The role of Wee1 and Myt1 in breast cancer

by

Cody Wayne Lewis

A thesis submitted in partial fulfillment of the requirements for the degree of

Doctor of Philosophy
in
Cancer Sciences

Department of Oncology
University of Alberta

Abstract

To ensure faithful cell division, entry into mitosis must be inhibited in cells with damage or under-replicated DNA. Wee1 and Myt1 are two partially redundant kinases that inhibit mitotic entry through the phosphorylation of the Cdk1/cyclin B complex. Cdk1 is an essential mitotic kinase that regulates essentially all mitotic processes including chromosome condensation and nuclear envelop breakdown. Ectopic Cdk1 activation causes cells to prematurely enter mitosis with under-replicated DNA leading to chromosome fragmentation. Moreover, failure to inhibit Cdk1 during the metaphase to anaphase transition can induce a mitotic arrest. Centromere fragmentation and mitotic arrest induce cell death by mitotic catastrophe.

Mitotic catastrophe is a common mode of cell death that occurs in tumour cells in response to various genotoxic therapies including irradiation. However, many cancer cells upregulate Wee1 expression, which promotes cancer cell survival through Cdk1 inhibition. To enhance the efficacy of genotoxic anticancer therapies, the Wee1 inhibitor Adavosertib was developed. Adavosertib is currently being tested in the clinic against various cancer types alone and in combination with different genotoxic agents.

Our lab has found that monotreatment with Adavosertib is enough to induce cell death in a subset of cancer cells. In these cells, Adavosertib has two major effects on the cell cycle: premature mitotic entry leading to chromosome fragmentation *and* prolonged mitotic arrest, which is not dependent on chromosome fragmentation. Cell sensitivity to Adavosertib is directly correlated with Myt1 protein expression; cells with high Myt1 protein levels are resistant to Adavosertib (and vice versa). Likewise, Myt1-induced overexpression reduces cell sensitivity to Adavosertib. Furthermore, cells selective for

Adavosertib resistance have upregulated Myt1 protein levels. Adavosertib resistant cells have less *in vitro* Cdk1 activity, do not undergo premature mitosis or centromere fragmentation, and do not arrest in mitosis following Wee1 inhibition, suggesting that Adavosertib resistance is mediated through reduced Cdk1 activity.

Cdk1 phosphorylation on Y15 is catalyzed by Wee1 and to a lesser extent Myt1 whereas Cdk1 phosphorylation on T14 is strictly regulated by Myt1. We found that Adavosertib treatment reduced pY15-Cdk1 levels but not pT14-Cdk1 levels, which suggests that Adavosertib inhibits Wee1 but not Myt1 activity. siRNA knockdown of Myt1 sensitizes Adavosertib resistant cells to Wee1 inhibition; these cells have increased *in vitro* Cdk1 activity, are prone to premature mitosis, undergo centromere fragmentation, and arrest in mitosis. This data confirm that Myt1 is an important driver of Adavosertib resistance.

Our data shows that Myt1 is overexpressed in breast cancer tissue and that high Myt1 levels are associated with a worse clinical outcome. Myt1 is also reported to be overexpressed in other cancer types including colorectal, lung, and head and neck cancers. Currently, there are no selective Myt1 small molecule inhibitors available for preclinical or clinical use, but our data provides a rationale for the development of such inhibitors.

Given the lack of selective small molecule Myt1 inhibitors, we investigated alternative treatment strategies for enhancing Adavosertib sensitivity in cancer cells. We focused our study on small molecule inhibitors that were either approved for clinical used or had the potential for clinical use. Checkpoint kinases such as ATR and Chk1 function in a parallel pathway to Wee1 and Myt1. Several ATR and Chk1 inhibitors are being tested in the clinic. Both ATR and Chk1 inhibitors induce premature mitosis and synergistic

cancer cell killing when used in combination with Adavosertib. Additionally, antimitotic agents that delay mitotic exit (e.g. paclitaxel and FTI inhibitor L-744-832) were also found to sensitize cancer cells to Adavosertib by inhibiting mitotic exit. Importantly, combination treatments with Adavosertib were found to be effective in cells that overexpressed Myt1. Our data highlight potential avenues for overcoming Myt1 induced Adavosertib resistance.

Preface

This thesis is an original work by Cody W Lewis. Portions of this thesis have been previously published as research articles or reviews as indicated below.

Chapter 1: Figure titled Cdk1/cyclin B activity is antagonized by PP2A-B55 panel B was published as Rata S, Suarez Peredo Rodriguez MF, Joseph S, Peter N, Echegaray Iturra F, Yang F, Madzvamuse A, Ruppert JG, Samejima K, Platani M, Alvarez-Fernandez M, Malumbres M, Earnshaw WC, Novak B, and H Hochegger, "Two Interlinked Bistable Switches Govern Mitotic Control in Mammalian Cells," Current Biology, volume 28, issue 23, 3824-3832 (2018). Copyright permission to use figure is granted under **Creative Commons Attribution 4.0 License** (CC BY 4.0). Figure titled "Mitotic checkpoint silencing figure" is published as Lewis CW and GKT Chan, "Role of cytoplasmic dynein and dynactin in mitotic checkpoint silencing," Dyneins: Structure, Biology and Disease: The Biology of Dynein Motors, Academic Press, Elsevier, volume 1, 516–533 (2018). Copyright permission to re-use figure and legend was obtained Elsevier.

Chapter 2: Published as Lewis CW, Jin Z, Macdonald D, Wei W, Qian XJ, Choi WS, He R, Sun X, and G Chan, "Prolonged mitotic arrest induced by Wee1 inhibition sensitizes breast cancer cells to paclitaxel," Oncotarget, volume 8, issue 43, 73705-73722 (2017). Copyright permission to use a copy of this article in chapter 2 is granted under **Creative Commons Attribution 3.0 License** (CC BY 3.0). I was responsible for the experimental design, data collection and analysis as well as the manuscript writing. Jin Z initiated project and contributed to experimental design, data collection and analysis for all figures except for experiments that used paclitaxel. Macdonald D and Wei W aided in the preparation of cell extracts and analysis of extracts by immunoblotting. Qian XJ, Choi WS, He R were

involved in the data collection and analysis of high-content live cell imaging. Sun X contributed to experimental design, data collection and analysis for high content imaging of immunofluorescent images. G Chan was the supervisory author and was involved with experimental design and manuscript writing. All figures have been re-numbered, and some supplementary figures have been incorporated as main figures.

Chapter 3: Published as Lewis CW, Bukhari AB, Xiao EJ, Choi WS, Smith JD, Homola E, Mackey JR, Campbell SD, Gamper AM, and GK Chan, "Upregulation of Myt1 promotes acquired resistance of cancer cells to Wee1 inhibition," (2019). Under the **copyright and permissions policies of the AACR** to which Cancer Research belongs, authors are permitted to use a copy of this article in my doctoral thesis. Lewis CW, Choi WS, Smith JD, Gamper AM, and GK Chan developed the concepts and designed the project. Lewis CW and Homola E developed methodology. Lewis CW, Bukhari AB, Xiao EJ, Choi WS, Smith JD, Gamper AM, and GK Chan acquired data, performed analysis, and interpreted data. Lewis CW, Bukhari AB, Smith JD, Mackey JR, Campbell SD, Gamper AM, and GK Chan. All figures have been re-numbered and supplementary figures and materials have been incorporated as main figures and text. Figure 3.3, Figure 3.7B & C, Figure 3.11 parts including T-46D cell lines, and Figure 3.13 were not included in the publication.

Chapter 4-5: Unpublished data (original work).

Appendixes A: This appendix includes published and unpublished data characterizing the effects of combined inhibition of Wee1 and ATR on mitosis in HeLa and other cancer cell lines. The Chan lab contributed to this project by providing stable fluorescent cell lines and performing some of the mitotic assays included in this appendix. Additionally, our lab

performed survival assays showing that siWee1 mimics the effects of Adavosertib in the presence of AZD6783. Portions of **Figure 8.1**, **Figure 8.2**, and **Figure 8.3** are published in Bukhari AB, Lewis CW, Pearce JJ, Luong D, Chan GK, and AM Gamper, "Inhibiting Wee1 and ATR kinases produces tumor-selective synthetic lethality and suppresses metastasis," The Journal of Clinical Investigations, volume 129, issue 3, 1329-1344 (2019). **Appendixes B-E**: Unpublished data (original work).

Dedication

In memory of Wayne Harry Lewis and Elsie Lewis, the most loving, caring, and supportive people I have even known.

Acknowledgements

I would like to thank my supervisor Dr. Gordon Chan for his patience, support, and mentorship through my PhD training. Dr. Chan's mentorship was invaluable and without his guidance I would not have been able to accomplish the work presented in this thesis. I would also like to thank all the members of the Chan laboratory (past and present) for their assistance. I would like to specially thank Dr. Dawn Macdonald for her help editing various documents for me and for her help with tissue culture during the early portion of my PhD. In addition, I would like to thank Joanne Smith for helping me with lab projects during the writing period of my thesis.

My PhD supervisory committee (Dr. Michael Weinfeld and Michael Hendzel) have played essential roles in fostering my skills as a scientist and I thank them for all their advice over the years. I also thank Dr. Shelagh Campbell, Dr. Zhigang Jin and Dr. Armin Gamper for providing reagents (antibodies, cell lines, etc.) and for the stimulating scientific conversations.

I would like to thank members of the Weinfeld, Godbout and Gamper laboratories for sharing equipment and reagents. Thanks to Dr. Roseline Godbout for the breast cancer cell lines. Special thanks to Mesfin Fanta for his technical advice in areas of protein purification and colony formation assay. Thanks to Michelle (Min Hsuan) Wu, Daniel (Won Shik) Choi, Xiaoyan Yang, Jennifer Dufour, Richard Yuen, and Bingcheng Jiang for help editing my thesis, attending the numerous mock presentations over the years, and for providing other useful advice. I also thank Amirali Bukhari for his help sorting cells, assisting me with setting up imaging experiments, and for his computer expertise.

I would also like to thank Dr. Xuejun Sun, and Gerry Barron in the Cell Imaging Facility (Oncology department) for providing rigorous training and expertise on the numerous imaging platforms utilized in my experiments. Thanks to Dr. Anne Galloway for sorting cells and for other technical advice in the laboratory.

The Oncology department is very fortunate to have several amazing laboratory assistants and I would like to personally acknowledge April Scott and Ray Ronald for all the help they provided in filling pipette tips, preparing solutions, autoclaving, and other tasks. Additionally, I thank April and Ray for the many stimulating lunchroom conversations.

Special thanks to my loving husband, Daniel James Hoot, for always supporting me throughout my career. Sorry you had to sit through all my practise presentations over the past 5 years!

I would also like to thank the following organizations for funding me during the tenure of my PhD: 1) Natural Sciences and Engineering Research (NSERC) Council of Canada for awarding me the *Alexander Graham Bell Canada Graduate Scholarships-Doctoral Program*; 2) the University of Alberta for awarding me two *Queen Elizabeth II graduate scholarships*, *Andrew Stewart Memorial Prize*, and *President's Doctoral Prize of Distinction*; 3) the Graduate Student Association (University of Alberta) for awarding me two travel awards; and 4) the Killam trust and University of Alberta for awarding me the *Izaak Walton Killam Memorial Scholarship*.

Contents

List of tables

List of Figures

List of Supplementary Figures

List of terms, abbreviations, and symbols

µg	Microgram
µM	Micromolar
µm	Micrometer
γH2XA	Gamma histone H2AX
ACA	Anti-centromere antigen
APC/C	Anaphase promoting complex/cyclosome
ARPP19	cAMP-regulated phosphoprotein 19 (also known as ENSA)
ATM	Ataxia telangiectasia mutated
ATP	Adenosine triphosphate
ATR	Ataxia telangiectasia and Rad3 related kinase
Bak	Bcl-2 antagonist/killer
Bax	Bcl-2 associated X
Bcl-2	B-cell lymphoma 2
Bcl-X_L	B-cell lymphoma extra large
Bid	BH3 interacting-domain death agonist
Bim	Bcl-2 interacting mediator of cell death
BRIP1	BRCA1 interacting protein C-terminal helicase 1
BSA	Bovine serum albumin
Bub1	Budding uninhibited by benzimidazole 1
BubR1	Bub1 related kinase 1
Bub3	Budding uninhibited by benzimidazole 3
C-terminus	Carboxyl terminus
CAK	CDK activating kinase
CCAN	Constitutive centromere associated network
CCLE	Cancer Cell Line Encyclopedia
cDNA	Complementary DNA
Cdc2	Cell division cycle 2 kinase (also known as Cdk1)
Cdc20	Cell division cycle 20
Cdc25A	Cell division cycle 25A phosphate
Cdc25B	Cell division cycle 25B phosphate
Cdc25C	Cell division cycle 25C phosphate
Cdc45	Cell division cycle 45
Cdk1	Cyclin-dependent kinase 1 (also known as Cdc2)
Cdk2	Cyclin-dependent kinase 2
Cdk4	Cyclin-dependent kinase 4
Cdk6	Cyclin-dependent kinase 6
Cdk7	Cyclin-dependent kinase 7
CENP-A	Centromere protein A
CENP-B	Centromere protein B
CENP-C	Centromere protein C

CENP-T	Centromeric protein T
Chk1	Checkpoint kinase 1
Chk2	Checkpoint kinase 2
cIAP1	Cellular Inhibitor of Apoptosis Protein-1
cIAP2	Cellular Inhibitor of Apoptosis Protein-2
Cip	CDK interacting protein
CPC	Chromosomal passenger complex
CPT	Camptothecin
CRD	C-terminal regulatory domain
DAPI	4’,6-diamino-2-phenylindole
DNA	Deoxyribonucleic acid
DMEM	Dulbecco’s Modified Eagle’s Medium
EGFR	Epidermal growth factor receptor
ENSA	α-Endosulfine
FA	Fanconi anemia
FANCJ	Fanconi anemia J (also known as BRIP1)
FANCM	Fanconi anemia M
Fcp1	RNA polymerase II-carboxy-terminal domain phosphatase
FGFR1	Fibroblast growth factor receptor 1
FTI	Farnesyl transferase inhibitor
G1	Gap phase 1
G2	Gap phase 2
GFP	Green fluorescence protein
GST	Glutathione-S-transferase
GTP	Guanosine triphosphate
h	Hours
H2A	Histone H2A
H2B	Histone H2B
H3	Histone H3
H4	Histone H4
HR	Hazard ratio
INK4	inhibitors of Cdk4
KDa	Kilo dalton
Kip	Kinase inhibitory protein
KNM	Knl1, Ndc80, and Mis12
M	Mitosis phase
Mad1	Mitotic arrest deficient 1
Mad2	Mitotic arrest deficient 2
Mad2-C	Closed mitotic arrest deficient 2
Mad2-O	Open mitotic arrest deficient 2
MEK1	Mitogen-activated protein kinase kinase
MCAK	Mitotic centromere-associated kinesin
MCC	Mitotic checkpoint complex

mCherry	Monomeric Cherry fluorescent protein
Mcl-1	Myeloid cell leukemia 1
Mik1	Mitosis inhibitor protein kinase 1
min	Minutes
Mps1	Monopolar spindle 1
mRuby	Monomeric ruby fluorescent protein
Myt1 (PKMYT1)	Protein kinase, membrane associated tyrosine/threonine 1
n	Number of samples
N-terminus	Amino terminus
NEBD	Nuclear envelope breakdown
NES	Nuclear export signal
NLS	Nuclear localization signal
ng	Nanogram
nm	Nanometer
nM	Nanomolar
NPAT	Nuclear protein, co-activator of histone transcription
NRD	N-terminal regulatory domain
NS	Not significant
OD_{600}	Optical density at 600 nm
PALB2	Partner and Localizer of BRCA2
PARP	Poly-ADP ribose polymerase
PBS	Phosphate buffered saline
PDGFRb	Platelet-derived growth factor receptor b
PKB	Protein kinase B (also known as Akt1)
Plk1	Polo-like kinase 1
PP1	Protein phosphatase 1
PP1Cα	Protein phosphatase 1Cα
PP2A	Protein phosphatase 2A
qRT-PCR	Quantitative reverse transcription-polymerase chain reaction
RIF1	Replication Timing Regulatory Factor 1
RT-PCR	Reverse transcription-polymerase chain reaction
RZZ	Roughdeal, Zwilch and Zeste-white 10
S	Synthesis (DNA replication) phase
SAC	Spindle assembly checkpoint
SD	Standard deviation
SDS	Sodium dodecyl sulfate
SEM	Standard error of mean
siSc	Scrambled small interfering ribonucleic acid
siMyt1	Myt1 small interfering ribonucleic acid
siRNA	Small interfering ribonucleic acid
siWee1	Wee1 small interfering ribonucleic acid
Ska	spindle and kinetochore associated complex
Slx1	Structure-specific endonuclease subunit Slx1

Slx4	Structure-specific endonuclease subunit Slx4 (also known as FANCP)
Src	Sarcoma (also known as c-Src)
TBS	Tris buffered saline
TBS-T	Tris buffered saline with tween
tdTomato	Tandem repeat tomato fluorescent protein
TSAP6	Tumour suppressor activate pathway 6 (also known as Steap3)
WT	Wild type
XIAP	X-linked inhibitor of apoptosis
ZW-10	Zeste-white 10

1 Chapter 1. Background

1.1 Cell cycle

The cell cycle is composed of two major parts: interphase and M-phase (**Figure 1.1**). Interphase is further divided into three phases referred to as Gap 1 (G1), synthesis (S), and Gap 2 (G2). During the Gap phases, cells obtain mass and accumulate biomolecules necessary for DNA replication and cell division, whereas in S phase cells replicate their DNA. M-phase is divided into two parts, mitosis (division of chromosomes) and cytokinesis (division of cytoplasm). Mitosis consists of five stages (prophase, prometaphase, metaphase, anaphase, and telophase) (**Figure 1.1**). Following cytokinesis, cells can either re-enter the cell cycle at G1 or enter a non-dividing state referred to as quiescence or G0.

The cell-cycle is monitored by four major checkpoints: G1/S, intra-S, G2/M, and the mitotic checkpoint (also known as the spindle assembly checkpoint (SAC)) [reviewed in (Lewis and Chan, 2017; Musacchio, 2015)]. These checkpoints can induce a cell-cycle arrest if a problem affecting faithful cell division is detected. Damaged DNA, which arises from endogenous processes and exogenous sources, is a major trigger for the activation of the G1/S, intra-S, and G2/M checkpoints. Additionally, incomplete DNA replication can trigger the activation of the G2/M checkpoint. Once the problem that gave rise to the checkpoint has been resolved (i.e. damaged DNA is repaired and DNA replication is completed), the interphase checkpoints will be turned off and the cell will continue onto the next phase. The mitotic checkpoint prevents cells from undergoing anaphase if bi-polar alignment of duplicated chromosomes is not sensed or if other mitotic defects are detected

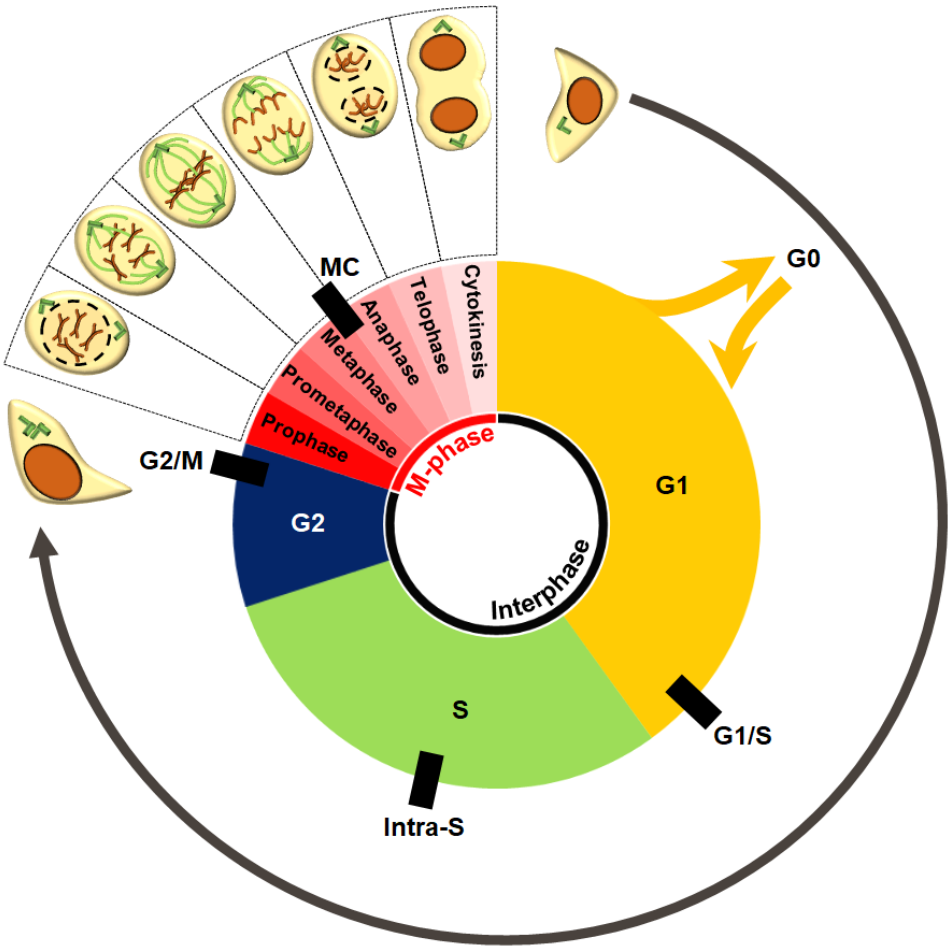

Figure 1.1. The Cell cycle and cell-cycle checkpoints.
The cell cycle is composed of four distinct phases: G1, S, G2, and M. Collectively, G1, S and G2 make up interphase (black inner ring) whereas mitosis and cytokinesis make up M-phase (red inner ring). Mitosis can be divided into 5 stages (depicted): prophase, the stage in which the nuclear envelop breaks down and chromosome condensation begins; prometaphase, the stage in which spindle fibers (microtubules) attach to the chromosome kinetochores; metaphase, the state in which chromosomes alignment and bipolar kinetochore tension is achieved; anaphase, the stage in which sister chromatids are separated and; telophase, the stage in which the nuclear envelop reforms around daughter nuclei and chromosome de-condensation occurs. While telophase is occurring, the cell undergoes cytokinesis resulting in two daughter cells. Black boxes on outer ring indicate the four major cell-cycle checkpoints. MC refers to the mitotic checkpoint.

[Reviewed in (Liu and Zhang, 2016)]. Collectively, the main purpose of these cell-cycle checkpoints is to ensure genomic stability is maintained during cell division, as the disruption of genomic stability can induce cell death and promote diseases such as cancer.

Many cancer cells have one or more defective checkpoint(s), which makes them susceptible to genomic changes.

1.2 CDK/cyclin complexes drive the cell cycle

The cell cycle is driven by a highly conserved group of the serine/threonine kinases, known as cyclin-dependent kinases (CDKs). In lower eukaryotic organisms, such as *Saccharomyces cerevisiae* and *Schizosaccharomyces pombe*, a single CDK controls the cell cycle (Russell and Nurse, 1986b). This CDK was designated cell division cycle-28 (Cdc28) and cell division cycle-2 (Cdc2) in *Saccharomyces cerevisiae* and *Schizosaccharomyces pombe* respectively. In humans, thirteen different CDKs have been identified, but only four of these (Cdk1, Cdk2, Cdk4, and Cdk6) are directly involved in cell cycle regulation [reviewed in (Malumbres and Barbacid, 2009)]. CDK activation requires dimerization with regulatory subunits known as cyclins. The binding of cyclin induces a conformational change to the ATP binding region of the CDK. This CDK conformational change is further stabilized by CDK activating kinase (CAK, a trimeric complex consisting of Cdk7, cyclin H and Mat1), which phosphorylates CDKs within the T-loop (T161 and T160 on Cdk1 and Cdk2, respectively) (Solomon et al., 1992). Four different cyclins regulate cell-cycle CDKs: cyclin A, cyclin B, cyclin E, and cyclin D. These cyclins undergo cyclical changes, which regulates cell-cycle phase transition by confining CDK activity to specific phases (Zerjatke et al., 2017) (**Figure 1.2A**). Cyclin downregulation can be used to restrict cell division and conserve energy in quiescent cells (Zerjatke et al., 2017). Additionally, cyclin downregulation in the presence of damaged DNA can reinforce DNA damage checkpoints and induce a cell-cycle arrest (Agami and Bernards, 2000; Kikuchi et al., 2010; Nakayama et al., 2009; Pontano et al., 2008).

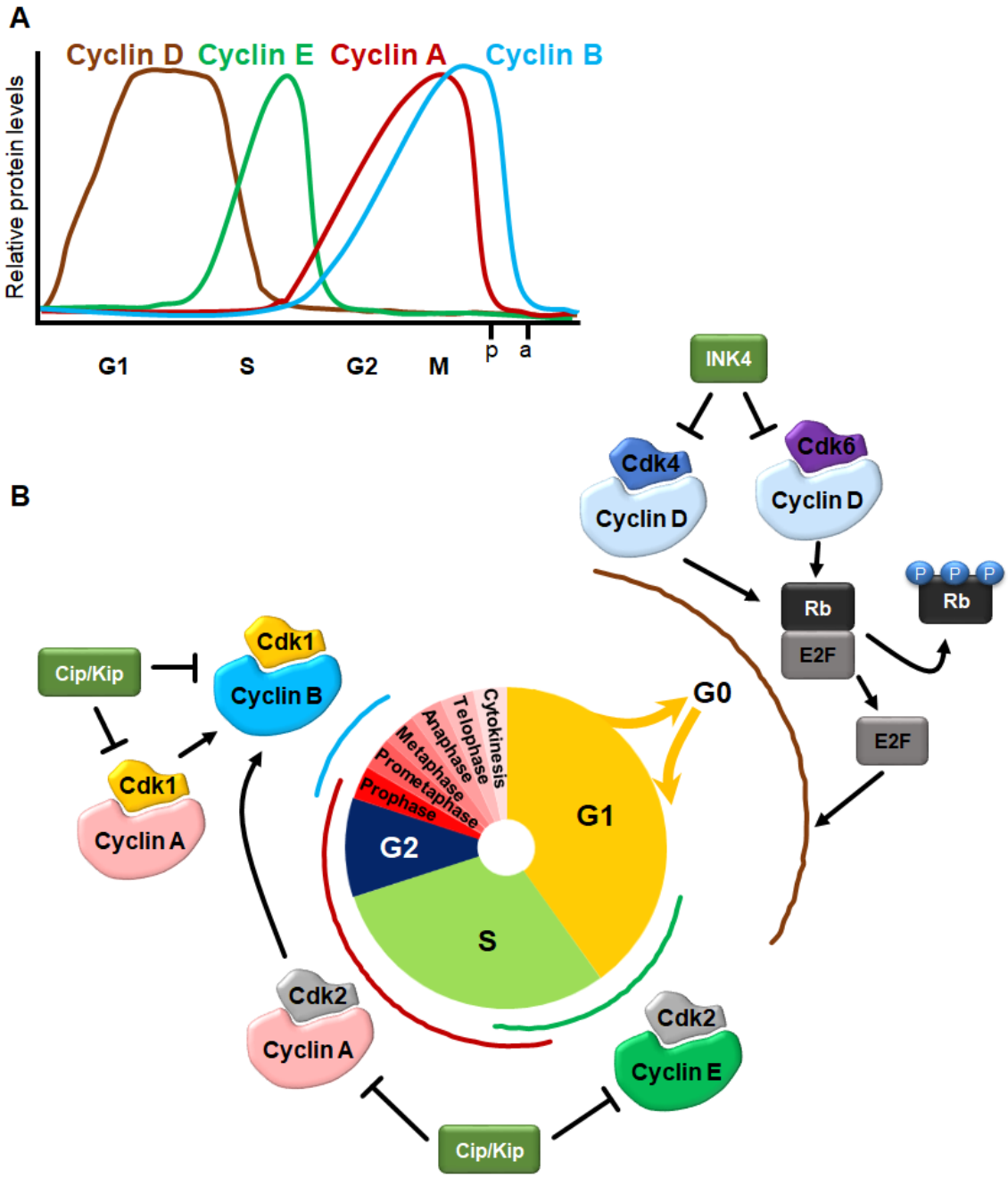

Figure 1.2. CDKs regulate the cell cycle.
A) Graph shows the cyclic changes in relative protein levels of human cyclin A (red), B (blue), E (green), and D (brown). Lower case 'p' and 'a' denote prometaphase and anaphase. Cyclin A and D levels are based on data presented in (Fung et al., 2007; Zerjatke et al., 2017), cyclin B levels are based on data presented in (Fung et al., 2007; Gavet and Pines, 2010; Zerjatke et al., 2017) whereas cyclin E levels were based on data presented in (Dong et al., 2018). **B)** Model showing when and where the different Cdk/cyclin complexes exhibit activity. Cdk4 and Cdk6 (brown line) are active in G1 phase, where they inhibit Rb and promote E2F activation. Cdk2/cyclin E (green line) promotes transition from G1 to S phase. Cdk2/cyclin A transitions cells into G2 phase after DNA replication. Cdk1/cyclin B promotes entry into mitosis following

activation by other Cdk/cyclin complexes. CDKs can be inhibited by two inhibitor families INK4 and Cip/Kip through direct binding.

Six CDK/cyclin complexes regulate the cell cycle in human somatic cells (**Figure 1.2B**). Mitogenic signalling in quiescence cells induces cyclin D synthesis and promotes its assembly with Cdk4 and Cdk6 in G1 phase (Matsushime et al., 1994; Meyerson and Harlow, 1994; Zerjatke et al., 2017). Cdk4/cyclin D and Cdk6/cyclin D then partially inhibit the Retinoblastoma (Rb) (Harbour et al., 1999; Matsushime et al., 1994; Meyerson and Harlow, 1994) and RB related proteins (p107 and p310), a group of cell cycle inhibitors known as the pocket protein family. Non-phosphorylated Rb binds to, and inhibits, the E2F family of activating transcription factors (E2F1, E2F2, and E2Fa) in quiescent cells, blocking transcription of downstream genes required for cellular proliferation [reviewed in (Trimarchi and Lees, 2002)]. However, Rb phosphorylation by Cdk4 and Cdk6 induces a conformational change to Rb, which weakens the interaction with E2F allowing transcription of cyclin E (Harbour et al., 1999). Once synthesized, cyclin E forms a complex with Cdk2, a process that promotes the transition from G1 into S phase. Cdk2/cyclin E adds additional phosphates to Rb, which further disrupts its interaction with E2F leading to the transcription of cyclin A and cyclin B (Harbour et al., 1999; Lundberg and Weinberg, 1998). In mid-S phase, cyclin E is ubiquitinated by the Skp1/Cul1/F-box protein (SCF) complex and then degraded by the proteasome complex [reviewed in (Nakayama and Nakayama, 2006)]. Following cyclin E degradation, Cdk2 complexes with cyclin A, which facilitates the end of DNA synthesis and the transition into the G2 phase (Woo and Poon, 2003). At the end of G2 phase, Cdk2 and Cdk1 in complex with cyclin A

promote the activation of the mitotic promoting complex, Cdk1/cyclin B (Fung et al., 2007).

1.2.1 Cdk1 is an essential CDK that is required for mitosis

Genetic studies in mice have shown that Cdk1 can interact with other cyclin molecules to maintain cell cycle progression if one or more interphase CDK(s) (e.g. Cdk2) is knocked out (Santamaria et al., 2007). This suggests that interphase CDKs are not essential for cell division, at least during early mammalian development. In contrast, Cdk1 is essential for mitosis and its deletion induces a permanent G2 arrest that cannot be rescued by the ectopic expression of other CDKs or cyclins (Fung et al., 2007; Santamaria et al., 2007).

Cdk1 directly phosphorylates at least two hundred different proteins during mitosis (Ubersax et al., 2003), which trigger several key processes including nuclear envelope breakdown (NEBD), chromosome condensation, centriole disengagement, mitotic checkpoint activation, and endoplasmic reticulum and Golgi fragmentation.

NEBD occurs during prophase and results in the release of nuclear contents (e.g. chromosomes) into the cytoplasm. During interphase, lamin A and lamin C proteins form a dense intermediate filament network that provides mechanical support to the nucleus. However, Cdk1 phosphorylation of lamin A and lamin C triggers the disassembly of the lamin network, which contributes to NEBD (Heald and McKeon, 1990; Peter et al., 1990; Szmyd et al., 2019).

Chromosome condensation is required to prevent chromosomes from becoming entangled during chromosome segregation. Cdk1/cyclin B induces chromosome condensation through the phosphorylation of histones (Langan et al., 1989; Peter et al., 1990; Seibert et al., 2019) and through the activation of condensin II subunits (Abe et al.,

2011). To ensure biorientation of the microtubules and bipolar attachment of chromosomes, centrioles must separate and migrate to opposite poles. Cdk1/cyclin B induces centriole separation through the phosphorylation of different proteins including the kinesin motor Eg5 (Cahu et al., 2008; Smith et al., 2011). As discussed in **section 1.1**, the mitotic checkpoint inhibits chromosome segregation until chromosome bipolar attachment is achieved, a process that ensures faithful chromosome division. Cdk1 regulates the activation and localization of several key mitotic checkpoint proteins including Aurora B and mono-polar spindle 1 (Mps1) (discussed in detail in **section 1.4.2**). Cdk1 also has a role in promoting the fragmentation of membranous organelles. During prophase, membranous organelles such as the Golgi, endoplasmic reticulum, and mitochondria are fragmented into thousands of vesicles and tubules, which ensures equal division between daughter cells during cell division (Shorter and Warren, 2002). Cdk1 promotes the fragmentation of these organelles through phospho-inactivation of proteins that positively regulate membrane fusion (Nakajima et al., 2008; Shorter and Warren, 2002). In summary, Cdk1 is essential for cell division because it drives nearly all mitotic processes.

1.3 The Wee1/Myt1-Cdk1-Cdc25 axis regulates mitotic timing

1.3.1 Wee1 and Myt1 negatively regulate mitosis through Cdk1 phosphorylation

Although Cdk1 protein levels are stable throughout the cell cycle (Welch and Wang, 1992) the absence of cyclin B prevents Cdk1 from inducing mitosis during G1 and early S phase (Fung et al., 2007; Gavet and Pines, 2010; Zerjatke et al., 2017) (**Figure 1.3A**). As cells progress through S-phase, cyclin B levels slowly increase and peak during the G2/M transition. Cdk1/cyclin B complexes that form prior to the G2/M transition are inhibited

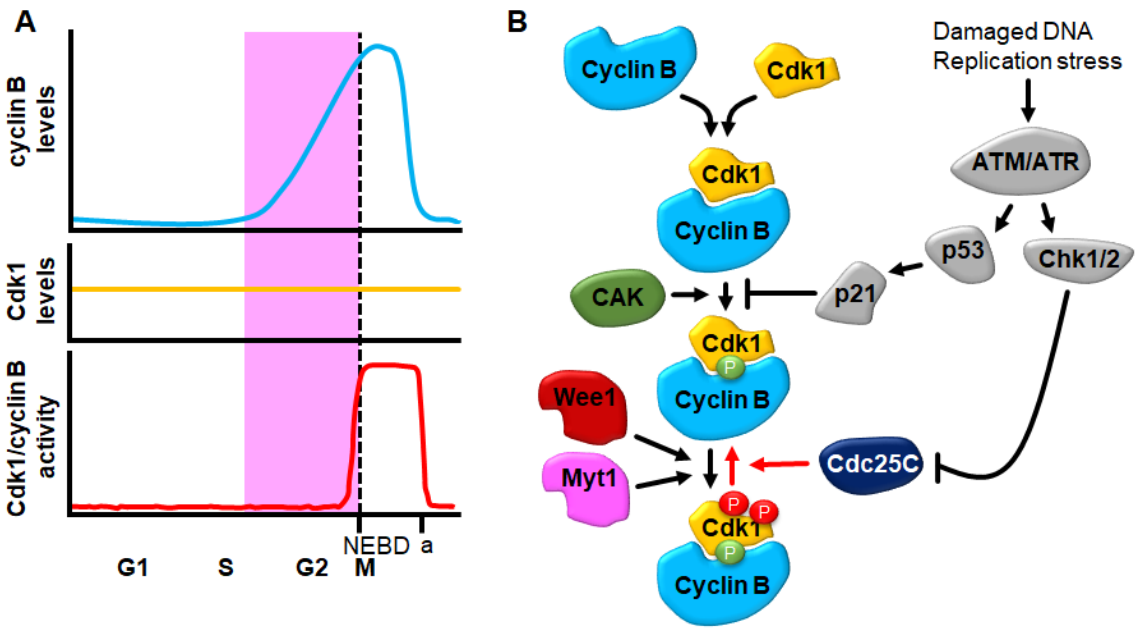

Figure 1.3. Cdk1/cyclin B activity is inhibited during S and G2 phase.
A) Graph shows the relative protein levels of cyclin B (top; blue line) and Cdk1 (middle; yellow line). Bottom graph show the relative activity of Cdk1/cyclin B over the cell cycle (red line). The pink region between mid S-phase and NEBD represents the region in which Cdk1/cyclin B activity is inhibited by Wee1 and Myt1. Cyclin B levels and Cdk1/cyclin B activity are modeled based on data presented in (Fung et al., 2007; Gavet and Pines, 2010; Zerjatke et al., 2017). **B)** Cdk1 and cyclin B bind in late S-phase. Cdk1 is then phosphorylated by CAK on T161 (depicted with green circle), which is required for Cdk1/cyclin B activation. However, phosphorylation of Cdk1 on T14 and Y15 (depicted with red circles) by Myt1 and Wee1 during interphase inhibits Cdk1/cyclin B. Damaged DNA or replication stress can induce the activation of interphase checkpoints, which downregulate Cdk1/cyclin B activity. ATM and ATR activate effector kinases Chk1 and Chk2, which phosphorylate and inhibit Cdc25C. In parallel, ATM and ATR can induce transcription of p53 leading to the transcription of the CDK inhibitor p21. Stimulatory phosphates are shown with green circles whereas inhibitory phosphates are shown with red circles. Red arrows in indicate pathways that are downregulated during interphase.

through phosphorylation of Cdk1 on Y15 (and T14 in multicellular eukaryotes) by the highly conserved Wee1 and Wee1 related kinases (**Figure 1.3B**).

Wee1 (also known as Wee1A in humans) was originally identified in *Schizosaccharomyces pombe*, and was named "wee" based on the resulting small-cell size phenotype observed in Wee1 mutant cells (Russell and Nurse, 1987). Following that discovery, additional Wee1 related kinase were identified: Mitosis inhibitor protein kinase

1 (Mik1) in *Schizosaccharomyces pombe* (Lundgren et al., 1991); Protein kinase membrane associated tyrosine/threonine 1 (PKMYT1) also known as Myt1 in metazoans (Cornwell et al., 2002; Mueller et al., 1995; Palmer et al., 1998); and Wee2 (Wee1B) in vertebrate cells (Leise and Mueller, 2002; Nakanishi et al., 2000). In mammalian cells, Wee2 is only expressed in germ tissue in the testes and ovaries and not in somatic tissue; therefore, Wee2 does not regulate Cdk1 and mitotic entry in somatic cells (Han et al., 2005; Nakanishi et al., 2000). In contrast, Wee1 and Myt1 are ubiquitously expressed in all tissue types and are therefore key regulators of mitotic entry.

Wee1 is an atypical tyrosine kinase that exclusively phosphorylates Cdk1 (and Cdk2) on Y15 of the ATP binding region (Jin et al., 2008; Russell and Nurse, 1987; Watanabe et al., 1995). In contrast, Myt1 is a dual tyrosine/threonine kinase that phosphorylates Cdk1 on both T14 and Y15 (Jin et al., 2008; Liu et al., 1997; Mueller et al., 1995). However, in human cells Myt1 preferentially phosphorylates Cdk1 on T14 (Liu et al., 1997). Initial studies on Myt1 and Wee1 kinase activities reported that Myt1 could not phosphorylate Cdk2 (Booher et al., 1997). Low levels of pT14-Cdk2 in complex with cyclin A have been observed by 2-D gel electrophoresis in HeLa cells, suggesting that Cdk2 is also a Myt1 substrate *in vivo* (Coulonval et al., 2011), however pY15-Cdk2 is the main phospho-inhibited form of Cdk2 observed in human cells (Coulonval et al., 2003; Coulonval et al., 2011). In addition to having slightly different substrate specificities, Wee1 and Myt1 also exhibit different subcellular localizations. During most of interphase, Wee1 localizes to the nucleus (Baldin and Ducommun, 1995; Heald et al., 1993; McGowan and Russell, 1995; Russell and Nurse, 1987), whereas Myt1 localizes to the Golgi and

endoplasmic reticulum (Liu et al., 1997; Mueller et al., 1995; Nakajima et al., 2008; Villeneuve et al., 2013).

Wee1 and Myt1 negatively regulate Cdk1 activity in a partially redundant manner; however, the subcellular localization of each protein has given rise to non-redundant specialized Cdk1 regulatory roles. For instance, the nuclear localization of Wee1 ensures that Cdk1/cyclin complexes entering the nucleus do not induce premature chromosome condensation or NEBD until G2/M transition. Due to its localization at the Golgi and endoplasmic reticulum, Myt1 functions as an essential component of an "organelle-based checkpoint", which prevents Cdk1 induced premature fragmentation of Golgi and endoplasmic reticulum during G2 phase [(Villeneuve et al., 2013) and reviewed in (Valente and Colanzi, 2015)]. Myt1 is also essential for Golgi and endoplasmic reticulum reassembly following chromosome segregation (Nakajima et al., 2008). In *Drosophila*, Myt1 inhibition of Cdk1/cyclin A is required to maintain the integrity of the endoplasmic reticulum derived fusome in premeiotic G2-arrested spermatocytes (Varadarajan et al., 2016). Additionally, Myt1 inhibition of Cdk1/cyclin A prevents premature centriole disengagement, a process that can lead to the formation of multipolar spindles (Varadarajan et al., 2016).

The primary structure of Wee1 is composed of a N-terminal regulatory domain (NRD), a kinase domain, and a short C-terminal domain [reviewed in (Enders, 2010)] (**Figure 1.4A**). The NRD contains both a nuclear export signal (NES) (Li et al., 2010) and a nuclear localization signal (Squire et al., 2005), which are needed to traffic Wee1 out of the nucleus during the G2/M transition and then back into the nucleus following nuclear envelope reformation in telophase. The NRD also contains a highly conserved negative

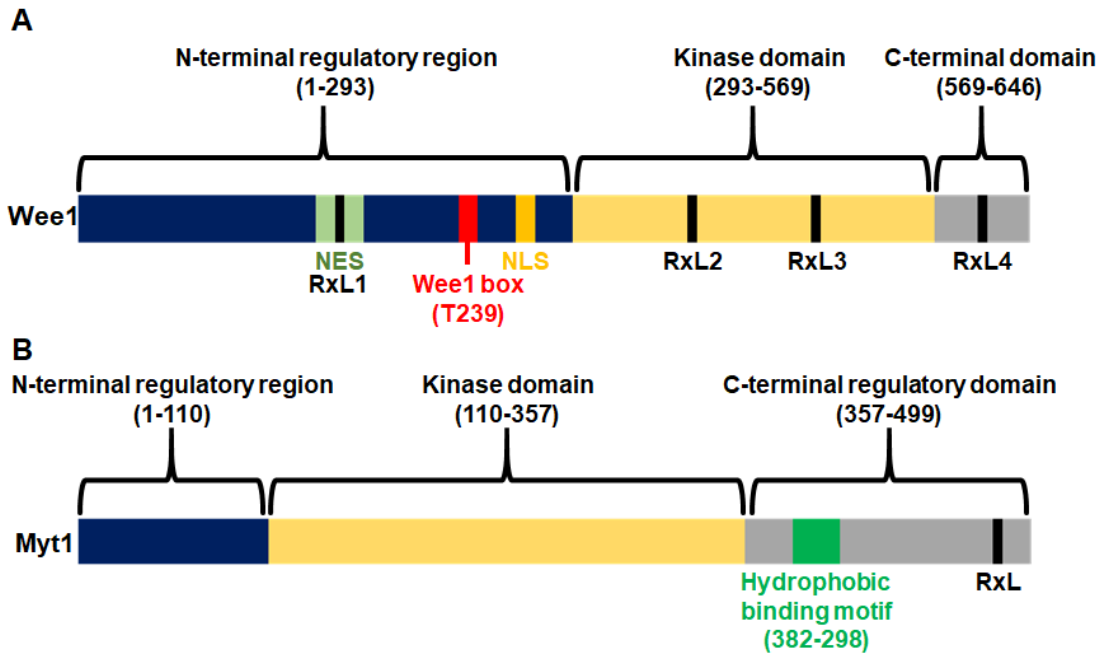

Figure 1.4. Primary structures of Wee1 and Myt1.
A) Wee1 is composed a N-terminal regulatory domain (dark blue), a kinase domain (tan), and a short C-terminal domain (grey). Wee1 also contains four cyclin binding motifs (RxL1, RxL2, RxL3, and RxL4), a highly conserved regulatory Wee1 box (red), a nuclear localization sequence (orange), and a nuclear export sequence (light green). **B)** Myt1 is composed of a short N-terminal regulatory domain, a kinase domain, and a regulatory C-terminal domain. Myt1 also contains a hydrophobic binding (membrane-associated) motif and a cyclin binding motif.

regulatory element known as the Wee box (Kim et al., 2005; Li et al., 2010; Okamoto and Sagata, 2007) (discussed in **section 1.3.1**). Wee1 contains four cyclin binding motifs (RxL1, RxL2, RxL3, and RxL4), which facilitate the interaction with CDK-cyclin (Li et al., 2010). The primary structure of Myt1 is less well characterized, but is also composed of three domains: a N-terminal regulatory domain; a kinase domain (Mueller et al., 1995; Wells et al., 1999); and a C-terminal regulatory domain (CRD) (Wells et al., 1999) (**Figure 1.4B**). In contrast to Wee1, Myt1 contains only one cyclin binding motif (RxL) (Liu et al., 1999), which facilitates Cdk1 interaction. Myt1 also contains a hydrophobic membrane

associated motif, which is required for localization to the Golgi and endoplasmic reticulum respectively (Liu et al., 1997).

1.3.2 p21 binding down regulates Cdk1 activity in normal cells

CDK activity is negatively regulated by two inhibitor families: INK4 (inhibitors of Cdk4) and Cip/Kip (CDK interacting protein/Kinase inhibitory protein) [reviewed in (Malumbres and Barbacid, 2005; Malumbres and Barbacid, 2009)] (**Figure 1.2**). The INK4 family only interacts with Cdk4 and Cdk6, whereas the Cip/Kip family can interact with all four cell-cycle CDKs *in vitro*. Cip (commonly known as p21) primarily inhibits Cdk2, an essential process for maintaining the G1/S DNA damage checkpoint (Aleem et al., 2005). In addition to Cdk2, p21 also binds to Cdk1 (Satyanarayana et al., 2008). p21 prevents phospho-activation of the T-loop (pT161-Cdk1) by CAK (Charrier-Savournin et al., 2004), a process that increases *in vitro* Cdk1 activity by hundred fold (Solomon et al., 1992). p21 is transcriptionally regulated by the tumour suppressor p53, a protein that is downregulated in at least 50% of all cancers (Cancer Genome Atlas Research, 2008; Cancer Genome Atlas Research, 2012; Olivier et al., 2010; Rausch et al., 2012). As such, most cancer cells have a defective G1/S checkpoints and must rely on the inhibition of Cdk1 by Wee1 and Myt1 to initiate a cell cycle arrest [Reviewed in (Aleem et al., 2005; Visconti et al., 2016)].

1.3.3 DNA damage checkpoints downregulate Cdk1 activity by inhibiting Cdc25 phosphatases

DNA damage checkpoints activate in response to damaged DNA or replication stress, which leads to the downregulation of Cdk1 activity (**Figure 1.3B**). Activation of these checkpoints is mediated by apical kinases Ataxia telangiectasia mutated (ATM) and Ataxia

telangiectasia and Rad3 related (ATR), which upregulate effector kinases checkpoint kinase 2 (Chk2) and checkpoint kinase 1 (Chk1) respectively. Among the key Chk1 and Chk2 targets is the Cdc25 family, a group of functionally redundant phosphatases consisting of Cdc25A, Cdc25B, and Cdc25C [Reviewed in (Shaltiel et al., 2015)]. The Cdc25 family functions to remove inhibitory phosphates from Cdk1 and Cdk2 (Russell and Nurse, 1986a). However, Chk1 and Chk2 mediated phosphorylation of the Cdc25 family neutralizes their activity. For instance, Chk1 and Chk2 phosphorylation on Cdc25C on S216 promotes the association of 14-3-3 proteins and the subsequent sequestration of Cdc25C in the cytoplasm, which prevents it from activating Cdk1 in the nucleus (Peng et al., 1997; Sanchez et al., 1997). In parallel, ATM and ATR stabilize and upregulate p53, which in turn upregulates p21 synthesis [reviewed in (Sperka et al., 2012)]. Additionally, p53 is also reported to upregulate tumour suppressor activate pathway 6 [TSAP6 (also known as Steap3)], a transmembrane protein that has been reported to interact with Myt1, upregulating its activity (Passer et al., 2003).

1.3.4 Wee1 and Myt1 are downregulated during mitosis by several independent mechanisms

Wee1 and Myt1 are hyper-phosphorylated at the onset of mitosis. In the case of Myt1, hyper-phosphorylation inhibits kinase activity, but does not appear to affect protein levels or localization (Nakajima et al., 2008; Villeneuve et al., 2013). In contrast, Wee1 phosphorylation inhibits kinase activity and promotes protein degradation. Moreover, Wee1 phosphorylation also promotes translocation out of the nucleus (Katayama et al., 2005; Li et al., 2010).

Myt1 phosphorylation at the Golgi and endoplasmic reticulum is mediated by MEK1 (Villeneuve et al., 2013). Myt1 mediated phosphorylation by MEK1 is required for normal Golgi and endoplasmic reticulum fragmentation, a process regulated by Cdk1 (Nakajima et al., 2008; Shorter and Warren, 2002; Villeneuve et al., 2013). Wee1 and Myt1 are both phosphorylated by Cdk1 and Cdk2 on several residues, which subsequently provide binding motifs for the peptidyl-isomerase Pin1 (**Figure 1.5A**) (Kim et al., 2005; Okamoto and Sagata, 2007; Visconti et al., 2015; Visconti et al., 2012; Wells et al., 1999). Pin1 induces inactivating conformational changes to Wee1 and Myt1 through prolyl isomerization (Shen et al., 1998). For instance, Cdk1/2 phosphorylation and Pin1 prolyl isomerization of T239 within the wee regulatory box of Wee1, greatly diminishes kinase activity (Kim et al., 2005; Okamoto and Sagata, 2007; Visconti et al., 2015; Visconti et al., 2012) (**Figure 1.4A** and **Figure 1.5A**; top panel). T239 phosphorylation may also create binding motifs for other kinases, which reinforce Wee1 inhibition by catalyzing the addition of secondary phosphates. HeLa and U-2 OS cells transfected with a Wee1 mutant that cannot be phosphorylated on T239 (T239A) cannot enter mitosis and instead arrest in G2 phase (Li et al., 2010). In contrast, cells transfected with the phospho-mimetic T239D Wee1 mutant cannot phosphorylate Cdk1 (Visconti et al., 2015; Visconti et al., 2012). Myt1 phosphorylation on T455 by Cdk1 is another Pin1 substrate (Inoue and Sagata, 2005; Wells et al., 1999) (**Figure 1.5A**; bottom panel). However, in this context Pin1 prolyl isomerization does not directly inhibit Myt1 activity and is thought to create a binding motif that is recognized by other kinases, which then help downregulate Myt1 kinase activity (Inoue and Sagata, 2005). In *Xenopus*, phosphorylation of Myt1 on T478 (human

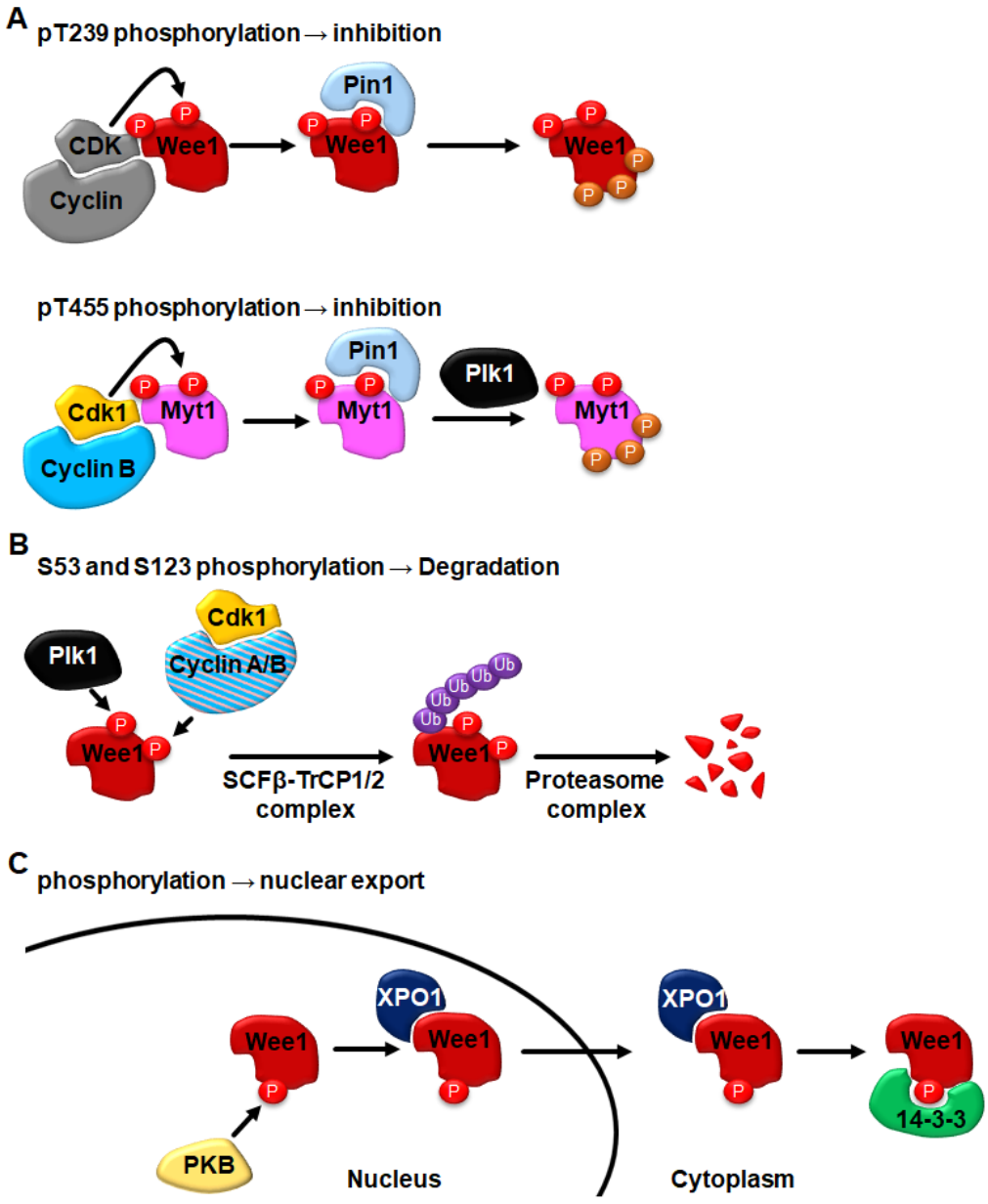

Figure 1.5. Mechanisms of downregulating Wee1 and Myt1 during the G2/M transition.
A) Cyclin binding to RxL motifs promotes CDK/cyclin phosphorylation of Wee1 and Myt1 on T239 and T455, respectively. Pin1 alters the protein structure of phosphorylated Wee1 and Myt1 through proline isomerization of CDK/cyclin phosphorylation sites. Additional kinases may be required to completely inhibit Wee1 and Myt1. CDK phosphorylations are shown in red, while non-CDK phosphorylations are shown in orange. CDK/cyclin refers to either Cdk1/cyclin A/B or Cdk2/cyclin A **B)** Wee1 phosphorylation on S53 and S123 by Plk1 and Cdk1/cyclin, respectively, promote the association of the SCFβ-TrCP1/2 complex, which poly-ubiquitinates Wee1 labelling it for degradation by the proteasome complex. **C**) XPO1 binds to Wee1 via the NES and facilitates translocation out of the nucleus. Phosphorylation of Wee1 on the short C-

terminal domain (S642) by PKB promotes association with 14-3-3 proteins and cytoplasmic retention.

T455) creates a binding motif for Plx1 (human Plk1), which then adds additional inhibitory phosphates to the CRD (Inoue and Sagata, 2005).

Wee1 phosphorylation on S53 and S123 by Plk1 and Cdk1/2 induces ubiquitin mediated protein degradation by the SCF complex (Watanabe et al., 2004) (**Figure 1.5B**). Moreover, the NRD of Wee1 also contains three PEST sequences (Watanabe et al., 1995; Zhu et al., 2017). PEST sequences are signal peptides rich in proline (P), glutamic acid (E), serine (S), and threonine (T), which can be used to induce rapid protein degradation (Rogers et al., 1986).

Wee1 contains an XPO1 nuclear export signal (**Figure 1.4A**), which facilitates XPO1 binding and subsequent translocation out of the nucleus (Li et al., 2010) (**Figure 1.5C**). Although it is not clear what stimulates XPO1 binding, it has been suggested that Wee1 phosphorylation at an unidentified site by Cdk2/cyclin A enhances Wee1 translocation out of the nucleus [reviewed in (Enders, 2010)]. Furthermore, Wee1 phosphorylation on S642 of the short C-terminal domain by Protein kinase B (PKB, also known as Akt) can promote cytoplasmic retention via the association of 14-3-3 proteins (Katayama et al., 2005). In the absence of Wee1, the nucleus becomes a refuge for Cdk1/cyclin B activation.

1.3.5 Cdk1/cyclin B is activated during the G2/M transition

Wee1 and Myt1 downregulation is one of two steps required for Cdk1/cyclin B activation at the G2/M transition. The second step is Cdc25 upregulation. The inhibitory phosphates

that were added to Cdc25 proteins during interphase are removed and new phosphates are added, which stabilize protein levels, enhance phosphatase activity, and alter protein subcellular localization [Reviewed in (Boutros et al., 2007; Shaltiel et al., 2015)]. For instance, Cdc25C is dephosphorylated on S216 and then phosphorylated on S198 by Plk1, which both increase catalytic activity and promote translocation into the nucleus (Cho et al., 2015; Toyoshima-Morimoto et al., 2002). Cdk1/cyclin B complexes that enter the nucleus are then dephosphorylated by Cdc25 (Russell and Nurse, 1986a). Since Wee1 is also translocated out of the nucleus at this time (Li et al., 2010), Cdk1/cyclin B activity is protected against re-phosphorylation (**Figure 1.6A**). Cdk1/cyclin B activation is a positive feedback system because activated complexes in turn inhibit Wee1 and Myt1 **(Figure 1.6B**). Furthermore, Cdk1/cyclin B also upregulate Cdc25 proteins. However, Cdk1/cyclin B is antagonized by protein phosphatase 2A (PP2A) and its subunit B55, which upregulate Wee1/Myt1 and downregulate Cdc25C [reviewed in (Kishimoto, 2015)] (**Figure 1.7A**). To overcome the PP2A-B55 antagonistic pathway, Cdk1 upregulates Greatwall kinase (Gwl). Gwl reinforces Cdk1 activity and together the two kinases upregulate PP2A-B55 inhibitory molecules α-Endosulfine (ENSA) and cAMP-regulated phosphoprotein 19 (ARPP19) (Hegarat et al., 2014; Okumura et al., 2014). ENSA and ARPP19 bind to B55 preventing its association with PP2A (Gharbi-Ayachi et al., 2010; Hached et al., 2019; Mochida et al., 2010; Williams et al., 2014). The downregulation of PP2A-B55 by Cdk1 and Gwl induces a secondary positive feedback system. As such, higher levels of Cdk1/cyclin B activity are required for mitotic entry compared to the amount required to sustain mitosis (Rata et al., 2018) (**Figure 1.7B**).

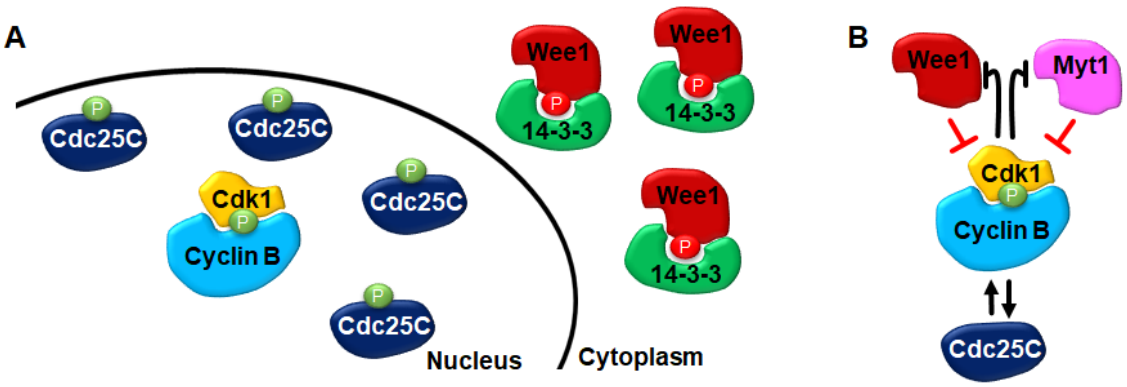

Figure 1.6. Cdk1 activation is a positive feedback system.
A) During the G2/M transition Wee1 is downregulated and transported out of the nucleus and Cdc25C is translocated into the nucleus. This provides a safe harbor for Cdk1/cyclin B activation. **B)** Cdk1/cyclin B inhibits Wee1 and Myt1 and activates Cdc25C, which results in a positive feedback system. Stimulatory phosphates are shown with green circles whereas inhibitory phosphates are shown with red circles. Black lines depict pathways that are upregulated in mitosis, whereas red lines depict pathways that are downregulated.

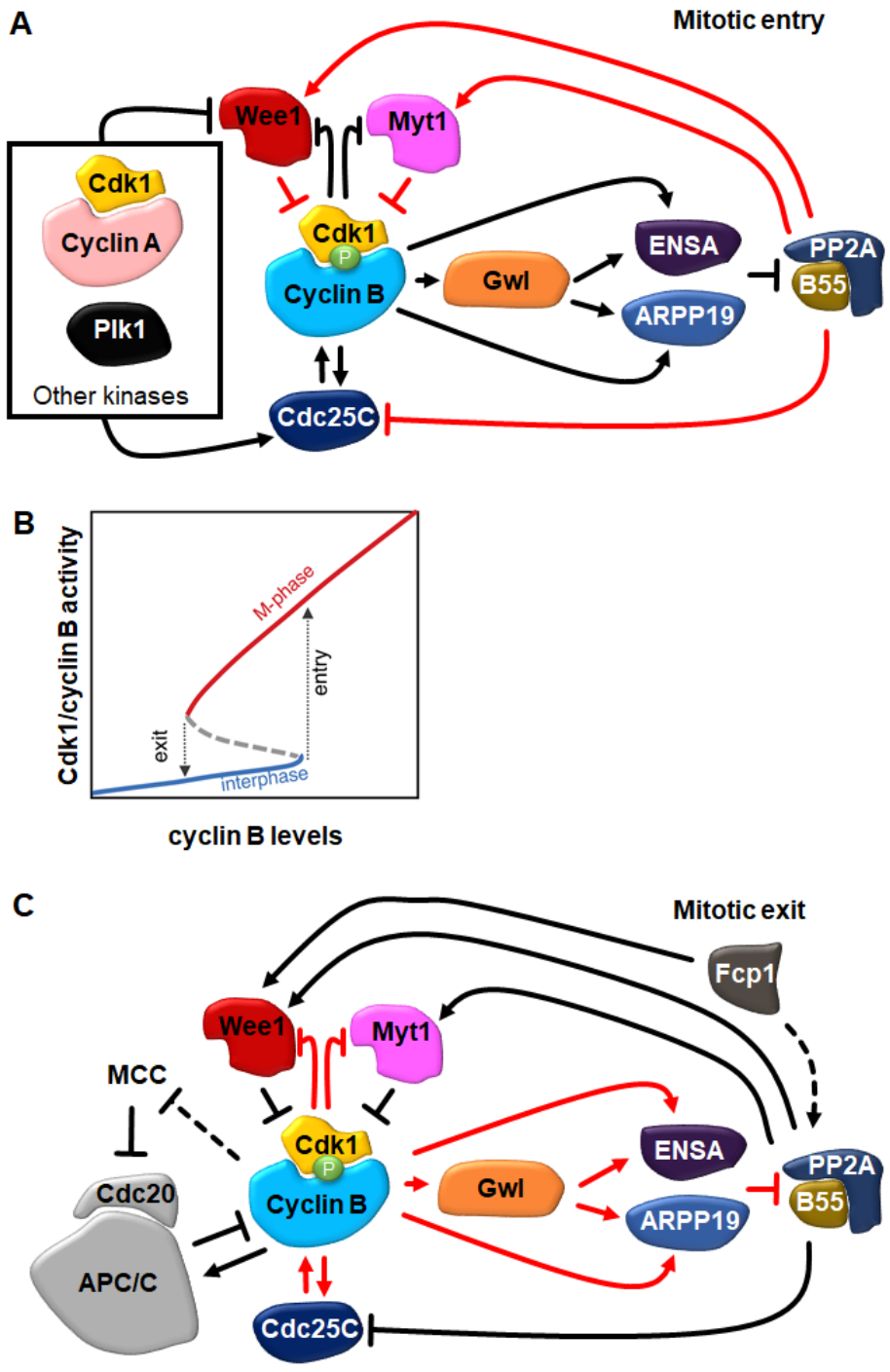

Figure 1.7. Cdk1/cyclin B activity is antagonized by PP2A-B55.
A) Mitotic entry. Cdk1 activation during the G2/M transition requires downregulation of Wee1 and Myt1 and upregulation of Cdc25C. This can be achieved by kinases such as Cdk1/2/cyclin A and Plk1. Once active, Cdk1/cyclin B can further inhibit Wee1 and Myt1 and activate Cdc25C. Cdk1/cyclin B activation is reinforced by Gwl. Together, Cdk1/cyclin B and Gwl activate ENSA and ARPP19, inhibitors of the PP2A subunit B55. This prevents

PP2A-B55 antagonism of Cdk1/cyclin B. **B)** Bistable switch of mitotic regulation. Graph models the amount of Cdk1/cyclin B1 activity relative to the total amount of cyclin B needed for mitotic entry and exit. Graph was adapted from (Rata et al., 2018). **C)** Mitotic exit. During the metaphase to anaphase transition, Cdk1/cyclin B activity is counteracted by the upregulation of PP2A-B55 and Fcp1. First, Fcp1 removes activating phosphates on ARPP19 and ENSA promoting PP2A-B55 upregulation. PP2A-B55, in concert with PP1 (not shown), dephosphorylates Gwl resulting in its inactivation. PP2A-B55 and Fcp1, upregulate Wee1 and Myt1 and downregulate Cdc25C leading to the re-phosphorylation of Cdk1 on Y15 and T14. Additionally, ubiquitin mediated degradation of cyclin B by APC/C, released from the inhibition of the mitotic checkpoint complex (MCC), inhibits Cdk1 activity. Black lines indicate upregulated pathways and red lines indicate downregulated pathways (B & C). Dotted lines indicate indirect regulation whereas solid lines represent direct regulation.

1.3.6 Cdk1 phosphorylation and cyclin B degradation occurs during mitotic exit

During the metaphase to anaphase transition, Cdk1 activity is downregulated by cyclin B degradation. Cyclin B degradation requires polyubiquitination, which is mediated by the anaphase promoting complex/cyclosome (APC/C), an E3 ubiquitin ligase (**Figure 1.3A & Figure 1.7C**). Cyclin B contains a degron sequence known as the destruction box (D-box), which is recognized by the APC/C adaptor protein, cell division cycle 20 (Cdc20) (Di Fiore et al., 2016). Cdk1 promotes Cdc20 loading onto the APC/C complex through the phosphorylation of APC/C subunits including Apc1 and Apc3 [also known as cell division cycle 27 (Cdc27)] (Fujimitsu et al., 2016). However, prior to anaphase, Cdc20 is bound by mitotic arrest-deficient 2 (Mad2) protein, which together with Budding uninhibited by benzimidazole 3 (Bub3) and Bub1 related kinase 1 (BubR1) form the mitotic checkpoint complex (MCC) (Sudakin et al., 2001). The MCC is a physiological inhibitor of the APC/C complex that responds to kinetochore-microtubule attachment and tension and prevents anaphase onset until bipolar-chromosome alignment is achieved (discussed in detail in **section 1.4.1**). During the metaphase to anaphase transition the MCC is deactivated and the APC/C-Cdc20 complex initiates cyclin B ubiquitination. In parallel, the PP2A-B55

pathway is upregulated by a phosphatase known as Fcp1, which dephosphorylates the B55 inhibitors ENSA and ARPP19 leading to their inactivation (Hegarat et al., 2014). Subsequently, PP2A-B55, along with other phosphatases (e.g. PP1) (Rogers et al., 2016), removes the activating phosphates from Gwl (Hegarat et al., 2014) and then downregulates Cdc25C and upregulates Wee1 and Myt1 (**Figure 1.7C**). In addition to inhibiting ENSA and ARPP19, Fcp1 has also been shown to directly activate Wee1 during mitotic exit by removing the inhibitor phosphate on T239 (Visconti et al., 2015; Visconti et al., 2012). Wee1 and Myt1 then re-phosphorylate Cdk1 (Harvey et al., 2011; Hegarat et al., 2014; Visconti et al., 2015; Visconti et al., 2012). The re-phosphorylation of Cdk1 during mitotic exit is suggested to be a failsafe mechanism, which ensure Cdk1 is inhibited in the event that cyclin B degradation is retarded (Chow et al., 2011; Jin et al., 1998).

During telophase Cdk1 phosphorylation is essential for Golgi and endoplasmic reticulum re-assembly (Nakajima et al., 2008). A small amount of cyclin B that is not initially degraded during anaphase onset, maintains Cdk1 activity and antagonizes Golgi and endoplasmic reticulum re-assembly throughout anaphase and telophase (Nakajima et al., 2008). However, Myt1 inhibits Cdk1 activity during anaphase and telophase, which allows these organelles to reassemble. Given that Myt1 knockdown prevents re-assembly of the Golgi and endoplasmic reticulum in HeLa cells expressing Wee1, regulating Golgi and endoplasmic reassembly is likely a specialized function of Myt1.

1.4 Mitotic checkpoint

1.4.1 The kinetochore is a platform for microtubule attachments and MCC activation

Chromosome alignment at the metaphase plate and the subsequent separation of sister chromatids in anaphase require forces that are generated by the mitotic spindle. The mitotic spindle is a bipolar array of microtubules, which attach to chromosomes via a massive protein structure known as the kinetochore. The kinetochore is composed of hundreds of proteins that assemble on the centromere, a heterochromatin region that is characterized by repetitive DNA sequences (satellite DNA) that are bound by CENP-B, CENP-C and dedicated nucleosomes consisting of histone H3 variant CENP-A [reviewed in (Musacchio and Desai, 2017)] (**Figure 1.8A**). CENP-A nucleosomes form a platform for the constitutive centromere-associated network (CCAN). The CCAN and CENP-C bridge centromere DNA to microtubule binding complexes Knl1, Ndc80, and Mis12, collectively known as the KNM network (**Figure 1.8B**). In the absence of microtubule binding, the mitotic checkpoint kinase Monopolar spindle 1 (Mps1) localizes to the kinetochore via Ndc80 [reviewed in (Nilsson, 2015)]. Once bound to Ndc80, Mps1 then phosphorylates Knl1 at specific Met-Glu-Lue-Thr (MELT) motifs (**Figure 1.8A**). Phosphorylated Knl1 acts as a scaffold for a number of essential mitotic checkpoint proteins including Bub3 kinase and Budding uninhibited by benzimidazole (Bub1) (Ji et al., 2017; Vleugel et al., 2013). Bub1 in complex with Bub3 recruit Roughdeal, Zeste-white 10 (ZW10) and Zwilch (collectively known as the RZZ complex) and RZZ associated proteins (e.g. Spindly) [Reviewed in (Zhang et al., 2015b)]. Bub1 and the RZZ complex recruit Mad1-Mad2 tetramers to unattached kinetochores (Rodriguez-Rodriguez et al., 2018). Once localized at the kinetochore, inactive “open” Mad2 is converted to active “closed” Mad2 (Luo and

Yu, 2008; Tipton et al., 2013; Tipton et al., 2011), which then binds to Cdc20 along with Bub3 and BubR1 to form the MCC.

1.4.2 Cdk1 modulates the mitotic checkpoint

The formation of the kinetochore and activity of the mitotic checkpoint is directly and indirectly orchestrated by Cdk1/cyclin B [reviewed in (Hayward et al., 2019b)]. The interaction between centromeric proteins CENP-A and CENP-C is required for normal kinetochore assembly and long-term cell viability. This interaction is in part mediated through the phosphorylation of the C-terminal region of CENP-C on T651 by Cdk1 (Watanabe et al., 2019). A non-phosphorylatable CENP-C mutant (T651A) fails to interact with CENP-A or localize to the kinetochore (Watanabe et al., 2019). Cdk1 activity also facilitates the interaction between the CCAN and the KNM network. For example, Cdk1 phosphorylation of the CCAN subunit CENP-T on T11 and T85 mediates binding and kinetochore recruitment of Ncd80 (Rago et al., 2015). Mutating the Cdk1 phosphorylation sites on CENP-T abrogates Ncd80 binding and kinetochore recruitment resulting in chromosome segregation defects (Rago et al., 2015).

Cdk1/cyclin B modulates the activity of the mitotic checkpoint through the phosphorylation of several mitotic checkpoint proteins including Aurora B, Mps1, Bub1, BubR1, and Cdc20 [reviewed in (Hayward et al., 2019b)] (**Figure 1.8A**). Aurora B kinase along with inner-centromere protein (INCENP), Survivin, and Borealin form the chromosome passenger complex (CPC), which functions in resolving erroneous microtubule-kinetochore attachments (discussed in **section 1.4.4**). Cdk1 phosphorylates all

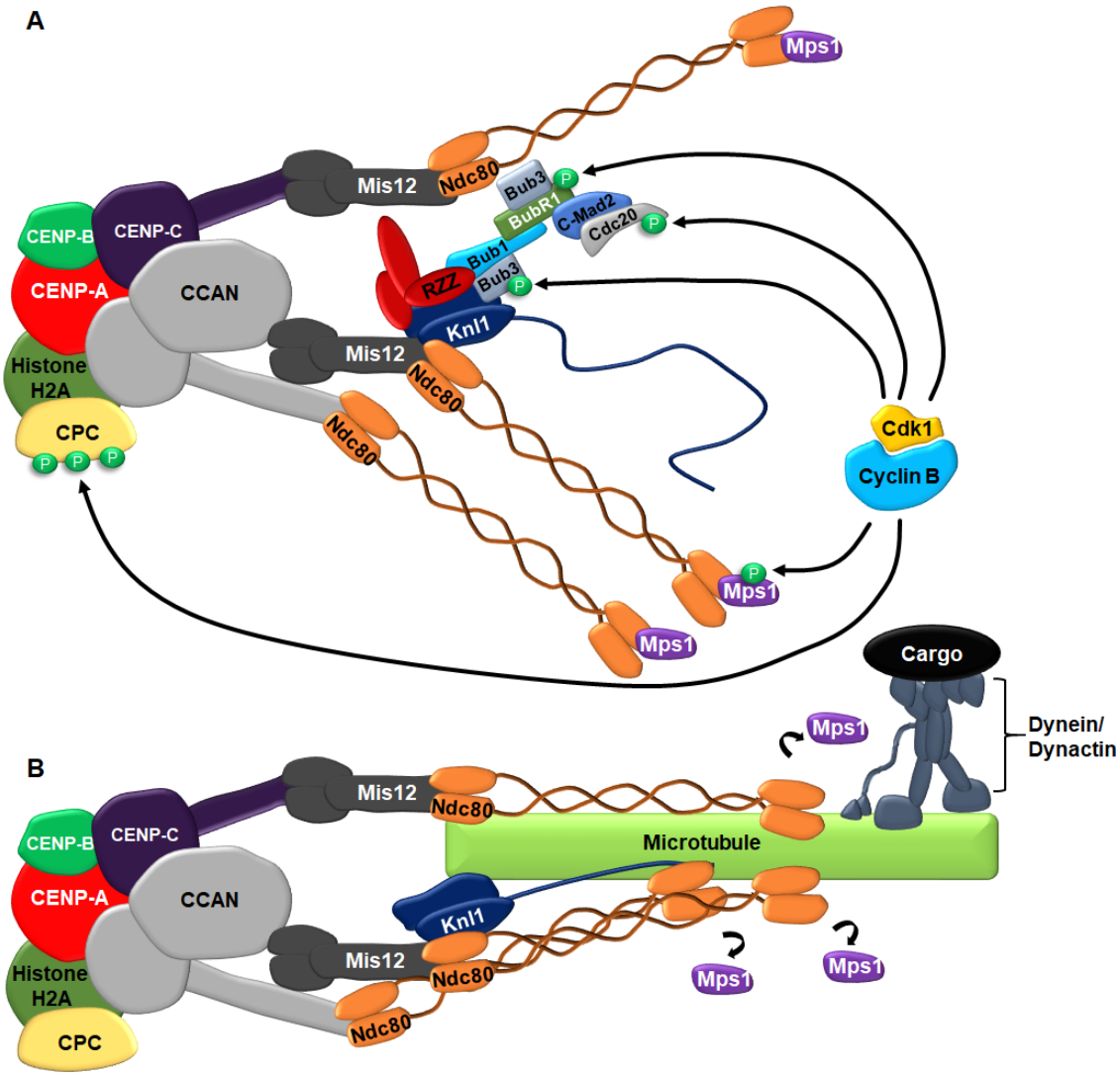

Figure 1.8. The kinetochore bridges centromeric DNA to microtubules. **A)** Centromere DNA is bound by specialized nucleosomes consisting of histone H3 variant CENP-A along with DNA binding proteins CENP-B and CENP-C. CENP-A nucleosomes form a platform for the constitutive centromere associated network, which forms the inner layer of the kinetochore. The CCAN and CENP-C then form a platform for the KMN network consisting of Knl1, Mis12, and Ndc80 complexes. In the absence of microtubule binding, Ndc80 provides a binding site for Mps1 kinase. Mps1 and Plk1 (not shown) then phosphorylate a series of MELT motifs along Knl1. The resulting phosphorylated MELT motifs are required for the binding of additional mitotic checkpoint proteins (e.g. Bub1 and Bub3). Bub1 and Bub3 then bind to Knl1, which is required for the subsequent binding of the RZZ complex (Roughdeal, Zeste-white 10, and Zwilch) and MCC (BubR1, Bub3, C-Mad2, and Cdc20). The CPC binds to the inner kinetochore via phosphorylated histone H2A. Cdk1/cyclin B phosphorylate several mitotic checkpoint proteins (depicted with green circles) promoting their activation and/or kinetochore localization. **B)** The KMN network binds microtubules via the Knl1 and Ndc80 complexes. End-on

kinetochore microtubule attachments displace Mps1 from the kinetochore and promote dynein/dynactin mediated shedding of mitotic checkpoint proteins RZZ and MCC (represented as “cargo”).

four components of the CPC, which are required for CPC activation, kinetochore localization, and/or interaction with other mitotic checkpoint protein [reviewed in (Carmena et al., 2012)]. For example, the phosphorylation of human Borealin by Cdk1/cyclin B promotes interaction with shugoshin proteins bound to H2B at the centromere (Tsukahara et al., 2010). Cdk1 phosphorylation of INCENP inhibits the interaction with kinesins responsible for removing the CPC from the centromere during anaphase (Hummer and Mayer, 2009). Mps1 is directly and indirectly regulated by Cdk1. The phosphorylation of Mps1 on S821 and S281 by Cdk1 is essential for Mps1 activation and kinetochore localization, respectively (Diril et al., 2016; Hayward et al., 2019a). Additionally, Mps1 localization requires the phosphorylation of Hec1 by Aurora B (Saurin et al., 2011). Cdk1 phosphorylation of Bub1 and BubR1 facilitates the kinetochore recruitment of Mad1-Mad2 tetramers (Ji et al., 2017) and Plk1 (Elowe et al., 2007), respectively. Newly recruited Plk1 enhances Mps1 mitotic checkpoint signalling by phosphorylating additional Knl1 MELT motifs (von Schubert et al., 2015). Additionally, Plk1 in concert with Cdk1 adds additional phosphates to BubR1 promoting the recruitment of PP2A-B56 phosphatase (Huang et al., 2008). PP2A-B56 counteracts mitotic checkpoint kinases like Mps1, Plk1, and Aurora B at the kinetochore during mitotic checkpoint silencing (e.g. dephosphorylates Knl1 MELT motifs) (Espert et al., 2014). N-terminal phosphorylation of Cdc20 by Cdk1 and other kinases enhances Cdc20 binding affinity to MCC and reduces Cdc20 affinity to the APC/C complex (Yudkovsky et al., 2000).

Together, these examples highlight the fact that Cdk1 activity is essential for mitotic checkpoint activity.

1.4.3 Disruption of microtubule dynamics prolongs MCC activation

Microtubule dynamics are essential for chromosome congression. Loss of chromosome dynamics inhibits bipolar chromosome alignment and disrupts kinetochore-microtubule tension, which results in prolonged MCC activation and mitotic arrest. Microtubule dynamics can be inhibited by chemicals that either inhibit microtubule polymerization such as nocodazole or vinca alkaloids (e.g. vincristine, and vinblastine), or by small molecules that inhibit microtubule depolymerization (e.g. paclitaxel and other taxanes) [reviewed in (Jordan and Wilson, 2004)]. Both taxanes and vinca alkaloids are used in the clinic for the treatment of several different cancers [reviewed in (Mukhtar et al., 2014)]. Cancer cells treated with these inhibitors arrest in mitosis and undergo cell death that is at least partially mediated by Cdk1 (described in **section 1.6.4**).

1.4.4 Aurora B destabilizes kinetochore-microtubule attachments that are not conducive for faithful chromosome segregation.

Kinetochore localization of kinases such as Mps1, Plk1, Cdk1/cyclin, and Aurora B are essential for monitoring bipolar kinetochore microtubule tension (DeLuca et al., 2011; Dumitru et al., 2017; Elowe et al., 2007; Ji et al., 2015). Microtubule tension is used to detect kinetochore-microtubule attachments that are not conducive for faithful chromosome segregation. For instance, if microtubules from the same spindle pole attach to kinetochores on both sister chromatids (syntelic attachment) then sister chromatids would not have the force required to segregate sister chromatids between daughter cells. Additionally, if microtubules from opposite spindle poles attach to the same kinetochore

(merotelic attachment) chromosome breakage or aneuploidy can occur, which can promote genetic disorders like cancer (Barra and Fachinetti, 2018; Gordon et al., 2012).

Incorrect kinetochore-microtubule attachments can be destabilized through increased phosphorylation of the KMN network as well as the spindle and kinetochore associated (Ska) complex, which directly interface with microtubules (Powers et al., 2009; Wei et al., 2007; Welburn et al., 2009). Aurora B in concert with other kinases (e.g. Cdk1 and Plk1) participate in kinetochore-microtubule destabilization. Aurora B phosphorylates Ncd80 subunit Hec1 on several sites, which induce a charge repulsion between Ndc80 and the negatively charged C-terminal tail of tubulin weakening microtubule binding (Ciferri et al., 2008; DeLuca et al., 2006; DeLuca et al., 2011). Aurora B also phosphorylates the Mis12 complex subunit Dsn1, the N-terminal microtubule-binding domain of Knl1 (Welburn et al., 2010), and the Ska complex subunits Ska1 and Ska3 (Chan et al., 2012), which also disrupt kinetochore-microtubule binding. Moreover, Aurora B also downregulates the activity of the kinesin 13 mitotic centromere-associated kinesin (MCAK), a potent microtubule depolymerizing enzyme that facilitates chromosome movement (Lan et al., 2004; Wordeman et al., 2007). Micro-injection of antibodies against Aurora B (Kallio et al., 2002), small molecule Aurora B inhibitors (ZM447439 and Hesperadin) (Ditchfield et al., 2003; Isokane et al., 2016), and siRNA knockdown of Aurora B (Adams et al., 2001; Ditchfield et al., 2003) leads to defective chromosome congression. As a result, cells exit mitosis without proper chromosome alignment.

Following error correction of kinetochore-microtubule attachments, PP1 along with targeting subunits Sds22, repo man and PP2A-B56 dephosphorylate Aurora B substrates (Wurzenberger et al., 2012), allowing new bipolar attachments to be made. siRNA (or

shRNA) knockdown of Sds22, prevents dephosphorylation of Aurora B substrates leading to prolonged activation of the mitotic checkpoint, and mitotic arrest (Eiteneuer et al., 2014; Posch et al., 2010; Wurzenberger et al., 2012).

1.4.5 The mitotic checkpoint is downregulated during metaphase

Following bipolar chromosomal alignment, the mitotic checkpoint is downregulated by at least four major mechanisms: displacement of Mps1 from kinetochores following microtubule attachment, dephosphorylation of kinetochore proteins, disassembly of the MCC complex, and mitotic checkpoint protein shedding from the kinetochore [reviewed in (Lewis and Chan, 2017)] (**Figure 1.8B & Figure 1.9A-B**). Microtubule binding at kinetochores displaces the mitotic checkpoint kinase Mps1 from the Ndc80 complex, thus downregulating the mitotic checkpoint signal (Hiruma et al., 2015; Ji et al., 2015). Following chromosome bi-orientation, PP2A-B56 (recruited by BubR1) (Huang et al., 2008) and PP1-Repo man/SDS22 (recruited by the Ska and Knl1 complexes) (Liu et al., 2010; Sivakumar et al., 2016), initiate the removal of phosphates on kineto-chore proteins that provide binding motifs for other mitotic checkpoint proteins (e.g. Knl1 MELT motifs) (Espert et al., 2014; Sivakumar et al., 2016). Additionally, these phosphatases remove activating phosphates on mitotic kinases like Mps1 (London et al., 2012). MCC disassembly is mediated through the direct binding of checkpoint silencing proteins p31comet (Teichner et al., 2011; Xia et al., 2004) and thyroid hormone receptor 13 (TRIP13) (Wang et al., 2014a), CCT chaperonin (Kaisari et al., 2017), and CUEDC2 (Gao et al., 2011). Mitotic checkpoint proteins shedding is mediated by dynein/dynactin and adaptor protein Spindly (Chan et al., 2009; Famulski et al., 2011). During MCC shedding

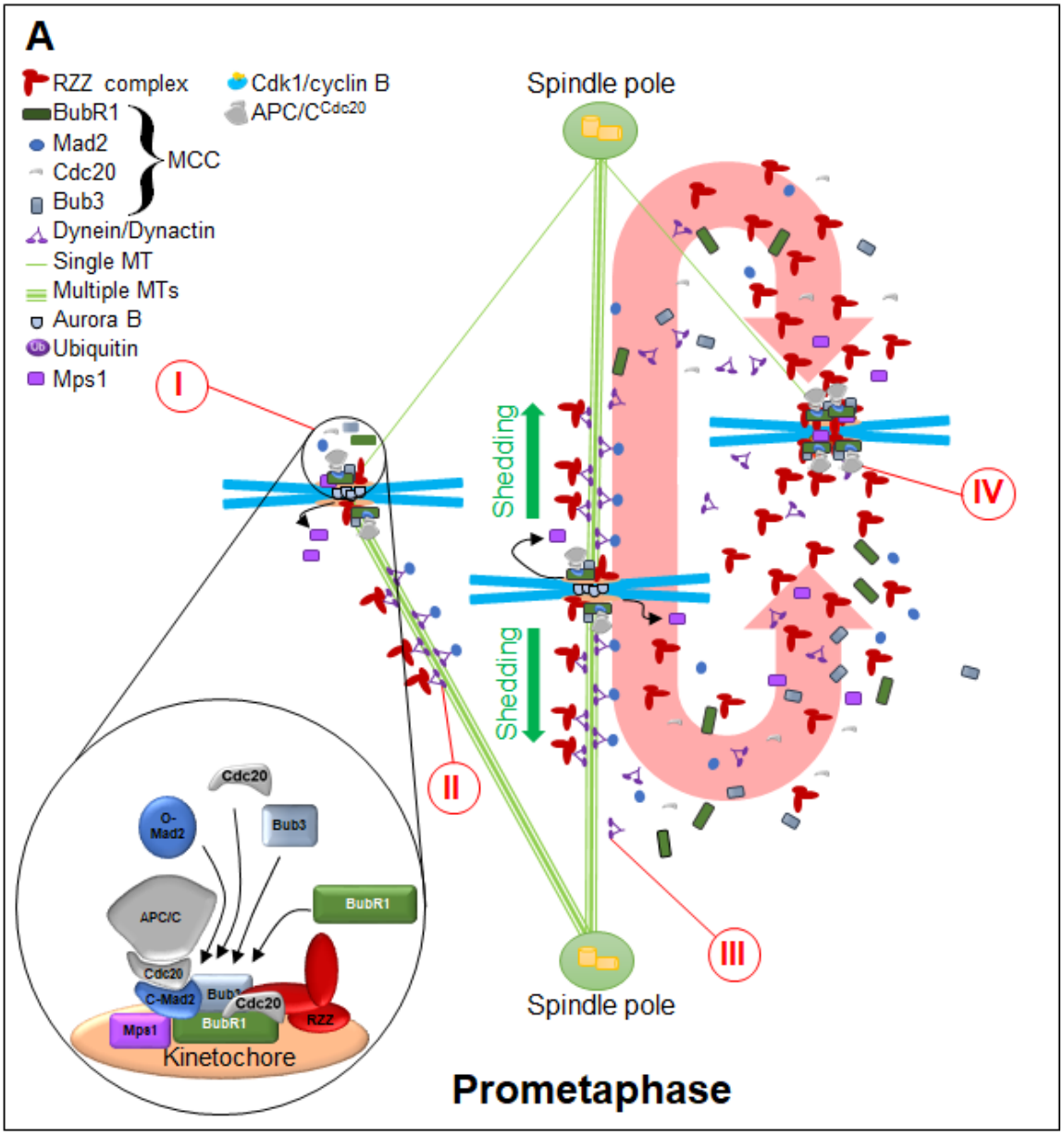
A
RZZ complex
BubR1
Mad2
Cdc20
Bub3
MCC
Cdk1/cyclin B
APC/C^Cdc20
Dynein/Dynactin
Single MT
Multiple MTs
Aurora B
Ub
Mps1
Spindle pole
I
II
III
IV
Shedding
Shedding
Cdc20
O-Mad2
Bub3
APC/C
BubR1
Cdc20
C-Mad2
Bub1
Cdc20
RZZ
Mps1
BubR1
Kinetochore
Spindle pole
Prometaphase

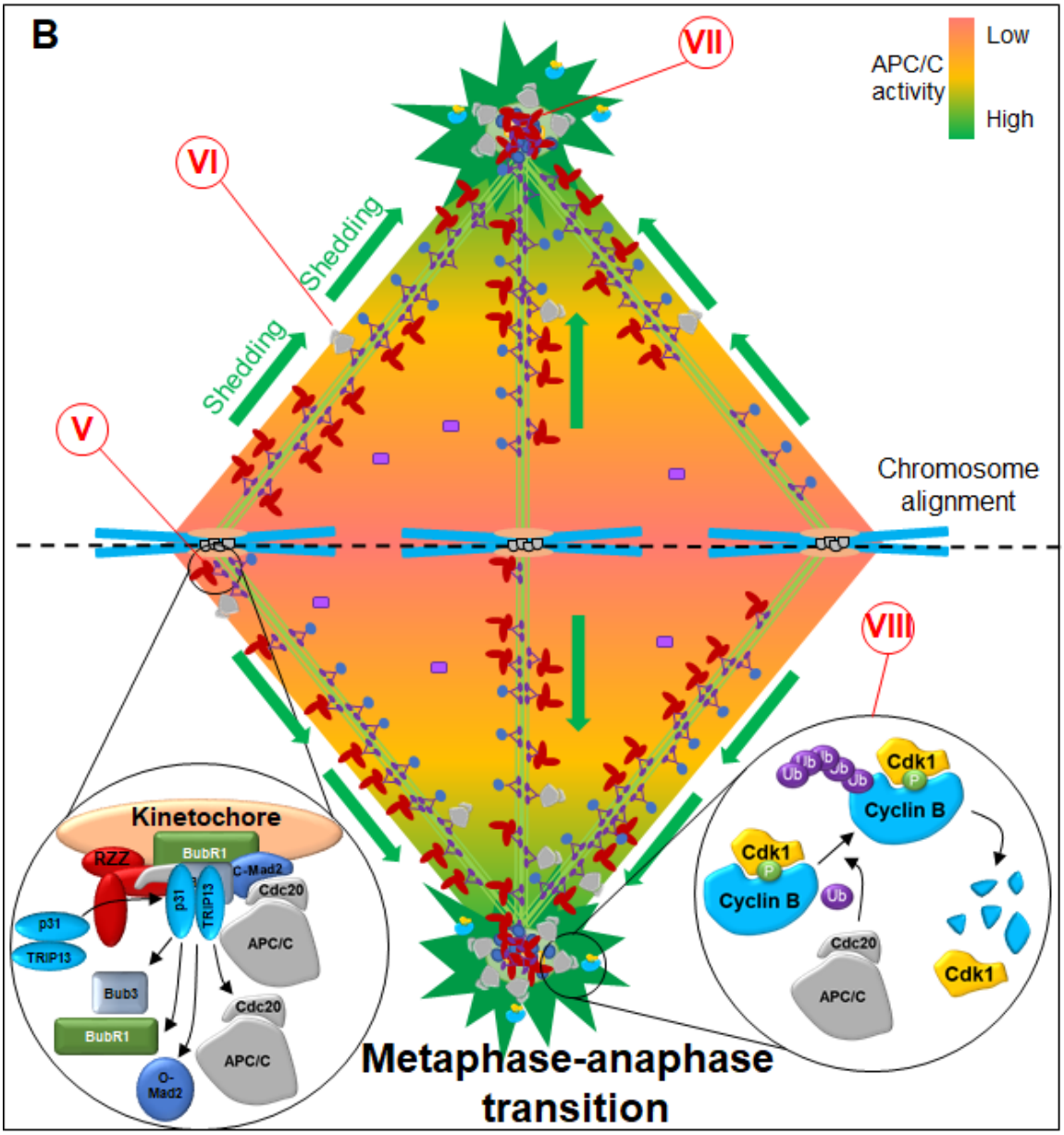

Figure 1.9. Mitotic checkpoint silencing.
A) During prometaphase, microtubules emanating from spindle poles attach to kinetochores. I. Unattached kinetochores or kinetochores lacking a "full" complement of MT attachments recruit dynein/dynactin and mitotic checkpoint proteins such as RZZ (Roughdeal, ZW10, and Zwilch) and Mad2. Here the kinetochore serves as a platform for the assembly of the mitotic checkpoint complex (MCC), which is composed of BubR1, Bub3, Mad2, and Cdc20; inactive O-Mad2 is converted to active C-Mad2 (see inset circle). II. Kinetochores that have achieved bipolar attachment engage dynein/dynactin-mediated transport of mitotic checkpoint proteins from the kinetochore toward the spindle poles (shedding). III. During transport, dynein/dynactin and the mitotic checkpoint proteins, which are not stably interacting with MTs, fall off the

mitotic spindle. IV. Dynein/dynactin and the mitotic checkpoint proteins are recruited back to unattached kinetochores to maintain the active state of the mitotic checkpoint. **B)** During metaphase, kinetochores achieve bipolar spindle attachment. V. Bipolar attachment of kinetochores stimulates the disassembly of MCC, which is partly facilitated by the binding of p31Comet and TRIP13 to Mad2 (see inset circle). VI. The disassembled MCC components as well as other mitotic checkpoint proteins undergo dynein/dynactin-mediated shedding to spindle poles. VII. Mitotic checkpoint proteins (e.g., Mad2 and the RZZ) and components of the APC/C (e.g., Cdc27) accumulate at the spindle poles. VIII. Once all kinetochore-microtubule attachments are made, mitotic checkpoint silencing occurs, which leads to the activation of the APC/C-Cdc20. The APC/C-Cdc20 is first activated at the spindle poles where it ubiquitylates cyclin B, but its activity spreads outward to the kinetochores to allow ubiquitylation of securin. Color gradient shows the progression of APC/C-Cdc20 activity. Figure adapted from (Lewis and Chan, 2017).

mitotic checkpoint proteins are transported from the kinetochores to the spindle poles thus silencing the checkpoint (Howell et al., 2000).

1.4.6 MCC shedding requires Spindly

Spindly and dynein/dynactin form an active trimer complex, which initiates MCC shedding following kinetochore-microtubule binding. Knockdown of Spindly by siRNA induces a metaphase arrest, possibly due to reduced MCC shedding (Holland et al., 2015; Moudgil et al., 2015). Furthermore, Spindly knockdown in lung cancer cell lines (NCI-H460 and A549) promotes cell death in mitosis and reduces clonogenic cell survival, which is further enhanced by low dose paclitaxel treatment (Silva et al., 2017). Kinetochore localization of Spindly requires the addition of a farnesyl group to the C-terminus and interaction with the RZZ complex. Mutation or deletion of the Spindly farnesyl motif (CPQQ) inhibits kinetochore localization and induces a metaphase-like arrest (Holland et al., 2015; Moudgil et al., 2015). Inhibition of Spindly farnesylation with farnesyl transferase inhibitors (L-744-832 or FTI-277) also prevents Spindly localization and induces a metaphase arrest (Moudgil et al., 2015).

1.5 Functional roles for Wee1 and Myt1 beyond Cdk1 regulation.

In the past twenty-five to thirty years, few Wee1 and Myt1 substrates have been identified. Wee1 phosphorylates both Cdk1 and Cdk2 *in vitro*, whereas Myt1 only phosphorylates Cdk1 (Booher et al., 1997). Low levels of pT14-Cdk2 in complex with cyclin A have been observed by 2-D gel electrophoresis in HeLa cells, suggesting that Myt1 can phosphorylate Cdk2 (Coulonval et al., 2011). However, the levels of pY15-Cdk2 were much higher than pT14-Cdk2 in this study, which is consistent with other studies that have reported Cdk2 is abundantly phosphorylated at Y15 but not T14 in human cells (Coulonval et al., 2003). Therefore, it remains unclear what role Myt1 plays in the regulation of Cdk2. Recently, Myt1 knockdown in colorectal cancer cells was reported to decrease cell migration and invasion in colorectal (Jeong et al., 2018) and lung cancer (Sun et al., 2019). Given that Cdk1 in complex with mitotic cyclins promotes cell adhesion and negatively correlates with metastasis, it is possible that Myt1 functions in other pathways that are independent of Cdk1 (Fang et al., 2015; Jones et al., 2018).

Wee1 phosphorylation of Cdk2 inhibits DNA replication, which ensures proper S-phase timing (Hughes et al., 2013). Cells expressing a non-phosphorylatable Cdk2 mutant (Cdk2 T14A/Y15F) prematurely enter S-phase, rapidly degrade cyclin E, and cause replication stress leading to genomic instability (Hughes et al., 2013). In addition to Cdk1 and Cdk2, Wee1 also phosphorylates histone H2B on Y37 in late S phase (Mahajan et al., 2012). pY37-H2B is an epigenetic modification that represses transcription of the histone gene cluster 1 (Hist1) (Mahajan et al., 2012), a region containing 55 histone genes (Marzluff et al., 2002). Following DNA replication, histone synthesis must be downregulated to avoid histone overproduction [reviewed in (Marzluff et al., 2008)]. Normally, during S phase non-phosphorylated Y37-H2B recruits transcriptional co-

activators NPAT (Nuclear Protein, Co-Activator of Histone Transcription) and RNA polymerase II, which promotes histone transcription. However, pY37-H2B recruits transcriptional co-repressor and histone chaperone HIRA, which leads to a significant reduction in mRNA transcript levels of core histones (H2A, H2B, H3, and H4) and linker histone H1 (Mahajan et al., 2012). Wee1 inhibition or knockdown following S-phase abolishes H2B phosphorylation on Y37 during late S and G2 phase, which results in abnormally high levels of histones (Mahajan et al., 2012).

1.6 Aberrant Cdk1 activity

1.6.1 Disruption of Cdk1 phosphorylation induces ectopic Cdk1 activity

In mice, monoallelic expression of a non-phosphorylatable Cdk1 mutant T14A/Y15F (Cdk1AF) induces uncontrolled mitotic entry and early embryonic lethality (around E3.5) and Cdk1AF induction in adult mice induces lethality within 6 days (Duda et al., 2016; Szmyd et al., 2019). HeLa and other human cells expressing Cdk1AF also exhibit uncontrolled mitotic entry and cell death (Heald et al., 1993).

Loss of Wee1 and Myt1 abrogates Cdk1 phosphorylation and mimics Cdk1AF expression. In mice, homozygous deletion of Wee1 alone disrupts Cdk1 regulation and induces early embryonic lethality (Tominaga et al., 2006). Similarly, *Drosophila* harboring homozygous Wee1 mutations derived from maternal mutants also exhibit early embryonic lethality (Price et al., 2000), suggesting that Wee1 is essential for development. Whether Myt1 deletion also results in embryonic lethality in mice remains unknown; however, *Drosophila* harboring homozygous Myt1 mutations fully develop, albeit with ectopic

mitosis in some organs/tissues (Jin et al., 2008; Jin et al., 2005). These studies suggest that Myt1 is not required for embryonic development.

Wee1 and Myt1 are functionally redundant in some systems. For example, zygotic viability in *Drosophila* does not require the presence of both Wee1 and Myt1 (Ayeni et al., 2014; Jin et al., 2008; Price et al., 2000). However, homozygous mutations to both kinases completely disrupt Cdk1 phosphorylation and results in synthetic lethality (Ayeni et al., 2014; Jin et al., 2008). The functional redundancy between Wee1 and Myt1 is lost in many human cancer cells. For example, Wee1 is essential for Cdk1 regulation in HeLa, U-2 OS, and a subset of breast cancer cell lines, and its inhibition or knockdown induces ectopic Cdk1 activation overriding DNA damage checkpoints leading to premature mitosis and mitotic cell death (Aarts et al., 2012; Chow and Poon, 2013; Coulonval et al., 2011; Hirai et al., 2009; Nakajima et al., 2008; Wells et al., 1999). In at least some of these cells (HeLa and U-2 OS), siRNA knockdown of Myt1 alone does not affect either mitotic timing or the competency of DNA damage checkpoints (Chow and Poon, 2013; Nakajima et al., 2008). However, Myt1 is essential for regulating mitotic timing in a subset of human glioblastoma cells in which Wee1 is downregulated (Toledo et al., 2015). In glioblastoma cells, Myt1 knockout or knockdown results in cell death, which is preceded by a prolonged mitotic arrest (Toledo et al., 2015).

Overexpression of Cdc25 family members also reduces Cdk1 phosphorylation. Cdc25B overexpression induces premature mitosis through the activation of Cdk1 (Karlsson et al., 1999; Timofeev et al., 2010). The mechanism of action of small molecule Chk1 and ATR inhibitors is at least partially attributed to the upregulation of the Cdc25

family [reviewed in (Qiu et al., 2018)]. Both Chk1 and ATR inhibitors induce ectopic Cdk1 activity and cell death (Moiseeva et al., 2019b).

1.6.2 Checkpoint adaptation induces ectopic Cdk1 activity

In response to extreme DNA damage, cancer cells can downregulate the S and G2 DNA damage checkpoints and enter mitosis in a process known as checkpoint adaptation (Kubara et al., 2012; Lewis and Golsteyn, 2016; Rezacova et al., 2011; Swift and Golsteyn, 2016). Initially ATM, ATR, and Chk1 of the DNA damage checkpoint are activated in response to genotoxic agents leading to a cell-cycle arrest. However, despite the presence of numerous double stranded DNA breaks, Chk1 is eventually downregulated leading to Cdk1 activation (Kubara et al., 2012; Rezacova et al., 2011; Swift and Golsteyn, 2016). As such, cells arrested in S and G2 phase enter mitosis with under-replicated and/or damaged DNA (Kubara et al., 2012).

Although the precise mechanism of checkpoint adaptation remains unclear, Wee1/Myt1 downregulation and/or Cdc25 upregulation likely contribute to checkpoint adaptation. Chk1 negatively regulates the Cdc25 family during checkpoint activation, but overexpression of Cdc25 proteins can override the Chk1-mediated arrest through Cdk1 dephosphorylation (Varmeh and Manfredi, 2008; Xiao et al., 2003). Consistent with this data, chemical inhibition of Chk1 enhances checkpoint adaptation through Cdc25 upregulation (Lewis and Golsteyn, 2016). Loss of Wee1 activity also promotes checkpoint adaptation. Chemical inhibition or siRNA knockdown of Wee1 induces mitosis in various cancer cell types exposed to ionizing radiation (Bridges et al., 2011; Chow and Poon, 2013; Mir et al., 2010; PosthumaDeBoer et al., 2011). Wee1 inhibition also induces mitosis in cancer cells treated with camptothecin, gemcitabine, cisplatin, and 5-fluorouracil (Aarts et

al., 2012; Hauge et al., 2017; Hirai et al., 2010; Hirai et al., 2009; Zheng et al., 2017). Although the role of Myt1 in the DNA damage checkpoint is less clear, siRNA knockdown in HeLa cells induces mitosis in some cells exposed to ionizing radiation (Chow and Poon, 2013). Furthermore, Myt1 knockdown accelerates the rate at which cells enter mitosis when combined with Wee1 or Chk1 chemical inhibitors following irradiation (Chow and Poon, 2013). These data strongly suggest that checkpoint adaptation requires the down regulation of Wee1/Myt1 and the upregulation of Cdc25.

1.6.3 Ectopic Cdk1 activity in S phase induces chromosome fragmentation

Mitotic cells that undergo checkpoint adaptation following genotoxic treatment exhibit numerous chromosome breaks and high levels of damaged DNA as signalled by the phosphorylation of histone variant H2AX on S139 (γH2AX) (Kubara et al., 2012; Rezacova et al., 2011; Swift and Golsteyn, 2016). However, even in the absence of pre-existing DNA damage, ectopic Cdk1 activity during S-phase induces *de novo* damage through several independent mechanisms (**Figure 1.10**). Cells acquire damaged DNA during periods of persistent replication stress and fork collapse [reviewed in (Alexander and Orr-Weaver, 2016)]. Ectopic Cdk1 activity induces replication stress and fork collapse through the depletion of deoxyribonucleotides (dNTPs) and aberrant replication origin firing (Beck et al., 2012; Hauge et al., 2017; Pfister et al., 2015). Cdk1 phosphorylation of the ribonucleotide reductase (RNR) subunit RRM2 induces ubiquitin mediated degradation during DNA synthesis resulting in a 70% drop in dNTPs (Pfister et al., 2015). Ectopic Cdk1 activity may also trigger aberrant replication firing through increased loading of replication initiating factor Cdc45 (Hauge et al., 2017), likely through increased phosphorylation of a Cdc45-interacting protein known as Treslin (Sld3 in *Saccharomyces*

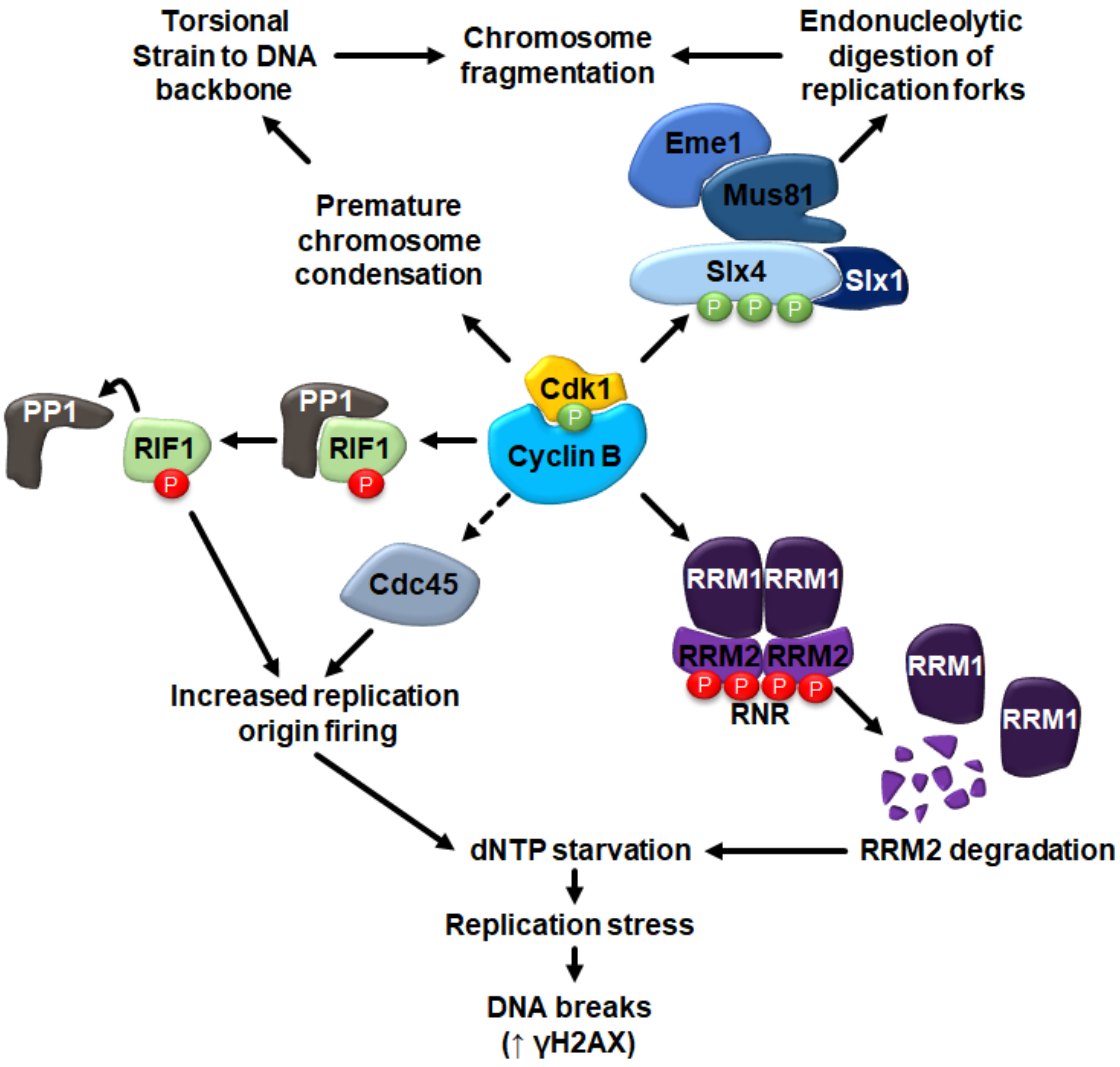

Figure 1.10. Ectopic Cdk1 activity in S-phase induces damage to DNA. Ectopic Cdk1 activity upregulates the Mus81-Eme1-Slx4-Slx1 endonuclease, which cleaves replication forks leading to chromosome fragmentation. Ectopic activation of Cdk1 also induces premature chromosome condensation, which causes torsional strain to the DNA backbone leading to chromosome breakage. Cdk1 upregulates DNA initiating factor Cdc45 (via Treslin phosphorylation) and downregulates PP1 activity through the phosphorylation of RIF1 leading to aberrant replication origin firing. Cdk1 also downregulates ribonucleotide reductase (RNR) subunit RRM2 through phosphorylation. Together this leads to increased replication origin firing and deoxyribonucleotide (dNTP) starvation, which in turn causes replication stress and damaged DNA. Inhibitory phosphates are labelled with red circles, whereas activating phosphates are labelled with green circles. Solid lines indicate direct interactions, whereas dotted lines indicate indirect interactions.

cerevisiae) (Kumagai et al., 2011). Aberrant origin firing is also induced through Cdk1 phosphorylation of chromatin factor RIF1, a protein that is required for PP1 recruitment (Moiseeva et al., 2019a; Moiseeva et al., 2019b). Normally, PP1/RIF1 counteract Cdk2 activity during S-phase to prevent the firing of dormant replication origins (Yamazaki et al., 2012). However, Cdk1 phosphorylation of RIF1 disrupts PP1 binding leading to firing of additional origins (Moiseeva et al., 2019b). Moreover, ectopic Cdk1 activation upregulates the endonuclease complex Mus81-Eme1-(and/or Eme2)-Slx1-Slx4 during S-phase, which triggers widespread endonucleolytic digestion of replication forks resulting in massive chromosome pulverization (Dominguez-Kelly et al., 2011; Duda et al., 2016; Szmyd et al., 2019). Normally, during the G2/M transition Cdk1 activates the Mus81-Eme1-Slx1-Slx4 complex through hyper-phosphorylation of Slx4 (also known as FANCP) (Wyatt et al., 2013), which cleaves any branched structures that resemble replication forks, thereby preventing chromosome tangling and promoting faithful segregation. Ectopic Cdk1 activity also promotes condensation of under-replicated chromosomes, which causes torsional strain to the DNA backbone leading to centromere fragmentation or chromothripsis (Beeharry et al., 2013; El Achkar et al., 2005; Holland and Cleveland, 2012; Zhang et al., 2015a). Chromosome regions, such as the centromere, which are replicated slower due to a low prevalence of replication origins, are more prone to breakage during premature condensation or cleavage by Mus81-Eme1-Slx1-Slx4 (Beeharry et al., 2013; Madan et al., 1976). As such, chromosome fragmentation may manifest as centromere fragmentation (double stranded DNA breaks at the centromere) (Beeharry et al., 2013).

1.6.4 Chromosome fragmentation and mitotic arrest are indicators of mitotic catastrophe

Chromosome fragmentation and other types of DNA damage in mitosis are an indicator of mitotic catastrophe, a common mode of tumour cell death that occurs during *or* following an aberrant mitosis [reviewed in (Galluzzi et al., 2012; Vakifahmetoglu et al., 2008; Vitale et al., 2011)]. Mitotic catastrophe lacks a mechanistic definition, but growing evidence suggests that it is at least partially facilitated by cysteine-aspartate proteases known as caspases (Galluzzi et al., 2012; Vakifahmetoglu et al., 2008). Caspases are essential for apoptosis (programed cell death) and their activation is negatively regulated by anti-apoptotic proteins known as the B-cell lymphoma family-2 (Bcl-2), a family which includes Bcl-2, B-cell lymphoma extra large (Bcl-X_L), and myeloid cell leukemia 1 (Mcl-1). Together, Bcl-2, Bcl-X_L, and Mcl-1 inhibit pro-apoptotic proteins Bcl-2 antagonist/killer (Bak) and Bcl-2 associated X (Bax). In the absence of Bcl-2, Bcl-X_L and Mcl-1, Bak and Bax aggregate to form channels in the mitochondria resulting in cytochrome C release, a molecule that triggers caspase-9 activation [reviewed in (Green and Llambi, 2015)] (**Figure 1.11**).

Excessive damaged DNA can trigger apoptosis during interphase through continuous signalling of the DNA damage checkpoint leading to p53 mediated apoptosis. However, during mitosis, DNA damage checkpoint signalling is turned off. This suggests that DNA damage checkpoint signalling does not mediate apoptosis in mitotic cells. Importantly, mitotic cells with damaged chromosomes are unable to satisfy the mitotic checkpoint due to the presence of damaged chromosomes and instead arrest in prometaphase (Beeharry et al., 2013; Chang et al., 2007; Mikhailov et al., 2002). However, continuous mitotic checkpoint signalling is also not necessary for apoptosis during mitosis.

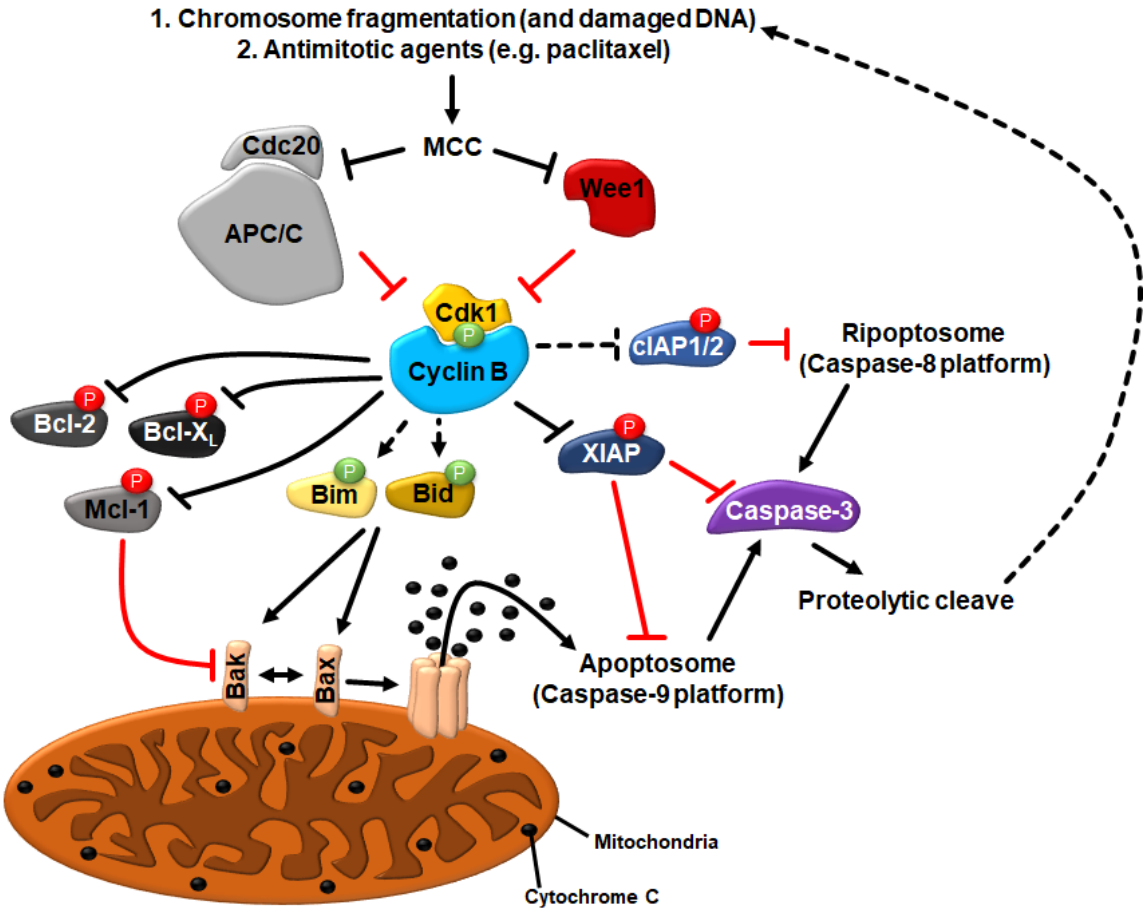

Figure 1.11. Cdk1/cyclin B upregulates caspase activity during a mitotic arrest.
Disruption of chromosomal alignment (e.g. chromosome fragmentation or paclitaxel) and/or failure to down regulate Cdk1/cyclin B during the metaphase to anaphase transition induces a mitotic arrest. Cdk1 downregulates anti-apoptotic proteins (Bcl-2, Bcl-X_L, Mcl-1, XIAP, cIAP1, and cIAP2) and upregulates pro-apoptotic proteins (Bim and Bid) through phosphorylation. This leads to the aggregation of Bak and Bax leading to the releases of cytochrome C and the subsequent formation of the caspase-9 platform (apoptosome). Downregulation of cIAP1 and cIAP2 promote the activation of the caspase-8 platform (ripoptosome), which leads to the activation of executioner caspases such as caspase-3. Black lines indicate pathways that are upregulated, red lines indicate pathways that are downregulated, solid lines represent directly regulated processes, and dotted lines represent indirect regulated processes. Inhibitory phosphates are labelled with red circles, whereas activating phosphates are labelled with green circles.

Mitotic cells that express a non-degradable cyclin B mutant (Clijsters et al., 2014; Jin et al., 1998; Potapova et al., 2011), are transfected with siRNA against Cdc20 (Chow et al., 2011), or treated with MG132 (Chow et al., 2011; Potapova et al., 2011), are able to satisfy

the mitotic checkpoint, but arrest in metaphase due to high levels of Cdk1. Importantly, cells arrested in metaphase by the outlined mechanism still degrade and/or inhibit anti-apoptotic proteins (Mcl-1, Bcl-2, and Bcl-X_L), resulting in apoptosis (Sloss et al., 2016). Likewise, inhibiting Cdk1 re-phosphorylation during metaphase by inhibiting Wee1 or knocking down Fcp-1 also delays mitotic exit and promotes Mcl-1 degradation (Chow et al., 2011; Potapova et al., 2011; Visconti et al., 2015).

Several studies have shown that Cdk1 in concert with other kinases phosphorylate Bcl-2, Bcl-X_L, and Mcl-1 in cells arrested in mitosis by various anti-mitotic agents (siRNA knockdown of Cdc20, vinblastine, vincristine, paclitaxel, colchicine, and nocodazole) (Eichhorn et al., 2013; Harley et al., 2010; Poruchynsky et al., 1998; Sloss et al., 2016; Terrano et al., 2010). Mcl-1 phosphorylation by Cdk1 induces degradation, whereas Blc-2 and Bcl-X_L phosphorylation leads to their inactivation (Eichhorn et al., 2013; Harley et al., 2010; Poruchynsky et al., 1998; Sloss et al., 2016; Terrano et al., 2010). Cdk1 mediated phosphorylation of Mcl-1 is also been observed in HeLa cells arrested in mitosis following Wee1 knockdown or inhibition (Visconti et al., 2015). Prolonged mitosis also promotes the accumulation of phosphorylated pro-apoptotic proteins such as Bcl-2 interacting mediator of cell death (Bim) and BH3 Interacting Domain Death Agonist (Bid). Bim, Bid, and other pro-apoptotic protein such as NOXA inhibit anti-apoptotic Bcl-2 proteins and help activate Bak and Bax. Knockdown of Bim, Bid, and NOXA reduce cell sensitivity to antimitotic agents (Topham et al., 2015). Normally, phosphorylated Bim and Bid are inhibited by degradation and dephosphorylation, respectively, during anaphase (Wan et al., 2014; Wang et al., 2014b). However, cells arrested in mitosis by paclitaxel or nocodazole retain high levels of phosphorylated Bim and Bid (Wan et al., 2014; Wang et al., 2014b).

In addition to Bcl-2 family members, Cdk1 also phosphorylates X-linked inhibitor of apoptosis (XIAP) (Hou et al., 2017). XIAPs bind to activated caspases and inhibit their activity [reviewed in (Eckelman et al., 2006)], but Cdk1 phosphorylation of XIAP on S40 disrupts this binding in cells arrested in mitosis and induces cell death by apoptosis (Hou et al., 2017). Likewise, downregulation of cellular inhibitor of apoptosis protein 1 and 2 (cIAP1 and cIAP2), inhibitors of the caspase-8 platform (Ripoptosome) [reviewed in (Eckelman et al., 2006; Feoktistova et al., 2012)], also increase apoptosis in cells arrested in mitosis (Jin and Lee, 2006). Together, these studies show that Cdk1 directly regulates several apoptotic proteins and suggest that prolonged Cdk1 activity is the main trigger of apoptosis in mitosis.

1.7 Competing networks model determines whether mitotic cell death or mitotic slippage occurs

Prolonged mitotic arrest can result in cell death during mitosis or after mitotic exit (Galluzzi et al., 2012; Gascoigne and Taylor, 2008; Gascoigne and Taylor, 2009). Mitotic slippage, a process in which cells exit mitosis without completing cell division, can precede cell death following treatment with antimitotic agents. However, mitotic slippage is also a mechanism of cellular resistance to anti-mitotic agents (Topham et al., 2015). Cell death in mitosis is not always dependent on the type or concentration of the anti-mitotic agent (Gascoigne and Taylor, 2008; Gascoigne and Taylor, 2009). Inter- and intra-cell line variation can result in portions of a cell population dying in both mitosis and interphase (following mitotic slippage) even when treated with the same antimitotic agent. Gascoigne and Taylor proposed a “competing-networks model” to help explain how and why such variations exist (Gascoigne and Taylor, 2008; Gascoigne and Taylor, 2009) (**Figure 1.12**).

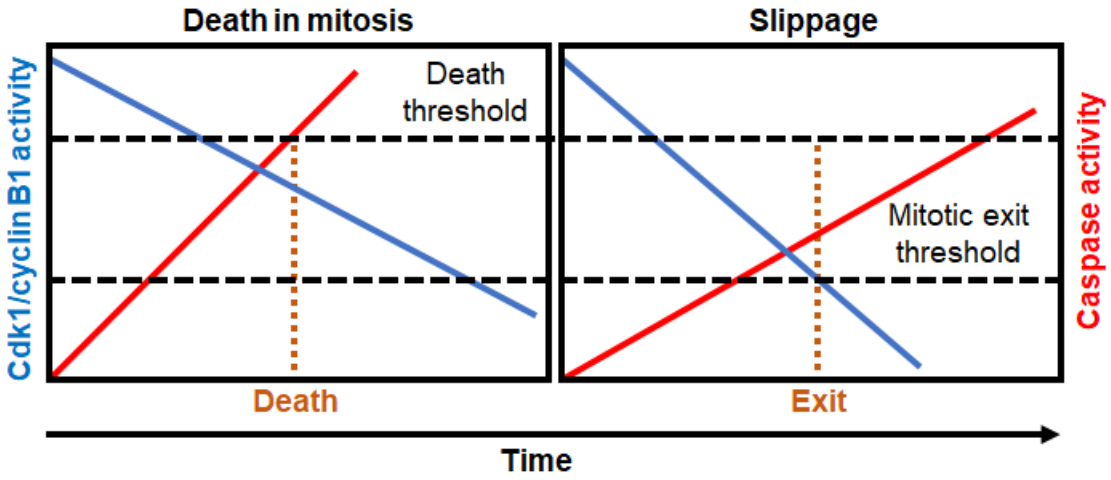

Figure 1.12. Cells arrested in mitosis can die in mitosis or interphase. Competing-networks model proposed and adapted from Gascoigne and Taylor (Gascoigne and Taylor, 2008; Gascoigne and Taylor, 2009). Cells that slowly downregulate Cdk1 (blue line) and/or quickly activate apoptotic pathways (red line) die in mitosis (left panel), whereas cells that quickly downregulate Cdk1 or slowly activate apoptotic pathways exit mitosis and undergo senescence or die in interphase (right panel). Mitotic exit and cell death thresholds are indicated in dotted lines.

In this model, if cell death pathways activate faster than inhibitory Cdk1 pathways (e.g. cyclin B degradation), then cell death will occur in mitosis. Conversely, if Cdk1 is downregulated prior to the activation of cell death pathways, then cells will undergo mitotic slippage. HeLa, HT-29 (colorectal cancer), and RKO (colon cancer) cells treated with Eg5 inhibitor AZ138 slowly degrade cyclin B and frequently die in mitosis (Gascoigne and Taylor, 2008). In contrast, DLD-1 (colon cancer) cells treated with AZ138 degrade cyclin B more efficiently, and frequently die in interphase rather than mitosis. Topham *et al*., showed breast cancer sensitivity to docetaxel is correlated with high levels of mitotic checkpoint proteins (e.g. Mad1, Mad2, Bub1, BubR1, Mps1, Bub3, Aurora B) (Topham et al., 2015), which suggest that robust mitotic checkpoint activity is necessary to prevent cyclin B degradation and induce mitotic cell death.

Pan-caspase inhibitor Boc-D-FMK when used in combination with AZ138 can induce mitotic slippage in cells that are prone to mitotic cell death (Gascoigne and Taylor, 2008; Gascoigne and Taylor, 2009). Similarly, Bcl-X_L inhibition by WEHI-539 in the presence of paclitaxel induces mitotic cell death in cells that are prone to mitotic slippage (Topham et al., 2015). Topham *et al*. reported that the expression of the transcription factors c-Myc and Egr1 may be key determinants of mitotic cell death (Topham et al., 2015). RKO cells are prone to mitotic cell death when treated with paclitaxel and other anti-mitotic agents, but siRNA depletion of either c-Myc or Egr1 reduces mitotic cell death in paclitaxel treated cells resulting in mitotic slippage. Interestingly, depletion of either c-Myc or Egr1 does not reduce the duration of the mitotic arrest but does affect transcriptional levels of apoptotic regulators. siRNA knockdown of c-Myc reduces the transcription of pro-apoptotic proteins (Bim, Bid, and NOXA) and increases the transcription of anti-apoptotic proteins (XIAP, Bcl-X_L, and cFlip), which suggest that c-Myc and Egr1 are upstream modulators of mitotic cell death pathways (Topham et al., 2015). Likewise, c-Myc overexpression reduces Bcl-X_L levels and increases Noxa levels, which promotes mitotic cell death in the presence of different antimitotic agents (paclitaxel, nocodazole, GSK923295 (CENP-E inhibitor), BI2536 (Plk1 inhibitor) and AZ138 (Eg5 inhibitor)) (Littler et al., 2019). Finally, breast tumours with high c-Myc expression exhibit higher sensitivity to docetaxel (Topham et al., 2015). Collectively, these data argue that robust apoptotic signalling during mitotic arrest induces mitotic cell death.

1.8 Cell death following mitotic slippage is dependent on the DNA damage response

Apoptotic cell death or senescence are common outcomes of mitotic slippage [Reviewed in (Galluzzi et al., 2012)]. Additionally, cells may re-enter mitosis in an attempt to complete cell division *or* continue onto DNA replication resulting in increased cell ploidy (Colin et al., 2015; Lambrus et al., 2016). The fate of cells that undergo mitotic slippage is dependent on factors such as the amount of DNA damage (Hain et al., 2016; Orth et al., 2012), length of the mitotic arrest (Colin et al., 2015; Lambrus et al., 2016; Uetake and Sluder, 2010), robustness of cell death pathways (Topham et al., 2015), and/or status of tumour suppressors (e.g. p53) (Colin et al., 2015; Lambrus et al., 2016; Orth et al., 2012).

Damaged DNA is not repaired during mitosis and can result in a strong DNA damage response following mitotic slippage [reviewed in (Giunta and Jackson, 2011)]. Antimitotic agents that delay mitotic exit induce *de novo* DNA damage through the activation of caspase-activated DNase (CAD) (Colin et al., 2015; Orth et al., 2012) and telomere de-protection (Hain et al., 2016; Hayashi et al., 2012; Hayashi and Karlseder, 2013). Normally, CAD activity is inhibited through the binding of inhibitor of CAD (ICAD). However, mitotic arrest can induce partial activation of caspase-3, -7, and -9, which does not induce full blown apoptosis (also known as sublethal apoptosis), resulting in ICAD cleavage (Hain et al., 2016; Orth et al., 2012). Orth *et al*. reported that activated CAD can lead to hundreds of double-stranded DNA nicks in mitotically arrested cells (Orth et al., 2012). Inhibiting caspase activity with the pan-caspase inhibitor Z-VAD-FMK, reduces both CAD activity and damaged DNA (Colin et al., 2015; Orth et al., 2012). Caspase activation can also lead to the cleavage of shelterin complex protein telomeric repeat-binding factor 2 (TRF2) during mitotic arrest (Hain et al., 2016). As such, telomere

DNA is particularly vulnerable to CAD cleavage (Hain et al., 2016). Importantly, longer mitotic arrest cause cells to accumulate more damaged DNA (Colin et al., 2015), which in turn results in a greater probability of cell death following slippage. Longer mitotic arrests are also more likely to induce senescence or apoptotic cell death in cells with functional p53 (Colin et al., 2015; Lambrus et al., 2016; Orth et al., 2012). Therefore, longer mitotic arrest is more detrimental to cancer cell survival and proliferation even if mitotic cell death is avoided.

1.9 Wee1 inhibitor Adavosertib (also known as MK-1775 and AZD1775)

Wee1 is reported to be overexpressed in triple negative breast cancer (Iorns et al., 2009; Murrow et al., 2010), glioblastomas (Mir et al., 2010; Wuchty et al., 2011), malignant melanomas (Magnussen et al., 2012), malignant squamous cell carcinomas (Magnussen et al., 2013) and osteosarcomas (PosthumaDeBoer et al., 2011).

Next to surgery, radiation and other DNA damaging therapies are the most common treatments for these cancers [Reviewed in (Baskar et al., 2012)]. The purpose of these treatments is to induce lethal amounts of DNA damage in cancer cells. However, Wee1 overexpression can promote cell survival by reinforcing the DNA damage checkpoints and preventing mitotic catastrophe (Mir et al., 2010). Furthermore, Wee1 overexpression can lead to repression of histone synthesis via the phosphorylation of histone H2B on Y37 (Mahajan et al., 2012), which can lead to inefficient DNA packaging making DNA more accessible to the DNA damage repair machinery [reviewed in (Mahajan and Mahajan, 2013)]. As such, increased Wee1 levels may promote resistance to DNA damaging agents independent of CDK regulation. As a means of enhancing cancer cell sensitivity to DNA

damaging therapies, the small molecule Wee1 inhibitor, Adavosertib (also known as AZD1775 and MK-1775) was developed (Hirai et al., 2009).

Currently, Adavosertib is being tested in the clinic against various cancers including triple negative metastatic breast cancer, glioblastoma, small cell lung cancer, prostate, ovarian, cervical, and colorectal cancers (**ClinicalTrial.gov**). These clinical trials are examining Adavosertib alone (Bauer et al., 2016; Do et al., 2015; Leijen et al., 2016; Sanai et al., 2018) and in combination with genotoxic therapies such as cisplatin and gemcitabine (Leijen et al., 2016; Mendez et al., 2018).

Wee1 inhibition by Adavosertib has been shown to enhance DNA damage induced by ionizing radiation and genotoxin chemicals such as 5-fluorouracil, cisplatin, camptothecin, and gemcitabine *in vitro* and *in vivo* (Aarts et al., 2012; Hauge et al., 2017; Hirai et al., 2010; Zheng et al., 2017) . DNA damaging agents that specifically interfere with DNA synthesis and arrest cells in S-phase exhibit high synergy with Adavosertib (Aarts et al., 2012; Hauge et al., 2017). Cotreating CAL120 (breast cancer) cells with Adavosertib and gemcitabine, a molecule that disrupts S-phase, forces cells into mitosis resulting in chromosome fragmentation. Cotreatment with Adavosertib and gemcitabine also reduces tumour volume five-fold in pancreatic cancer xenografts derived from patient tumours (Rajeshkumar et al., 2011).

As a single agent, Adavosertib induces replication stress through the upregulation of Cdk1 and Cdk2, which leads to aberrant origin firing, depletion of dNTPs, and increased endonucleolytic cleavage by the Mus81/Eme1/Slx1/Slx4 complex (Hauge et al., 2017; Pfister et al., 2015) (**section 1.6.3**). Furthermore, Adavosertib forces HeLa and a subset of breast cancer cells that are arrested in S phase into mitosis with under replicated DNA

(Aarts et al., 2012; Dominguez-Kelly et al., 2011; Duda et al., 2016). Premature mitosis coincides with high levels of DNA damage and mitotic arrest (Aarts et al., 2012; Dominguez-Kelly et al., 2011; Duda et al., 2016). Nevertheless, some tumours do not respond to Adavosertib in the clinic (Do et al., 2015; Van Linden et al., 2013); and the mechanisms underpinning clinical resistance are unknown. As such, researchers are focussed on identifying specific vulnerabilities, which can increase Wee1 sensitivity in cancer cells.

1.9.1 High levels of mitotic cyclins enhance Adavosertib induced mitotic cell death

Both cyclin A and cyclin B play essential roles in promoting and maintaining mitosis (Fung et al., 2007; Li et al., 2010). Cyclin A in complex with Cdk1 and Cdk2 is required for the initial inactivation of Wee1/Myt1 and activation of Cdc25 during the G2/M transition (Fung et al., 2007; Li et al., 2010), a key step that promotes Cdk1/cyclin B activation. Consistent with the role of cyclin A in Cdk1/cyclin B activation, a RNAi screen in pancreatic cancer cells showed that depletion of cyclin A reduced the amount of cell death induced by Adavosertib (Chang et al., 2016). Likewise, high levels of cyclin B are required for mitosis (Fung et al., 2007) and are strongly correlated with increased Adavosertib sensitivity in breast cancer cells (Aarts et al., 2012). These data suggest that tumours with high levels of mitotic cyclins will be more sensitive to Adavosertib treatment.

1.9.2 Adavosertib enhances cell death in a subset of p53 deficient cancer cells

The first paper to identify Adavosertib as a Wee1 inhibitor reported that Wee1 inhibition selectively killed p53 deficient cancer cells (Hirai et al., 2009). p53 knockdown in the presence of Adavosertib increases the mitotic index and amount of cell death observed in

breast and ovarian cancer cells compared to scrambled control (Aarts et al., 2012; Hirai et al., 2009). Additionally, p53 mutations strongly correlate with non-small lung cancer sensitivity to Adavosertib (Ku et al., 2017). *In vivo*, p53-deficient pancreatic cancers in mouse xenografts display high sensitivity to Adavosertib and gemcitabine relative to cancers with wild-type p53 (Rajeshkumar et al., 2011).

It should be noted that in at least some cancers, p53 status is not correlated with Adavosertib sensitivity. For instance, p53 functional status does not correlate with acute myelogenous leukemia cell sensitivity to combination treatments with Adavosertib and cytarabine (Van Linden et al., 2013). Additionally, a recent phase I clinical trial reported that p53 mutational status did not correlate with solid tumour response to Adavosertib (Do et al., 2015). However, it should be noted that most of these studies do not specifically address how the p53 mutations in each of the cancer affects the many transcriptional targets of p53. Part of the Adavosertib selectivity in p53 deficient cells has been attributed to reduced expression of the CDK inhibitor p21 (Aarts et al., 2012). p21 knockdown mimics p53 knockdown and enhances Adavosertib efficacy (Aarts et al., 2012). Furthermore, high p21 expression in cancer cells is associated with Adavosertib resistance (Aarts et al., 2012; Hauge et al., 2019). Therefore, enhanced Adavosertib sensitivity in p53-mutant tumours may only be enhanced if p21 transcription is impaired.

1.9.3 Adavosertib synergizes with Chk1 downregulation

A functional genetic screen in WiDr (colorectal cancer cells) with Adavosertib identified that cells depleted of Chk1 were highly sensitive to Wee1 inhibition (Aarts et al., 2015). In this same study, siRNA knockdown of Chk1 in the presence of 300 nM Adavosertib, reduced metabolic activity by up to 60% and increased the number of mitotic cells with

damaged DNA by 10% in a subset of breast cancer cell lines (MCF7, SK-BR-3, SUM44, and CAL120). Consistent with this study, two Chk1 inhibitors (AZD7762 and LY2603618) were identified in a drug screen for compounds that cause increased DNA damage in S-phase when combined with Adavosertib in Reh leukemia cells (Hauge et al., 2017). Combination treatments with Adavosertib and either AZD7762 or LY2603618 elicited a synergistic effect in inducing replication stress and premature mitosis in U-2 OS cells. Adavosertib and AZD7762 also enhance premature mitotic entry and DNA damage in a subset of breast cancer cell lines (Aarts et al., 2012).

Both *de novo* and acquired resistance to Adavosertib have been linked to the upregulation of phospho-activated Chk1. An analysis of a panel of small cell lung cancer (SCLC) cells showed that cells exhibiting intrinsic or acquired Adavosertib resistance had upregulated receptor tyrosine kinases AXL and MET (Sen et al., 2017). AXL and MET upregulation correlated with increased Akt/mTOR and ERK/p90RSK signalling as determined by increased phospho-activation of Akt (pS73), S6 (pS240, pS244, pS235 and pS236), pERK1/2 (pT202/204), and p90RSK (pT359 and pS363) (Sen et al., 2017). Chk1 is a downstream effector of both pathways. Increased p90RSK activation and mTOR signalling can facilitate nuclear accumulation of Chk1 through phosphorylation on S280 (Li et al., 2012; Sen et al., 2017). Nuclear accumulation and activation of Chk1 is further induced by S317 and S345 phosphorylation by ATM and ATR (Liu et al., 2000; Zhao and Piwnica-Worms, 2001) and autophosphorylation on S296 (Kasahara et al., 2010). Reverse-phase protein assay revealed significantly higher levels of nuclear Chk1 that was phosphorylated on these three sites as well as higher levels of phospho-activated ATR (pS428) in Adavosertib resistant cells relative to sensitive cells (Sen et al., 2017). In

addition to Chk1 inhibitors, Adavosertib co-treatment with either mTORC1 inhibitor (RAD001) or AXL inhibitor (TP0903) significantly reduces phosphorylated Chk1 levels and overcomes resistance to Wee1 inhibition *in vitro* and *in vivo* (Sen et al., 2017).

1.9.4 Adavosertib selectively targets cancer cells with deficient Fanconi anemia and homologous recombination pathways

A functional genetic screen with Adavosertib identified four Fanconi anemia (FA) genes and six homologous recombination genes, which when knocked down, selectively killed Wee1 inhibited cells (Aarts et al., 2015). The major function of the FA pathway is to remove barriers such as DNA intra-strand crosslinks, which interfere with DNA replication and gene transcription. As such, the FA pathway assist in both DNA replication and DNA repair. Two of the top gene hits included Fanconi anemia M (FANCM) and the helicase Fanconi anemia J (FANCJ) [also known as BRCA1 interacting protein C-terminal helicase 1 (BRIP1)]. FANCM is an essential core component of the FA complex, which is activated in response to damaged DNA induced by replication stress [reviewed in (Nalepa and Clapp, 2018; Wang et al., 2018)]. Formation of the FA complex leads to the activation of several downstream FA proteins that are essential for homologous recombination such as BRIP1 [reviewed in (Nalepa and Clapp, 2018)]. siRNA knockdown of FANCM and BRIP1 in the presence of Adavosertib resulted in an increased percentage of mitotic cells with pan nuclear staining of histone γH2AX (Aarts et al., 2015). Breast cancer 1 (BRCA1), Breast cancer 2 (BCRA2), and Partner and Localizer of BRCA2 (PALB2) proteins involved in homologous recombination, were also identified as gene hits, but were not validated as synthetic lethal partners of Wee1 (Aarts et al., 2015). BCRA1, BRCA2, and PALB2 mutations are commonly observed in triple negative breast and ovarian cancers (Van

Cutsem et al., 2004), which may allow Adavosertib to selectively kill tumour cells carrying these mutations. In support of this idea, a recently published phase I clinical trial reported that patient tumours with BCRA1 mutations exhibit a strong response to Adavosertib treatment (Do et al., 2015). Whether tumours carrying BCRA2 or PALB2 mutations will respond to Adavosertib remains unclear.

1.9.5 Adavosertib synergizes with microtubule inhibitors

Low dose paclitaxel inhibits microtubule depolymerization, which disrupts microtubule dynamics leading to prolonged activation of the MCC and delayed mitotic exit (Jordan et al., 1993). Wee1 inhibition by Adavosertib enhances the mitotic arrest induced by paclitaxel in HeLa cells (Visconti et al., 2015). HeLa and leukemia cell lines (MOLT-4 and TOM-1) that are cotreated with paclitaxel are more prone to apoptosis as assayed by Annexin-V staining and caspase 3 cleavage (Visconti et al., 2015). Consistent with this finding, co-treatment with Adavosertib and vincristine, which inhibits microtubule polymerization, decreases trypan-blue exclusion (cell viability assay) in patient derived leukemia cells compared to either inhibitor alone (Visconti et al., 2015). Prolonging mitotic arrest or delaying mitotic exit highlights a previously unexplored vulnerability that may enhance cell sensitivity to Adavosertib and may also help identify crucial mitotic proteins that when dysregulated, may alter cell sensitivity to Wee1 inhibition. For instance, a previous study showed that overexpression of Fcp1 reduced the duration of mitotic arrest and decreased the percentage of cells that undergo apoptosis in the presence of paclitaxel (Visconti et al., 2012), but it remains unclear if Fcp1 expression would affect cell sensitivity to Adavosertib.

1.10 Breast cancer

Breast cancer is the most diagnosed cancer and accounts for the second highest cancer-related deaths among women in North America and Europe [reviewed in (Ferlay et al., 2015; Senkus et al., 2015)]. As mentioned in **section 1.9** Wee1 is overexpressed in breast cancers (Iorns et al., 2009; Murrow et al., 2010). Thus, we selected breast cancer as a model system to study the effects of Adavosertib.

Breast cancer can be classified into different subtypes based on the status of three cell-surface receptors: estrogen hormone receptor (ER), progesterone hormone receptor (PR), and human epidermal growth factor receptor 2 (HER2) (Dai et al., 2015). Based on these receptors, breast cancers are categorized as being luminal A, luminal B, Her2 positive (non-luminal), or basal-like (also known as triple-negative) [reviewed in (Dai et al., 2015; Senkus et al., 2015)] (**Table 1.1**). Luminal A cancers are characterized by expressing ER and PR, but not Her2. These cancers are typically lower grade, well differentiated, less aggressive, and have a good prognosis (Sorlie et al., 2003). Luminal B cancers express ER, but little to no PR. These cancers have an intermediate prognosis and usually exhibit a higher tumour grade than luminal A (Cheang et al., 2009; Sorlie et al., 2003). Luminal B cancers that express Her2 have a worse prognosis relative to those that do not (Cheang et al., 2009). After the tumour is surgically removed, selective therapies can be used to target ER and PR in the luminal cancers including aromatase inhibitors and gonadotropin releasing hormone agonists, which downregulate estrogen and progesterone synthesis [reviewed in (Senkus et al., 2015)]. Additionally, estrogen-ER binding can be inhibited by Tamoxifen (also known as Nolvadex). Tamoxifen is a prodrug that once activated binds to ER with high affinity. Tamoxifen prevents ER from interacting with transcriptional co-

Table 1.1. Breast cancer subtypes
¥ all listed therapies include surgery
* Prognosis is worse if Her2 is overexpressed
** Therapy may also be included Trastuzumab if Her2 is overexpressed
*** Chemotherapy and radiation may also be necessary for high grade tumours

Molecular subtype	**Luminal A**	**Luminal B**	**Her2+**	**Triple negative**
Prevalence	40%	20%	10-15%	15-20%
Prognosis	Good	Good*	Intermediate	Poor
Therapy¥	Endocrine	Endocrine**	Trastuzumab***	Chemotherapy and radiation

activators leading to the recruitment of repressor proteins, thus inhibiting ER response genes (Teft et al., 2011). Her2-positive cancers are characterized by the overexpression of Her2 and the absence of ER and PR. These cancers are associated with increased metastasis in comparison to luminal cancers and have a poor clinical outcome (Sorlie et al., 2003). Some Her2-positive cancers can be successfully treated with a combination of chemotherapy and trastuzumab (also known as Herceptin), a monoclonal antibody that prevents Her2 activation through dimerization. Finally, basal-like cancers are characterized by the absence of PR, ER, and Her2. These cancers are associated with a high tumour grade, frequent metastasis, and poor clinical outcome (Sorlie et al., 2003; Tseng et al., 2013). Unlike luminal or Her2-positive cancers, there are currently no selective therapies like Tamoxifen or Herceptin that target basal-like cancers. Basal-like cancers are treated with surgery, radiation and chemotherapies such as taxanes, cyclophosphamide, methotrexate, and fluorouracil [reviewed in (Senkus et al., 2015)].

The benefit of studying Adavosertib in breast cancer cells (including the basal-like subtype) is that data obtained from our study may have clinical implications. For instance, in this study we identified Myt1 as a driver of Adavosertib resistance in breast cancer cells.

Furthermore, we determined high Myt1 expression in breast cancer is associated with a poor clinical outcome. As such, detecting of high Myt1 expression in breast tumours may help identify aggressive and hard to treat tumours. In this study we confirmed that antimitotic agents such as paclitaxel enhance Adavosertib induced breast cancer killing regardless of Myt1 expression, which may help in the treatment of drug resistant tumours.

2 Chapter 2. Prolonged mitotic arrest induced by Wee1 inhibition sensitizes breast cancer cells to paclitaxel

2.1 Abstract

Wee1 kinase is a crucial negative regulator of Cdk1/cyclin B1 activity and is required for normal entry into and exit from mitosis. Wee1 activity can be chemically inhibited by the small molecule MK-1775, which is currently being tested in phase I/II clinical trials in combination with other anti-cancer drugs. MK-1775 promotes cancer cells to bypass the cell-cycle checkpoints and prematurely enter mitosis. In our study, we show premature mitotic cells that arise from MK-1775 treatment exhibited centromere fragmentation, a morphological feature of mitotic catastrophe that is characterized by centromeres and kinetochore proteins that co-cluster away from the condensed chromosomes. In addition to stimulating early mitotic entry, MK-1775 treatment also delayed mitotic exit. Specifically, cells treated with MK-1775 following release from G1/S or prometaphase arrested in mitosis. MK-1775 induced arrest occurred at metaphase and thus, cells required 12 times longer to transition into anaphase compared to controls. Consistent with an arrest in mitosis, MK-1775 treated prometaphase cells maintained high cyclin B1 and low phospho-tyrosine 15 Cdk1. Importantly, MK-1775 induced mitotic arrest resulted in cell death regardless of the cell-cycle phase prior to treatment suggesting that Wee1 inhibitors are also anti-mitotic agents. We found that paclitaxel enhances MK-1775 mediated cell killing. HeLa and different breast cancer cell lines (T-47D, MCF7 and MDA-MB-231) treated with low dose MK-1775 showed increased sensitivity to paclitaxel with T-47D and MDA-MB-

231 showing the highest sensitivity to the co-treatments. Our data highlight a new potential strategy for enhancing MK-1775 mediated cell killing in breast cancer cells.

2.2 Introduction

Cyclin dependent kinase (Cdk)-1/cyclin B1 is the key complex, that when active, initiates mitosis with subsequent inactivation triggering mitotic exit [reviewed in (Malumbres and Barbacid, 2009)]. Cdk1 activity is tightly regulated in interphase by Wee1 and Myt1 kinases, which add inhibitory phosphates to Cdk1 on threonine 14 and tyrosine 15 thus preventing premature mitosis (Jin et al., 2008; Liu et al., 1997; Mueller et al., 1995; Russell and Nurse, 1987; Watanabe et al., 1995). In this way, Wee1 and Myt1 kinases maintain competent G1/S, intra-S and G2/M checkpoints that ensure cells have completed DNA synthesis as well as repaired any damaged DNA is prior to mitosis (Chow and Poon, 2013). When mitosis begins, the inhibitory phosphates on Cdk1 are removed by Cdc25 phosphatases (Timofeev et al., 2010) and Wee1 and Myt1 are subsequently inactivated (and degraded) (Watanabe et al., 2004). However, a small amount of inactive Wee1 remains throughout mitosis (Chow et al., 2011; Vassilopoulos et al., 2014; Visconti et al., 2015; Visconti et al., 2012). At the end of mitosis, mitotic exit is characterized by the re-phosphorylation and inhibition of Cdk1 and degradation of cyclin B1 (Chow et al., 2011). In the absence of Wee1 activity, mitotic cells maintain high levels of cyclin B1 and low levels of phosphorylated tyrosine 15-Cdk1 (Chow et al., 2011; Jin et al., 1998; Visconti et al., 2015).

Wee1 is reported to be overexpressed in several cancers including breast (De Witt Hamer et al., 2011; Iorns et al., 2009; Matheson et al., 2016a; Murrow et al., 2010). High

Wee1 activity helps reinforce the DNA damage checkpoint and facilitates DNA repair, which in turn allows cancer cells to resist genotoxic therapies (Magnussen et al., 2012). Thus, Wee1 has become a target of therapeutic interest. Wee1 activity can be chemically inhibited by the small molecule inhibitor MK-1775 (Hirai et al., 2009), which is undergoing phase I/II clinical trials in combination with several different genotoxic therapies including cisplatin and radiation (clinicaltrials.gov). The rationale of these clinical trials is largely supported by human cell line studies, including recent publications, which report that MK-1775 sensitizes cancers of the brain (Matheson et al., 2016b) and head and neck (Osman et al., 2015) to the genotoxic drug cisplatin as well as pancreatic cancer cells to gemcitabine (Kausar et al., 2015).

The mechanism of MK-1775-mediated cell death in breast and other cancers has been largely attributed to either premature mitosis or entry into mitosis with damaged DNA following exposure to genotoxic agents (Aarts et al., 2012; Matheson et al., 2016b). These treatment strategies induce chromosome defects that are incompatible with viable mitosis. MK-1775 treatment is shown to force HeLa and breast cancer cells into mitosis that were previously arrested in G1/S by treatment with thymidine, gemcitabine, or hydroxyurea (Aarts et al., 2012). While in mitosis these cells display defects including chromosome pulverization and abnormal microtubule organization. A similar morphology has been described in Chinese hamster ovarian (CHO) cells (Brinkley et al., 1988) and pancreatic cancer cells (Beeharry et al., 2013) that underwent mitosis with under-replicated genomes (MUG), a morphological marker of mitotic catastrophe. Mitotic catastrophe is a major mode of cell death in tumours following genotoxic treatment, however, its molecular mechanism is poorly defined (Galluzzi et al., 2012). In the MUG studies, cells were first

treated with etoposide, gemcitabine, or thymidine to induce an S phase arrest and then treated with either caffeine (ATM/ATR inhibitor) or UCN-01 (Chk1/2 inhibitor) to bypass the S and G2/M checkpoints and force cells into mitosis (Beeharry et al., 2013). The resulting mitotic cells exhibited centromere fragmentation due to torsional strain caused by incomplete centromeric DNA replication leading to abnormal DNA condensation resulting in a prolonged mitotic arrest (Beeharry et al., 2013; Brinkley et al., 1988). In our study, we will refer to the MUG morphology as centromere fragmentation. Whether inhibiting Wee1 with MK-1775 also induces centromere fragmentation has yet to be confirmed but elucidating the role of Wee1 in this process is important in terms of understanding the molecular pathways leading to mitotic catastrophe. These observations explain in part the synergistic activity of MK-1775 with genotoxic agents in the clinic.

In addition to enhancing the efficacy of genotoxic therapeutics, there is also evidence that MK-1775 can be used as a mono-treatment, particularly in cells that lack p53 (Aarts et al., 2012; Hirai et al., 2009). This observation implies that inhibiting Wee1-mediated mitotic exit may on its own promote cell death, although the steps are not clear. In addition to inducing cell death in G1/S synchronized cells, MK-1775 also prolongs mitosis in cells with fully replicated chromosomes that are released from prometaphase as marked by high cyclin B1 levels and a mitotic specific phosphorylation on serine 10 of histone H3 (Visconti et al., 2015). Prolonging mitosis with anti-mitotic drugs such as nocodazole, paclitaxel, and the Eg5 kinesin inhibitor AZ-138 have been previously shown to induce cell death (Gascoigne and Taylor, 2008). To our knowledge no study has determined the cell fate of a mitotic arrest induced by the loss of Wee1. We believe that MK-1775 disrupts the cell cycle and induces cell death by two different mechanisms, both

of which cause a mitotic arrest: 1) premature mitosis in cells with under replicated DNA and 2) unregulated Cdk1 activity in prometaphase cells. We hypothesize that the key to the MK-1775 induced cell death in both cases is dependent on a prolonged mitotic arrest. We predict that the addition of other clinical agents that also induce a mitotic arrest, such as the microtubule poison paclitaxel, will enhance the induction of Wee1 mediated cell death. MK-1775 was recently shown to enhance the efficacy of paclitaxel in HeLa cells and another microtubule poison vincristine, in leukemia cells (Visconti et al., 2015). Importantly, paclitaxel and its derivatives are a first line treatment against breast cancer [Reviewed in(Crown et al., 2004)]. However, no preclinical or clinical trials have specifically explored the effects of MK-1775 and paclitaxel in solid tumours affecting the breast. Here we will show that breast cancer cell lines (T-47D, MDA-MB-231, and MCF7) undergo a prolonged mitotic arrest in response to MK-1775 treatment. We also show that MK-1775 can sensitize breast cancer cells to paclitaxel treatment. Therefore, our data provide a strong rationale to explore the potential benefits of combining MK-1775 and paclitaxel in future clinical studies on breast cancer.

2.3 Methods

2.3.1 Cell culture and synchronization

HeLa, U2-OS, MDA-MB-468, and MDA-MD-231 cells were grown as a monolayer in high-glucose DMEM supplemented with 2 mM L-glutamine and 10% (vol/vol) FBS. T-47D cells were grown in RPMI1640 supplemented with 2 mM L-glutamine, 10% (vol/vol) FBS, 0.01 mg/ml insulin, and 1 mM sodium pyruvate. MCF7 cells were grown in high-glucose DMEM supplemented with 2 mM L-glutamine, 10% (vol/vol) FBS, and 0.01

mg/ml insulin. MCF 10A cells were grown in MEBM supplemented with SingleQuots (Lonza; CC-3150) (0.5 mL of gentamicin sulfate amphotericin B, 2 mL of bovine pituitary extract, 0.5 mL hydrocortisone, 0.5 mL epidermal growth factor (rHEGF), and 0.5 mL insulin). All cell lines were cultured in a humidified incubator at 37°C with 5% CO2.

2.3.2 Small molecule inhibitors

All small molecule inhibitors were stored as 10 mM stock solutions in DMSO at -20°C. Where applicable, cells were treated with 1 μM (unless otherwise indicated) MK-1775 (Chemie Tek; 955365-80-7), 1 μM UNC-01 (Sigma-Aldrich; 112953-11-4), 10 μM CR8 (Sigma-Aldrich; C3249-5MG), 2 μM AZ3146 (Selleckchem; s2731), 2.5-10 nM paclitaxel (Sigma; T7191).

2.3.3 Cell synchronization

Cells were synchronized in G1/S phase by double thymidine block as previously described (Moudgil *et al*., 2015) (Moudgil et al., 2015). Cells were treated with 2 mM thymidine for 16 h with an 8 h release interval between thymidine treatments. Cell synchronization in prometaphase was performed 8 h post release from thymidine treatment by the addition of 200 ng/mL of nocodazole (Cell Signalling; 2190S) for 4 h. Cell synchronization described in **Figure 2.8**, **Figure 2.9**, and **Figure 2.10** (measuring NEBD to anaphase), cells were released from 2nd thymidine block for 9 h and then subjected to indicated treatments. Cell synchronization in metaphase was achieved using 25 μM MG-132 (Sigma-Aldrich; M7449).

2.3.4 RNAi

siRNA for Wee1 (5'-CAUCUCGACUUAUUGGAAAtt-3'), Myt1 (5'-GGACAGCAGCGGAUGUGUUtt-3') or a scrambled control siRNA (5'-UGGUUUACAUGUCGACUAA-3') from Thermo Fisher Scientific were used at a concentration of 20 nM with 0.2% Lipofectamine RNAiMax (Thermo Fisher Scientific) for 24 h. siRNA transfections were initiated after the first thymidine block. Knockdown efficiency was analyzed by western blotting and normalized to tubulin levels.

2.3.5 Western blotting

Cells were harvested and processed for western blot as described previously (Vos *et al*., 2011) (Vos et al., 2011). 10 µg of protein extract were separated on 12% polyacrylamide gels for 1 h at 150V. PageRuler Plus Prestained protein ladder (Fermentas; Thermo Fisher Scientific) was used as a molecular weight marker. Proteins were transferred on to Polyvinylidene difluoride (PVDF) membrane (Bio-Rad Laboratories electroblotter system) for 17 h at 30 V. Membranes were blocked with Odyssey blocking buffer (LI-COR Biosciences). Membranes were probed with the following primary antibodies: anti-Wee1 antibodies (Santa Cruz; sc-5285; 1:200 dilution), anti-Myt1 antibodies (Cell Signalling; 4282; 1:300 dilution), anti-Cdk1 antibodies (Santa Cruz; sc-54; 1:500 dilution), anti-phospho-tyrosine 15 Cdk (Signalway Antibodies; 11244-2; 1:500 dilution), anti-phospho-threonine 14 Cdk (Cell Signalling; 2543; 1:1000 dilution), anti-tubulin antibodies (Sigma; T5168; 1:4000 dilution), and anti-cyclin B1 antibodies (Santa Cruz; sc-752; 1:200 dilution). Membranes were then incubated with Alexa Fluor—680 conjugated anti-rabbit (Thermo Fisher Scientific; A21109; 1:1000 dilution) or anti-mouse (Thermo Fisher Scientific; A21057; 1:1000 dilution). Membranes were scanned by Odyssey IR imager

system (LI-COR Biosciences) and then analyzed by Odyssey V3.0 for quantification (Eaton et al., 2014).

2.3.6 Fluorescence microscopy

Cells were processed for immunofluorescence as previously described (Famulski *et al*., 2011) (Famulski et al., 2011). Cells were seeded on to coverslips at a density of 5×10^4 cells/ml in a 35-mm dish. Following cell synchronization cells were treated with the following inhibitors alone or in combination: 1 μM (unless otherwise indicated) MK-1775 (Chemie Tek; 955365-80-7), 1 μM UNC-01 (Sigma-Aldrich; 112953-11-4), 10 μM CR8 (Sigma-Aldrich; C3249-5MG), and 2 μM AZ3146 (Selleckchem; s2731). Treatments were maintained for 4 h and 0.1% DMSO was used as a control in all experiments. siRNA transfections were performed as outlined in the RNAi section. DNA was stained with 0.1 μg/ml DAPI. Coverslips were stained with the following antibodies: anti-phospho-Ser10 Histone H3 (PH3) antibodies (Abcam; ab5176; 1:1000 dilution), anti-tubulin antibodies (Sigma; T5168; 1:4000 dilution), Anti-centromere antibody (ACA) sera (gift from M. Fritzler, University of Calgary, Calgary, Canada; 1:4000 dilution), anti-Rod antibodies (N-terminal 809-aa antigen; Chan et al., 2000; 1:1500 dilution). Coverslips were mounted with 1 mg/ml Mowiol 4-88 (EMD Millipore) in phosphate buffer, pH 7.4. Alexa Fluor 488–conjugated anti–rat (1:1000 dilution; Molecular Probes), Alexa Fluor 555–conjugated anti–rabbit (1:1000 dilution; Molecular Probes), Alexa Fluor 555–conjugated anti–mouse (1:1000 dilution; Molecular Probes), and Alexa Fluor 647–conjugated anti–human (1:1000 dilution; Molecular Probes) secondary antibodies were used to visualize protein localization. A microscope (Imager.Z.1; Carl Zeiss) equipped with epifluorescence optics was used to collect the images. Cells were visualized with a 100× Plan-Apochromat

objective (Carl Zeiss) with 1.4 NA. Images were captured with a SensiCam (Cooke) charge-coupled device camera (PCOTECH, Inc.) controlled by Metamorph 7.0 software (Universal Imaging Corp.). Images were processed using Photoshop CC (Adobe).

2.3.7 High-content imaging of mitotic index

Wide field fluorescence images were taken with a High-content automated microscopy imaging system (MetaExpress Micro XLS, software version 6, Molecular Devices, Sunnyvale, CA, USA). Briefly, at least 36 images per treatment (covering an area of ~2 mm^2/image) were taken with a 10X (NA 0.3) objective with the equipped siCMOS camera using bandpass filters of 447/60 nm for DAPI and 536/40nm for Alexa488 respectively. The images were then analyzed with the MetaXpress Cell scoring module which segments each cell nucleus using the DAPI signal. Mitotic cells were detected by PH3 staining. Positive PH3 stained cells were scored using a combination of criteria: 1) a minimal staining intensity threshold; 2) using DAPI as a mask for area staining; and 3) counted as percentage of the total number of nuclei (cells). On average, each slide yielded at least 20000-60000 cells.

2.3.8 Live cell imaging

For analysis of mitotic timing, a HeLa cell line stably expressing EGFP-tubulin and mCherry H2B was used (Moudgil et al., 2015). Cells seeded in a 35-mm glass-bottom dish (MatTek Corporation or Flourodish World Precision Instruments) were placed onto a sample stage within an incubator chamber maintained at a temperature of 37°C in an atmosphere of 5% CO2. Cell media was replaced with imaging media (OPTI-MEM; Gibco) supplemented with 2 mM L-glutamine, 10% (vol/vol) FBS, and 14 mM Hepes

before imaging. Following releases from thymidine or nocodazole (see cell synchronization), cells were treated with either 1 μM MK-1775 or DMSO for up to 30 h.

Imaging was performed using a spinning disk confocal on an inverted microscope (Axiovert 200M; Carl Zeiss; with a 40× objective lens and 1.3 NA) equipped with an electron-multiplying charge-coupled device (EM-CCD) camera (ORCA-FLASH-4.0; Hamamatsu Photonics). Images were collected every 5 min for GFP and Cy3 channels using 100-ms exposure times, for 10–16 h using the velocity software (Perkin¬Elmer). Velocity 6.3.0 software was used to collect and export videos as AVI format using Microsoft video 1 compression. Videos were further converted to the mov format with Vegas Pro version 12.0 (Build 394; Sony Creative Software Inc.) using Sorenson 3 compression. Mitotic timing for cells was calculated manually. Still tiff format images from videos were exported using Velocity 6.3.0 software and processed using Photoshop CC. Statistical analysis was performed using GraphPad Prism version 5.04.

2.3.9 Crystal violet assay

G1/S released cells were seeded into 96-well plates for 9 h and then treated with increases concentrations of MK-1775 (125-1000 nM, 1:2 series dilution) alone or in combination with paclitaxel (2.5, 5, or 10 nM) for 48 h. After treatment, media was aspirated and then cells were stained with 0.5% crystal violet assay for 20 min as outlined by Feoktistova *et al*. (Feoktistova et al., 2016). Crystal violet was later removed, and plates were rinsed three times with water and left to air-dry for 24 h. Crystal violet stain was then resuspended in 100% methanol. Absorbance 570 nm (OD_{570}) was measured using Optima Plate reader powered by Optima software. Percent surviving attached cells was calculated by subtracting off blank wells and then normalizing DMSO controls to 100%. The first point

on each curve (64 nM) represents 0 nM MK-1775. Graphs were plotted using Graph Prisms V7.

2.3.10 Flow cytometry

At desired times after treatment, cells treated with either 1 μM MK-1775 or DMSO were collected by aspiration and trypsinization. Cells were washed in PBS and fixed in 90% ethanol (-20°C) for at least 24 h. Fixed cell suspensions were blocked for 1 h with labelling buffer (PBS, 5% serum, 1% BSA and 0.1% sodium azide) before 1 h of incubation with anti-phospho-Ser10- histone H3 (PH3) antibody (Abcam; ab5176; 1:1000 dilution), and 30 min of incubation with Alexa Fluor 488–conjugated anti–rabbit (Thermo Fisher Scientific; A-11034; 1:100 dilution) in labelling buffer, separated by wash/centrifuge steps in wash buffer (PBS, 1% BSA and 0.1% sodium azide). For analysis, samples were incubated for 20 min in wash buffer with 0.02 mg/ml propidium iodide (Invitrogen) and 0.2 mg/ml RNase A (Sigma) and analysed by a FACSCantoTM II flow cytometer (BD Biosciences) using BD FACSDivaTM software. Gating was set using control samples without primary antibody. Experiments were carried out three times.

2.4 Results

2.4.1 Inhibition of Wee1 promotes premature mitosis

To test if Wee1 inhibition induced premature mitosis in HeLa, cells were synchronized in G1/S phase by double thymidine block and then released into fresh media containing either MK-1775 or a solvent control (DMSO) (**Figure 2.1A**). Cells were fixed 4 h after treatment with MK-1775 and then examined for phospho-serine 10 histone H3 (PH3), which is a mitotic specific biomarker (Hendzel et al., 1997), by immunofluorescence microscopy (**Figure 2.1B**). We observed that ~20% of cells were positive for PH3 following MK-1775 treatment compared to ~1% in the DMSO controls (**Figure 2.1B & C**; student t-test; $P < 0.05$). Cells that stained positive for PH3 had condensed DNA (observed by DAPI staining) consistent with a mitotic morphology. We also treated three different breast cancer cell lines (MDA-MB-231, T-47D, and MCF7) and one non-tumorigenic breast cell line (MCF 10A) with MK-1775 following G1/S synchronization (**Figure 2.1C**). The molecular subtype and p53 status for each cell line is indicated in **Table 2.1**. We observed that MK-1775 treatment increased the percentage of cells positive for PH3 in HeLa ($P < 0.005$; student t-test), T-47D ($P < 0.005$; student t-test), and MDA-MB-231 ($P < 0.05$; student t-test) from 1-2% to ~20%. In contrast, MK-1775 treatment was less effective in MCF7 cells. Here the percent of cells positive for PH3 increased from 2% to 6% ($P < 0.05$; student t-test). No significant change was observed in the percentage of cells positive for PH3 in MCF 10A cells treated with MK-1775 compared to DMSO. Cells released from G1/S were also analyzed by flow cytometry following treatment with MK-1775 or DMSO for up to 8 h (**Figure 2.1D** and **Supplementary Figure 2.1**). At each of the treatment intervals analyzed (4, 6, and 8 h), a similar number of MK-1775-treated cells were positive for PH3

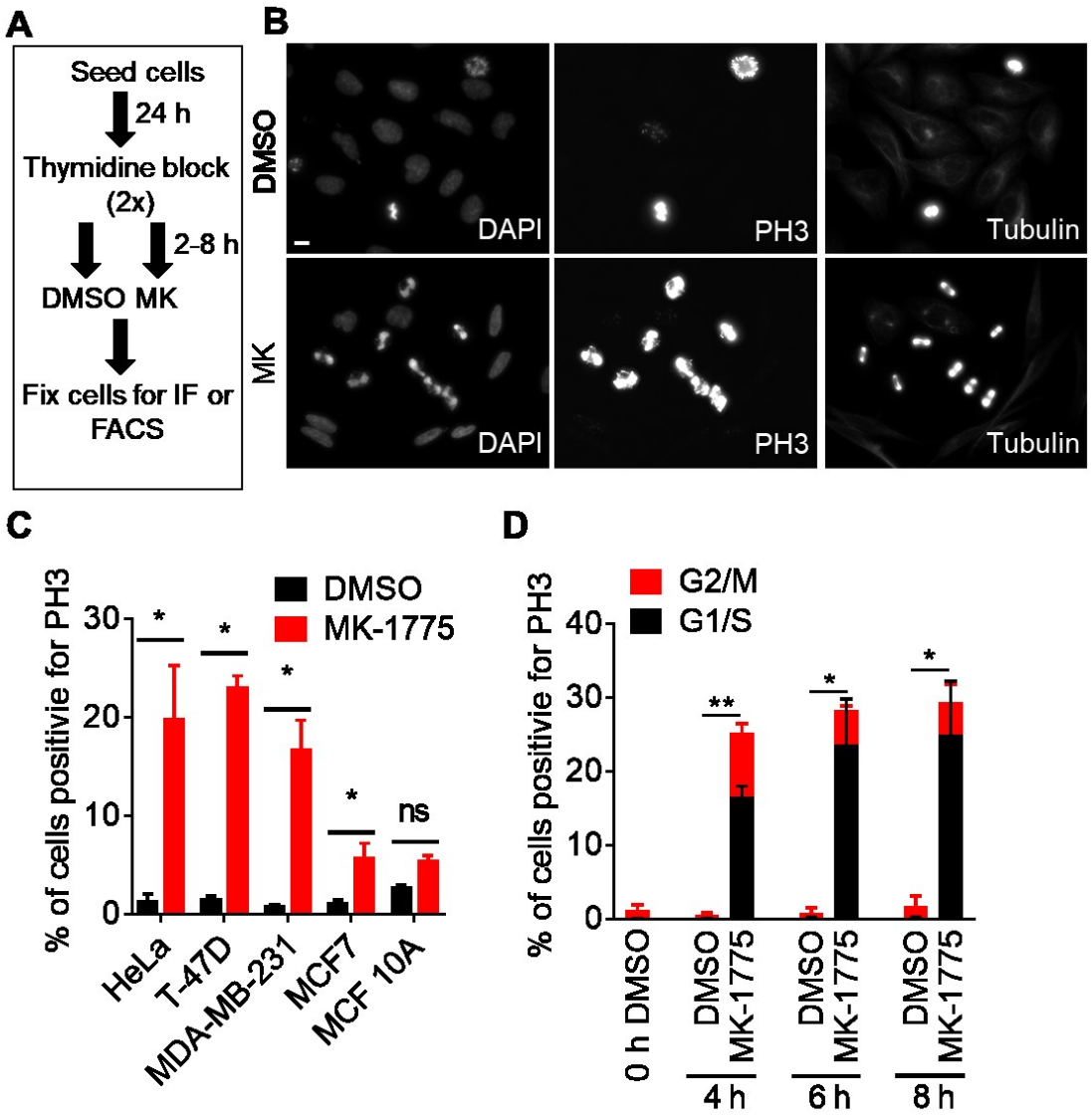

Figure 2.1. Inhibition of Wee1 kinase promotes premature entry into mitosis.
HeLa cells were released from G1/S phase into media containing either DMSO or MK-1775 (MK) and then fixed at indicated times. **A)** Experimental flow chart depicting treatments and times. **B)** Cells were stained for DNA, PH3, and microtubules and then analyzed by immunofluorescence microscopy 4 h post treatment. Scale bar = 10 μm. **C)** Indicated cell lines were treated with DMSO or MK-1775 for 4 h and then analyzed by immunofluorescence microscopy for PH3 and DNA. Percent total cells positive for PH3 is shown. Student t-test was used to determine significance between DMSO and MK-1775 (*p < 0.05). **D)** Cells stained for PH3 and DNA were analyzed by FACS to determined cell cycle phase (Supplementary Figure 2.1). Average percentage of cells positive for PH3 relative to DNA staining are shown. Error bars are standard error of the mean. Black bars represent cells in the G1/S phase and red bars represent cells in the G2/M phase. Statistical significance was determined by student t-test (*p < 0.05 and **p < 0.01).

Table 2.1. p53 status and molecule subtypes of cell lines.
p53 status for breast cancer cell lines is reviewed in (Muller and Vousden, 2014). Molecular subtypes were assigned based on ATCC classifications.

Cell line	Cell type (ATCC)	Tissue type (ATCC)	p53 status	Molecular sub-type
HeLa	Epithelial	Cervical	Wild type HPV E6 deactivated	N.A.
MDA-MB-231	Epithelial	Mammary gland/breast	Missense R273H	Basal (triple negative)
MDA-MB-468	Epithelial	Mammary gland/breast	Missense R280K	Basal (triple negative)
MCF 10A*	Epithelial	Mammary gland/breast	Wild type	Basal (triple negative)
MCF7	Epithelial	Mammary gland/breast	Wild type	Luminal A ER+/PR+
T-47D	Epithelial	Mammary gland	Missense L194F	Luminal A ER+/PR+

(25-29%), whereas less than 2% of cells treated with DMSO were positive for PH3 at any one time (**Figure 2.1D**). Analysis of DNA content by propidium-iodine staining showed that two-thirds of the cells positive for PH3 staining following MK-1775 treatment had less than 4N DNA. Together, this data confirms that inhibition of Wee1 kinase forces HeLa cells into mitosis directly from G1/S phase.

Knowing that inhibiting Wee1 induces premature entry into mitosis from G1/S phase, we tested if co-inhibition of other kinases involved in either the entry into or exit from mitosis would affect the number of PH3-positive cells. Cells synchronized in G1/S were released into media containing different kinase inhibitors (with and without MK-1775): UCN-01 (Chk1 inhibitor), AZ-3146 (Mps1 inhibitor), and CR8 (Cdk1 inhibitor) (**Figure 2.2A & B**). Of the listed inhibitors, only monotreatment with MK-1775 increased the percentage of cells positive for PH3 after a 4 h (~26% in MK-1775 compared to DMSO control ~0.5%) (One-way ANOVA and Dunnett's multiple comparisons test; $P < 0.0001$)

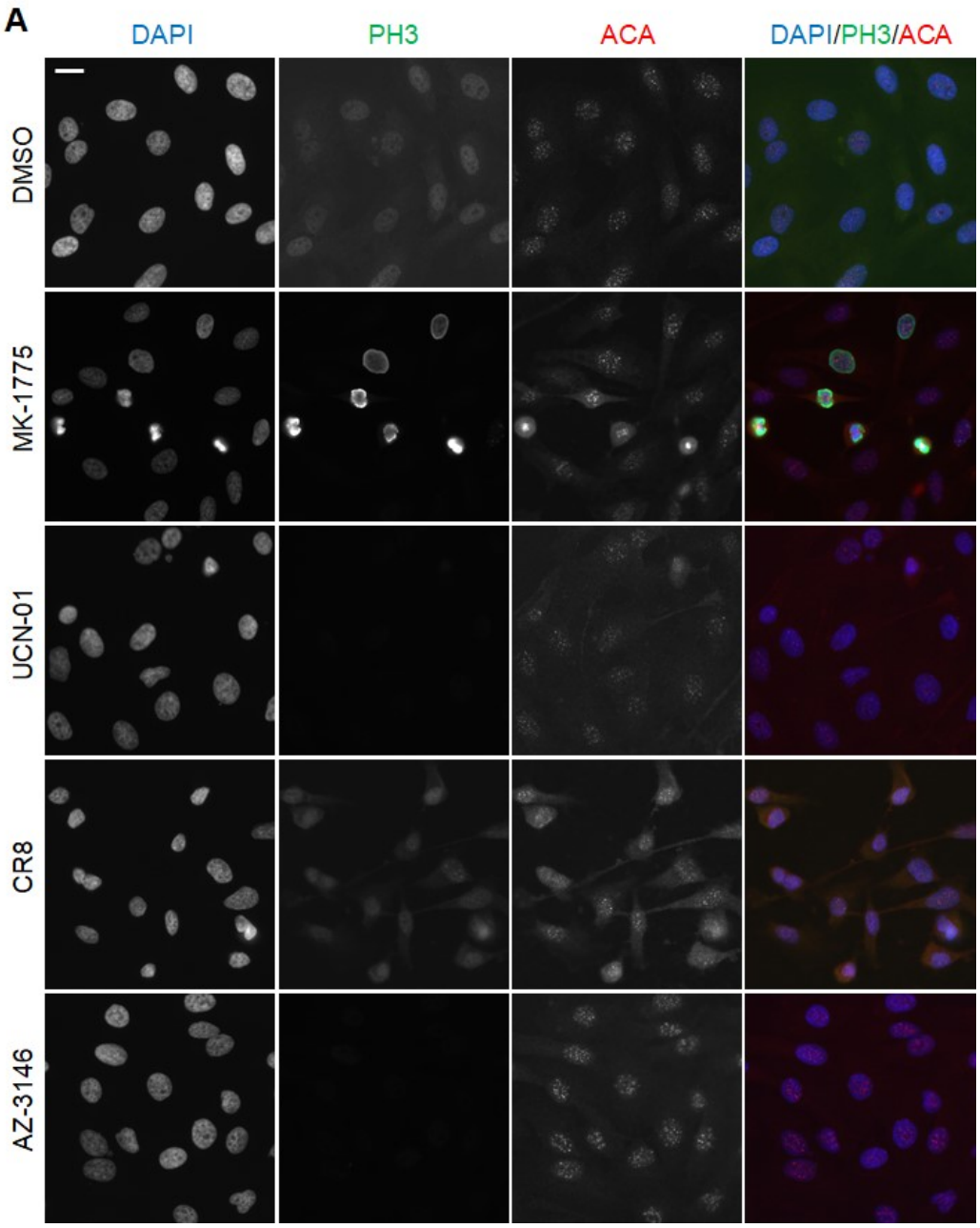
A
DAPI
PH3
ACA
DAPI/PH3/ACA
DMSO
MK-1775
UCN-01
CR8
AZ-3146

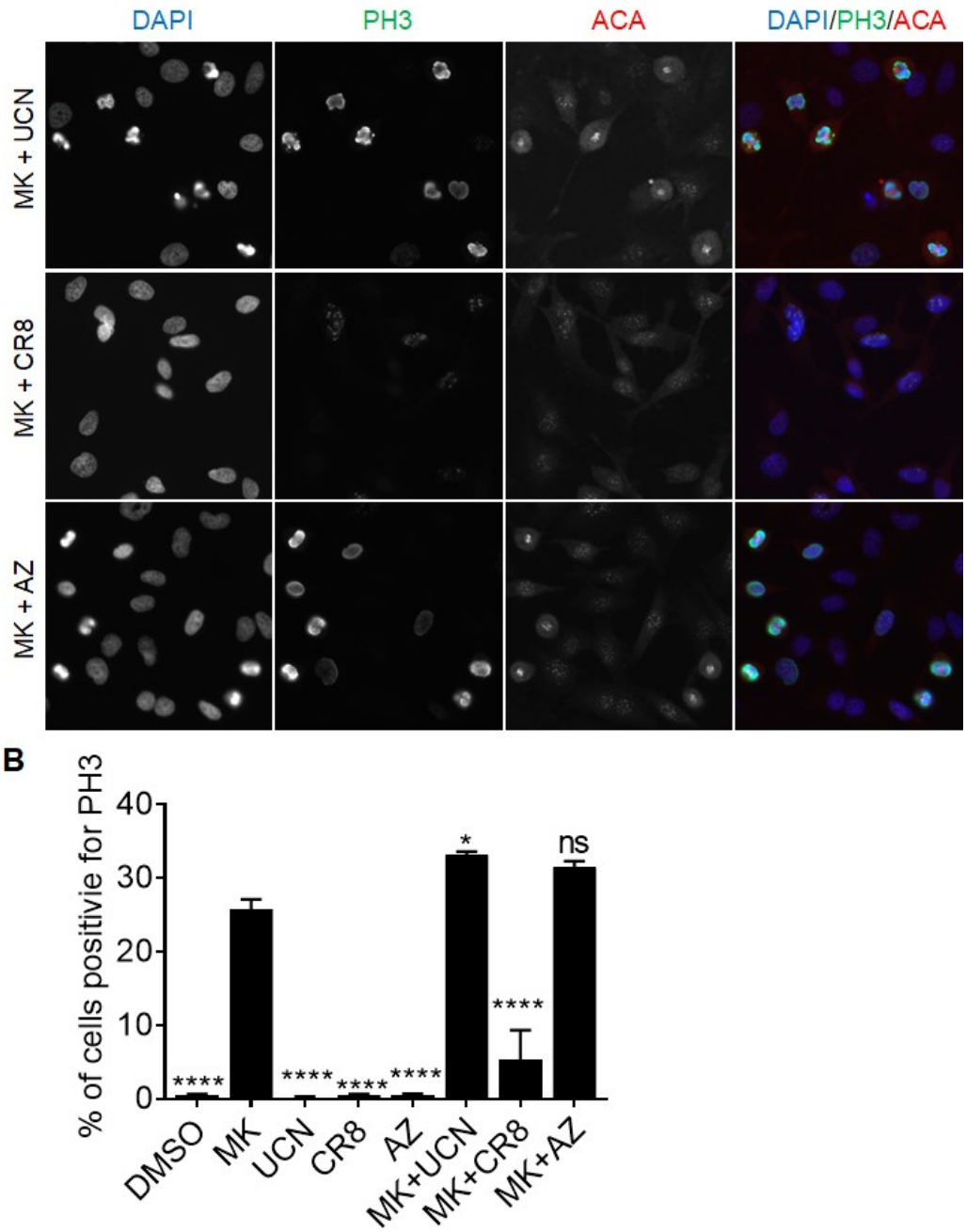

Figure 2.2. Co-inhibition of Wee1 and Chk1 increased premature entry into mitosis.

A) HeLa cells were released from G1/S phase and then treated with different kinase inhibitors (Chk1 inhibitor UCN-01 (UCN), Cdk1 inhibitor CR8, and Mps1 inhibitor AZ-3146 (AZ)) alone or in the presence of MK-1775. MK-1775 alone and DMSO were included as controls. After a 4 h treatment, cells were stained for DNA (DAPI), centromere (ACA), and PH3 and analyzed by immunofluorescence microscopy. Scale bar = 20 μM. **B)** The graph shows the average percentage of cells positive for PH3 relative to DNA staining for each

treatment. Error bars represent standard error of the mean. Experiment was repeated three times. One-way ANOVA and Dunnett's multiple comparisons test (MK verses treatment) were used to determine significance level (*$P < 0.05$; ****$P < 0.0001$).

(**Figure 2.2B**). Chk1 inhibition by UCN-01 increased the percentage of cells positive for PH3 from 26% (MK-1775 alone) to 33% (combined treatment) (One-way ANOVA and Dunnett's multiple comparisons test*;* $P < 0.05$). In contrast, inhibition of Cdk1 by CR8 decreased the percentage of cells positive for PH3 from 26% to 5% (One-way ANOVA and Dunnett's multiple comparisons test; $P < 0.0001$). No significant change in the percentage of PH3 positive cells was observed following co-inhibition of Mps-1 and Wee1 with AZ-3146 and MK-1775 versus inhibition of Wee1 alone.

2.4.2 Wee1 but not Myt1 kinase activity is required to prevent premature mitosis in HeLa cells

We confirmed that siRNA knockdown of Wee1 in G1/S synchronized HeLa cells also increased PH3 staining compared to scrambled siRNA (siSc) controls (**Figure 2.3A-H**; student t-test*,* $P < 0.05$). Since both Wee1 and Myt1 add inhibitory phosphates to Cdk1, we asked if the loss of both Wee1 and Myt1 kinase activity was required to induce premature mitosis in HeLa cells. MK-1775 is reported to be 100 times more potent against Wee1 than Myt1, but at concentrations above 300

nM both kinases may be inhibited (Hirai et al., 2009). To determine if premature mitosis requires loss of both Wee1 and Myt1, we knocked-down Wee1 and Myt1 alone and in combination by siRNA transfection in HeLa cells and then analyzed cells for PH3 (**Figure 2.3A-C**). Knockdown efficiencies of Wee1 and Myt1 were analyzed by immunoblotting (**Figure 2.3D-H**). We found that 11% of cells transfected with siRNA against Wee1 expressed PH3 whereas only 4% of cells transfected with scrambled control siRNA (siSc)

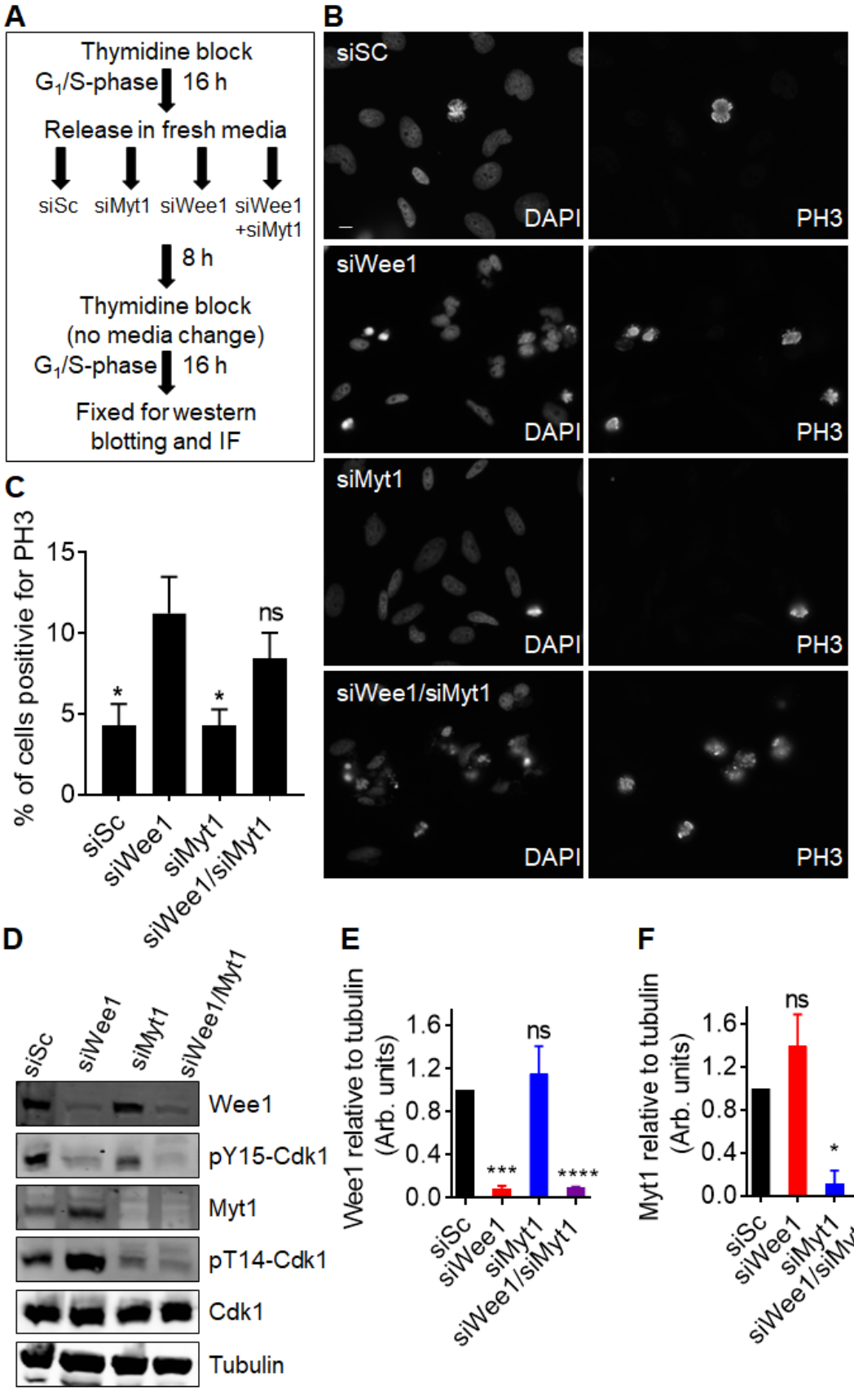
A
Thymidine block
G1/S-phase 16 h
Release in fresh media
siSc
siMyt1
siWee1
siWee1 +siMyt1
8 h
Thymidine block (no media change)
G1/S-phase 16 h
Fixed for western blotting and IF
B
siSC
siWee1
siMyt1
siWee1/siMyt1
DAPI
PH3
C
% of cells positivie for PH3
15
10
5
0
*
*
ns
siSc
siWee1
siMyt1
siWee1/siMyt1
D
siSc
siWee1
siMyt1
siWee1/Myt1
Wee1
pY15-Cdk1
Myt1
pT14-Cdk1
Cdk1
Tubulin
E
Wee1 relative to tubulin (Arb. units)
1.6
1.2
0.8
0.4
0.0
***
ns
****
siSc
siWee1
siMyt1
siWee1/siMyt1
F
Myt1 relative to tubulin (Arb. units)
1.6
1.2
0.8
0.4
0.0
ns
*
*
siSc
siWee1
siMyt1
siWee1/siMyt1

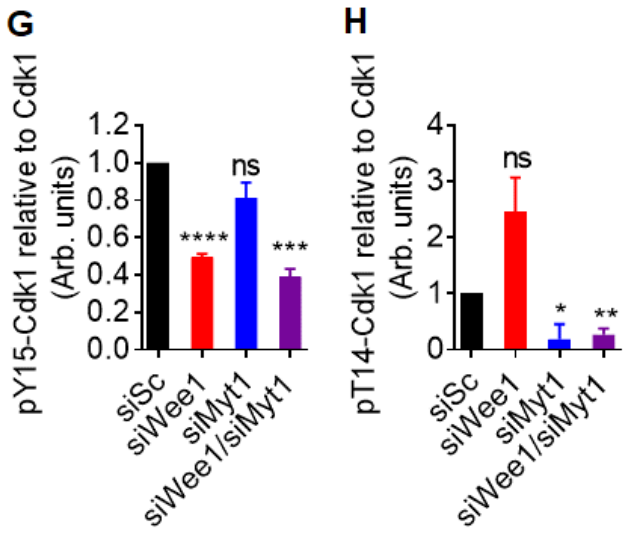

Figure 2.3. siRNA mediated knockdown of Wee1, but not Myt1, induces premature mitosis.
HeLa cells synchronized in G1/S phase were transfected with scrambled siRNA (siSc) and siRNAs against Wee1, Myt1, and both Wee1 and Myt1. **A)** Experimental flow chart depicting timing and treatments. **B)** Cells were fixed 24 h post siRNA transfection and then stained for DNA and PH3. Scale bar = 10 µm. **C)** The average percentage of cells positive for PH3 (relative to DNA staining) are graphed. Student t-test was used to determine statistical significance between siWee1 and other treatments (*$P < 0.05$). Standard error of the mean bars are shown. **D)** Following transfection, cell lysates were analyzed by immunoblot for total levels of Wee1, Myt1, pY15-Cdk1, pT14-Cdk1, Cdk1, and tubulin. Graphs show the average levels of (**E**) Wee1 and (**F**) Myt1 (relative to tubulin) and (**G**) pY15-Cdk1 and (**H**) pT14-Cdk1 (relative to Cdk1). Error bars represent standard error of the mean. Student t-test were used to determine significance (*$P < 0.05$, **$P < 0.005$, ***$P < 0.0005$ and ****$P < 0.0001$) F) Mitotic cells post transfection with scrambled siRNA or siRNA against Wee1 were fixed and then stained for histone H3 phospho-Ser10 (PH3), tubulin, anti-centromere antibody (ACA), and DNA. Experiments were repeated at least three times.

expressed PH3 (**Figure 2.3C**; student t-test; $P < 0.05$). In contrast to Wee1 knockdown, Myt1 knockdown did not affect the number of cells in mitosis; furthermore, combined knockdown of both Wee1 and Myt1 kinases did not enhance PH3 staining compared to Wee1 knockdown alone (8% vs 11%). These data suggest that Wee1 has a more dominant role in regulating Cdk1 activity in HeLa cells and that Myt1 alone cannot prevent premature mitosis.

2.4.3 Loss of Wee1 activity induces centromere fragmentation

We next examined the cellular morphology of MK-1775-treated cells that prematurely enter mitosis. Previous groups have reported that failure to complete DNA synthesis prior to mitotic entry can induce abnormal DNA condensation leading to torsional strain along the DNA backbone and centromere fragmentation (Beeharry et al., 2013; Brinkley et al., 1988). We asked if cells treated with MK-1775 also exhibited centromere fragmentation. G1/S synchronized cells treated with MK-1775 were analyzed for the localization of the mitotic checkpoint protein Rough Deal (Rod) (Chan et al., 2000) and centromeres (ACA) relative to the DNA by immunofluorescence microscopy (**Figure 2.4A**). In both MK-1775 and DMSO treatment, we found that Rod staining overlapped with ACA staining confirming activation of the mitotic checkpoint (Chan et al., 2000); however, the majority of the Rod/ACA in MK-1775-treated cells was clustered away from the main mass of chromosomes consistent with centromere fragmentation. We confirmed that siRNA knockdown of Wee1 also resulted in the centromere fragmentation morphology (**Figure 2.5**), which supports that observed morphology was dependent on Wee1 and not another off-target kinase.

We then asked if MK-1775 induced centromere fragmentation affected the ability of cells to complete mitosis. We released HeLa cells (stably transfected with mCherry-H2B and GFP-tubulin) from G1/S phase and then monitored the time cells spent in mitosis by time-lapse microscopy (**Figure 2.4B**). We found that cells released into MK-1775 remained in mitosis for a median time of 203 min whereas DMSO treated cells stayed in mitosis for 60 min (**Figure 2.4C**, student t-test; $P < 0.0001$). Most MK-1775-treated cells

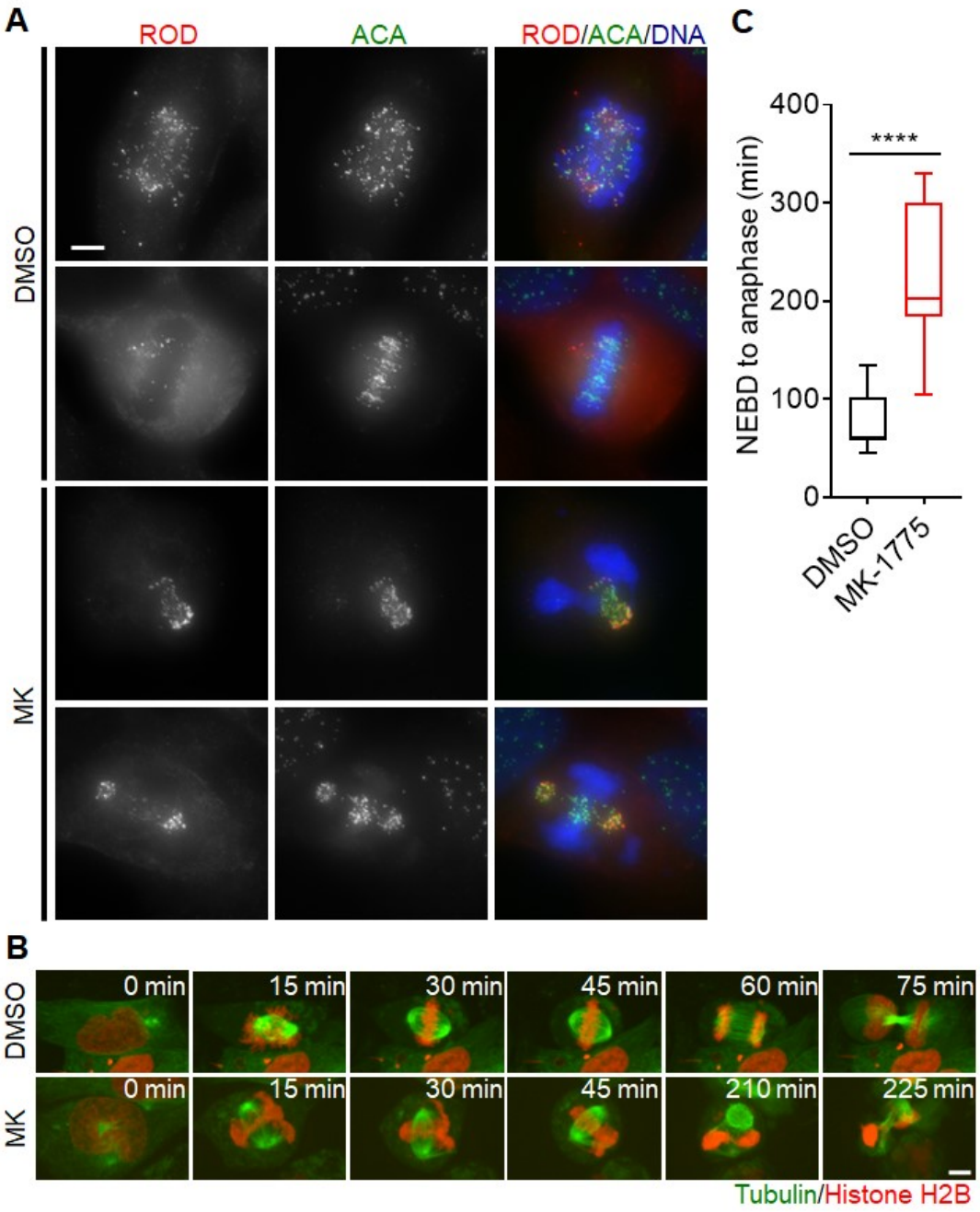
A
ROD
ACA
ROD/ACA/DNA
DMSO
MK
C
NEBD to anaphase (min)
400
300
200
100
0
****
DMSO
MK-1775
B
DMSO
MK
0 min
15 min
30 min
45 min
60 min
75 min
0 min
15 min
30 min
45 min
210 min
225 min
Tubulin/Histone H2B

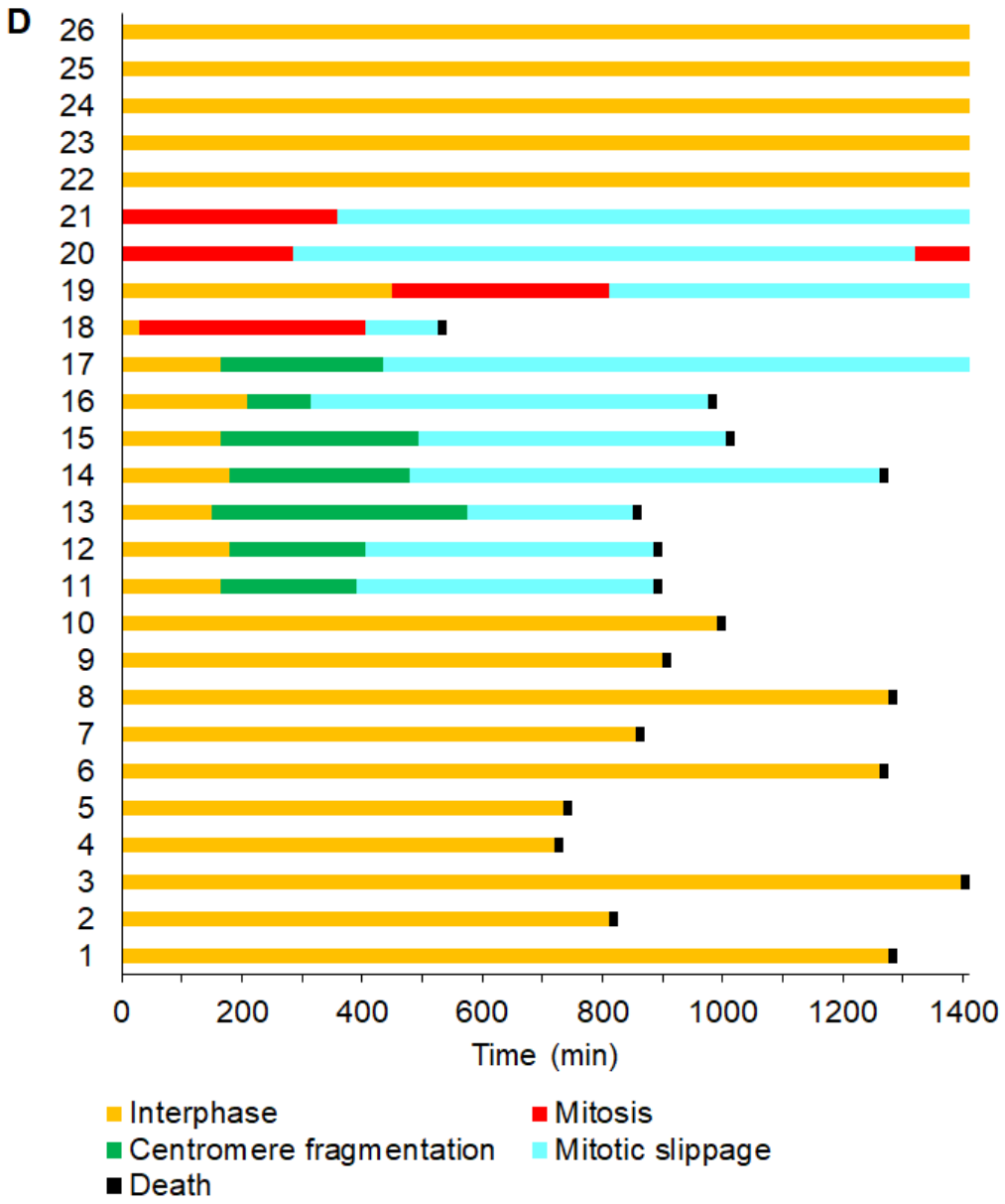

Figure 2.4. Inhibition of Wee1 induces centromere fragmentation and prolonged mitosis.
HeLa cells were synchronized in G1/S phase and then released into media containing either DMSO or MK-1775 (MK). **A)** Mitotic cells fixed 4 h post treatment with MK were compared to mitotic cells fixed post treatment with DMSO. Cells were stained for Rough deal (ROD), anti-centromere antibody (ACA), and DNA. Scale bar = 10 μm. **B)** HeLa cells stably expressing mCherry-H2B and EGFP-tubulin were treated with DMSO and MK and then analyzed by time-lapse microscopy to determine duration of mitosis (scale bar = 8 μm). Time is counted from NEBD in minutes. MK treated cells (lower panel) is also depicted as cell 11 in Supplementary Figure 4B. **C)** The duration of mitosis (NEBD to anaphase) is shown for 8 cells for each treatment. Boxes represent interquartile distributions and whiskers represent 10th and 90th percentiles.

Statistical significance was determined by student t-test (****p < 0.0001). **D)** 26 individual HeLa cells stably expressing mCherry-H2B and EGFP-tubulin were synchronized in G1/S phase and then released into fresh media containing MK-1775. Duration of each indicated events was measured by time-lapse microscopy.

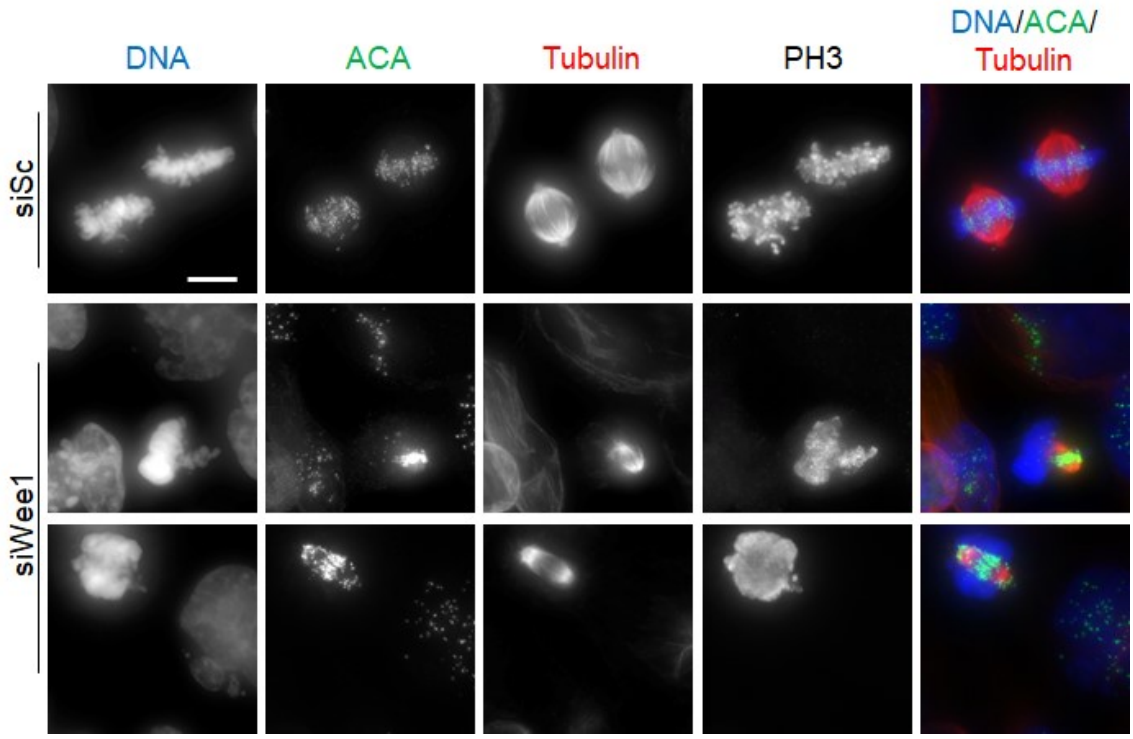

Figure 2.5. siRNA mediated knockdown of Wee1 induces centromere fragmentation.
HeLa cell extracts were prepared following transfections with scrambled siRNA or siRNAs against Wee1. Representative mitotic cells stained for histone H3 phospho-Ser10 (PH3), tubulin, anti-centromere antibody (ACA), and DNA are shown. Experiments were repeated at least three times.

did not achieve chromosome alignment and exited mitosis without chromosome segregation (**Figure 2.4D**). We monitored the MK-1775 treated cells for 24 hours and observed that 86% of cells that underwent centromere fragmentation (6/7) subsequently died in interphase (**Supplementary Figure 2.2**, cells labelled 11-17). These data suggest that MK-1775 treatment prolongs mitosis by preventing normal chromosome alignment and segregation, which ultimately leads to cell death.

2.4.4 Inhibition of Wee1 prevents normal mitotic exit

Although Wee1 inhibition during G1/S phase induces premature mitosis followed by a prometaphase-like arrest, it is not clear if Wee1 inhibition induces a mitotic arrest in cells with fully replicated (and undamaged) chromosomes. We synchronized HeLa cells (stably transfected with mCherry-H2B and GFP-tubulin) in prometaphase using nocodazole treatment (**Figure 2.6A**). We then released cells from nocodazole treatment into media containing either MK-1775 or DMSO and then measured the time required for cells to complete anaphase (**Figure 2.6B & C**). We found that the average time required to complete mitosis (metaphase to anaphase) was similar among DMSO treated cells (**Figure 2.6C**); however, MK-1775 treated cells arrested at metaphase (**Figure 2.6B**, right set of images). During this metaphase arrest, many cells experienced one or more spindle collapses resulting in the temporary loss of chromosome alignment. Overall, we found that the transition from metaphase to anaphase in cells treated with MK-1775 took a median time of 220 min with some cells requiring greater than 700 min to initiate anaphase (**Figure 2.6C**). In contrast, DMSO treated cells took only 20 min to transition from metaphase to anaphase (student t-test; $P = 0.0023$). To confirm the delay in mitotic exit, we also released cells synchronized in prometaphase into media containing either MK-1775 or DMSO for up to 2 h and then analyzed the levels of cyclin B1 and phospho-tyrosine 15 Cdk1 (pY15-Cdk1) by western blotting (**Figure 2.6D-F**). MK-1775-treated cells had low levels of pY15-Cdk1 and retained high levels of cyclin B1 (60% relative to time 0) after 2 h. In contrast, DMSO-treated cells had higher levels of pY15-Cdk1 and lower levels of cyclin B (15% relative to that at time 0) after 2 h (One-way ANOVA and Dunnett's multiple comparisons test; $P < 0.0005$). We tested if proteasome inhibition by MG-132 could further

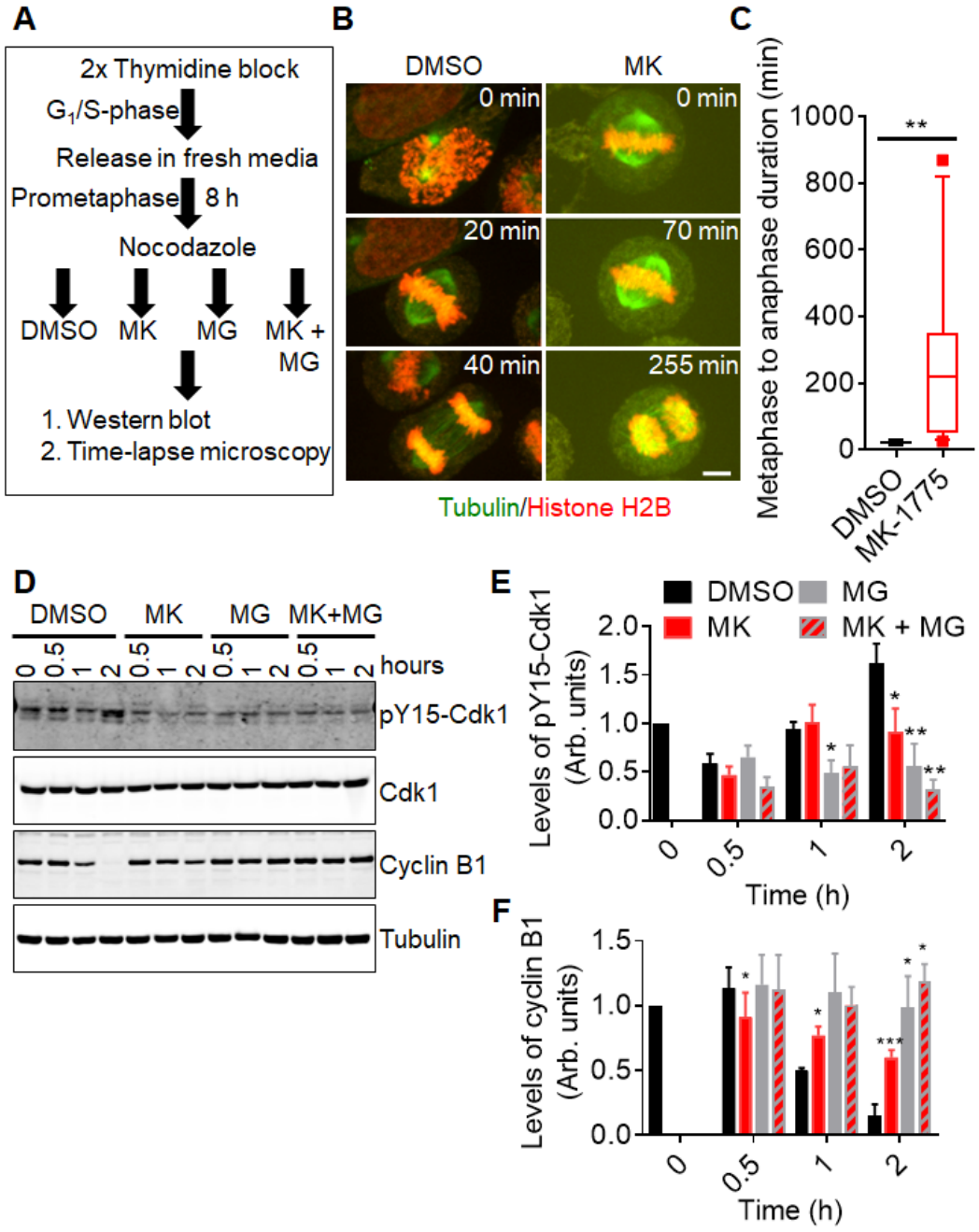

Figure 2.6. Inhibition of Wee1 prevents normal mitotic exit.
HeLa cells were synchronized and then released into media containing DMSO, MK-1775 (MK), MG-132 (MG) or both MK and MG for two hours. **A)** Experimental flow chart of treatment conditions. **B)** HeLa cells stably expressing mCherry-H2B and EGFP-tubulin were released into DMSO and MK and monitored by time-lapse microscopy. Scale bar = 8 μm. **C)** The duration of the transition between metaphase and anaphase was measured for 12 cells for each treatment. Boxes represent interquartile distributions and whiskers represent 10th and 90th percentiles. Square dots represent outliers. Statistical significance was determined by student t-test (**p < 0.005). **D)** Cell extracts

were prepared from treated cells at indicated times. Extracts were then analyzed by western blot for the levels of pY15-Cdk1, Cdk1, cyclin B1, and tubulin. **E)** Average levels of pY15-Cdk1 (relative to Cdk1) and **F)** cyclin B1 (relative to tubulin) were measured over time. Levels of pY15-Cdk1 and Cyclin B1 at time zero were set as 1. Error bars represent standard error of the mean. Statistical significance was determined using One-way ANOVA and Dunnett's multiple comparisons test (*p < 0.05 and *** p < 0.0005). Experiments were repeated at least three times.

enhance the effects of MK-1775 (Famulski and Chan, 2007). MG-132 treatment completely stabilized cyclin B levels in mitotic cells, but no significant differences were observed between cells co-treated with MG-132 and MK-1775 and those treated with MK-1775 alone (One-way ANOVA and Dunnett's multiple comparisons test; $P = 0.1246$; **Figure 2.6E & F**). We confirmed that treatment with MK-1775 inhibited Cdk1 phosphorylation and cyclin B1 degradation in three additional cell lines (U-2 OS, T-47D, and MDA-MB-231) (**Figure 2.7**). Together these data confirm that Wee1 activity is required for normal mitotic exit from prometaphase through a Cdk1/cyclin B1-dependent pathway.

2.4.5 Mitotic arrest induced Wee1 inhibition leads to cell death

Since inhibition of Wee1 in prometaphase cells extended mitosis compared to controls, we then asked if this increased time in mitosis affected cell viability. We treated mitotic synchronized HeLa cells (expressing GFP-H2B) with either MK-1775 or DMSO and then examined cell fate by time-lapse microscopy for up to 900 min (**Figure 2.8** and **Table 2.1**). We found that 26% (10/38) of mitotic cells examined, died without completing anaphase. We observed successful completion of mitosis in 68% (26/38) of cells monitored, but 27% (14/52) of resulting daughter cells exhibited extra-nuclear structures or micronucleation and 60% (31/52) of the daughter cells died in interphase several hours after anaphase. In

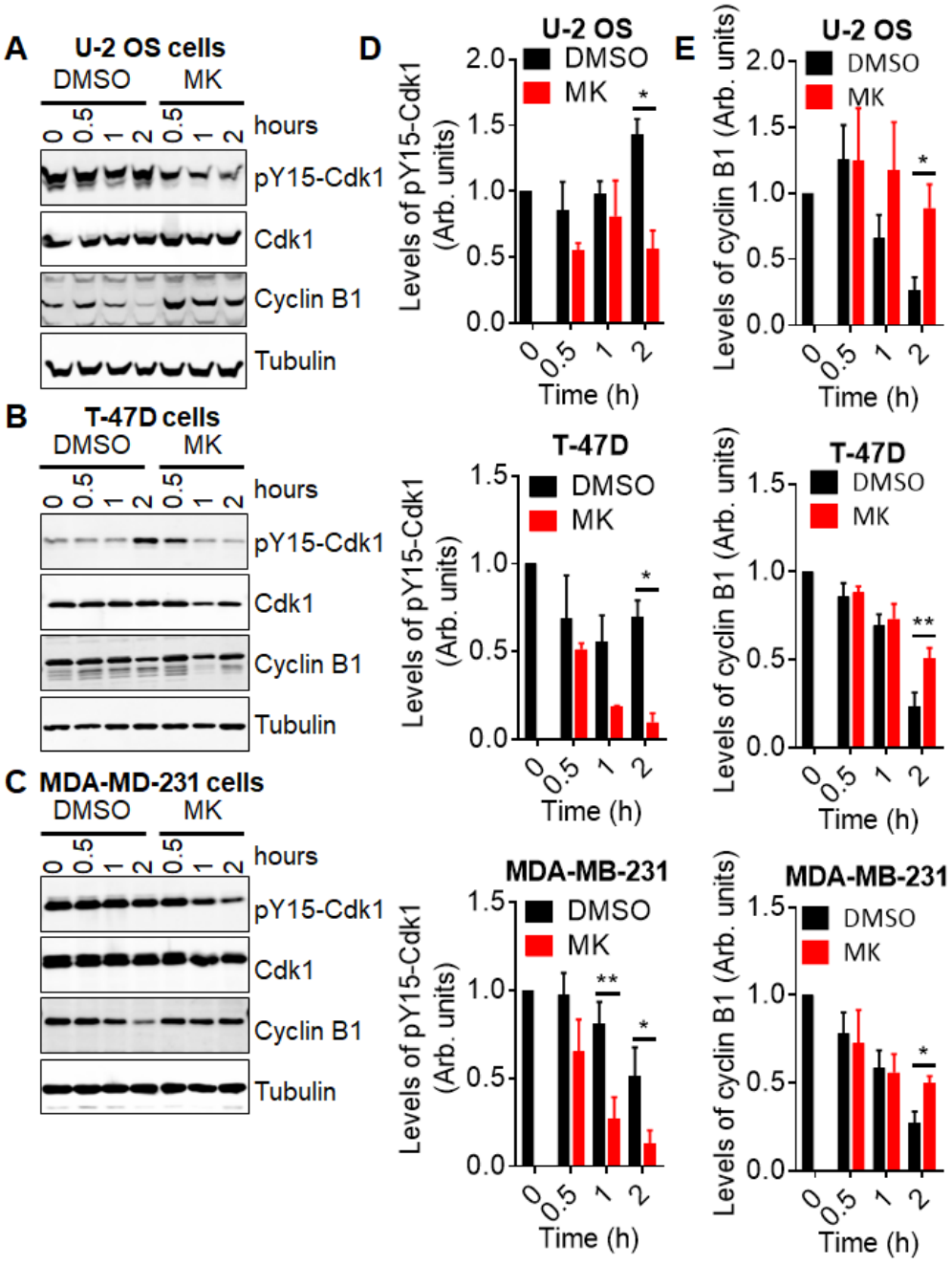

Figure 2.7. MK-1775 inhibits cyclin B degradation in cancer cells.
A) U2-OS, **B)** T47-D, and **C)** MDA-MD-231 cell lines were synchronized in prometaphase and then released into media containing either DMSO or MK-1775 (MK) for two hours. Cell extracts were prepared at indicated times. Extracts were analyzed by western blot for the levels of pY15-Cdk1, Cdk1, cyclin B1, and tubulin. **D)** Average levels of pY15-Cdk1 (relative to Cdk1) and **E)** cyclin B1 (relative to tubulin) were measured over time. Levels of pY15-Cdk1 and Cyclin B1 at time zero were set as 1. Error bars represent standard error of the mean. Statistical significance was determined using student t-test (*p < 0.05). Experiments were repeated at least three times.

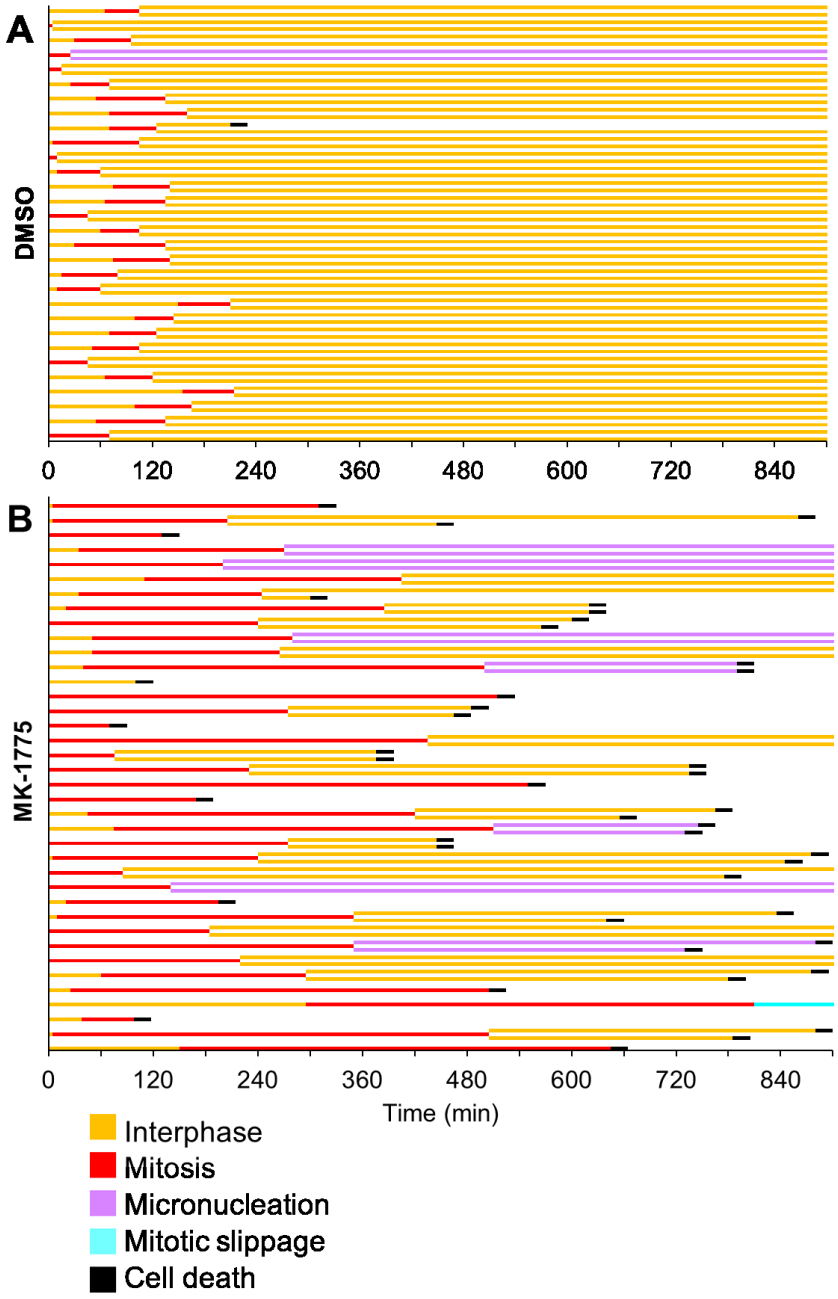

Figure 2.8. MK-1775 induced mitotic arrest promotes cell death.
HeLa cells expressing EGFP-H2B were released from double thymidine block for 9 hours and then treated with either A) DMSO or B) MK-1775 for 900 min. A line graph for 38 individual mitotic cells tracked by time-lapse microscopy is shown, which includes times for indicated cellular events. A fork in the line indicates cell division and cell fate of daughter cells is also shown.

Table 2.2. Duration of mitosis and percentage of cell death in HeLa cells treated with 1000 nM MK-1775.

	DMSO	MK-1775
Average mitotic timing (min)	56	277
% Cell death in mitosis	0% (0/30)	26% (10/38)
% Daughter cell death after mitosis	2% (1/60)	60% (31/52)
% Daughter cells with micronuclei	3% (2/60)	27% (14/52)

contrast, cell death or cells with micronuclei were rarely detected in DMSO controls. These data illustrate that Wee1 can induce mitotic cell death independent of premature mitosis.

2.4.6 Paclitaxel treatment enhances MK-1775 mediated cell killing

Knowing that Wee1 is required for normal mitotic exit, we tested if co-treatment with the anti-microtubule drug paclitaxel could prolong mitosis in Wee1 inhibited cells. Mitotic synchronized HeLa cells were treated with 10 nM paclitaxel alone or in the presence of different concentrations of MK-1775 (125 nM to 1000 nM) (**Figure 2.9** and **Table 2.3**). Mono-treatments of both paclitaxel and MK-1775 (at all tested concentrations) increased the average mitotic transit time (NEBD to anaphase) compared to DMSO controls (**Table 2.3**). The average mitotic transit time in the presence of paclitaxel was found to be longer compared to mono-treatments of MK-1775 at concentration of 125 nM to 500 nM (One-way ANOVA and Tukey's multiple comparisons test, $P < 0.0001$), but no difference was observed between paclitaxel and 1000 nM MK-1775. We also observed abnormal spindle formation (tri-polar spindles) with paclitaxel treatment alone consistent with previous groups (Zasadil et al., 2014). We found that combined treatments with paclitaxel and MK-1775 (500 nM to 1000 nM) prolonged average mitotic transit time (One-way ANOVA and Tukey's multiple comparisons test; $P < 0.0005$ *and* $P < 0.0001$). In addition to prolonging

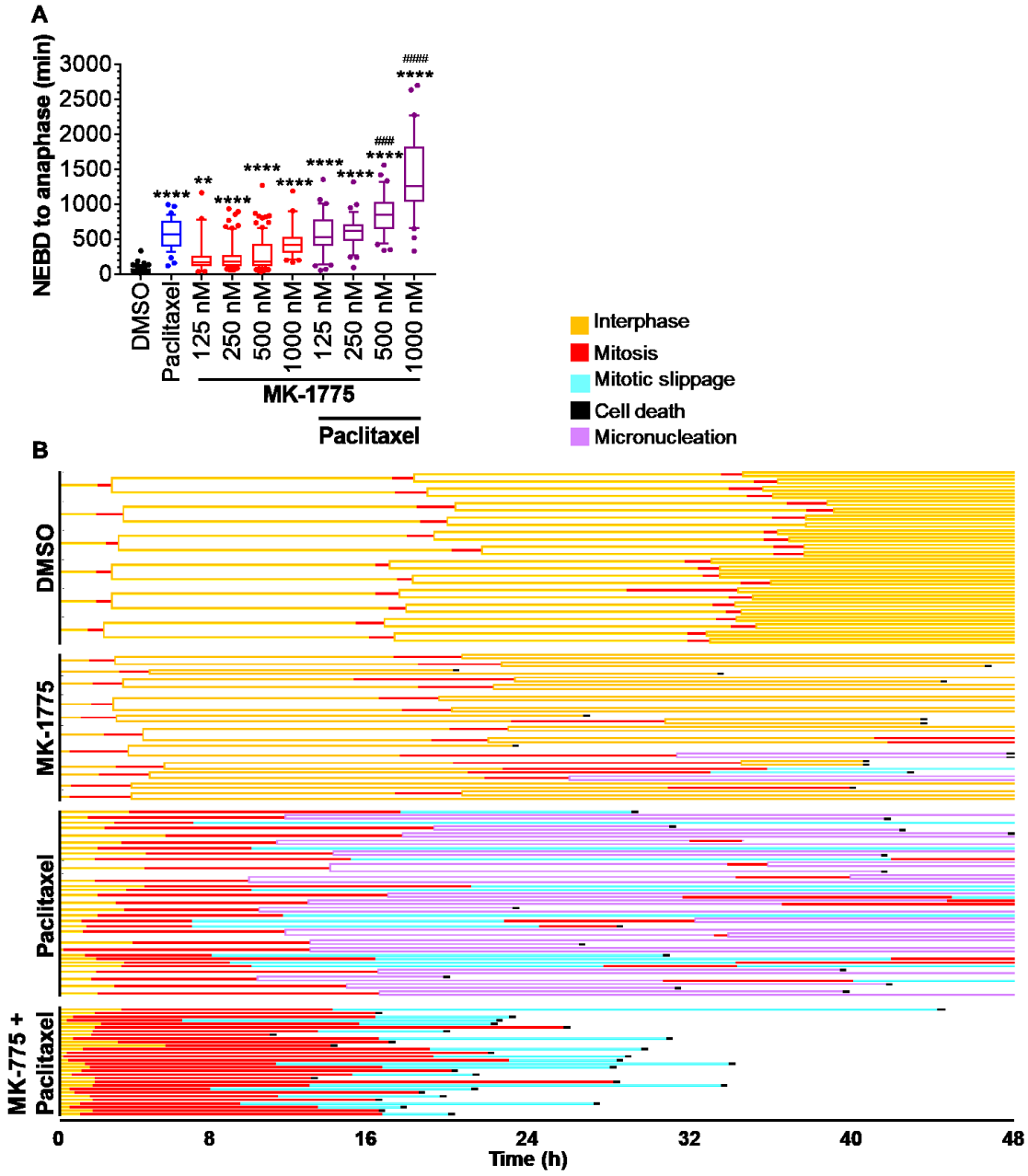

Figure 2.9. MK-1775 induced mitotic arrest is enhanced by co-treatment with paclitaxel.

HeLa cells stable expressing GFP-H2B were released from G1/S phase for 9 hours and then treated with DMSO, 10 nM paclitaxel, MK-1775 at indicated concentration alone, or both paclitaxel and MK-1775 for 48 h. **A)** Duration of mitosis (NEBD to anaphase) is shown for at least 30 cells for indicated treatments. Boxes represent interquartile distributions and whiskers represent 10th and 90th percentiles. Coloured dots represent statistical outliers. Statistical significance was determined by One-way ANOVA and Tukey's comparisons test. Asterisk (*) corresponds to significance between DMSO and indicated treatments (**$p < 0.005$ & ****$p < 0.0001$), whereas hashtag (#) corresponds to significant increases between co-treatments with paclitaxel and MK-1775

compared to paclitaxel alone (###p < 0.0005 & ####p < 0.0001). **B)** Cell fate dendrograms corresponding to DMSO, 500 nM MK-1775, 10 nM paclitaxel, or 500 nM MK-1775 and 10 nM Paclitaxel are presented. A line graph for individual mitotic cells tracked by time-lapse microscopy is shown, which includes time for an indicated cellular event. A fork in the line indicates cell division.

Table 2.3. Average time spent in mitosis and percentage of cell death in the presence of MK-1775 and paclitaxel.

	DMSO						10 nM Paclitaxel			
Treatment	DMSO	10 nM Paclitaxel	125 nM MK	250 nM MK	500 nM MK	1000 nM MK	125 nM MK	250 nM MK	500 nM MK	1000 nM MK
Mitosis (min)	72.1	570.6	245.1	258.0	280.7	432.3	567.4	600.1	847.7	1392.3
Mitotic cell death	0.0%	3.7%	0.0%	9.0%	5.4%	22.0%	12.0%	4.1%	37.5%	68.8%
Interphase cell death	0.6%	33.3%	18.3%	19.1%	27.0%	78.0%	52.0%	44.9%	62.5%	25.0%
Total cell death	0.6%	37.0%	18.3%	28.1%	32.4%	100.0%	64.0%	49.0%	100.0%	93.8%

mitosis, we observed that co-treatments increased cell death in mitosis and interphase (following mitosis exit). Mono-treatments of paclitaxel and 500 nM MK-1775 resulted in 37% and 32% cell death respectively; however, combination treatments with both paclitaxel and 500 nM MK-1775 resulted in the death of all cells monitored (**Figure 2.9B** and **Table 2.3**). This data support that prolonging the Wee1 induced mitotic arrest can be used to enhance cell killing.

Since combination treatments with MK-1775 and paclitaxel led to a greater mitotic transit time and increased cell death in HeLa cells, we then tested if combining paclitaxel and MK-1775 could enhance cell killing in different breast cancer cell lines (T-47D, MDA-MB-231, MDA-MB-468, and MCF7). We first treated the different cell lines with different concentrations of MK-1775 (125-1000 nM) alone or in the presence of different concentrations of paclitaxel (2.5-10 nM) for 48 h. We then measured the average percent survival (percent crystal violet OD) of attached cells by crystal violet assay (**Figure 2.10**).

Alone, both paclitaxel and MK-1775 significantly reduced the percentage of surviving attached cells as determined by a Two-way ANOVA test (**Table 2.4**, see the first two *P*-values corresponding to MK-1775 and paclitaxel for the indicated cell lines). As predicted the combination of paclitaxel and MK-1775 also had a significant interaction on cell survival in HeLa and the four breast cancer cell lines tested (**Figure 2.10A-E** and **Table 2.4**, see third *P*-value [interaction] for the corresponding cell lines). We also tested co-treatments with MK-1775 and paclitaxel in a non-tumorigenic breast cell line (MCF 10A), but we did not observe a significant interaction between MK-1775 and paclitaxel (**Figure 2.10F** and **Table 2.4**). These data support that inhibition of Wee1 in the presence of paclitaxel can enhance cell killing in breast cancer cell lines.

Please also see:

See Appendix A for additional data showing that co-inhibition of Wee1 and ATR induces premature mitotic entry, centromere fragmentation, and prolonged mitotic arrest (Bukhari et al., 2019).

See appendix B for additional (unpublished) data comparing the combined affects of MK-1775 with other anti-mitotic agents: Farnesyl transferase inhibitor (L-744-832), Aurora inhibitor (ZM447439), siRNA knockdown of PP1 subunit SDS22.

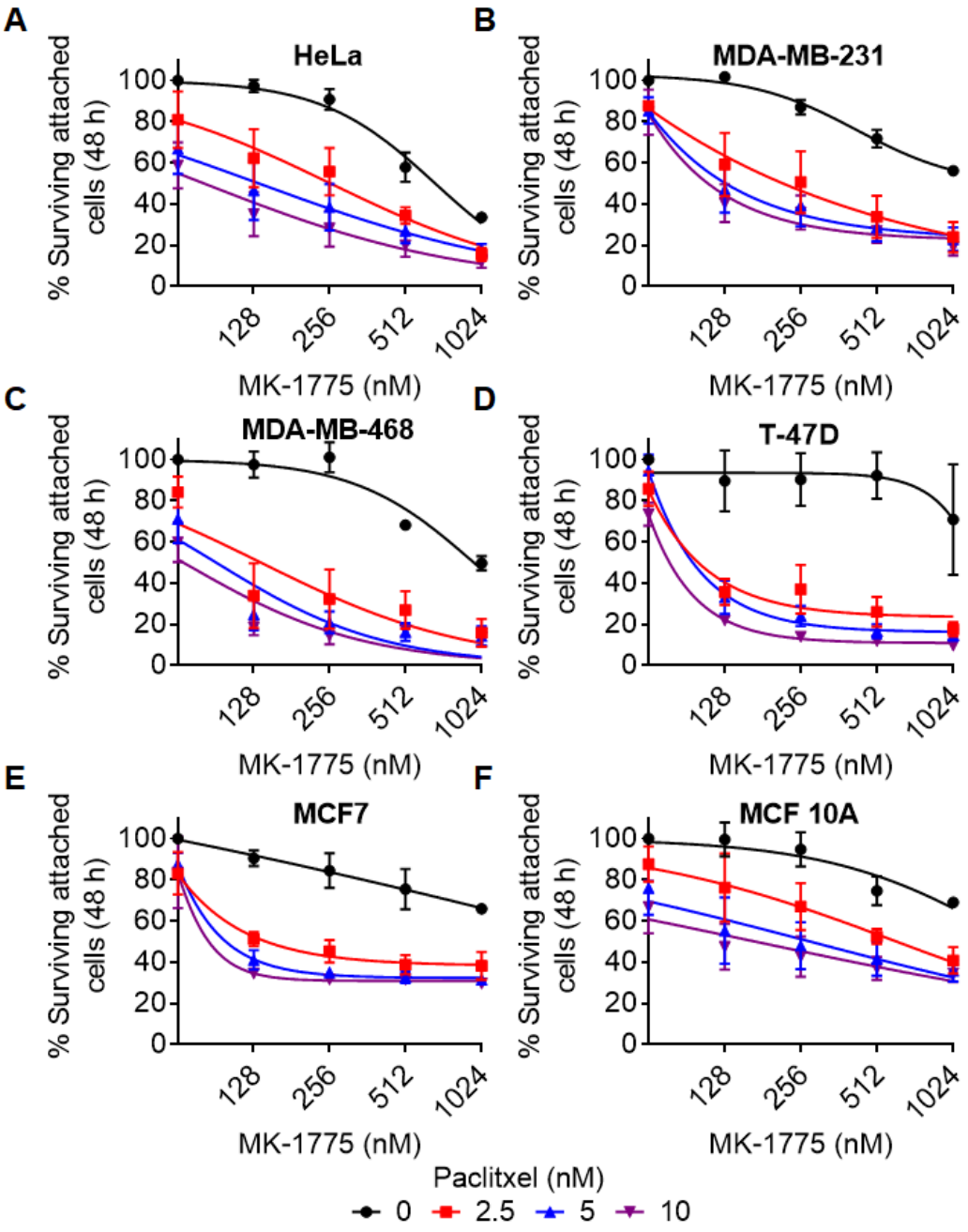

Figure 2.10. Paclitaxel enhances MK-1775 mediated cell killing in breast cancer cells.
A) HeLa, **B)** MDA-MB-231, **C)** MDA-MB-468, **D)** T-47D, **E)** MCF7, and **F)** MCF 10A cells were released from G1/S phase for 9 h and then treated with increasing concentration of MK-1775 alone (black curve) or in the presence of 2.5 nM (red curve), 5 nM (blue curve), or 10 nM (purple curve) paclitaxel for 48 h. Average percent surviving attached cells (% Crystal violet OD) is shown. Error bars represent standard error of mean (SEM). Statistical significance was determined by Two-way ANOVA.

Table 2.4. Paclitaxel and MK-1775 co-treatment significantly reduces cell survival.

Cells were treated with increasing concentration of MK-1775 alone or in the presence of increasing concentrations of paclitaxel. Table presented for each cell line shows statistical analysis of treatments determined by Two-way ANOVA. SS, DF, MS, FDn, and FDd are defined as sum of squares, degrees of freedom, mean square, degrees of freedom numerator, and degrees of freedom dominator respectively.

HeLa					
ANOVA table	SS	DF	MS	F (DFn, DFd)	P value
MK-1775	31590	4	7898	F (4, 12) = 31.43	P<0.0001
Paclitaxel	23037	3	7679	F (3, 9) = 15.63	P=0.0007
Interaction: MK-1775 x Paclitaxel	3120	12	260	F (12, 36) = 7.372	P<0.0001
Interaction: MK-1775 x Subjects	3016	12	251.3		
Interaction: Paclitaxel x Subjects	4423	9	491.4		
Subjects	9603	3	3201		
Residual	1270	36	35.27		
MDA-MB-231					
ANOVA table	SS	DF	MS	F (DFn, DFd)	P value
MK-1775	32916	4	8229	F (4, 12) = 29.33	**P<0.0001**
Paclitaxel	22250	3	7417	F (3, 9) = 16.53	**P=0.0005**
Interaction: MK-1775 x Paclitaxel	3039	12	253.3	F (12, 36) = 4.076	**P=0.0005**
Interaction: MK-1775 x Subjects	3367	12	280.6		
Interaction: Paclitaxel x Subjects	4039	9	448.7		
Subjects	6514	3	2171		
Residual	2237	36	62.14		
MDA-MB-468					
ANOVA table	SS	DF	MS	F (DFn, DFd)	P value
MK-1775	21388	4	5347	F (4, 8) = 40.47	**P<0.0001**
Paclitaxel	32402	3	10801	F (3, 6) = 24.76	**P=0.0009**
Interaction: MK-1775 x Paclitaxel	4878	12	406.5	F (12, 24) = 4.922	**P=0.0004**
Interaction: MK-1775 x Subjects	1057	8	132.1		
Interaction: Paclitaxel x Subjects	2618	6	436.3		
Subjects	1342	2	671.1		
Residual	1982	24	82.58		
T-47D					
ANOVA table	SS	DF	MS	F (DFn, DFd)	P value
MK-1775	26498	4	6624	F (4, 8) = 23.76	**P=0.0002**
Paclitaxel	34684	3	11561	F (3, 6) = 23.64	**P=0.0010**
Interaction: MK-1775 x Paclitaxel	5181	12	431.7	F (12, 24) = 3.288	**P=0.0063**
Interaction: MK-1775 x Subjects	2230	8	278.8		
Interaction: Paclitaxel x Subjects	2935	6	489.1		
Subjects	2235	2	1118		
Residual	3152	24	131.3		
MCF7					
ANOVA table	SS	DF	MS	F (DFn, DFd)	P value
MK-1775	11633	4	2908	F (4, 4) = 30.78	**P=0.0029**
Paclitaxel	10673	3	3558	F (3, 3) = 15.42	**P=0.0251**
Interaction: MK-1775 x Paclitaxel	1330	12	110.8	F (12, 12) = 4.56	**P=0.0068**
Interaction: MK-1775 x Subjects	378	4	94.5		
Interaction: Paclitaxel x Subjects	692.3	3	230.8		

Subjects	195	1	195		
Residual	291.6	12	24.3		
MCF 10A					
ANOVA table	SS	DF	MS	F (DFn, DFd)	P value
MK-1775	10581	4	2645	F (4, 8) = 30.49	**P<0.0001**
Paclitaxel	15637	3	5212	F (3, 6) = 8.241	**P=0.0150**
Interaction: MK-1775 x Paclitaxel	1026	12	85.5	F (12, 24) = 1.408	P=0.2291
Interaction: MK-1775 x Subjects	694.1	8	86.76		
Interaction: Paclitaxel x Subjects	3795	6	632.5		
Subjects	4908	2	2454		
Residual	1458	24	60.73		

2.5 Discussion

2.5.1 MK-1775 induces centromere fragmentation, a key morphological feature of mitotic catastrophe

Wee1 kinase is a pivotal negative regulator of Cdk1/cyclin B1 activity and is required for normal entry into and exit from mitosis. We find that loss of Wee1 activity promotes both premature mitosis and a prolonged mitotic arrest leading to cell death. Normally, HeLa cells that are released from G1/S phase require 8-10 h to complete DNA replication and to synthesize other crucial biomolecules before entering mitosis (Whitfield et al., 2002). However, in our experiments 4-6 h after treatment with MK-1775 one-quarter of G1/S-synchronized cells entered mitosis and half of these cells had less than 4N DNA. This data confirms that MK-1775-treated cells entered mitosis prematurely without completing DNA replication. Premature mitosis is typically associated with mitotic catastrophe, a mode of cell death that is yet to be defined by a molecular pathway (Galluzzi et al., 2012). In addition to premature mitosis, mitotic catastrophe is also associated with centromere fragmentation, micronucleation, and prolonged mitosis (Beeharry et al., 2013; Galluzzi et al., 2012).

We characterized the morphology of the premature mitotic cells and found that they exhibited key features of centromere fragmentation (Beeharry et al., 2013). Centromere fragmentation has been reported to occur in both Chinese hamster ovarian (Brinkley et al., 1988) and human cell lines (Beeharry et al., 2013) that are forced into mitosis with damaged DNA from an S-phase arrest. Cells treated with MK-1775 had centromeres (marked by ACA) and kinetochore proteins (marked by Rod) that co-localized away from condensed DNA (**Figure 2.4A**). This finding is consistent with that reported by Beeharry *et al*., who reported that during centromere fragmentation, the centromeres and kinetochore proteins such as Mis12, Aurora B, and CENP-F co-localized away from the bulk of the condensed DNA in pancreatic cancer cells (Beeharry et al., 2013). Furthermore, a previous study showed that cells that survive treatment with MK-1775 often exhibit micronuclei or micronucleation (Aarts et al., 2012), which is a consistent outcome for cells that have previously undergone an abnormal mitosis (Fenech et al., 2011), such as centromere fragmentation. Our data confirms for the first time that loss of Wee1 activity in G1/S synchronized cells induces centromere fragmentation, which prevents chromosome alignment and segregation.

2.5.2 Wee1 exhibits dominant regulation over Cdk1 in HeLa cells

Wee1 and Myt1 exhibit partial functional redundancy in the regulation of Cdk1 in some model system such as *Drosophila* (Jin et al., 2008). However, both the inhibition and knockdown of Wee1 induced premature mitosis in HeLa and some breast cancer cell lines, whereas Myt1 knockdown alone did not induce premature mitosis or centromere fragmentation (**Figure 2.3** and **Figure 2.5**). This suggests that Wee1 exhibits a dominant role in regulating Cdk1 and mitosis in HeLa cells. Our results are consistent with others

who have reported that Myt1 knockdown does not affect entry or exit of mitosis in unperturbed HeLa cells (Coulonval et al., 2011; Nakajima et al., 2008). We also did not observe an increase in the number of cells in mitosis following combined knockdown of Wee1 and Myt1 compared to that of Wee1 alone after 24 h, which suggest that the levels of Myt1 in non-transfect HeLa cells are already too low to protect most cells from premature mitosis. However, we cannot rule out the possibility that a longer siMyt1 transfection time (> 24 h) may enhance the effects of Wee1 inhibition or knockdown.

2.5.3 MK-1775 treatment induces cell death in a manner consistent with other anti-mitotic drugs

We confirmed that Wee1 inhibition prolongs mitosis (Chow et al., 2011; Lianga et al., 2013; Vassilopoulos et al., 2014; Visconti et al., 2015; Visconti et al., 2012), and we show that increased time in mitosis results in cell death. We found that cells released from both G1/S phase and prometaphase exhibited longer times in mitosis (**Figure 2.4B & C**), which is commonly observed during mitotic catastrophe. Cells that exhibited centromere fragmentation remained in mitosis for several hours before exiting and subsequently dying (**Figure 2.4C** and **Supplementary Figure 2.2**). However, while in mitosis Rod was localized to the kinetochore (**Figure 2.4A**) suggesting that the mitotic checkpoint was active (Chan et al., 2000; Karess, 2005). Mitotic checkpoint activation and mitotic arrest will occur if there are chromosome attachment errors (Foley and Kapoor, 2013). Therefore, a mitotic arrest was expected in cells exhibiting centromere fragmentation because normal bipolar chromosome attachment could not be achieved. However, we observed that Wee1 inhibition prolonged mitosis in cells that did not prematurely enter mitosis or undergo centromere fragmentation. This observation is consistent with others who have reported

that Wee1 inhibition or knockdown delays mitotic exit in cells previously synchronized in prometaphase (Chow et al., 2011; Visconti et al., 2015; Visconti et al., 2012). In support of this, we found that prometaphase synchronized cells with fully replicated chromosomes that were capable of normal bipolar attachment, still arrested in mitosis when treated with MK-1775. We used time-lapse microscopy and resolved that this arrest occurred in metaphase but was not due to centromere fragmentation. During the metaphase arrest, cells experienced multiple spindle collapses and overall were found to require ~5 times longer to complete mitosis (or ~12 times longer to transition from metaphase to anaphase) compared to DMSO controls (**Figure 2.6**). Following this mitotic arrest, 26% of cells died in mitosis and 60% of cells died in interphase within ~12 h of anaphase (**Figure 2.8** and **Table 2.2**). Cell death in both mitosis and interphase following prolonged mitosis has been previously documented in HeLa, A549, and HCT-116 cells that were treated with other anti-mitotic drugs such as nocodazole, paclitaxel, and a small molecule inhibitor of Eg5 (AZ-138) (Gascoigne and Taylor, 2008). The driving mechanism of MK-1775 mediated cell killing has been suggested to be premature entry into mitosis from S-phase (Aarts et al., 2012; Hirai et al., 2009). However, our data show that MK-1775 also causes cell death by delaying mitotic exit (independent of centromere fragmentation or premature mitosis). This mode of cell death is consistent with that of other anti-mitotic drugs (Foley and Kapoor, 2013; Gascoigne and Taylor, 2008; Gascoigne and Taylor, 2009). We also detected further evidence of mitotic catastrophe; 27% of daughter cells exhibited either micronucleation or contained extra-nuclear structures (Galluzzi et al., 2012; Vitale et al., 2011), which likely arose due to repeated spindle collapses (Marcelain et al., 2012).

2.5.4 Sustained Cdk1 activity prolongs mitosis leading to cell death

We believe that sustained Cdk1 activity in the presence of MK-1775 initiates cell death. Treatment with other anti-mitotic drugs such as paclitaxel or nocodazole are reported to induce the upregulation of pro-apoptotic proteins (Bax) and downregulation of anti-apoptotic proteins (Mcl-1, Bcl2, Bcl-X_L, and XIAPs) (Bennett et al., 2016; Colin et al., 2015; Hain et al., 2016; Shi et al., 2008; Sloss et al., 2016). Cdk1 initiates the degradation or inhibition of at least some of these factors (Mcl-1, Bcl2, and Bcl-X_L) through phosphorylation during a mitotic arrest (Sloss et al., 2016; Terrano et al., 2010) and the inhibition of Cdk1 by Wee1 inhibits apoptosis and promotes cell survival (Guzman et al., 2009). In our study, high levels of cyclin B and low levels of pY15-Cdk1 were observed in HeLa, U-2 OS, MDA-MB-231 and T-47D cells arrested in mitosis following treatment with MK-1775 (**Figure 2.6D-F** and **Figure 2.7**). Our findings are consistent with those of Visconti *et al*. who reported prometaphase synchronized cells exposed to MK-1775 or transfected with a inactive Wee1 mutant (Wee1-T239D) retain high cyclin B1 and low pY15-Cdk1 levels for up to 10 hours (Visconti et al., 2015). Failure to phosphorylate Cdk1 and degrade cyclin B indicate that Cdk1 is active in cells treated with MK-1775, which would allow Cdk1 to initiate apoptosis.

2.5.5 MK-1775 sensitizes breast cancer cells to paclitaxel

Since inhibition of Wee1 activity with MK-1775 prevents normal mitotic exit, we tested if co-treating cells with the microtubule poison paclitaxel could be used to enhance cell killing compared to treating cells with either paclitaxel or MK-1775 alone. Paclitaxel is used in adjuvant therapy in breast cancers as well as a single agent therapy for metastatic cancers (Senkus et al., 2015). Paclitaxel treatment also prolongs mitosis, which has been suggested to be a driving mechanism of cell death (Foley and Kapoor, 2013; Gascoigne

and Taylor, 2009). Importantly, many patients do not respond with monotherapies with either MK-1775 or paclitaxel.

In our experiments, we examined the response of breast cancer cell lines to cotreatment with paclitaxel and MK-1775. We found that combining paclitaxel with MK-1775 (500-1000 nM) significantly increased total time in mitosis compared to either treatment alone in HeLa cells (**Figure 2.9**). We also observed an increase in the percentage of cells that died in co-treated conditions compared to mono-treatments (**Figure 2.9B** and **Table 2.3**). These experiments were consistent with crystal violet assay results, where we found that paclitaxel enhanced MK-1775 in four different breast cancer cell lines tested (T-47D, MDA-MB-231, MDA-MB-468, and MCF7) and vice versa (**Figure 2.10B-E**) but not in the non-tumorigenic breast cell line (MCF 10A). Since MK-1775 did not enhance MCF 10A cell sensitivity to paclitaxel, combined treatments maybe more selective towards cancer cells but this would need to be validated in a panel of normal cell lines. In either case, our findings are consistent with a recent study that showed MK-1775 sensitized MOLT-4 cells and patient derived Acute Lymphoblastic Leukemia (ALL) cells to paclitaxel and other microtubule poisons (vincristine, and nocodazole) as marked by an increase in apoptosis and a reduction in cell viability (Visconti et al., 2015). Interestingly, breast cancer cells treated with paclitaxel are reported to down-regulate Wee1 expression (Choi and Yoo, 2012), suggesting that loss of Wee1 activity is an important step in paclitaxel mediated-cell killing. Therefore, if paclitaxel induced cell death requires inactivation of Wee1, then it makes sense that co-treating cells with MK-1775 will result in additional cell killing.

Our data highlight a new potential strategy for enhancing MK-1775 mediated cell killing in breast cancer cells. Currently, paclitaxel is an approved treatment for breast cancer (Gligorov and Richard, 2015) and though MK-1775 is currently undergoing phase I/II clinical evaluations with different anti-cancer agents for the treatment of solid tumours affecting organ such as the cervix, ovaries, lungs, and pancreas, there are no dedicated studies examining the response of breast cancer to MK-1775 and paclitaxel (https://clinicaltrials.gov). Therefore, our data provide a rationale for combining MK-1775 and paclitaxel to treat breast cancer.

2.5.6 Conclusion

MK-1775 is a potent small molecule inhibitor that has two modes of cell killing. First, it can induce premature mitosis leading to centromere fragmentation in G1/S cells. Second, it induces a metaphase arrest because of dysregulated Cdk1 activity in cells synchronized in mitosis. In both cases, the abnormal mitosis induced by MK-1775 results in cell death in mitosis or cell death in interphase several hours following an extended mitosis. Paclitaxel also disrupts and induces a prolonged mitosis. Combining paclitaxel with low dose MK-1775 allows greater cell killing than either treatment alone in breast cancer cell lines.

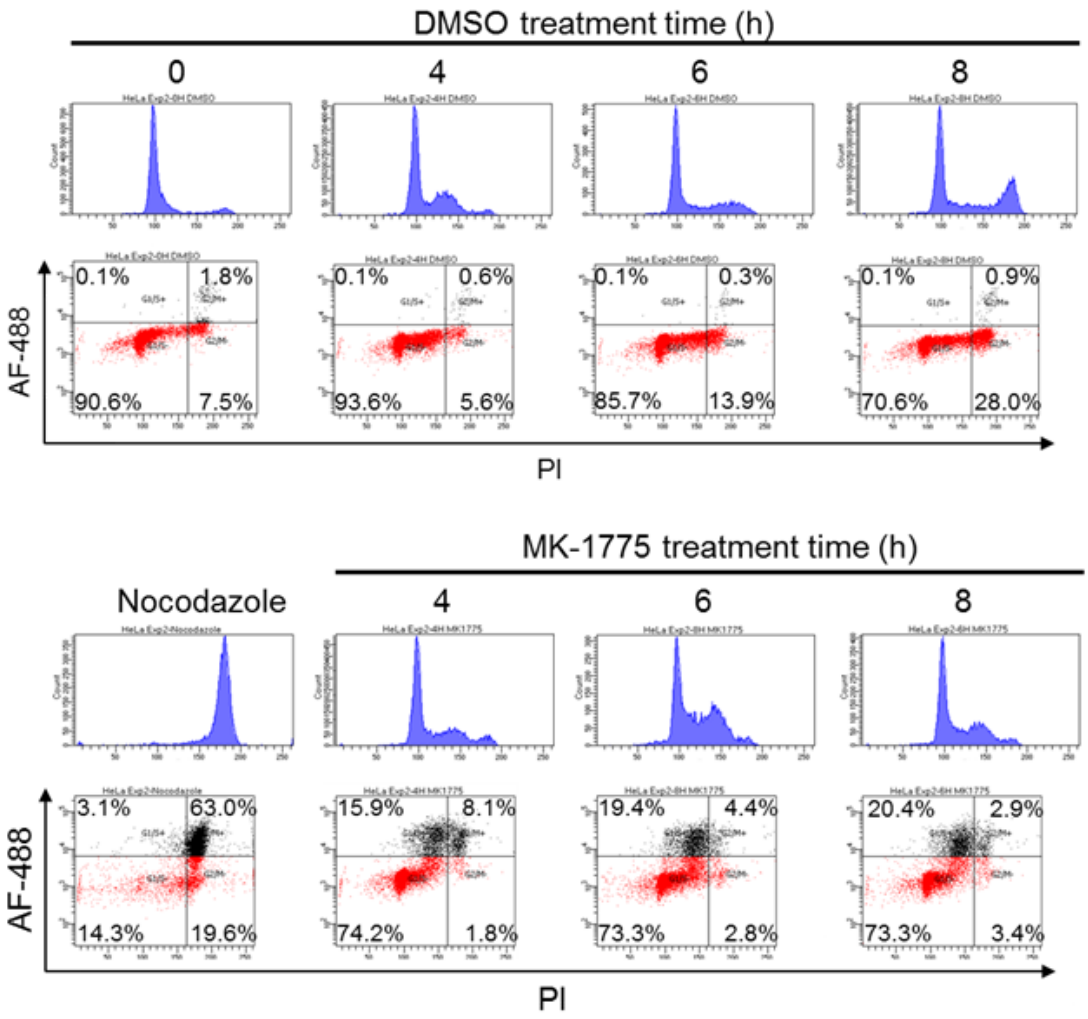

Supplementary Figure 2.1. MK-1775 induces premature mitosis in G1/S synchronized cells.
HeLa cells were synchronized in G1/S phase by double thymidine block and then released into media containing with DMSO or MK-1775. Cells were fixed at indicated times, then stained for phospho-Ser10-histone H3 (PH3) and DNA and analyzed by FACS to determined cell cycle phase. Histogram of DNA content is shown for indicated treatments at each time. Scatterplots show cells positive for PH3 (Black = positive; Red = negative). Right side of each dot blot represents cells in G2/M whereas left side represents cells in G1/S.

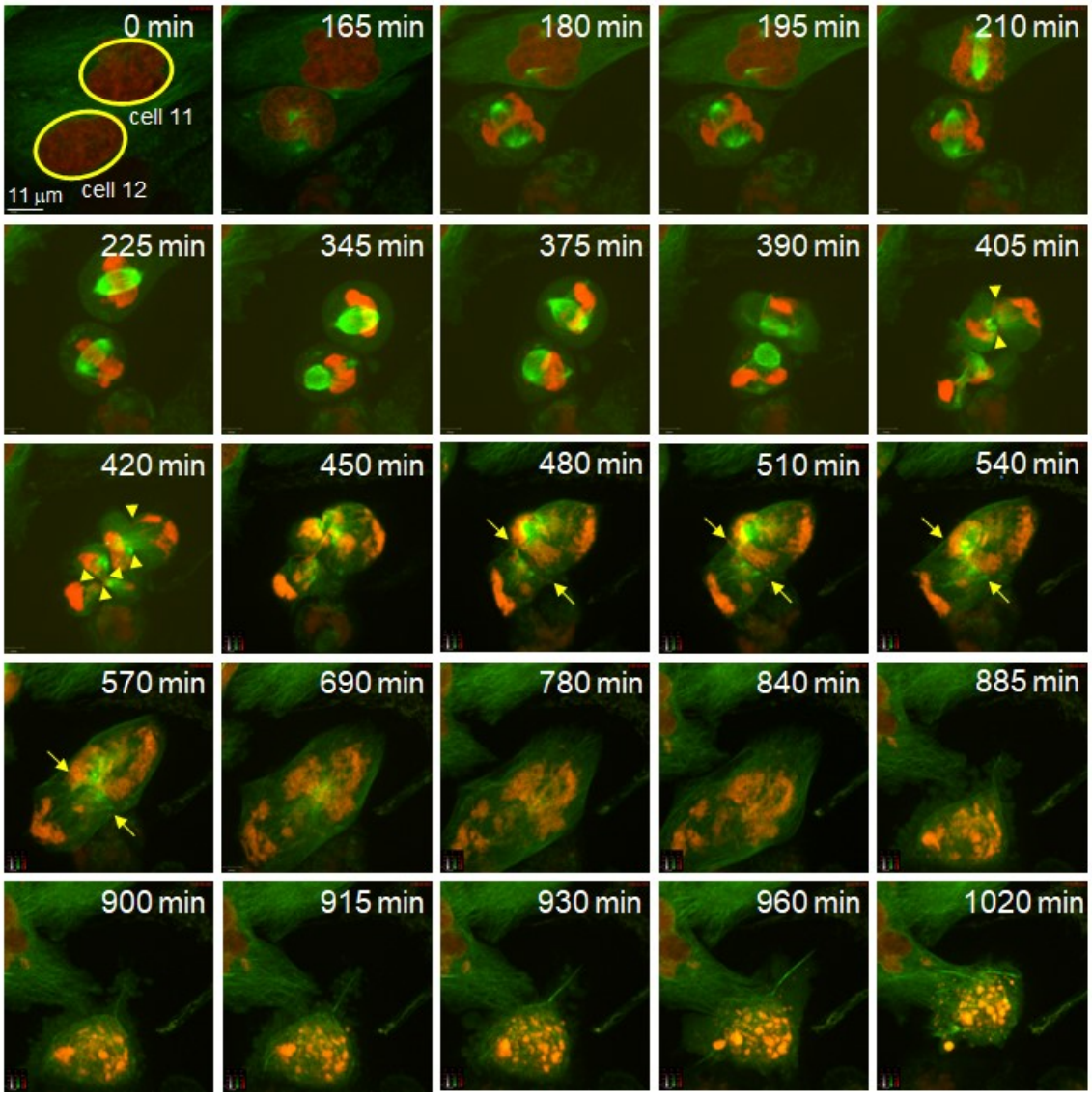

Supplementary Figure 2.2. Inhibition of Wee1 kinase induces prolonged mitosis and cell death.
Timelapse panels of movie showing cells 11 and 12 as an example of the prolonged mitotic arrest and cell death phenotype. Red – mCherry histone H2B; green – EGFP-tubulin; yellow arrow heads indicate planes of cleavage of attempted anaphase; yellow arrows indicate plane of fusion of cells 11 and 12 at approximately 540 min of the movies; scale bar = 11 μm. Time is duration from the start of the timelapse movie. Cell 12 is the same cell depicted in Fig 3B lower panel.

3 Chapter 3. Cancer cells acquire resistance to the Wee1 inhibitor Adavosertib through Myt1 upregulation

3.1 Abstract

Adavosertib (also known as AZD1775 or MK1775) is a small molecule inhibitor of the protein kinase Wee1, with single agent activity in multiple solid tumours, including sarcoma, glioblastoma, and head and neck cancer. Adavosertib also shows promising results in combination with genotoxic agents such as ionizing radiation or chemotherapy. Previous studies have investigated molecular mechanisms of primary resistance to Wee1 inhibition. Here, we investigated mechanisms of acquired resistance to Wee1 inhibition, focusing on the role of the Wee1-related kinase Myt1. Myt1 and Wee1 kinases were both capable of phosphorylating and inhibiting Cdk1/cyclin B, the key enzymatic complex required for mitosis, demonstrating their functional redundancy. Ectopic activation of Cdk1 induced aberrant mitosis and cell death by mitotic catastrophe. Cancer cells with intrinsic Adavosertib resistance had higher levels of Myt1 compared to sensitive cells. Furthermore, cancer cells that acquired resistance following short-term Adavosertib treatment had higher levels of Myt1 compared to mock-treated cells. Downregulating Myt1 enhanced ectopic Cdk1 activity and restored sensitivity to Adavosertib. These data demonstrate that upregulating Myt1 is a mechanism by which cancer cells acquire resistance to Adavosertib.

3.2 Graphical abstract (Cancer Research submission)

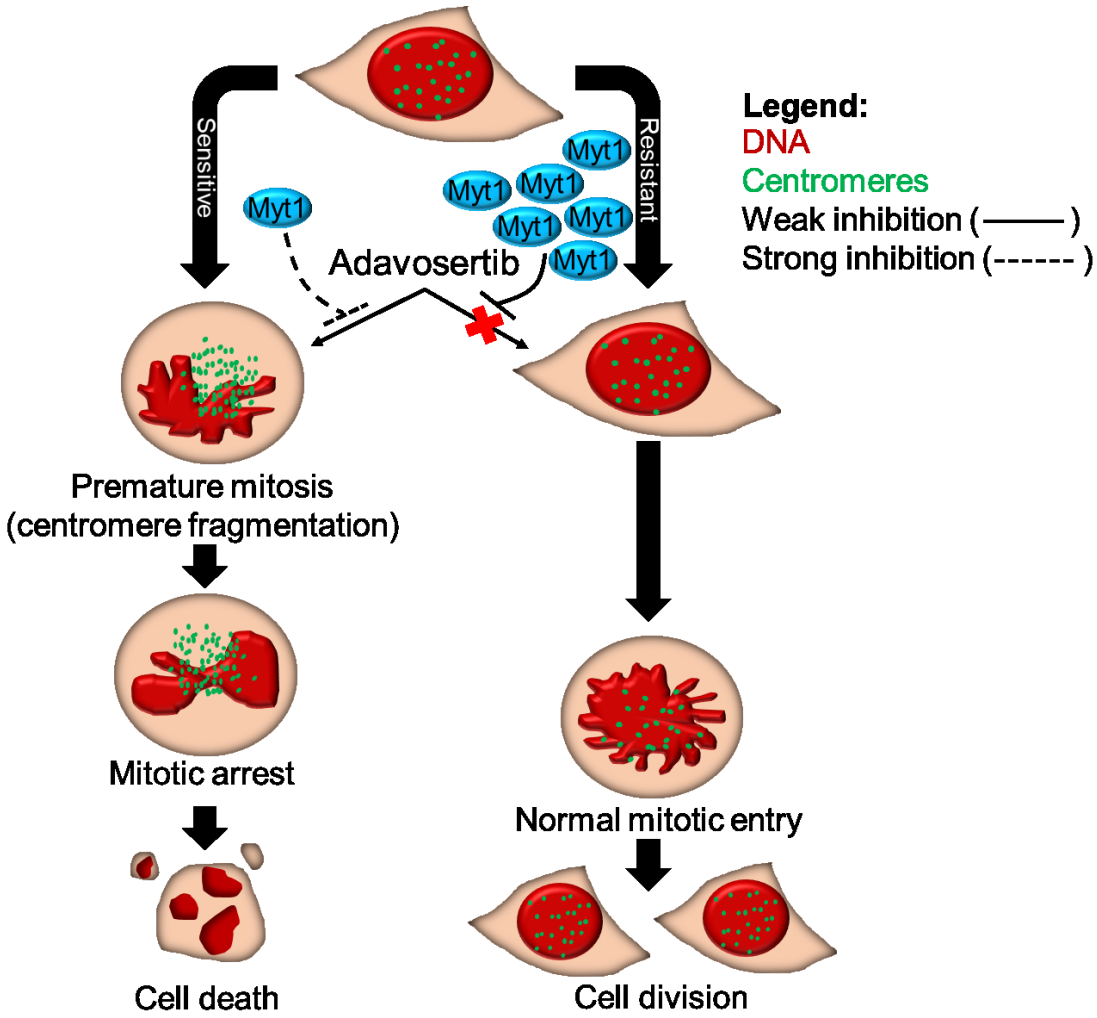

3.3 Introduction

Adavosertib (also known as AZD1775 or MK1775) is a narrow spectrum inhibitor of the protein kinase Wee1 that has single agent clinical activity in multiple solid tumours, including sarcoma, glioma, head and neck cancer, and ovarian cancer (Do et al., 2015; Sanai et al., 2018).

Wee1 activity is crucial for maintaining the S- and G2/M-phase DNA damage checkpoints (Mir et al., 2010; PosthumaDeBoer et al., 2011; Zheng et al., 2017) and as such Adavosertib sensitizes cancer cells to genotoxic treatments including ionizing radiation, gemcitabine, cisplatin and camptothecin (Aarts et al., 2012; Chow and Poon, 2013; Hirai et al., 2010; Hirai et al., 2009; Osman et al., 2015). On its own, Adavosertib treatment forces S-phase HeLa (cervical cancer cells) and breast cancer cells to directly enter mitosis (Aarts et al., 2012; Bukhari et al., 2019; Duda et al., 2016; Lewis et al., 2017). This causes premature condensation of under replicated-chromosomes leading to double-stranded breaks at the centromeres (centromere fragmentation) (Beeharry et al., 2013; Brinkley et al., 1988; Lewis et al., 2017). Subsequently, these cells arrest and die in prometaphase or following mitotic slippage (Lewis et al., 2017). Nevertheless, some tumours do not respond to Adavosertib in the clinic (Do et al., 2015; Van Linden et al., 2013); and the mechanisms underpinning clinical resistance are unknown.

In eukaryotes, Wee1 and the related Myt1 kinase (PKMYT1) (Mueller et al., 1995) exhibit functionally redundant roles in the inhibition of the mitosis promoting complex – Cdk1/cyclin B (Ayeni et al., 2014; Okumura et al., 2002; Palmer et al., 1998). Wee1 phosphorylates Cdk1 on Y15 whereas Myt1 phosphorylates Cdk1 on both T14 and Y15 (Jin et al., 2008; Mueller et al., 1995). When cells are ready to enter mitosis, the

phosphatase Cdc25C removes these inhibitory phosphates from Cdk1 (Russell and Nurse, 1986a; Timofeev et al., 2010). Cdk1 is re-phosphorylated by Wee1 during mitotic exit – again inhibiting its activity (Chow et al., 2011; Lewis et al., 2017; Visconti et al., 2015; Visconti et al., 2012).

Because Wee1 and Myt1 exhibit functional redundancy in Cdk1 inhibition, compensatory Myt1 activation is a candidate mechanism for Adavosertib resistance. However, several studies show that knockdown or inhibition of Wee1 alone is sufficient to abrogate the S- and G2/M DNA damage checkpoints and to cause cells to prematurely enter mitosis (Chow and Poon, 2013; Coulonval et al., 2011; Nakajima et al., 2008; Wells et al., 1999). In contrast, the loss of Myt1 (in the presence of Wee1) neither affects the timing of mitosis nor abrogates DNA damage checkpoints (Chow and Poon, 2013; Coulonval et al., 2011; Nakajima et al., 2008; Wells et al., 1999). These observations led some researchers to conclude that Myt1 is not required for Cdk1 inhibition in cancer cells. However, a more recent study showed that Myt1 is essential for cell survival in a subset of glioblastoma cells that have downregulated Wee1 expression (Toledo et al., 2015). In these glioblastoma cells, loss of Myt1 induced a mitotic arrest followed by cell death (Toledo et al., 2015). Additionally, Chow and Poon reported that the combined knockdown of Wee1 and Myt1 causes more HeLa cells to enter mitosis with damaged DNA compared to Wee1 knockdown alone (Chow and Poon, 2013). Furthermore, Myt1 knockdown enhances Adavosertib induced cell killing in cell lines derived from brain metastases (Guertin et al., 2013).

Although Adavosertib is in clinical development in multiple cancer types, ongoing trials include patients with advanced and metastatic breast cancer. Given the high breast

cancer incident and mortality in North America and Europe (Ferlay et al., 2015), we studied Adavosertib resistance in breast cancer models, and report that Myt1 upregulation mediates intrinsic and acquired Adavosertib resistance through the inhibition of ectopic Cdk1 activity.

3.4 Methods

3.4.1 Cell culture

HeLa cells were received directly from ATCC whereas breast cancer cells were received from Dr. Roseline Godbout (also ordered from ATCC) who amplified, aliquoted, and then froze cells at early passage (P3) in liquid nitrogen. A P3 aliquot was subsequently received and then re-amplified, aliquoted, and frozen by our lab (P6-9). Cell lines were tested for mycoplasma contamination by DAPI staining and confocal imaging. HeLa, MDA-MB-468, MDA-MB-231, SK-BR-3, and BT-474 cells were grown as a monolayer in high-glucose DMEM supplemented with 2 mM L-glutamine and 10% (vol/vol) FBS. T-47D and MCF7 cells were grown in high-glucose DMEM supplemented with 2 mM L-glutamine, 10% (vol/vol) FBS, and 0.01 mg/ml insulin. MCF 10A and HME-1 cells were grown in MEBM supplemented with SingleQuots (Lonza; CC-3150). Cell lines were maintained in culture for a maximum of 2 months (~20-25 passages). MDA-MB-231 cells expressing mCherry-H2B and EGFP-tubulin were generated as outlined by Moudgil *et al*. (Moudgil et al., 2015). MDA-MB-231 cells were transfected with mClover3-10aa-H2B (Bajar et al., 2016). HeLa cells were transfected with mClover3-10aa-H2B (Bajar et al., 2016) and tdTomato-CENPB-N-22 (Gao et al., 2012). All cell lines were cultured in a humidified incubator at 37°C with 5% CO2.

3.4.2 Cell synchronization.

Cells were synchronized in G1/S phase by double thymidine block as outlined in Moudgil *et al*. (Moudgil et al., 2015). Cells were treated with 2 mM thymidine for 16 h with an 8 h release interval between thymidine treatments. For cell synchronization (measuring premature entry into mitosis), cells were released from the 2nd thymidine block for 4 h and then subjected to indicated treatments.

3.4.3 Small molecule inhibitors.

Adavosertib (Chemie Tek; 955365-80-7), RO-3306 (Sigma; SML0569), and thymidine (Sigma; T1895) were prepared as 10 mM solutions in DMSO and then stored at -20°C.

3.4.4 Transfections

siRNA for Wee1 5'-CAUCUCGACUUAUUGGAAAtt-3' (Ambion; siRNA ID: s21), Myt1 5'-GGACAGCAGCGGAUGUGUUtt-3' (Ambion; siRNA ID: s194985) and 5'-GCGGUAAAGCGUUCCAUGUtt-3' (Ambion; siRNA ID: s194986) and a scrambled control siRNA 5'-UGGUUUACAUGUCGACUAA-3' from Thermo Fisher Scientific were used at a concentration of 20 nM (unless otherwise indicated) with 0.2% Lipofectamine RNAiMax (Thermo Fisher Scientific) for 24 h prior to treatments with Adavosertib. In the siWee1 dilution assay, the amount of RNAiMax Lipofectamine used was fixed at 0.2%. Knockdown efficiency was analyzed by western blot and normalized to tubulin or actin 48 h post transfection.

3.4.5 Orthotopic breast cancer xenograft and drug treatments

2 x 10^6 MDA-MB-231-*fluc2-tdT* cells were mixed with Matrigel (Corning, USA) and 1X PBS (1:1) and injected using a 1 cc syringe with 26G needle in 50 µL volume orthotopically

into inguinal mammary fat pad of 6-8 week old female NSG (NOD/SCID gamma) mice procured from Dr. Lynne Postovit's breeding colony at the University of Alberta. Tumor volume was measured every 4 days with a Vernier caliper and volume was calculated as [length x $(width)^2$] / 2. When tumors reached a volume of about 150 mm^3, mice were randomly segregated into 2 groups (n = 3 per group). Mice received daily treatment with either vehicle (0.5% methylcellulose dissolved in sterile water) or 60 mg/kg Adavosertib via oral gavage for 26 days. Tumors were harvested 24 h post last drug treatment and fixed with 10% formalin for 48 h prior to embedding. All animal work was approved by the *Cross Cancer Institute* Animal Care Committee in accordance with the Canadian Council on Animal Care guideline.

3.4.6 DNA microarray

Total RNA was isolated from frozen breast tumour biopsies, gene microarray analysis, data processing, and reverse transcription-polymerase chain reaction (RT-PCR) were processed as outlined in (Germain et al., 2011; Liu et al., 2011; Liu et al., 2012). One Wee1 (A_23_P127926) and two Myt1 primers (A_24_P105102 and A_23_P398515) were available for analysis. Myt1 primers were then averaged together after confirming that mRNA detection was similar by comparative analysis.

3.4.7 Immunoblot

Cells were harvested and processed for western blot as described previously by Chan *et al*. (Famulski et al., 2011). Protein extracts were separated on 12% polyacrylamide gels for 7-15 min at 200 V. PageRuler Plus Prestained protein ladder (Thermo Fisher Scientific; 26619) was used as a molecular weight marker. Proteins were transferred on to

nitrocellulose for 7-15 min at 25 V by Trans-Blot® Turbo Transfer System. Membranes were blocked with Odyssey blocking buffer (LI-COR Biosciences). Membranes were probed with the following primary antibodies: anti-Wee1 antibodies (Cell Signalling; 4936; 1:1000 dilution), anti-Myt1 antibodies (Cell Signalling; 4282; 1:1000 dilution), anti-Cdc25C antibodies (Cell Signalling; 4688; 1:11000), anti-Cdk1 antibodies (Santa Cruz; sc-54; 1:500 dilution), anti-phospho-tyrosine 15 Cdk1 (Cell Signalling; 9111; 1:1000 dilution), anti-phospho-threonine 14 Cdk1 (1:1000 dilution), anti-tubulin antibodies (Sigma; T5168; 1:4000 dilution), anti-PARP antibodies (Cell Signalling: 9542; 1:1000 dilution), anti-pT320-PP1Cα antibody (Abcam: ab62334; 1:30000), and anti-GST antibody (Rockland: 600-401-200; 1:2000 dilution). Membranes were then incubated with Alexa Fluor-680 conjugated anti-rabbit (Thermo Fisher Scientific; A21109; 1:1000 dilution), anti-mouse (Thermo Fisher Scientific; A21057; 1:1000 dilution), IR800 anti-mouse (LI-COR Biosciences; 827-08364 1:1000 dilution) and IR800 anti-rabbit (LI-COR Biosciences; 926-32211; 1:1000). Membranes were scanned by the Odyssey Fc (LI-COR Biosciences) and then analyzed by Image Studio Lite software.

3.4.8 Immunofluorescence

Cells were processed for immunofluorescence as previously described by (Famulski et al., 2011). Cells were seeded on to coverslips at a density of 5×10^4 cells/ml in a 35-mm dish. Following cell synchronization, cells were treated with either DMSO or Adavosertib at indicated concentrations. Treatments were maintained for 4 h and 0.1% DMSO was used as a control in all experiments. siRNA transfections were performed as outlined in the RNAi section. DNA was stained with 0.1 µg/ml DAPI. Coverslips were stained with the following antibodies: anti-phospho-Ser10 Histone H3 (PH3) antibodies (Abcam; ab5176;

1:1000 dilution), anti-tubulin antibodies (Sigma; T5168; 1:4000 dilution), and anti-centromere antibody (ACA) sera (gift from M. Fritzler, University of Calgary, Calgary, Canada; 1:4000 dilution). Coverslips were mounted with 1 mg/ml Mowiol 4-88 (EMD Millipore) in phosphate buffer, pH 7.4. Alexa Fluor 488–conjugated anti–mouse and anti-rabbit (1:1000 dilution; Molecular Probes), Alexa Fluor 647–conjugated anti–human (1:1000 dilution; Molecular Probes) secondary antibodies were used to visualize protein localization. Images were captured at 63X magnification using a Zeiss LSM 710 Meta Confocal Microscope (Carl Zeiss, Germany). The pinhole diameter was set at 1 airy unit for all channels, and the exposure gain for each channel was kept constant in between image acquisition of all samples.

3.4.9 Immunohistochemistry

Immunohistochemistry was performed on formalin fixed paraffin embedded (FFPE) tissue samples using standard procedures as previously described (Varghese et al., 2014). Briefly, 4 μm slices were sectioned on precleaned Colorfrost Plus microscope slides (Fisher Scientific, USA) using a microtome (Leica, Germany). Tissue samples were baked at 60°C for 2 h and deparaffinized 3 times in xylene for 10 mins each and subsequently rehydrated in a gradient of ethanol washes (100%, 80%, and 50%). Tissue sections were subjected to antigen retrieval in a pressure cooker using 0.05% citraconic anhydride antigen retrieval buffer (pH – 7.4). Tissue samples were blocked with 4% BSA for 30 mins and incubated with primary antibody against Myt1 (1:50; Cell Signalling; 4282) overnight at 4°C. Next day, endogenous peroxidase activity was blocked for 30 mins using 3% H_2O_2, followed by incubation with anti-rabbit HRP labelled secondary antibody (Dako EnVision+ System; K4007) for 1 h at room temperature in the dark. Samples were incubated with DAB+

substrate chromogen (Dako, USA) for brown colour development, counter stained with hematoxylin, and mounted with DPX mounting medium (Sigma, USA). Images were captured using the Zeiss Axioskop2 plus upright microscope (Carl Zeiss) equipped with AxioCam color camera. Images were then analyzed using IHC profiler plugin (Varghese et al., 2014) for ImageJ as previously described (Kumar et al., 2014) . Briefly, images were color deconvoluted to unmix pure DAB and hematoxylin stained areas using the nuclear stained image option in the IHC profiler plugin. DAB stained (brown) nuclei were marked using the threshold feature of ImageJ and assigned an automated score using the IHC profiler macro. The automated score is calculated based on the following formula: Score = [(Number of pixels in a zone) x (Score of the zone)] / (Number of pixels in the image). Wherein, the score of the zone is assigned as 4 for the high positive (+3) zone, 3 for the positive (+2) zone, 2 for the low positive (+1) zone and 1 for the negative (+0) zone (Varghese et al., 2014).

3.4.10 Live cell imaging on spinning disk microscope

Cells were seeded in a 35 mm glass bottom dishes (MatTek Corporation). Glass bottom plates were placed on a motor-controlled stage within an incubator chamber maintained at 37°C and 5% CO_2. Live cell imaging was carried out with the Ultraview ERS Rapid confocal imager (PerkinElmer) on an Axiovert 200M inverted microscope (Carl Zeiss) and a CMOS camera (ORCA-Flash4.0, Hamamatsu) using the 40X objective lens. Images were captured at 5 mins interval for 24 h using the Volocity software. The 488 nm and 561 nm lasers were set at 20% power and 200 ms exposure time. Movie files were exported as OME-TIFF files and further processed in Imaris 9.0.1 (Bitplane) for background subtraction and noise reduction.

3.4.11 High content analysis

Images were taken with a high-content automated microscopy imaging system (MetaXpress Micro XLS, software version 6, Molecular Devices, as outline in Lewis *et al*. (Lewis et al., 2017). Briefly, MDA-MB-231 and HeLa cells were seeded onto a 96 well plate at a density of 4000 cells per well. Single images were captured in each well with a 20× (NA 0.75) objective with the equipped siCMOS camera using bandpass filters of 536/40nm and 624/40 nm. On average 200 cells per well were imaged. The images were then manually analyzed with the MetaXpress software using the mCherry-H2B to mark changes in DNA organization. Mitotic timing was calculated by the interval between nuclear envelope break down (NEBD, indicated by the first evidence of chromosome condensation) to the onset of anaphase (or chromosome decondensation in the case of mitotic slippage). Only cells that entered mitosis were analyzed for mitotic timing experiments and the fates of the mitotic cells (and resulting daughter cells) were tracked for the duration of the experiment (48 h). Cell death was determined by the formation of apoptotic bodies, loss of cell attachment, and/or loss of membrane integrity.

3.4.12 Generation of pT14-Cdk1 antibody

The phospho-specific antibody against pT14-Cdk1 was generated by immunizing rabbits with a synthetic peptide phosphorylated at the T14 residue (conjugated to KLH). Sera was first depleted of antibodies against the unphosphorylated epitopes with a non-phosphorylated peptide column. Cdk1-pT14 antibodies were then affinity-purified with a pT14 peptide column. Specificity of the antibodies was demonstrated by no signal in western blot of mutant myt1 fly extracts.

3.4.13 Crystal violet assay

Cells were seeded into 96-well plates and transfected with siRNAs against Wee1, Myt1, and scrambled control for 24 h. Cells were then treated with increasing concentrations of Adavosertib (16-4000 nM, 1:2 serial dilution). After 96 h treatment, media was aspirated and then cells were stained with 0.5% crystal violet for 20 min as outlined by Bukhari *et al*. (Bukhari et al., 2019). Crystal violet was then removed, and plates were rinsed three times with water and left to air-dry for 24 h. Crystal violet within stained cells was resuspended in 100% methanol. Absorbance at 570 nm was measured using FLUOstar OPTIMA microplate reader (BMG Labtech). Percent cell survival was calculated by subtracting blank wells and then normalizing DMSO controls to 100%. The first point on each curve represents 0 nM Adavosertib. Graphs were plotted using GraphPad Prism V7.

3.4.14 Kinase assay

Cdk1 kinase assays were completed as outlined in Lewis *et al*. (Lewis et al., 2016; Lewis et al., 2013). Briefly, 20 ng of GST fused with a 9 amino acid PP1Cα peptide (GRPITPPRN) was combined with 2000 cells in 2x Cdk1 phospho-buffer (100 mM β-glycerophosphate, 20 mM $MgCl_2$, 20 mM NaF, 2 mM DTT), 400 μM ATP and then incubated at 37°C for 15 min. Reactions were then terminated with Laemmli sample buffer (BioRad; 161-0747) and then analyzed by western blot. The ratio of pT320-PP1Cα to GST, minus "no lysate" control, was calculated for each sample. DMSO was set to one for Adavosertib serial dilution and HeLa for baseline Cdk1 experiment.

3.5 Results

3.5.1 Upregulation of Myt1 confers resistance to Wee1 inhibition in vitro

To test acquired resistance to the Wee1 inhibitor Adavosertib, we derived Adavosertib resistant cell lines from HeLa (cervical cancer) and MDA-MB-231 (breast cancer) cell lines. We and others have previously shown that HeLa and MDA-MB-231 are highly sensitive to Adavosertib as single agent treatment (Aarts et al., 2012; Bukhari et al., 2019; Lewis et al., 2017). We selected for resistant cells by culturing these cell lines in medium containing 500 nM Adavosertib for approximately 2 months (**Figure 3.1A**). The resulting cell populations were tested for Adavosertib sensitivity by crystal violet assays (Bukhari et al., 2019). In the case of both MDA-MB-231 and HeLa, Adavosertib-selected cells (denoted as "R500") showed much higher resistance to the Wee1 inhibitor compared to mock-treated (Parental, "P") cells (**Figure 3.1B-C**). Selection increased the IC50 from 305 nM to 1090 nM in HeLa and from 349 nM to 1217 nM in MDA-MB-231. Since the activities of two related kinases Myt1 and Wee1 were found to be redundant in Cdk1 regulation in various organisms/tissues (Jin et al., 2008; Okumura et al., 2002; Palmer et al., 1998; Toledo et al., 2015), we hypothesized that upregulation of Myt1 could underline Wee1 inhibitor resistance. We therefore compared Myt1 protein levels in the derived Adavosertib-resistant cell lines to the parental cell lines. Indeed, resistant cell populations had increased Myt1 levels; 2.0-fold in HeLa and 3.1-fold in MDA-MB-231 relative to parental cell populations. To test if decreasing Myt1 levels could re-sensitize resistant cells to Adavosertib, we used two different siRNAs to knockdown Myt1 (siMyt1 #1 and #2) and compared Adavosertib sensitivity to siRNA scrambled control treated cells (siSc). Myt1 knockdown in R500 HeLa cells decreased the IC50 from 1261 nM in siSc-treated cells to 283 nM and 373 nM in siMyt1 (#1 and #2) transfected cells respectively (**Figure 3.1D**). In R500 MDA-MB-231 cells, Myt1 knockdown decreased the IC50 from 1447 nM (siSc) to

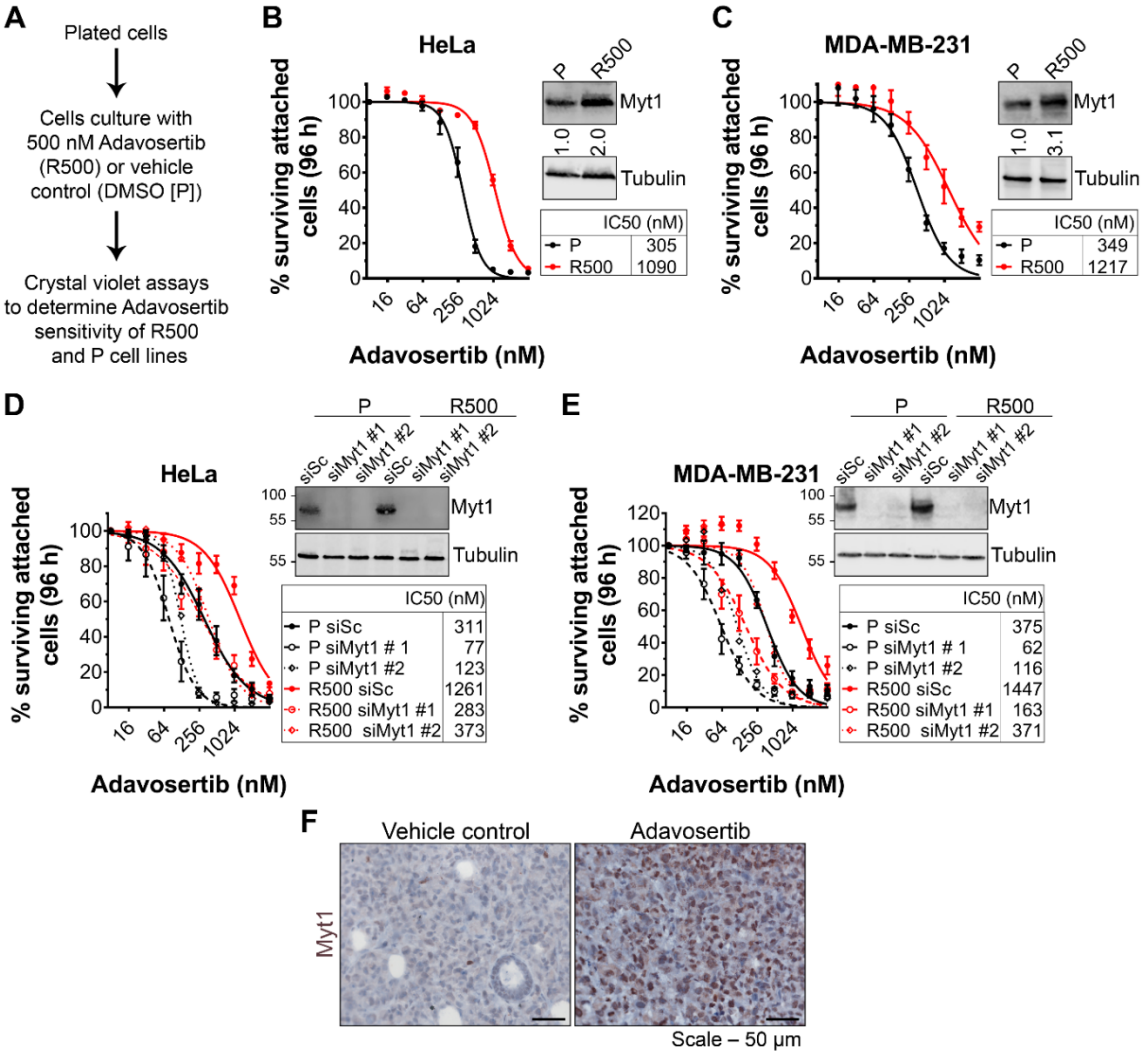

Figure 3.1. Adavosertib acquired resistance correlates with Myt1 upregulation *in vitro* and *in vivo*.
A) Flow chart depicting the generation of Adavosertib resistant cell lines. Adavosertib sensitivity was tested in parental (P) and resistant (R500) HeLa **(B)** and MDA-MB-231 **(C)** cells by crystal violet assays. Error bars represent SEM. Myt1 and tubulin expression was analyzed by immunoblot. Representative images and quantitation of average Myt1 levels (n = 4) relative to tubulin are shown to the right. Adavosertib sensitivity was re-tested in **D)** HeLa and **E)** MDA-MB-231 cells following Myt1 knockdown by siRNA. Myt1 knockdown was confirmed by western blot. **F)** MDA-MB-231 xenograft tumours of mice treated with vehicle control or 60 mg/kg Adavosertib for 26 days were excised on the last day of drug administration. Paraffin embedded tumour slices were analyzed for Myt1 expression by immunohistochemistry. Scale bar = 50 µm.

163 nM and 371 nM for siMyt1 #1 and #2, respectively (**Figure 3.1E**). These data suggest that Myt1 upregulation is a driver of resistance in the R500 HeLa and MDA-MB-231 cell lines.

3.5.2 Selection for Wee1 resistance leads to Myt1 upregulation in vivo

We previously tested the efficacy of Adavosertib treatment in an orthotopic breast cancer xenograft model (Bukhari et al., 2019). In that study using a luciferase labelled MDA-MB-231 cell line, mice were treated with 60 mg/kg of Adavosertib for 26 days. Although Adavosertib treatment caused significant tumor growth delay, no tumor shrinkage was observed (Bukhari et al., 2019). This indicates that the tumours had at least partially acquired Adavosertib resistance. To investigate whether increased Myt1 expression contributed to tumor resistance, we harvested MDA-MB-231-derived tumors from NSG (NOD/SCID gamma) mice immediately after a 26-day treatment with 60 mg/kg of Adavosertib. Tumor slices were analysed for Myt1 expression and Wee1 inhibition by immunohistochemistry (**Figure 3.1F**; n = 3 per group). Tumors treated with Adavosertib showed increased Myt1 expression (+2; positive) compared to vehicle control treated mice (+1; low positive). These results strongly support Myt1 upregulation as a mechanism for acquired Adavosertib resistance *in vivo*.

3.5.3 Cellular Myt1 levels determine Adavosertib sensitivity

To confirm that upregulation of Myt1 can confer Adavosertib resistance, we transiently overexpressed Myt1 tagged with GFP (GFP-Myt1) or GFP alone in HeLa and MDA-MB-

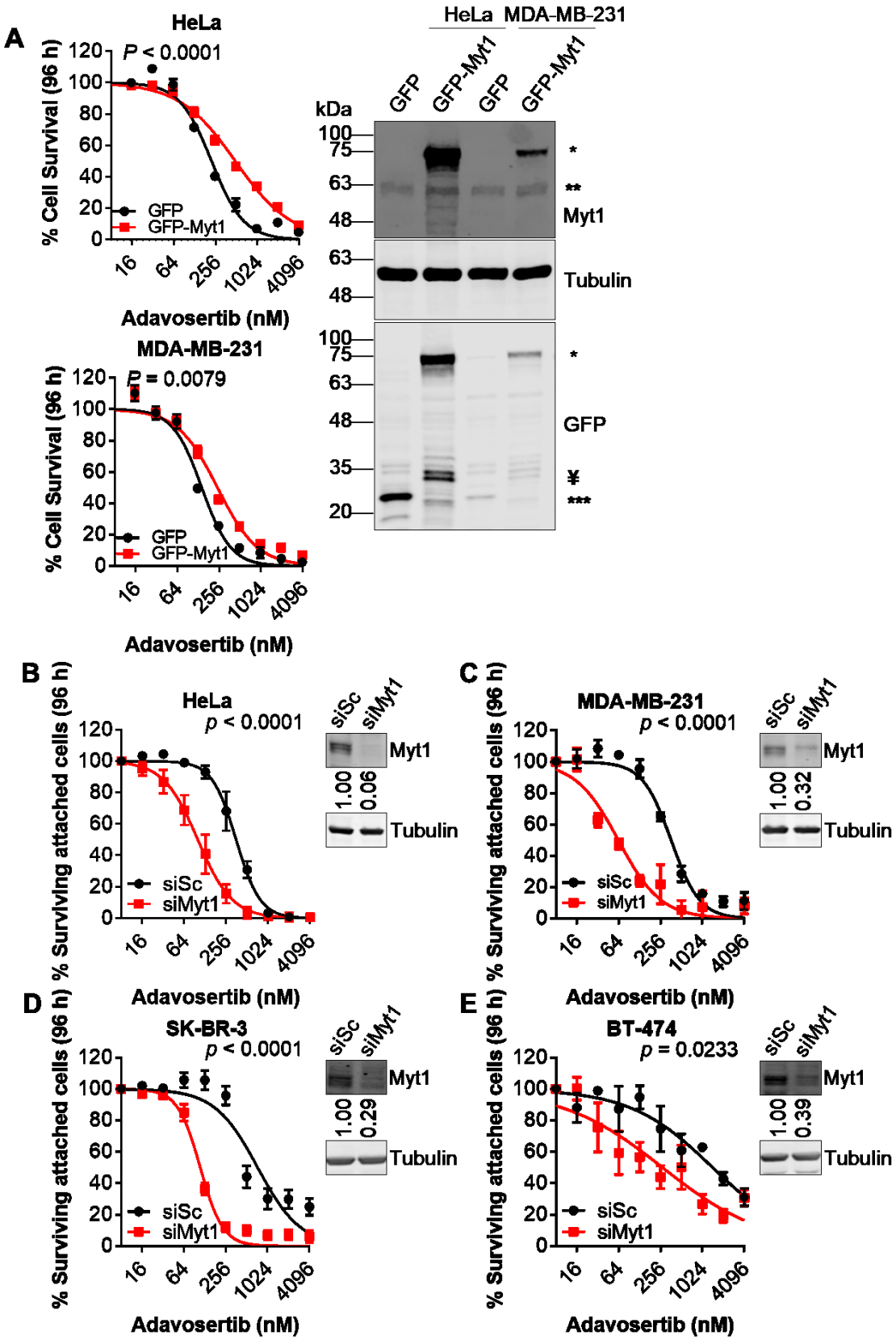
A
HeLa
P < 0.0001
% Cell Survival (96 h)
GFP
GFP-Myt1
Adavosertib (nM)
MDA-MB-231
P = 0.0079
HeLa MDA-MB-231
GFP
GFP-Myt1
kDa
Myt1
Tubulin
GFP
B
HeLa
p < 0.0001
% Surviving attached cells (96 h)
siSc
siMyt1
1.00
0.06
C
MDA-MB-231
p < 0.0001
1.00
0.32
D
SK-BR-3
p < 0.0001
1.00
0.29
E
BT-474
p = 0.0233
1.00
0.39

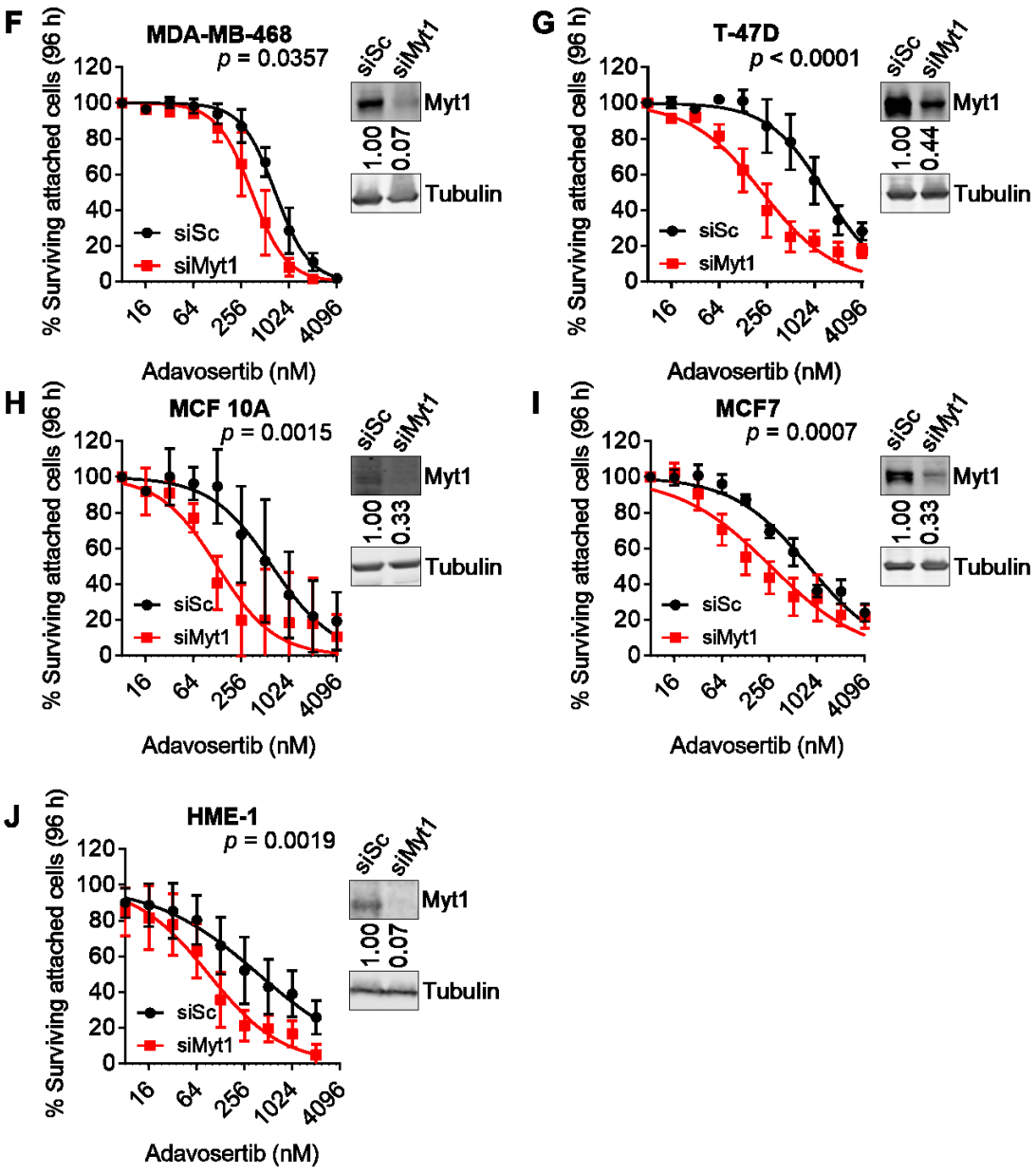

Figure 3.2. Transient overexpression of Myt1 promotes resistance to Adavosertib, whereas Myt1 knockdown enhances sensitivity.
A) HeLa and MDA-MB-231 cells were transiently transfected with either GFP (solid line) or GFP-Myt1 (dotted line) for 24 h and then treated with Adavosertib for 96 h. Cell survival was analyzed by crystal violet assay. Error bars represent SEM. P-values are indicated (Two-way ANOVA). Protein levels of Myt1, tubulin, and GFP were analyzed in both HeLa and MDA-MB-231 cell lines. Exogenous GFP-Myt1 (*) and endogenous Myt1 bands (**) are indicated. *** and ¥ denote untagged GFP and a GFP-Myt1 degradation product respectively. **B)** HeLa, **C)** MDA-MB-231, **D)** SK-BR-3, **E)** BT-474, **F)** MDA-MB-231, **G)** T-47D, **H)** MCF 10A, **I)** MCF7, and **J)** HME-1 cells were transfected with siSc (solid line) or siMyt1 (dotted line) and then treated with Adavosertib for 96 h and surviving attached cells measured by crystal violet assays. Error bars represent SEM. P-

values are indicated (Two-way ANOVA). Myt1 knockdown was determined by immunoblot (right panel) (quantitation of Myt1 relative to tubulin is shown). All experiments were repeated at least three times.

231 cells and then measured cell sensitivity to Adavosertib by crystal violet assays (**Figure 3.2A**). GFP-Myt1 overexpression resulted in a modest but significant increase in the Adavosertib IC50s for both cell lines relative to GFP transfected controls (2.2-fold and 1.7-fold increase in HeLa ($P < 0.001$; Two-way ANOVA) and MDA-MB-231 ($P = 0.0079$; Two-way ANOVA) respectively. Although HeLa exhibited a greater increase in the Adavosertib IC50 compared to MDA-MB-231, HeLa also exhibited higher GFP-Myt1 expression levels compared to MDA-MB-231. Since increased Myt1 expression induced Adavosertib resistance in HeLa and MDA-MB-231, we wondered if endogenous Myt1 expression in other cell lines could be used as a biomarker to predict Adavosertib sensitivity. Adavosertib sensitivity was screened in a panel of breast cell lines (5 cancer and 2 non-tumorigenic [**Table 3.1]**). HeLa and MDA-MB-231 cells were included as positive controls for Adavosertib sensitivity. Cell lines were transfected with siMyt1 or siSc and then treated with Adavosertib for 96 h. Adavosertib treatment reduced cell number in a dose dependent manner in all 9 cell lines tested, and as expected Myt1 knockdown (confirmed by immunoblot) further reduced cell number (**Figure 3.2B-J**). The reduced cell number was associated with an increase in PARP cleavage (a biomarker for apoptosis) in HeLa and MDA-MB-231 cells transfected with siSc or siMyt1 and treated with Adavosertib (250-500 nM) (**Figure 3.3**).

We calculated IC50 values for each cell line (**Table 3.2**). HeLa, MDA-MB-231, and HME-1 cell lines had IC50 values in the 300 nM range, but the remaining 6 cell lines (MCF10A, MDA-MB-468, SK-BR-3, MCF7, T-47D, and BT-474) had IC50 values that

Table 3.1. p53 and molecular subtypes of breast cell lines.
* indicate non-tumorigenic cell lines.

Cell line	Cell type (ATCC)	Tissue type (ATCC)	p53 status (67,68)	Molecular sub-type (69,70)
HeLa	Epithelial	Cervical	Wild type HPV E6 deactivated	N.A.
MDA-MB-231	Epithelial	Mammary gland/breast	Missense R280K	Basal (triple negative)
MDA-MB-468	Epithelial	Mammary gland/breast	Missense R273H	Basal (triple negative)
MCF7	Epithelial	Mammary gland/breast	Wild type	Luminal A (ER+/PR+)
T-47D	Epithelial	Mammary gland	Missense L194F	Luminal A (ER+/PR+)
BT-474	Epithelial	Mammary gland/breast	Missense E285K	Luminal B (PR+/ER-/HER+)
SK-BR-3	Epithelial	Mammary gland/breast	Missense R175H	HER2+ (ER-/PR-)
MCF 10A*	Epithelial	Mammary gland/breast	Wild type	N.A.
HME-1*	Epithelial	Mammary gland/breast	Wild type	N.A.

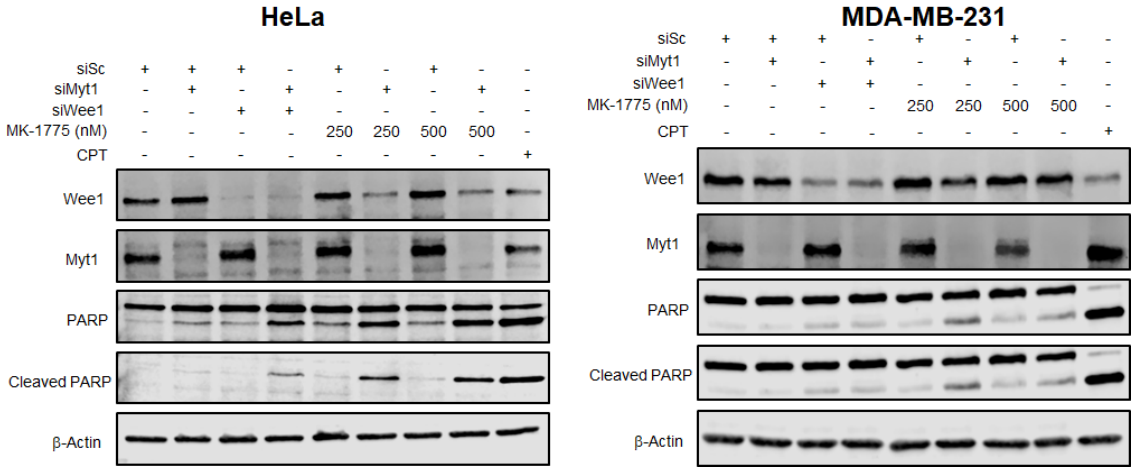

Figure 3.3. Myt1 knockdown induces apoptosis in cells treated with Adavosertib.
HeLa and MDA-MB-231 cells were transfected with siMyt1, siWee1, or siSc for 24 h and then treated with Adavosertib (250-500 nM) for additional 24 h. Cell lysates were prepared and analyzed for total levels of Wee1, Myt1, total PARP, cleaved PARP, and actin by immunoblot. This data was not published in the original manuscript.

Table 3.2. Cell line sensitive to Adavosertib in the presence of siSc or siMyt1.

Cell line	IC50 (nM)		Fold Change
	siSc	siMyt1	
HeLa	356	100	3.5
MDA-MB-231	363	63	5.8
HME-1	388	91	4.3
MCF 10A	630	128	4.9
MDA-MB-468	686	346	2.0
SK-BR-3	736	110	6.7
MCF7	800	267	3.0
T-47D	1400	226	6.2
BT-474	1441	274	5.3

were approximately 2-4 times higher. To investigate how the high IC50 values correlated with Myt1 levels, Myt1 protein levels (normalized to total protein content) were quantified in each cell line **(Figure 3.4A**; top panel) and then plotted against the corresponding IC50 values. Linear analysis revealed a strong correlation between calculated IC50 values and Myt1 protein levels (**Figure 3.4B**; top panel; R^2 = 0.6903) in agreement with our prediction. We also tested if the levels of Wee1 or Cdc25C (the phosphatase responsible for reversing Cdk1 phosphorylation, by Wee1 and Myt1) correlated with cell sensitivity to Adavosertib, but no significant correlations were observed (**Figure 3.4A-B**). These data strongly support that Myt1 levels can be used as predictive biomarkers for cell sensitivity to Adavosertib.

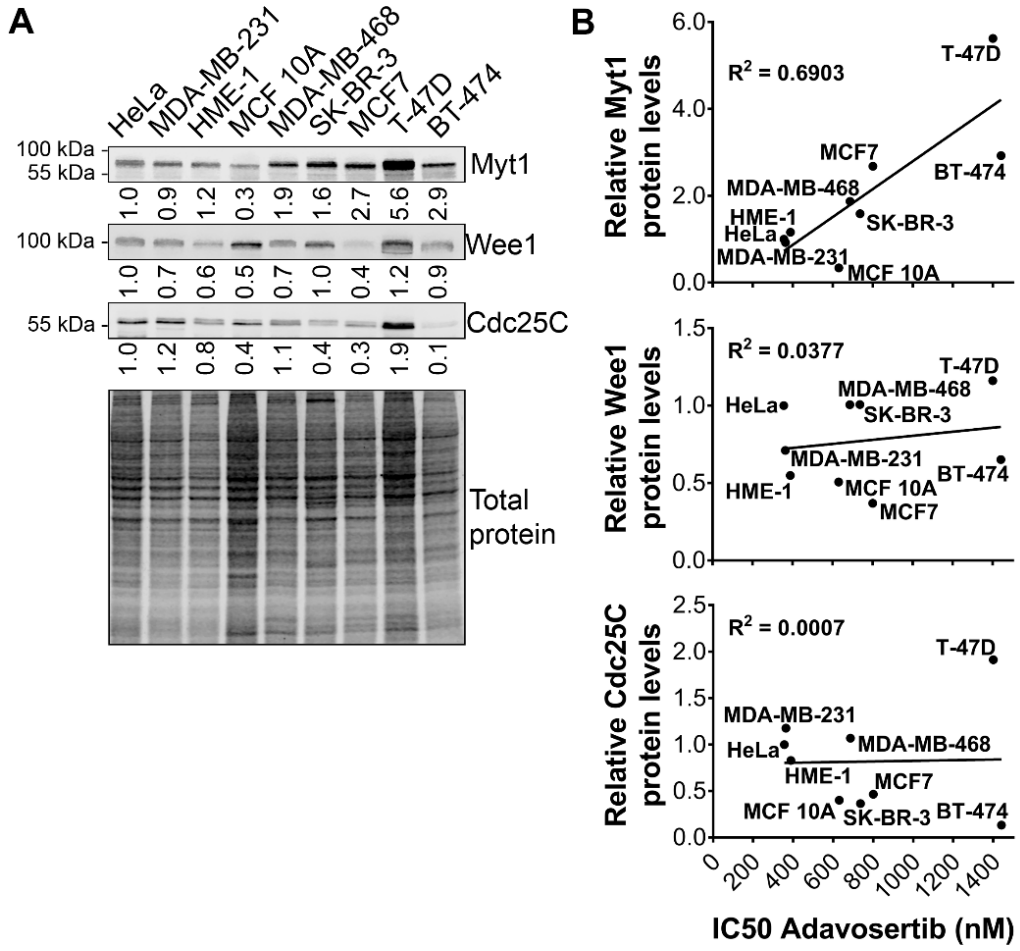

Figure 3.4. High Myt1 protein levels correlate negatively with cancer cell sensitivity to Adavosertib.
A) Cell extracts were prepared from cell lines and analyzed for total Myt1, Wee1, Cdc25C, and total protein by immunoblot. HeLa protein levels were used as reference. Quantitation of Myt1, Wee1, and Cdc25C levels (normalized to total protein) are shown below. **B)** Protein levels of Myt1, Cdc25C, and Wee1 were plotted against Adavosertib IC50 concentrations for various cell lines (**Table 3.2**). Experiments were repeated at least three times.

3.5.4 siRNA knockdown of Wee1 mimics Adavosertib treatment in the presence of siMyt1

In addition to Wee1, Adavosertib also exhibits activity against Polo-like kinse-1 (Plk1) in some cell types including small cell lung carcinoma cells (Serpico et al., 2019; Wright et al., 2017). However, Adavosertib treatment induces premature mitosis in cells consistent with the inhibition of Wee1, whereas inhibition of Plk1 prolongs G2 phase (Gheghiani et al., 2017). To confirm that the reduced cell survival observed following

Adavosertib/siMyt1 treatment was dependent on loss of Wee1 activity and not an off-target effect of Adavosertib, we substituted the treatment with Adavosertib for a validated siRNA targeting Wee1 (siWee1) (Lewis et al., 2017). Select cell lines (HeLa, MDA-MB-231, MDA-MB-468, and T-47D) were transfected with increasing amounts of siWee1 in the background of either siSc or siMyt1 (**Figure 3.5A-D**). siWee1 transfection decreased cell survival in a dose dependent manner. However, cells transfected with siMyt1 + siWee1 had fewer surviving attached cells compared to siSc + siWee1 controls in all four cell lines ($P < 0.0001$; Two-way ANOVA). The reduced surviving attached cells following transfection with siWee1 + siMyt1 was also associated with increased PARP cleavage (**Figure 3.3**). These data corroborate that the observed cell death with Adavosertib and siMyt1 is due to loss of Wee1 and Myt1 activity.

3.5.5 Adavosertib does not inhibit Cdk1 phosphorylation by Myt1

Due to the role of Myt1 in cell cycle regulation, we suspected that Myt1 promotes Adavosertib resistance by maintaining Cdk1 inhibition. Structure-function studies have reported that Adavosertib does not strongly interact with Myt1 and is 100 times more selective towards Wee1 (Hirai et al., 2009; Zhu et al., 2017). To confirm this, we treated MDA-MB-231 and MDA-MB-468 cells with Adavosertib, and then assayed Myt1 and Wee1 activity by examining Cdk1 phosphorylation. In the presence of Adavosertib, the cellular levels of pT14-Cdk1 (a surrogate biomarker for Myt1 activity) remained stable, whereas the levels of pY15-Cdk1 (a surrogate biomarkers of Wee1 activity) declined (**Figure 3.6A & B**). These data show that even 1000 nM Adavosertib does not inhibit Myt1.

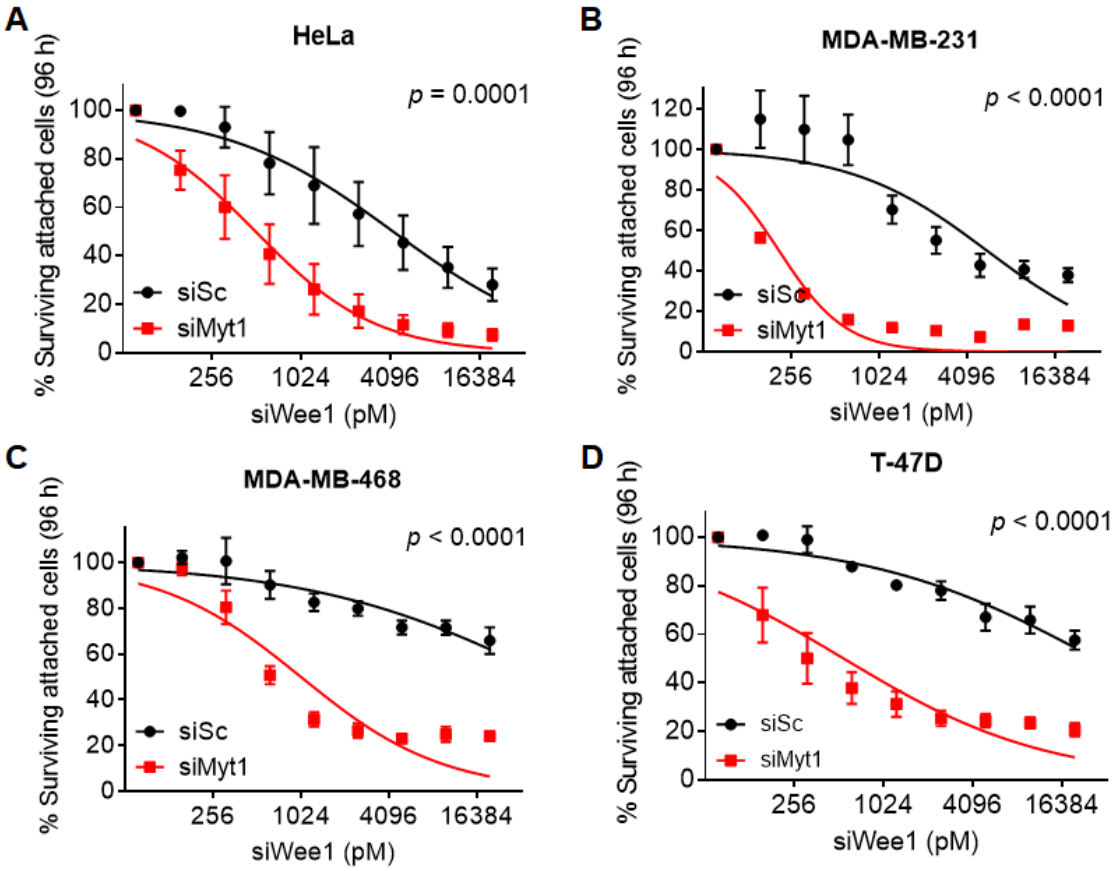

Figure 3.5. Wee1 knockdown mimics Adavosertib treatment.
A) HeLa, **B)** MDA-MB-231, **C)** MDA-MB-468, and **D)** T-47D cells were transfected with siMyt1 or siSc in the presence of increasing concentrations of siWee1 and 0.2% lipofectamine for 96 h. The average percent surviving attached cells was analyzed by violet assay. Error bars represent SEM. Experiments were repeated at least three times. P values are indicated (Two-way ANOVA).

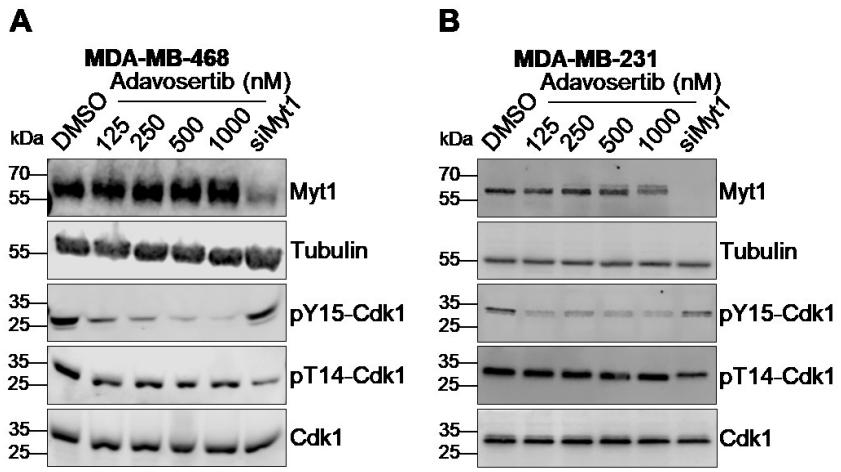

Figure 3.6. Adavosertib does not inhibit Myt1 activity.
Cell lysates were prepared from **A)** MDA-MB-231 and **B)** MDA-MB-468 cells treated with either DMSO or 125-1000 nM Adavosertib for 4 h or transfected with siMyt1 for 48 h. Lysates were analyzed for total levels of Wee1, Myt1, tubulin, pY15-Cdk1, pT14-Cdk1, and Cdk1 by western blot. Experiments were repeated at least three times.

3.5.6 Adavosertib resistant cells have low Cdk1 activity

To confirm that high Myt1 levels inhibit Cdk1 activity even in the presence of Adavosertib, we assayed *in vitro* Cdk1 activity (Lewis et al., 2013). First, we examined if R500 cells had lower activity relative to parental cells. R500 and parental HeLa and MDA-MB-231 were treated with Adavosertib for 4 h following G1/S release. Lysates were then prepared and incubated with a recombinant Cdk1 substrate, GST-PP1Cα. Total levels of pT320 GST-PP1Cα (an indicator of Cdk1 activity) were then quantified by immunoblot (Kwon et al., 1997; Lewis et al., 2013) (**Figure 3.7A**). Adavosertib treatment increased *in vitro* Cdk1 activity in a dose dependant manner; however, R500 HeLa and MDA-MB-231 had significantly less *in vitro* Cdk1 activity relative to parental cells (**Figure 3.7B-C**). Next, we directly tested if transient overexpression of Myt1 could suppress Cdk1 activity in HeLa and MDA-MB-231 parental cells. Cells were transfected with GFP or GFP-Myt1 and then

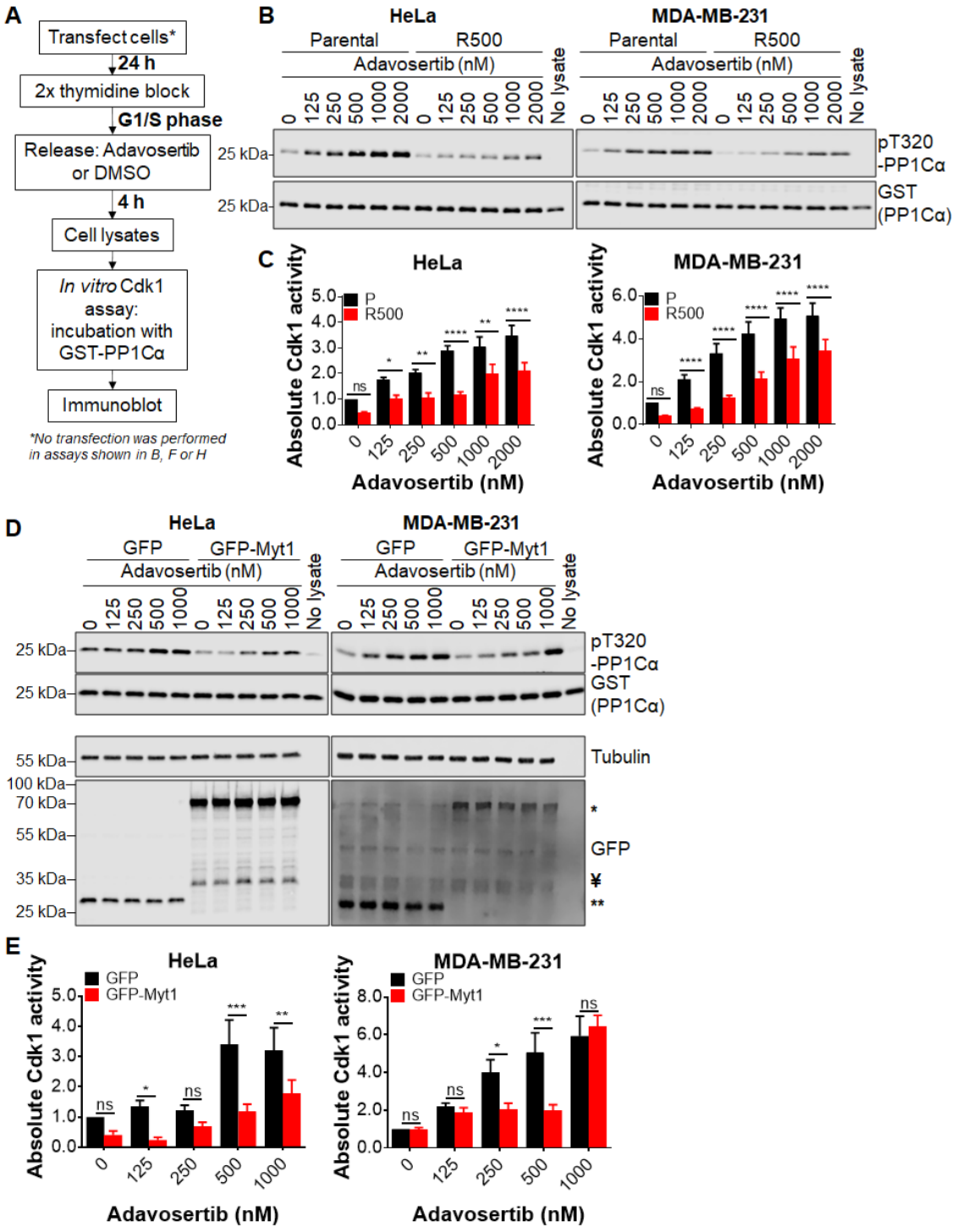
A
Transfect cells*
24 h
2x thymidine block
G1/S phase
Release: Adavosertib or DMSO
4 h
Cell lysates
In vitro Cdk1 assay: incubation with GST-PP1Cα
Immunoblot
*No transfection was performed in assays shown in B, F or H
B
HeLa
MDA-MB-231
Parental
R500
Adavosertib (nM)
0 125 250 500 1000 2000
No lysate
25 kDa
pT320 -PP1Cα
GST (PP1Cα)
C
HeLa
MDA-MB-231
Absolute Cdk1 activity
P
R500
ns
Adavosertib (nM)
D
HeLa
MDA-MB-231
GFP
GFP-Myt1
Adavosertib (nM)
No lysate
25 kDa
pT320 -PP1Cα
GST (PP1Cα)
55 kDa
Tubulin
100 kDa
70 kDa
55 kDa
35 kDa
25 kDa
GFP
*
¥
**
E
HeLa
MDA-MB-231
Absolute Cdk1 activity
GFP
GFP-Myt1
ns
Adavosertib (nM)

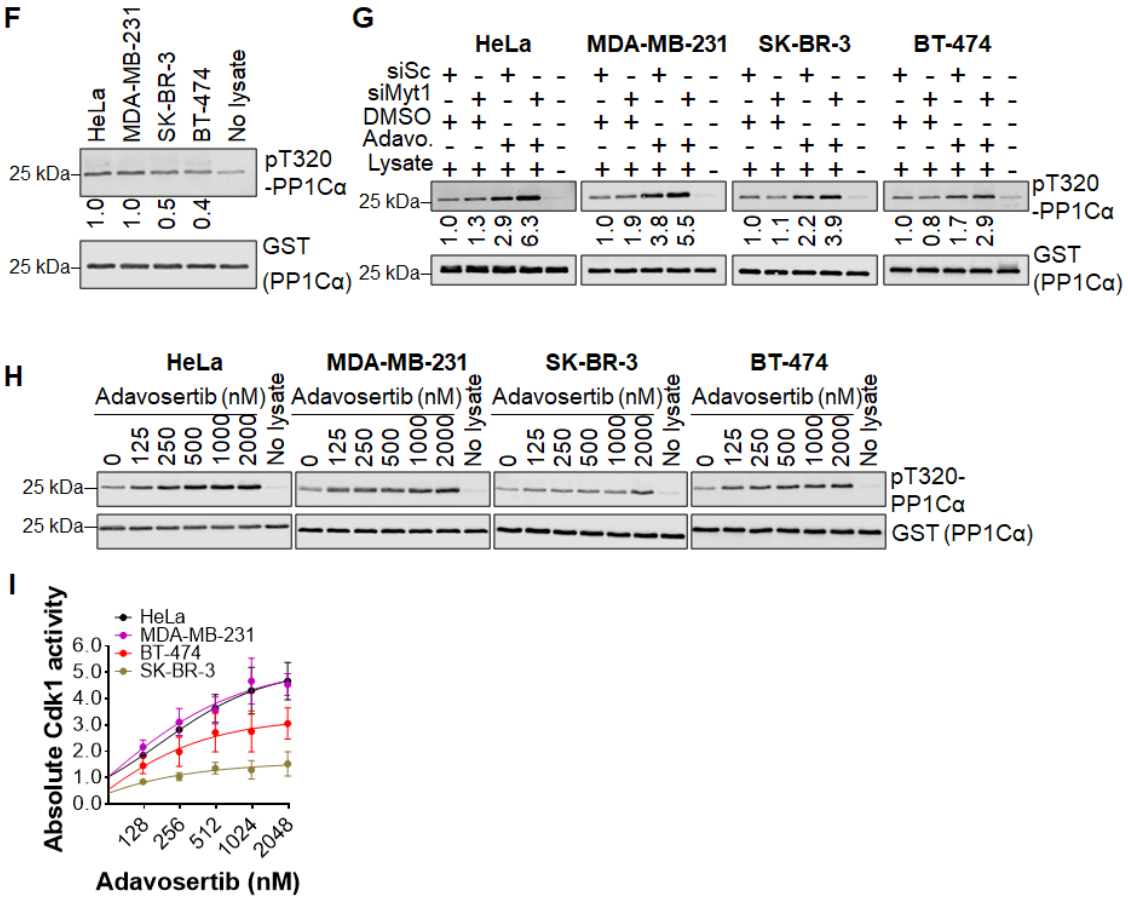

Figure 3.7. Myt1 inhibits ectopic Cdk1 activity induced by Adavosertib. **A)** Flow chart depicts *in vitro* kinase assay. Cdk1 activity in lysates from cells 4 h after G1/S release was assessed *in vitro* by incubation with GST-PP1Cα (a Cdk1 substrate). Total pT320-PP1Cα peptide and GST levels were determined by immunoblot. Where indicated cells were transfected prior to synchronization. **B)** *In vitro* Cdk1 activity was analyzed in R500 and parental (P) HeLa and MDA-MB-231 cells treated with Adavosertib. **C)** Graphs show quantitation of average Cdk1 activity (normalized to control parental/DMSO). Error bars represent SEM. **D)** *In vitro* Cdk1 activity (top two panels) HeLa and MDA-MB-231 were transiently transfected with GFP or GFP-Myt1 and then treated with DMSO or Adavosertib. GFP, GFP-Myt1, and tubulin levels were analyzed by immunoblot (bottom two panels). * denotes GFP-Myt1, whereas ** and ¥ denote untagged GFP and GFP-Myt1 degradation products respectively. **E)** Graph shows the quantitation of average Cdk1 activity (relative to control GFP/DMSO). Error bars represent SEM. **F)** Baseline Cdk1 activity was analyzed in HeLa, MDA-MB-231, SK-BR-3, and BT-474 cells 4 h post release from G1/S. Average *in vitro* Cdk1 activity is shown (normalized to HeLa). **G)** HeLa, MDA-MB-231, SK-BR-3, and BT-474 were transfected with siSc or siMyt1. 24 h after knockdown, cells were released from G1/S with DMSO or 250 nM Adavosertib before testing *in vitro* Cdk1 activity in cell lysates. Average *in vitro* Cdk1 activity is shown below (normalized to DMSO). **H)** *In vitro* Cdk1 activity was analyzed in HeLa, MDA-

MB-231, SK-BR-3, and BT-474 treated with DMSO or Adavosertib. **I)** Graph shows absolute *in vitro* Cdk1 activity (normalized to total cellular protein) in cell lines. Error bars represent SEM. All experiments were repeated at least three times. *, **, ***, and **** indicate P values < 0.05, < 0.01, 0.001 and < 0.0001 (Two-way ANOVA). Parts B and C were not published component in the original *Cancer Research* manuscript.

treated with Adavosertib for 4 h following G1/S release. GFP-Myt1 overexpression (confirm by immunoblot) significantly reduced absolute *in vitro* Cdk1 activity in both HeLa and MDA-MB-231 cells relative to cells expressing only GFP (**Figure 3.7D-E**).

Next, we tested if Adavosertib-resistant cell lines (SK-BR-3 and BT-474) exhibited less *in vitro* Cdk1 activity compare to HeLa or MDA-MB-231. We first established the baseline Cdk1 activity in cell lines in the absence of Adavosertib. Cell lysates were prepared from cells 4 h after release from G1/S arrest and normalized by total protein (**Figure 3.7A**; no transfection). SK-BR-3 and BT-474 had 50-60% less *in vitro* Cdk1 activity compared to the more Adavosertib sensitive HeLa and MDA-MB-231 (**Figure 3.7F**).

Next, we tested the effects on Cdk1 activity of combining Myt1 knockdown with Adavosertib. HeLa, MDA-MB-231, and two Adavosertib resistant cell (SK-BR-3, and BT-474) were transfected with siSc or siMyt1 and then treated with Adavosertib (**Figure 3.7G**). Low *in vitro* Cdk1 activity was observed in siSc and siMyt1 transfected cells in the absence of Adavosertib. Adavosertib treatment in siSc transfected cells increased Cdk1 activity 2- to 4-fold compared to DMSO. However, the highest Cdk1 activity was observed in cells treated with Adavosertib and transfected with siMyt1. Together these data show that high Myt1 levels suppress Cdk1 activity in the presence of Adavosertib.

Subsequently, we treated each cell line with increasing concentrations of Adavosertib (**Figure 3.7H**). To compare the absolute change in Cdk1 activity between cell lines, the baseline Cdk1 activity (normalized to total protein) (**Figure 3.7F**) was multiplied

by the change in *in vitro* Cdk1 activity within each cell line. We found that resistant cell lines (SK-BR-3 and BT-474) had less absolute Cdk1 activity in the presence of Adavosertib compared to that of HeLa and MDA-MB-231 (**Figure 3.7I**). To investigate whether the observed Cdk1 activity correlated with entry into mitosis, Adavosertib treated cells were stained for pS10 histone H3 (PH3) (a mitosis biomarker) (Hendzel et al., 1997) and analyzed by immunofluorescence microscopy (**Figure 3.8A**). Consistent with *in vitro* Cdk1 kinase assay, even at 2000 nM Adavosertib, <10% of SK-BR-3 and BT-474 cells stained positive for PH3 compared to 40-50% in HeLa and MDA-MB-231 (**Figure 3.8A & B**). Together these data strongly support that high Myt1 expression drives Adavosertib resistance by supressing Cdk1 activity.

3.5.7 Myt1 protects cells from Adavosertib induced mitotic arrest

Wee1 is required for normal mitotic exit and the loss of Wee1 causes cells to arrest in mitosis (Chow et al., 2011; Visconti et al., 2015; Visconti et al., 2012). Similarly, Myt1 knockout in glioblastoma cells has been previously shown to prolong the duration of mitosis leading to cell death (Toledo et al., 2015). We therefore wondered whether Myt1 levels may affect how long cancer cells arrest in mitosis following Adavosertib treatment. We transfected MDA-MB-231 cells expressing mCherry-H2B and GFP-tubulin with siMyt1 or siSc and then treated cells with Adavosertib or DMSO. Next, we measured the duration of mitosis by timelapse microscopy (**Figure 3.9A & B**). No significant differences were observed between siMyt1 or siSc transfected MDA-MB-231 cells in the absence of Adavosertib (**Figure 3.9B**; 0 nM); cells exhibited normal chromosome alignment and mitotic timing. In contrast, Adavosertib (in the background of siSc) increased the total time

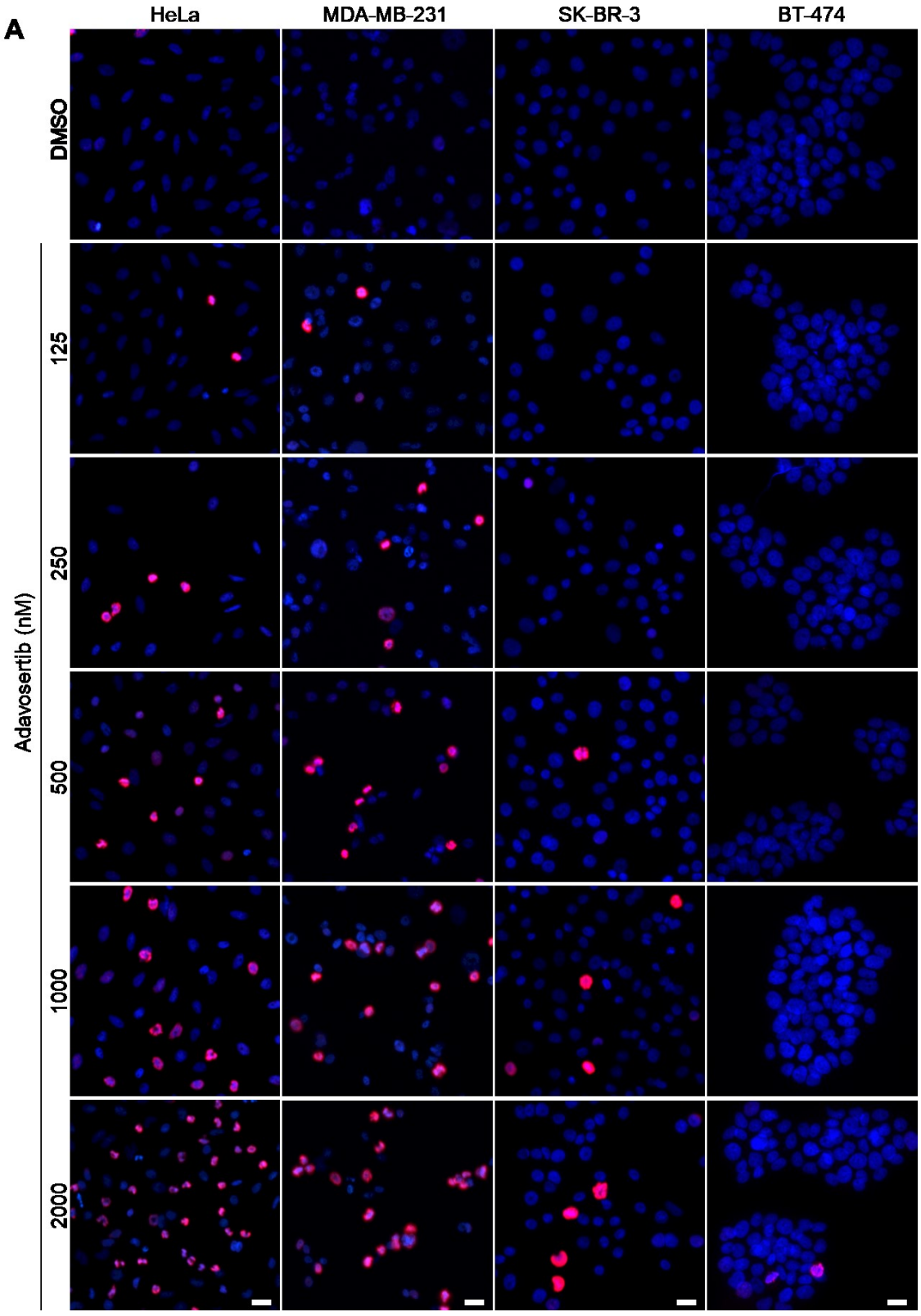
A
HeLa
MDA-MB-231
SK-BR-3
BT-474
DMSO
Adavosertib (nM)
125
250
500
1000
2000

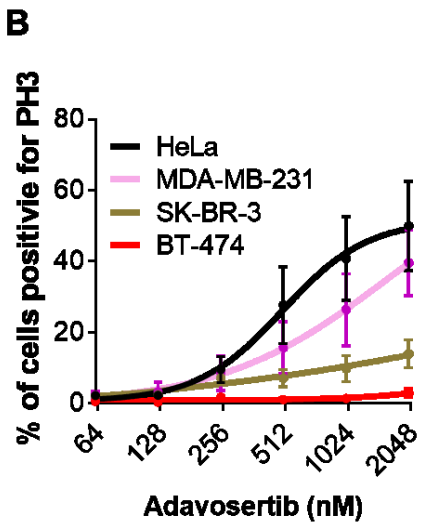

Figure 3.8. Adavosertib resistant cells do not prematurely enter mitosis. Adavosertib sensitive (HeLa and MDA-MB-231) and resistant (BT-474, and SK-BR-3) cell lines were released from G1/S phase into media containing 125-2000 nM Adavosertib. **A)** Cells were analyzed for positive PH3 by immunofluorescence microscopy. Scale bar = 25 µm. **B)** Percentage of PH3 cells (relative to DAPI) are presented in the graph. Error bars represent SEM. Experiments were repeated at least three times.

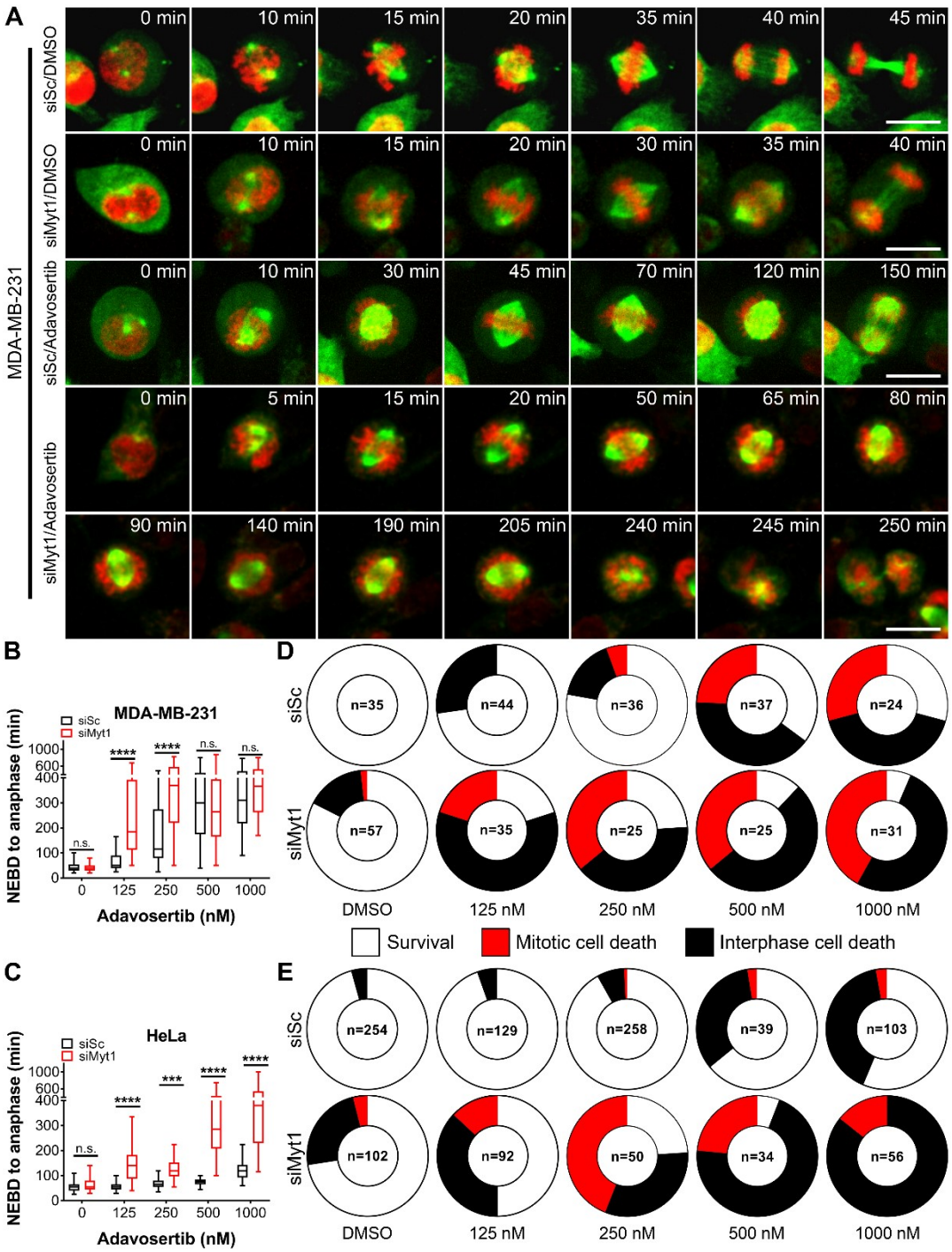

Figure 3.9. Myt1 knockdown and Adavosertib cooperatively lead to mitotic arrest and cell death.

A) MDA-MB-231 cells expressing GFP-tubulin (green) and mCherry-H2B (red) were transfected with siSc or siMyt1 for 24 h and then treated with Adavosertib or vehicle control (DMSO). Cells were then analyzed by time-lapse imaging. Representative images are shown. Whisker-box plots show the duration of mitosis for MDA-MB-231 **(B)** and HeLa **(C)** treated as indicated (0 nM = DMSO). **(D, E)** Donut plots showing the proportion of cell survival (white) and cell death

in mitosis (red) or interphase (black) following mitotic arrest. The number of cells analyzed is indicated in the inner circle of the donut plots. *** and **** indicate P values < 0.001 and < 0.0001 (Two-way ANOVA).

in mitosis compared to DMSO controls. Normal chromosome alignment and segregation was observed in most cells at low concentrations of Adavosertib (≤ 250 nM), but Adavosertib concentrations ≥ 500 nM induced abnormal chromosome condensation, which frequently was followed by in mitotic slippage (**Figure 3.10A & B**; two phenotypes are shown). Combined knockdown of Myt1 with Adavosertib (125-250 nM) prolonged mitosis more than Adavosertib alone (**Figure 3.9B**; $P < 0.0001$). siMyt1 combined with Adavosertib also increased the percentage of cells that exhibited abnormal chromosome condensation and/or mitotic slippage. No increases in the duration of mitosis were observed after siMyt1 transfection and Adavosertib concentrations ≥ 500 nM. To compare the effects on mitosis in MDA-MB-231 to another cell line, we repeated the experiment in HeLa cells expressing GFP-H2B (**Figure 3.9C**). Like MDA-MD-231, Adavosertib/siSc increased the duration of mitosis in HeLa compared to DMSO/siSc. Unlike in MDA-MB-231, siMyt1 significantly enhanced the duration of mitosis compared to Adavosertib /siSc in HeLa cells even at concentrations higher than 500 nM.

We measured the percentage of cell death in MDA-MB-231 and HeLa cells by time-lapse microscopy for up to 48 h (**Figure 3.9D-E**). Few cell deaths were observed in siSc/DMSO controls for either cell line; however, 18% of MDA-MD-231 and 25% of HeLa cells died during mitosis or after slippage in siMyt1/DMSO treated cells. Consistent with cell survival assay data (**Figure 3.2B-C**), we observed that Adavosertib alone induced cell death in a dose dependent manner in both MDA-MB-231 and HeLa, which was further enhanced by siMyt1. Mitotic cell death commonly occurred at high concentrations of

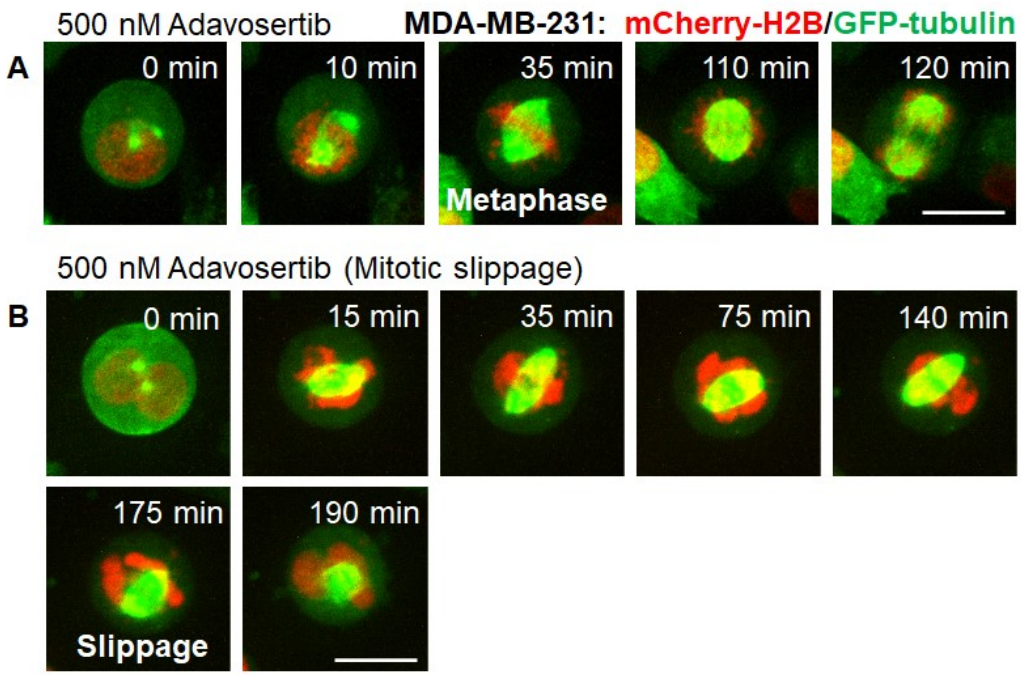

Figure 3.10. Adavosertib induced mitotic exit delays occur in cells with and without abnormal chromosome condensation and spindle organization.
MDA-MB-231 cells expressing EGFP-tubulin (green) and mCherry-H2B (red) were treated with 500 nM Adavosertib for 24 h and then analyzed by timelapse imaging. **A)** Mitotic cells with extended mitotic duration. **B)** Mitotic cells undergoing mitotic slippage (aborted mitosis).

Adavosertib (≥ 500 nM) in siSc-transfected cells and at lower doses of Adavosertib (125-250 nM) in siMyt1-transfected cells. These data suggest that loss of both Wee1 and Myt1 prolongs mitosis and induces mitotic cell death compared to loss of either kinase alone.

3.5.8 Myt1 knockdown induces centromere fragmentation in cancer cells treated with Adavosertib

Centromere fragmentation occurs when cells enter mitosis without completing DNA synthesis (Beeharry et al., 2013; Lewis et al., 2017). We previously reported that 20% of HeLa cells treated with 1000 nM Adavosertib underwent mitosis accompanied with centromere fragmentation (Lewis et al., 2017); however, at concentrations close to the IC50 of HeLa (250 nM), centromere fragmentation was rarely observed. Here we show that after

Myt1 knockdown, abnormal chromosome condensation and alignment (characteristic signs of centromere fragmentation (Beeharry et al., 2013; Lewis et al., 2017)) are observed in both MDA-MB-231 and HeLa cells treated with only 250 nM Adavosertib. HeLa and MDA-MB-231 cells were transfected with siSc or siMyt1, synchronized in G1/S, and then released into media containing Adavosertib or DMSO for 4 h (Lewis et al., 2017). Cells were then fixed and stained for centromeres, microtubules, and DNA and analyzed by immunofluorescence microscopy (**Figure 3.11A**). In the absence of Adavosertib, < 2% of HeLa and MDA-MB-231 cells transfected with siSc or siMyt1 entered mitosis; observed mitotic cells exhibited normal centromere localization, chromosome morphology and mitotic spindles. Treatment with 250 nM Adavosertib in the presence of siSc increased the percentage of mitotic cells to 12% and 17% in HeLa and MDA-MB-231 respectively (**Figure 3.11A & B**). Of these mitotic cells observed in the presence of Adavosertib alone, most exhibited abnormal chromosome condensation and had centromeres and microtubules that clustered away from the bulk of the chromosomes, consistent with centromere fragmentation (**Figure 3.11A & B**). However, 250 nM Adavosertib in the presence of siMyt1 increased centromere fragmentation 11-fold in HeLa, and 4-fold in MDA-MD-231 (**Figure 3.11B**). We repeated this experiment in an Adavosertib resistant cell lines (T-47D) using a higher concentration of the Wee1 inhibitor (1000 nM), consistent with HeLa and MDA-MB-231, Myt1 knockdown increased the number of cells exhibiting centromere fragmentation (**Figure 3.11A & B**)

To acquire higher resolution images of the chromosomes from mitotic cells, HeLa cells were prepared for karyotype analysis (**Figure 3.11C**). The chromosomes in DMSO

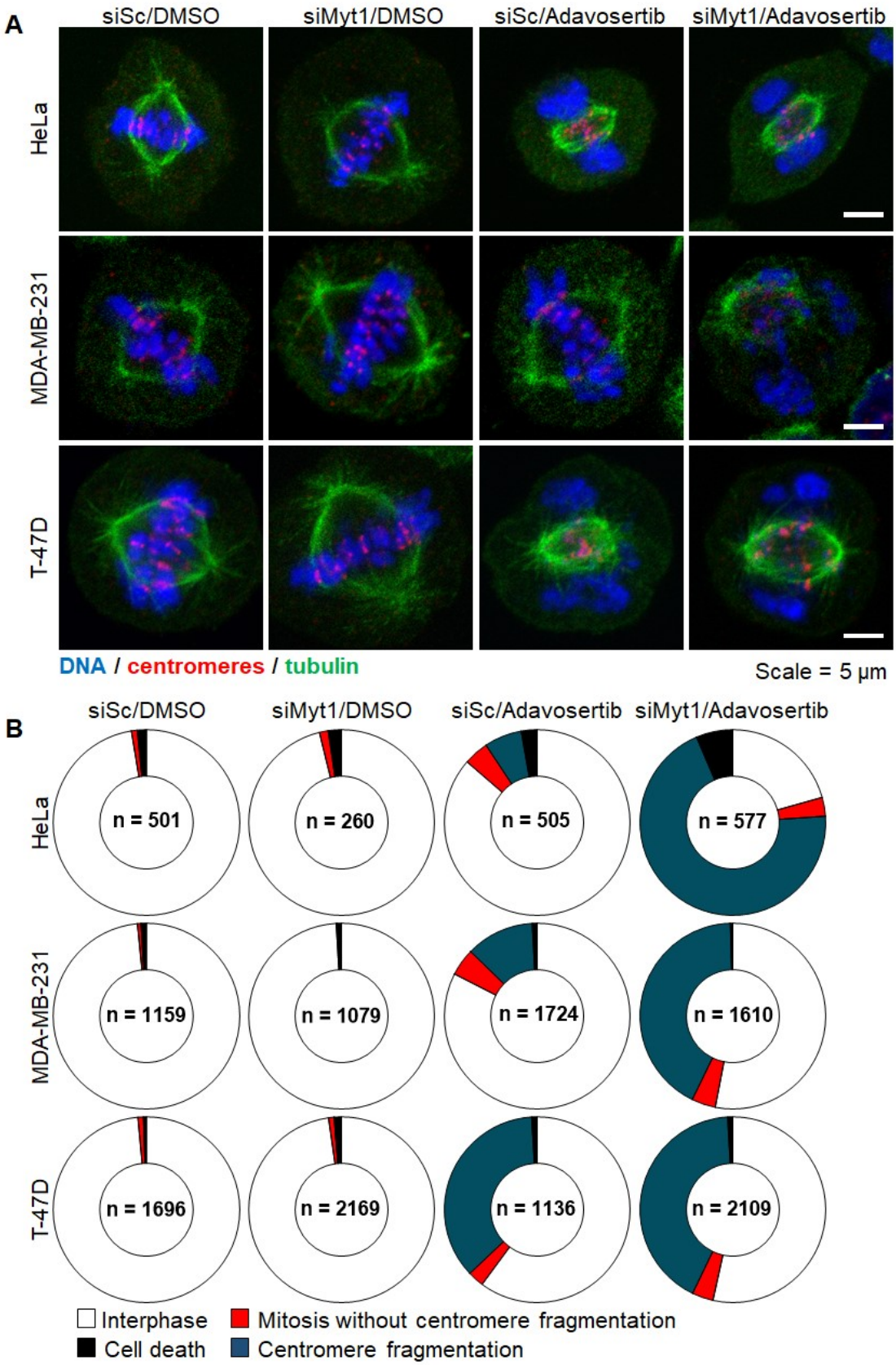
A
siSc/DMSO
siMyt1/DMSO
siSc/Adavosertib
siMyt1/Adavosertib
HeLa
MDA-MB-231
T-47D
DNA / centromeres / tubulin
Scale = 5 µm
B
siSc/DMSO
siMyt1/DMSO
siSc/Adavosertib
siMyt1/Adavosertib
HeLa
MDA-MB-231
T-47D
n = 501
n = 260
n = 505
n = 577
n = 1159
n = 1079
n = 1724
n = 1610
n = 1696
n = 2169
n = 1136
n = 2109
Interphase
Mitosis without centromere fragmentation
Cell death
Centromere fragmentation

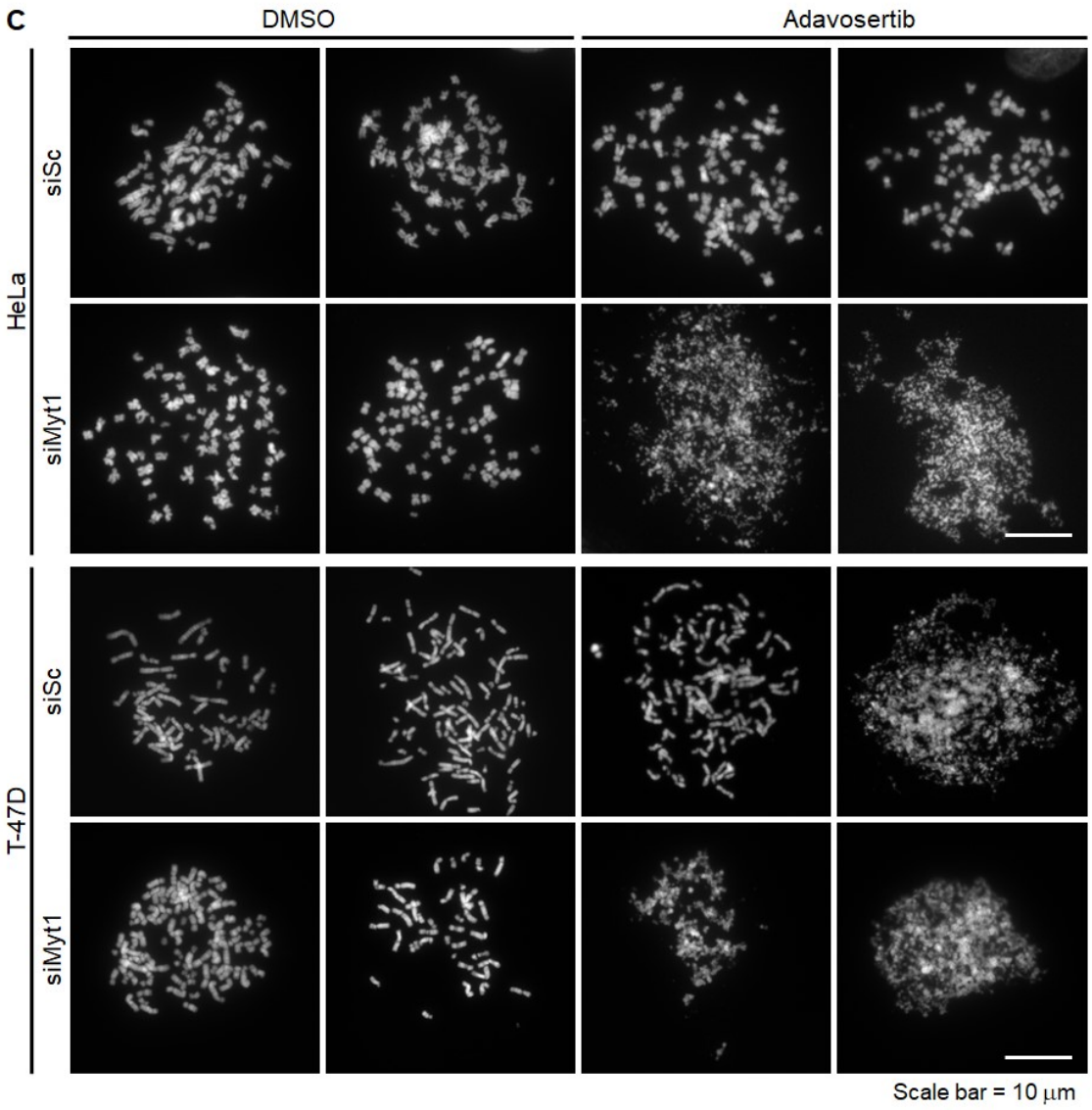
C
DMSO
Adavosertib
HeLa
siSc
siMyt1
T-47D
siSc
siMyt1
Scale bar = 10 μm

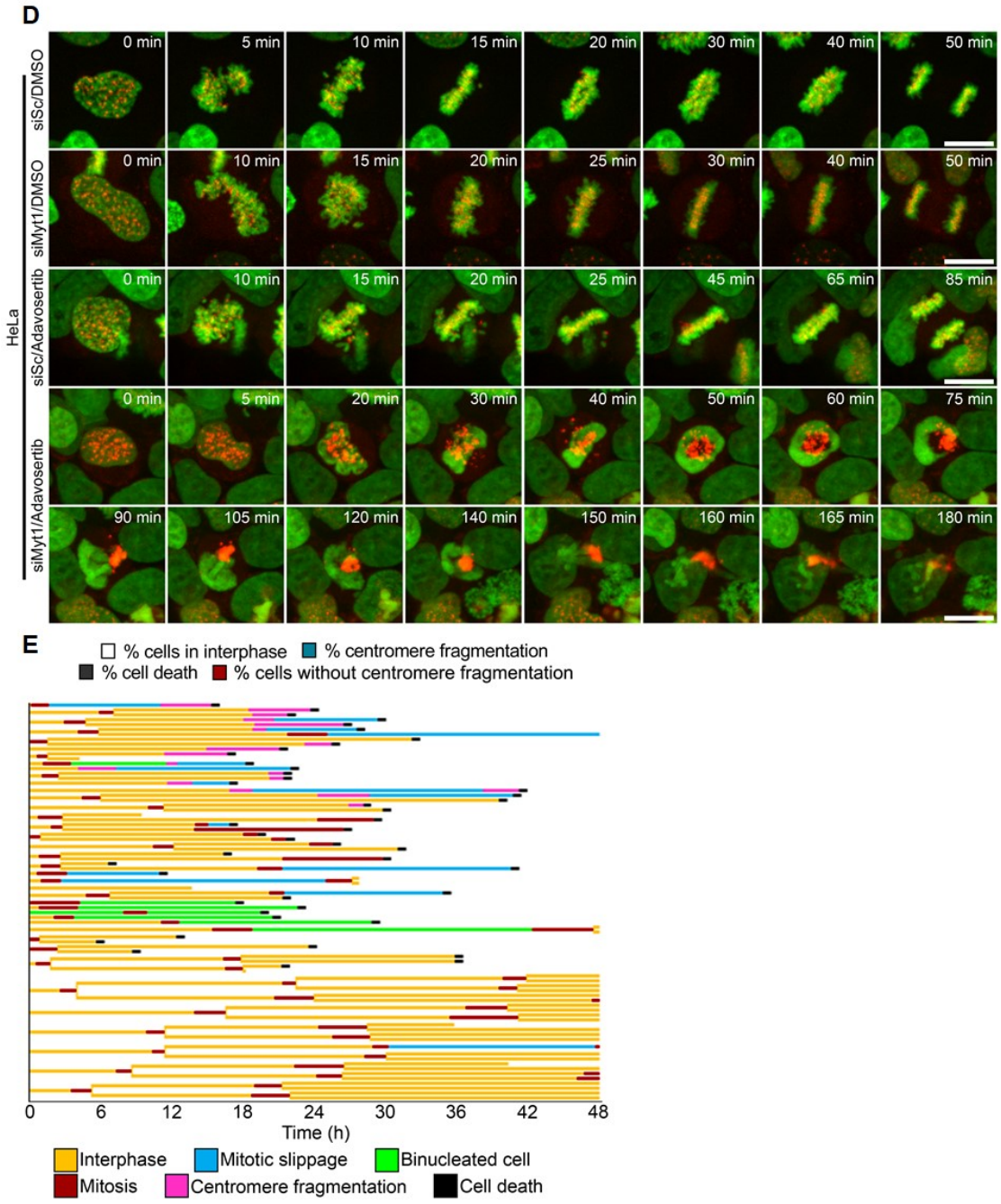

Figure 3.11. Myt1 knockdown enhances Adavosertib induced centromere fragmentation.

A) siSc or siMyt1 transfected cells were released from G1/S phase into media containing either DMSO or 250 nM (for HeLa and MDA-MB-231) or 1000 nM (for T-47D) for 4 h. Cells were then fixed and stained for tubulin (green), centromeres (red), and DNA (blue) and analyzed by confocal microscopy. Representative mitotic cells for each treatment are shown. **B)** Donut plots show the proportions of interphase (white), mitotic (red), centromere-fragmented (blue), and dead cells (black). The number of cells analyzed is indicated in the inner circle of the donut plots. **C)** Metaphase spreads of HeLa and T-47D cell

chromosomes following treatment conditions described in (A). **D)** HeLa cells expressing GFP-H2B (green) and td-Tomato-CENP-B (red) were analyzed by live cell imaging. **E)** Dendrograms show the cell fates of HeLa following transfection with siMyt1 and 250 nM Adavosertib treatment (n =39). Each line represents a single cell and forked lines indicate cell division. Capped black lines indicate cell death whereas uncapped lines represent cells that either survived treatment or exited the imaging field prior to the end of the experiment. T-47D data was not included as part of the original *Cancer Research* publication.

treated cells that were transfected with siSc or siMyt1 showed no signs of abnormalities. Likewise, in HeLa cells treated with 250 nM Adavosertib and were transfected with siSc had intact chromosomes with only a small number exhibiting signs of chromosome shattering. In contrast, treatment with Adavosertib resulted in chromosome shattering in nearly all mitotic spreads from Myt1 knockdown cells. Similar results were observed in the karyotype of T-47D cells transfected with siSc or siMyt1 and treated with DMSO or 1000 nM Adavosertib. Albeit high numbers of cells exhibiting chromosome shattering were observed in the presence of Adavosertib regardless of whether T-47D cells were transfected with siSc or siMyt1.

Finally, to further investigate the phenomenon of centromere fragmentation, a HeLa cell line expressing GFP-H2B and tdTomato-CENP-B was established to monitor chromosomes and centromeres respectively. Asynchronous cells were transfected with siMyt1 or siSc and then treated with either DMSO or 250 nM Adavosertib for 24 h. No centromere fragmentation was observed in cells treated with siSc/DMSO, siMyt1/DMSO, or siSc/250 nM Adavosertib (**Figure 3.11D & E** and **Table 3.3**). However, combining 250 nM Adavosertib with siMyt1 resulted in centromeres clustering away from the bulk of the chromosomes in 26.7% of cells (**Figure 3.11D** and **Table 3.3**). Cell death was observed in 100% of cells exhibiting centromere fragmentation (**Figure 3.11E**). To confirm that

Table 3.3. Cdk1 inhibition prevents centromere fragmentation.

Treatment (24 h)	Centromere fragmentation
siSc/DMSO	0% (0/72)
siSc/1000 nM Adavosertib	8.3% (2/24)
siMyt1/DMSO	0% (0/60)
siSc/250 nM Adavosertib	0% (0/35)
siMyt1/250 nM Adavosertib	26.7% (40/150)
RO-3306 + siMyt1/250 nM Adavosertib	0% (0/40)

centromere fragmentation was dependent on upregulated Cdk1 activity following loss of Wee1 and Myt1 activity, we treated cells with the small molecule Cdk1 inhibitor RO3306. We found that RO3306 completely supressed centromere fragmentation in siMyt1/Adavosertib treated cells (**Table 3.3**). Collectively, these findings may indicate that the ability of Myt1 to inhibit Cdk1 during DNA replication protects cells from undergoing centromere fragmentation when Wee1 is inhibited by Adavosertib.

3.5.9 High Myt1 expression is associated with a worse clinical outcome in breast cancer

Since most of our data were derived from breast cancer cell lines, we wanted to know if Myt1 was overexpressed in tumours from breast cancer patients. We compared Myt1 mRNA levels in breast cancer patient tissue (176 samples) (Germain et al., 2011; Liu et al., 2011; Liu et al., 2012) against normal breast tissue (10 samples) by cDNA microarray (Germain et al., 2011; Liu et al., 2011; Liu et al., 2012) and found that median mRNA

levels of Myt1 were approximately 14-fold higher in cancer tissue compared to normal tissue ($P = 0.0004$; student *t*-test) (**Figure 3.12A** and **Supplementary Figure 3.1A & B**; average of two primes). Nevertheless, we noted that Myt1 mRNA levels varied greatly among samples. We then correlated Myt1 expression with overall disease grade, mitotic grade, and hormone receptor status (basal like vs ER positive) (**Figure 3.12B-D** and **Supplementary Figure 3.1C-E**). We found that higher Myt1 expression was associated with a higher overall disease grade ($P < 0.0001$; student *t*-test) a higher mitotic grade ($P < 0.0001$; student *t*-test), and basal like (triple negative) hormone receptor status ($P = 0.009$; student *t*-test). We next evaluated whether Myt1 expression was associated with either disease recurrence (disease-free survival) or overall patient survival (**Figure 3.12E & F**). We therefore dichotomized the samples into high and low Myt1 expression groups with the low group representing the bottom quarter percentile of the samples, which is comparable to Myt1 expression in normal tissue. We found that higher Myt1 expression was associated with both a worse disease-free survival ($P = 0.0118$; Mantel-Cox test) and overall survival ($P = 0.0121$; Mantel-Cox test). Since our sample size (n = 176) was relatively small, we accessed the cBioPortal database to compare high and low Myt1 expressing breast cancers to confirm our findings. An analysis of 1423 additional samples confirmed high Myt1 levels were strongly associated with a lower overall survival (**Supplementary Figure 3.1F**; $P < 0.0001$; Mantel-Cox test) (Cerami et al., 2012; Gao et al., 2013). Previous studies have reported that Wee1 is overexpressed in various cancers including breast cancer (De Witt Hamer et al., 2011; Iorns et al., 2009; Matheson et al., 2016a; Murrow et al., 2010). In this study, no differences in Wee1 expression were observed between breast cancer and normal tissue samples (**Figure 3.13A**). Breast cancer

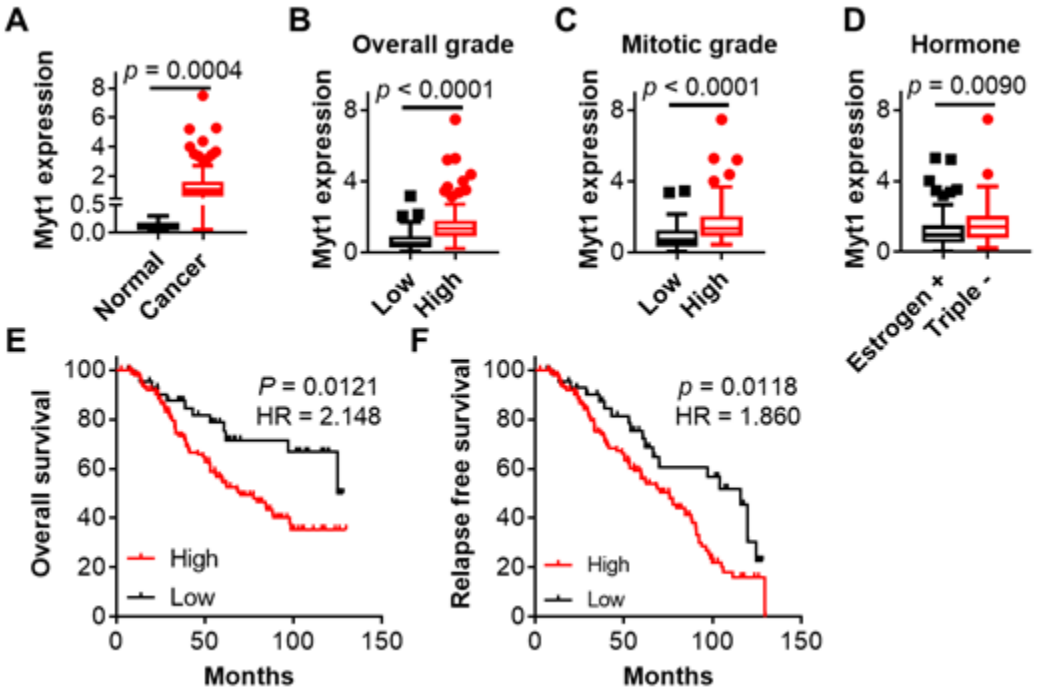

Figure 3.12. High Myt1 expression is associated with a worse clinical outcome in breast cancer.
Patient breast cancer tissue was analyzed for Myt1 mRNA expression by cDNA microarray (average of two primers; **Supplementary Figure 3.1**). **A)** Normalized Myt1 expression in breast cancer tissue (*n* =176) was compared to normal breast tissue (*n* = 10). **B)** Overall disease grade, **C)** mitotic grade and **D)** hormone status was compared with Myt1 expression. Tumour samples were grouped into high (above the 25th percentile; *n* = 132) and low (below the 25th percentile; *n* = 44) Myt1 expressing samples. Kaplan-Meier curves show **E)** overall survival and **F)** relapse free survival of breast cancer patients with tumours that express high and low levels of Myt1.

cells with Wee1 levels above the median expression were associated with a higher overall and mitotic grade (**Figure 3.13B & C**), but there were no differences in hormone status, overall survival, and disease-free survival (**Figure 3.13D-F**). Although it is worth pointing out that we examined only Myt1 mRNA levels, not Myt1 protein expression, these data suggest that Myt1 overexpression may be an important mechanism promoting cancer development.

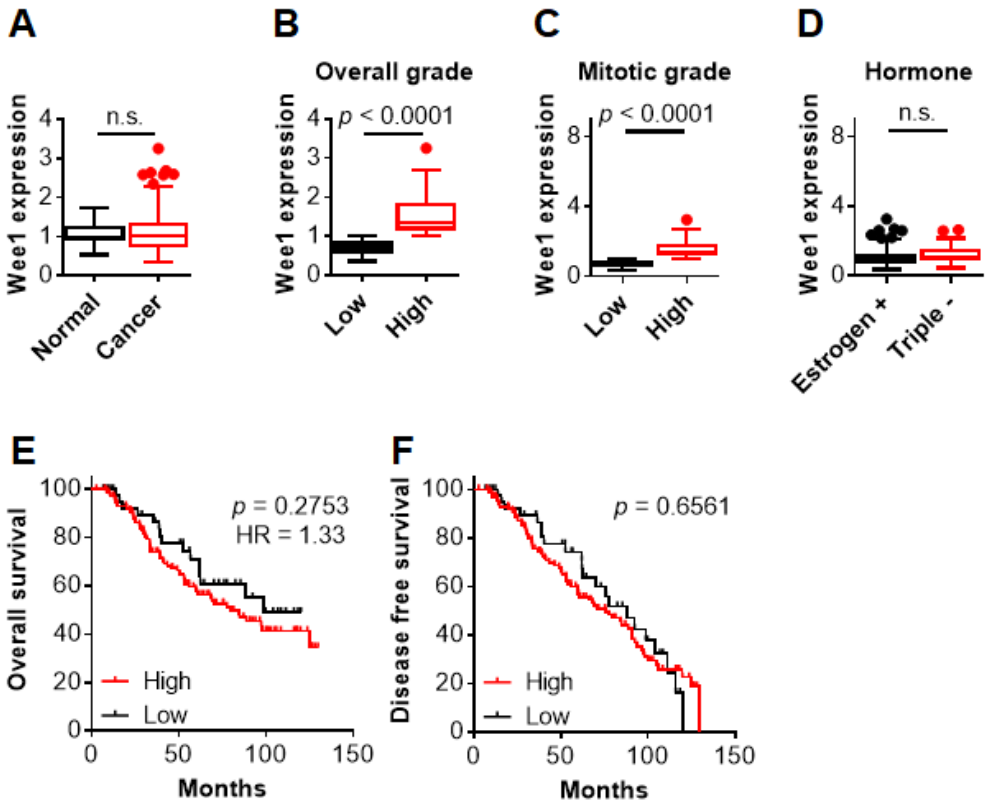

Figure 3.13. High Wee1 expression is associated with a higher tumour grade.
Normalized Wee1 expression in breast cancer tissue (*n* =176) was compared to normal breast tissue (*n* = 10). **A)** Overall disease grade, **B)** mitotic grade, and **C)** hormone status was compared between cancers with high (above the 50th percentile; *n* = 88) and low (below the 50th percentile; *n* = 88) Wee1 expression. Kaplan-Meier curves show **D)** overall survival and **E)** relapse free survival.

3.6 Discussion

Clinical trials show that Adavosertib treatment responses are variable, and some cancers do not respond to Adavosertib (Do et al., 2015; Van Linden et al., 2013); however, the mechanisms of drug resistance are unknown. We find that cancer cells can acquire resistance to Adavosertib through the upregulation of Myt1. HeLa and MDA-MB-231 cell lines, which initially exhibited high sensitivity to Wee1 inhibition, after selection acquired resistance to Adavosertib that was marked by a 2- to 3-fold increase in Myt1 expression

(**Figure 3.1B-C**). Additionally, *in vivo* experiments using an orthotopic breast cancer xenograft model demonstrated that tumours following 26 days of Adavosertib treatment had increased Myt1 expression compared to control treated tumour tissue (**Figure 3.1F**). Together, these data strongly suggest that Myt1 upregulation is a mechanism for tumour cells to acquire resistance to Wee1 inhibition. However, our data does not exclude the possibility that other proteins or pathways may also promote resistance to Adavosertib. Recently, proteomics study showed that primary resistance to Adavosertib is also associated with the upregulation of the mTOR pathway in small-cell lung carcinoma cells (Sen et al., 2017).

To validate that Myt1 upregulation had a direct role in Adavosertib resistance, we tested the effects of Myt1 knockdown and overexpression. Myt1 knockdown re-sensitized resistant HeLa and MDA-MB-231 cell lines to Adavosertib (**Figure 3.1D & E**), which suggested that Myt1 upregulation was required to sustain resistance in these cells. Furthermore, Myt1 knockdown also enhanced Adavosertib sensitivity in breast cancer cell lines initially exhibiting intrinsic resistance to the Wee1 inhibitor (**Figure 3.2**). Moreover, we were able to induce Adavosertib resistance directly in parental HeLa and MDA-MB-231 cells by transiently overexpressing GFP-Myt1 (**Figure 3.1A**). Collectively, these data argue that Myt1 upregulation directly drives Adavosertib resistance.

Our results suggest that Myt1 expression level is a candidate predictive biomarker for tumour sensitivity to Adavosertib. We compared Adavosertib sensitivity in cancer cell lines and identified a strong correlation ($R^2 = 0.69$) between Adavosertib resistance and Myt1 protein expression (**Figure 3.4** and **Table 3.2**), in agreement with a study suggesting a negative correlation of Myt1 mRNA levels with Wee1 inhibitor sensitivity (Guertin et

al., 2013). Although Wee1 and Cdc25C are important regulators of Cdk1 activity (Russell and Nurse, 1986a; Russell and Nurse, 1987; Timofeev et al., 2010), we did not observe any significant correlation between the expression of these proteins and Adavosertib sensitivity.

Developmental studies in model organisms have shown that Wee1 and Myt1 are at least partially redundant in the regulation of Cdk1 (Ayeni et al., 2014; Okumura et al., 2002; Palmer et al., 1998). This redundancy is important because ectopic Cdk1 activity is lethal due to the promotion of replication stress, premature entry into mitosis and the dysregulation of mitotic processes (Aarts et al., 2012; Duda et al., 2016; Jin et al., 2008). We confirmed that Myt1 retained its activity even in the presence of Adavosertib, indicating that Myt1 could compensate in Cdk1 regulation when Wee1 is inhibited (**Figure 3.6**) (Hirai et al., 2009; Zhu et al., 2017). However, we found that in cells with low levels of Myt1, such as HeLa and MDA-MB-231 (**Figure 3.4**), Myt1 activity is insufficient to suppress ectopic Cdk1 activity when Wee1 is inhibited (**Figure 3.7**). Upregulation of Myt1 in R500 HeLa and MDA-MB-231 reduced in vitro Cdk1 activity relative to parental cell controls (**Figure 3.7B & C**). Likewise, transient overexpression of GFP-Myt1 HeLa and MDA-MB-231 parental cells also reduced *in vitro* Cdk1 activity relative to GFP controls (**Figure 3.7D & E**), which argues that higher Myt1 levels can induce resistance in these cells by inhibiting Cdk1. Likewise, SK-BR-3 and BT-474 have high Myt1 levels (**Figure 3.4A & B**) and exhibit low Cdk1 activity in the presence of Adavosertib (**Figure 3.7H-I**). Myt1 knockdown enhanced ectopic *in vitro* Cdk1 activity induced by Adavosertib in all cell lines tested (**Figure 3.7G**), which further argues that Myt1 at least partially inhibits

Cdk1 activity if Wee1 is inhibited. Together, these data corroborate that Myt1 promotes resistance to Adavosertib through the inhibition of Cdk1.

Our data suggest Myt1 inhibition of ectopic Cdk1 activity protects cells from mitotic catastrophe, the mode of cell death induced by Wee1 inhibition (Aarts et al., 2012; Bukhari et al., 2019; Lewis et al., 2017). Mitotic catastrophe is not defined by a molecular pathway, but it can be identified by mitotic abnormalities including premature mitosis, centromere fragmentation (Beeharry et al., 2013; Brinkley et al., 1988) and mitotic exit delays (Gascoigne and Taylor, 2008; Orth et al., 2012; Uetake and Sluder, 2010). We observed that the type and incidence of these mitotic abnormalities prior to cell death varied depending on the concentration of Adavosertib used and cellular Myt1 levels. Despite HeLa and MDA-MB-231 cells having similar Myt1 protein levels and Adavosertib IC50s, we did note that siMyt1 transfection in the presence of Adavosertib had a more significant effect on the duration of mitosis in HeLa compared to MDA-MB-231 (**Figure 3.9**). This difference may be explained by other biological differences that may exist between the two cell lines. Apart from Myt1, differences in the expression (or activity) of other cell-cycle regulators may cause longer mitotic delays following Adavosertib treatment (**Figure 3.14**). The cellular levels of mitotic cyclins and their degradation rate in anaphase is known to affect the duration of mitosis in cells treated with other anti-mitotic drugs (Gascoigne and Taylor, 2008; Gascoigne and Taylor, 2009). The upregulation of mitotic cyclins (cyclin A/B) and the downregulation of CDK interacting protein p21 have been suggested to correlate with increased cancer cell sensitivity to Adavosertib (Aarts et al., 2012). Alternatively, differences in the activity of the upstream kinase/phosphatase signalling pathway that regulates Wee1, Myt1, or Cdc25C could also affect the duration of mitosis in

these cells. It is also possible that the loss of Myt1 and Wee1 activity may induce mitotic catastrophe by an unknown mechanism that is independent of Cdk1 activity.

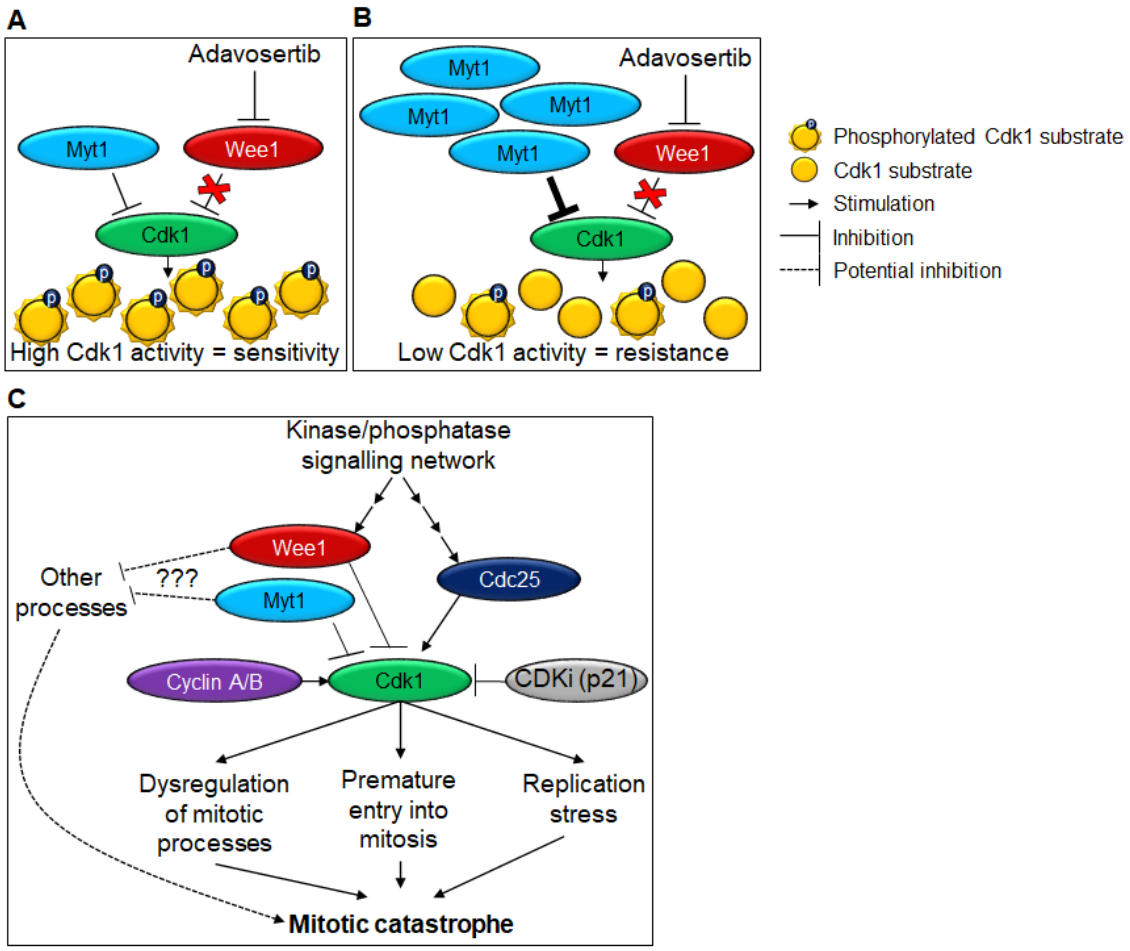

Figure 3.14. Model of Myt1 induced resistance in cancer cells.
Wee1 inhibition by Adavosertib induces ectopic Cdk1 activity in cells with low Myt1 expression **(A)** but not cells with high Myt1 expression **(B)**. **C)** Ectopic activation of Cdk1 promotes cell death by mitotic catastrophe. Other cell-cycle regulators may also contribute to cell sensitivity to Adavosertib through the regulation of Cdk1, Wee1, Myt1, Cdc25C, or through a parallel signalling pathway.

In the case of SK-BR-3 and BT-474, the amount of Myt1 expressed was enough to prevent premature mitosis in most cells treated with Adavosertib. At the highest concentration tested (2000 nM), less than 10% of SK-BR-3 or BT-474 prematurely entered

mitosis. In contrast, 10-20% of HeLa and MDA-MB-231 underwent premature mitosis at 250 nM and 40-50% of cells entered mitosis at 2000 nM Adavosertib. Although Myt1 did not protect most HeLa and MDA-MB-231 cells from mitotic catastrophe at high concentrations of Adavosertib (500-2000 nM), Myt1 was essential for cell survival at lower, more clinically relevant concentrations. Cells treated with 125-250 nM Adavosertib progressed through mitosis significantly slower than those treated with DMSO, but cell death was relatively low (10-20% cell death at 250 nM) (**Figure 3.9D & E**). Myt1 knockdown in combination with 125-250 nM Adavosertib caused cells to arrest in mitosis 2-3 times longer than in the case of Adavosertib alone and caused cell death to increase to 75%. Similarly, 10% of HeLa and 17% of MDA-MB-231 cells underwent premature mitosis associated with centromere fragmentation when treated with 250 nM Adavosertib (**Figure 3.11**). However, Myt1 knockdown in combination with Adavosertib induced mitosis associated with centromere fragmentation in 75% of HeLa and 50% of MDA-MB-231 cells. Together these data show that Myt1 and Wee1 cooperatively suppress cell death by mitotic catastrophe.

Our findings establish Myt1 level as a candidate predictive biomarker for tumour response after Adavosertib treatment. This could have wide-ranging clinical implications as Adavosertib enters the clinic. Currently, Adavosertib is undergoing phase I/II clinical trials against different cancer types alone and in combination with different anti-cancer agents. Although tumour response is observed in some patients, cancer progression continues in many other patients treated with Adavosertib (Do et al., 2015; Leijen et al., 2016). To our knowledge, clinical studies on Adavosertib do not take Myt1 expression levels into account prior to treating patients with this inhibitor. However, Myt1 expression

should be assessed in pre- and post-treatment tissue samples from participants in these studies to evaluate if there is a relationship between Myt1 expression and the clinical response to Adavosertib. If a correlation between high Myt1 levels and Adavosertib resistance is identified, Myt1 expression levels could be used to stratify cancer patients in a future clinical trial on Adavosertib. Our data shows that Myt1 is overexpressed in tumour tissue (relative to normal tissue) (**Figure 3.12A**). Likewise, Myt1 is also reported to be upregulated in other cancer types such as colorectal cancer and glioblastomas (Jeong et al., 2018; Toledo et al., 2015). If high Myt1 levels are indeed a predictive biomarker for tumour response to Adavosertib, it is unlikely that Adavosertib on its own will be effective in targeting these tumour types. Furthermore, the finding that Myt1 overexpression is associated with poor breast cancer prognosis suggests that those breast cancer patients most in need of new therapies are least likely to benefit from Adavosertib.

Combining Adavosertib with a small molecule Myt1 inhibitor will likely prove beneficial in overcoming resistance. However, there are additional reasons why a Myt1 inhibitor may be beneficial in the clinic. Myt1 level is a candidate prognostic biomarker, since high levels in breast cancer is associated with a higher tumour grade, triple negative status, reduced overall survival, and increased disease relapse (**Figure 3.12B-F**). Additionally, Myt1 upregulation is associated with cancer cell metastasis and lower overall survival in colorectal cancers (Jeong et al., 2018). Myt1 is also a crucial survival factor in a subset of glioblastomas (Toledo et al., 2015). Together these data suggest that Myt1 maybe a driver of tumour aggressiveness, which further provides a rationale for developing Myt1 inhibitors.

Acknowledgements: We thank Dr. Michael Weinfeld (and laboratory members), Dr. Michael Hendzel, and Chan laboratory members for their helpful discussion. We also thank Dr. Xuejun Sun and Geraldine Barron for assistance in the cell imaging facility. CWL is supported by the NSERC Alexander Graham Bell Canada Graduate Scholarship and Izaak Walton Killam Memorial Scholarship. ABB is supported by Alberta Cancer Foundation's Dr. Cyril M. Kay Graduate Scholarship. JDS was supported by the Queen Elizabeth II Graduate Scholarship. EJX was supported by a NSERC USRA award. The Chan laboratory was funded by NSERC, CIHR and the Cancer Research Society. The Gamper laboratory was funded by a start-up grant from the University of Alberta and a CIHR grant.

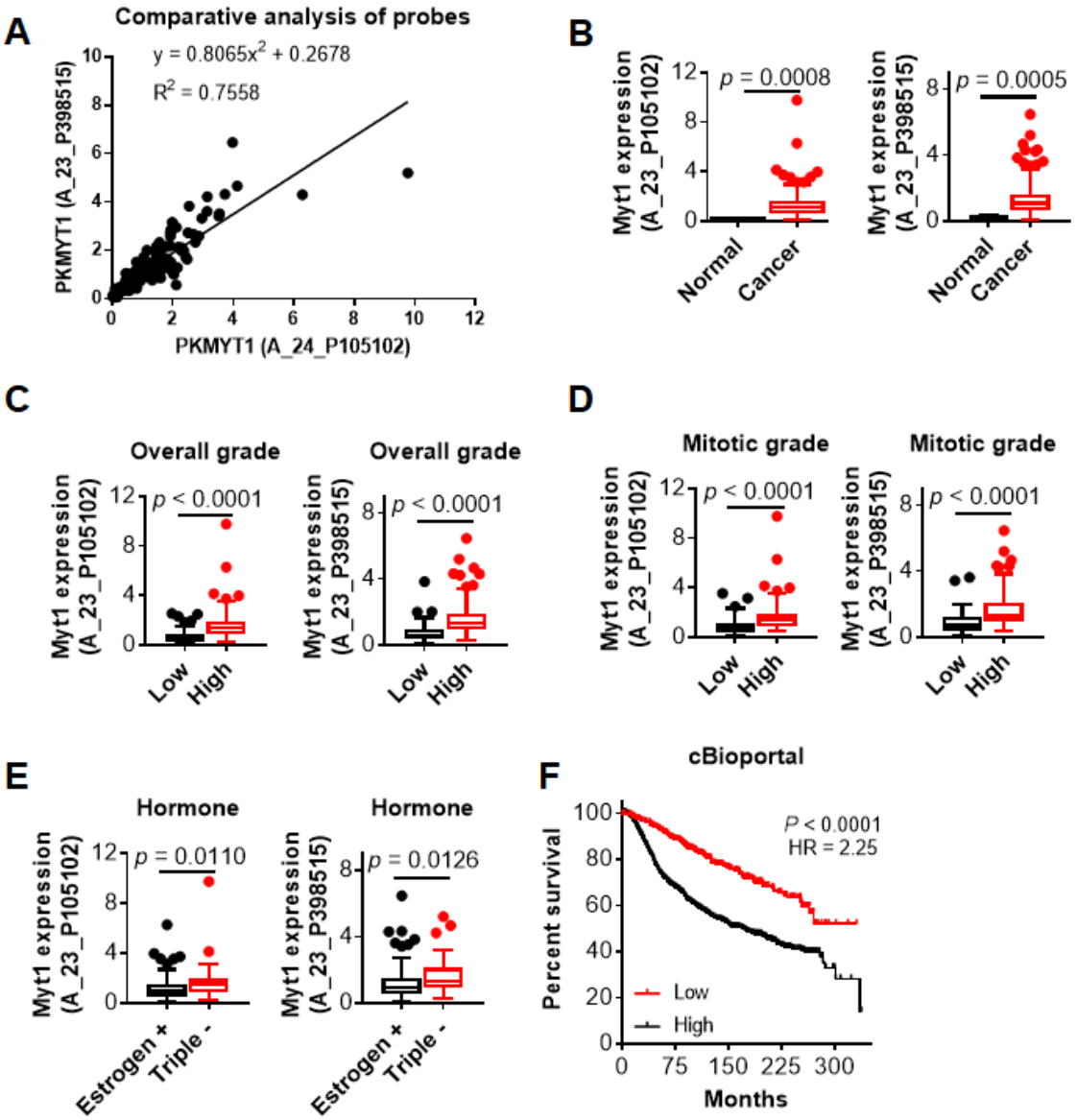

Supplementary Figure 3.1. Upregulation of Myt1 is associated with a worse clinical outcome

Patient breast cancer tissue was analyzed for Myt1 mRNA expression by DNA microarray. **A)** Comparative analysis of Myt1 probes (A_24_P105102 and A_23_P398515). Average of the two probes is shown in Figure 1. **B)** Normalized Myt1 expression (A_24_P105102 and A_23_P398515) in breast cancer tissue (n =176) was compared to normal breast tissue (n = 10). **C)** Overall disease grade, **D)** mitotic grade, and **E)**, hormone receptor status was compared between cancers with high (above the 25th percentile; n = 132) and low (below the 25th percentile; n = 44) Myt1 expression. **F)** Kaplan-Meier curves show overall survival in high and low Myt1 expressing cancer (1423 breast cancer patients; cBioPortal database).

4 Chapter 4. Myt1 overexpression restores Cdk1 regulation in Wee1 inhibited cancer cells

4.1 Background/rationale

We showed that transient overexpression of GFP-Myt1 in HeLa and MDA-MB-231 cells promoted Adavosertib resistance (Lewis et al., 2019); GFP-Myt1 reduced *in vitro* Cdk1 activity and promoted cell survival in Wee1 inhibited cells. However, we were unable to test the effects of GFP-Myt1 expression on mitosis directly due to high cytotoxicity induced by transfection. Furthermore, transfection efficiencies varied between experiments and we were unable to generate a stable cell line. To overcome these technical issues, we in collaboration with the Gamper lab developed a tetracycline inducible (Tet-On) Myt1 system using Flp-In^{TM} T-Rex^{TM} HeLa cells (a gift from Dr. Stephen Taylor, University of Manchester, UK) (Tighe et al., 2008). The Flp-In^{TM} element contains a site directed Flippase (Flp) recombination target (FRT) site (Sauer, 1994), which allows site directed gene integration of a plasmid containing a FTR site in the presence of the Flp [reviewed in (Ward et al., 2011)]. The T-Rex^{TM} element encodes a tetracycline repressor (tetR) (Yao et al., 1998), which recognizes and binds to a tetracycline operator (tetracycline operator 2) [reviewed in (Ward et al., 2011)] (**Figure 4.1A**). However, in the presence of tetracycline the tetR is inhibited permitting Myt1 expression. This system was advantageous in that we were able to generate a site directed isogenic inducible stable cell line to study the effects of Myt1 overexpression.

We cloned full length Myt1 into a plasmid vector containing the tetracycline-inducible promoter and the FRT site (pcDNA5/FRT/TO APEX2-GFP) (Padron et al.,

2019). The tetracycline-inducible promoter is consisted of a cytomegalovirus (CMV) promoter containing with two copies of the tetracycline operator 2 (Yao et al., 1998). The tetracycline inducible APEX2-GFP-Myt1 expression vector and a Flp recombinase expression vector (pOG44) were co-transfected into Flp-In™ T-Rex™ HeLa cells to generate a 110 kDa Myt1 fusion protein APEX2-GFP-Myt1 Flp-In™ T-Rex™.

The GFP tag was utilized for imaging experiments. The APEX2 tag is an engineered 28 kDa monomeric ascorbate peroxidase that catalyzes the oxidation of biotin-phenol to the short-lived (~1 ms) biotin-phenoxyl radical in the presence of H_2O_2 [reviewed (Trinkle-Mulcahy, 2019)]. The resulting biotin-phenoxyl radical then covalently attaches to adjacent amino acids of neighboring proteins. The APEX2 tagged was to be used in future experiments to label Myt1 interacting proteins but was not utilized in our experiments. For simplification, GFP-APEX2-Myt1 is referred to as GFP-Myt1 from here on out.

4.2 Results

4.2.1 Induction of Myt1 in HeLa cells does not affect cell division in not treated cells

To validate our inducible Myt1 system, Flp-In™ T-Rex™ HeLa cells containing GFP-Myt1 were either not treated or treated with 2 μM tetracycline. Within 24 h of tetratcycline treatment, we observed ubiquitous GFP-Myt1 expression by immunoblot and fluorescence microscopy (**Figure 4.1B & C**); however, in the absence of tetracycline, GFP-Myt1 was not detected. Given the functional role of Myt1 is to inhibit Cdk1, Myt1 overexpression may induce a cell cycle arrest (Liu et al., 1999; Mueller et al., 1995). To confirm that GFP-Myt1 induction did not induce a cell-cycle arrest in our system, we treated cells with tetracycline for 48 h and then fixed and stained cells with pS10-histone H3 (PH3) and

DAPI (**Figure 4.2A & B**). Similar proportions of PH3 positive cells were observed with or without tetracycline, confirming that GFP-Myt1 does not induce a cell-cycle arrest in interphase. Furthermore, mitotic cells expressing GFP-Myt1 exhibited normal chromosome condensation and segregation (**Figure 4.2C**).

GFP-Myt1 appeared as concentrated rounded hollow structures less than 2 μm in size outside the nucleus during interphase (**Figure 4.2C**; top two panels). The structures in question were absent in prometaphase and metaphase cells, but not in anaphase and telophase cells (**Figure 4.2C**; bottom three panels). This may suggest that these structures are disassembled during the onset of mitosis and then reassembled following anaphase. Diluting the amount of tetracycline from 2 μM down to 30 nM reduced GFP-Myt1 expression in some cells but did not affect the formation of these structures. Furthermore, similar structures were previously observed by our lab during transient transfection with an alternative GFP-Myt1 plasmid lacking APEX2 (pEGFP-Myt1-GW) in HeLa and MDA-MB-231, confirming that the formation of these structures is not unique to the Flp-In™ T-Rex™ GFP-APEX2-Myt1 HeLa system. Still, we are unclear of the precise nature of these structures.

4.2.2 Cells expressing GFP-Myt1 exhibit increased survival in the presence of Adavosertib

We previous showed that Adavosertib resistance is correlated with high Myt1 expression. To test if GFP-Myt1 induction promoted resistance in the HeLa Flp-In™ T-Rex™ system, cells were treated with Adavosertib in the presence or absence of tetracycline (**Figure 4.3**). Non-induced cells had a an IC50 of 101 nM, which was much lower that the IC50 previously observed in HeLa cells that did not contain the Flp-In™ T-Rex™ system.

Regardless, GFP-Myt1 induction increased the Adavosertib IC50 3-fold (Two-way ANOVA; $P < 0.049$).

4.2.3 GFP-Myt1 induction prevents mitotic entry from S-phase and promotes mitotic exit in Wee1 inhibited cells

Next, we tested if GFP-Myt1 could rescue cells from aberrant mitosis induced by Adavosertib. We first established stable Flp-In™ T-Rex™ GFP-Myt1 cells expressing mRuby-H2B. Asynchronous cell populations treated with either DMSO or 250 nM Adavosertib (+/- tetracycline) were then analyzed by time-lapse microscopy (**Figure 4.4A & B**). Induced and non-induced cells had similar median mitotic times (55 min and 50 min). Furthermore, GFP-Myt1 induced cells did not any display defects in chromosome alignment or segregation (**Figure 4.4A & C**). In contrast, nearly all Adavosertib-treated cells were unable to achieve chromosomal alignment in the absence of tetracycline; instead, cells arrested in prometaphase for several hours and then died without completing mitosis (**Figure 4.4A, C & D**). However, GFP-Myt1 induction in the presence of Adavosertib permitted chromosomal alignment and mitotic exit (**Figure 4.4A, C & D**).

We previously showed that Adavosertib disrupts the cell cycle by at least two independent mechanisms: forced mitotic entry from S phase and delayed mitotic exit. To test if GFP-Myt1 prevented cells from entering mitosis directly from S phase, G1/S synchronized cells were released from media containing either DMSO or Adavosertib in the absence or presence of tetracycline. The point at which cells enter mitosis was then analyzed by time-lapse microscopy (**Figure 4.5A**). Most DMSO-treated cells, with or without tetracycline, entered mitosis 9-11 h post G1/S release (**Figure 4.5A**; top two panels). Non-induced cells treated with 125-250 nM Adavosertib entered mitosis within 3-

5 h, indicating premature mitotic entry (**Figure 4.5A**; 3rd and 4th panel). In contrast, GFP-Myt1 induced cells treated with Adavosertib entered mitosis at a similar time to that of DMSO controls, which suggests Myt1 prevents premature mitotic entry in the absence of Wee1 activity. To further confirm this, *in vitro* Cdk1 activity was measured 4 h after releases from G1/S phase (**Figure 4.5B-D**). Consistent with imaging experiments, GFP-Myt1 induced cells exhibited significantly lower *in vitro* Cdk1 activity relative to non-induced cells in the presence of Adavosertib.

Next, we tested if Myt1 could facilitate mitotic exit in Wee1-inhibited cells that were synchronized in mitosis. G1/S phase cells were released for 8 h and then treated with Adavosertib and analyzed by time-lapse microscopy (**Figure 4.6A & B**). Most DMSO-treated cells (+/- tetracycline) underwent NEBD and chromosome segregation within 60-65 min, consistent with a normal mitotic duration for HeLa cells (Lewis et al., 2017). In contrast, non-induced cells that were treated with Adavosertib were more prone to prometaphase arrest and cell death in mitosis (**Figure 4.6A-C**). GFP-Myt1 induction decreased the number of cells that arrested in prometaphase and died in mitosis, which suggests that Myt1 promotes mitotic exit in the absence of Wee1 activity.

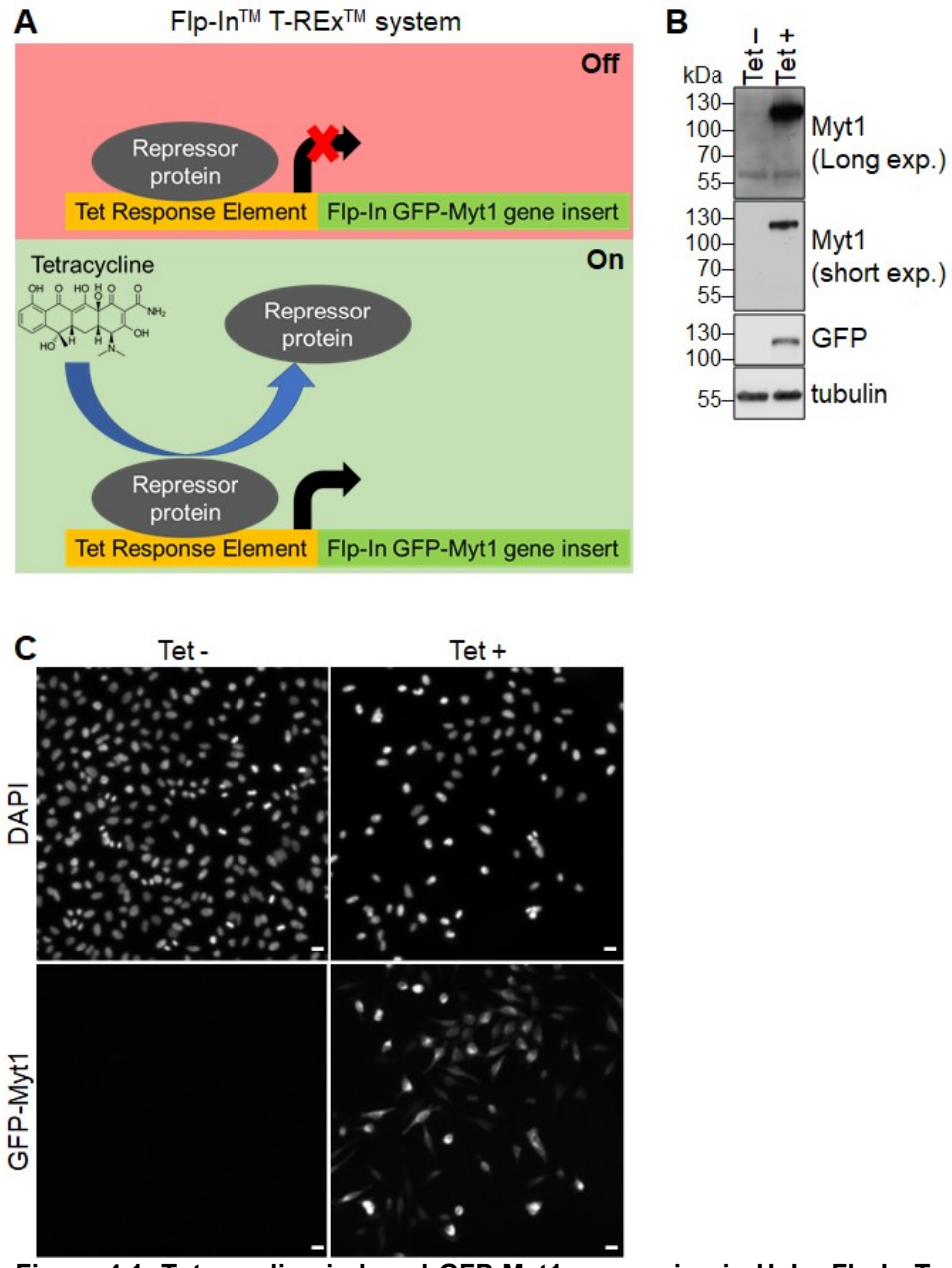

Figure 4.1. Tetracycline induced GFP-Myt1 expression in HeLa Flp-In T-REx cells.

A) Schematic of Flp-In™ T-REx™ system. In the absence of Tetracycline (top), transcription repressor protein binds to the tetracycline (Tet) response element inhibiting Myt1 expression. In the presence of tetracycline (bottom), the transcription repressor protein dissociates from the Tet-response element permitting GFP-Myt1 transcription. Scale bar = 20 μm **B)** Nontreated and tetracycline-treated HeLa cells were analyzed by immunoblot for total levels of Myt1, GFP, and tubulin. Long exposure shows endogenous Myt1 levels. **C)** Not-treated and tetracycline-treated HeLa cells were fixed and stained for DAPI.

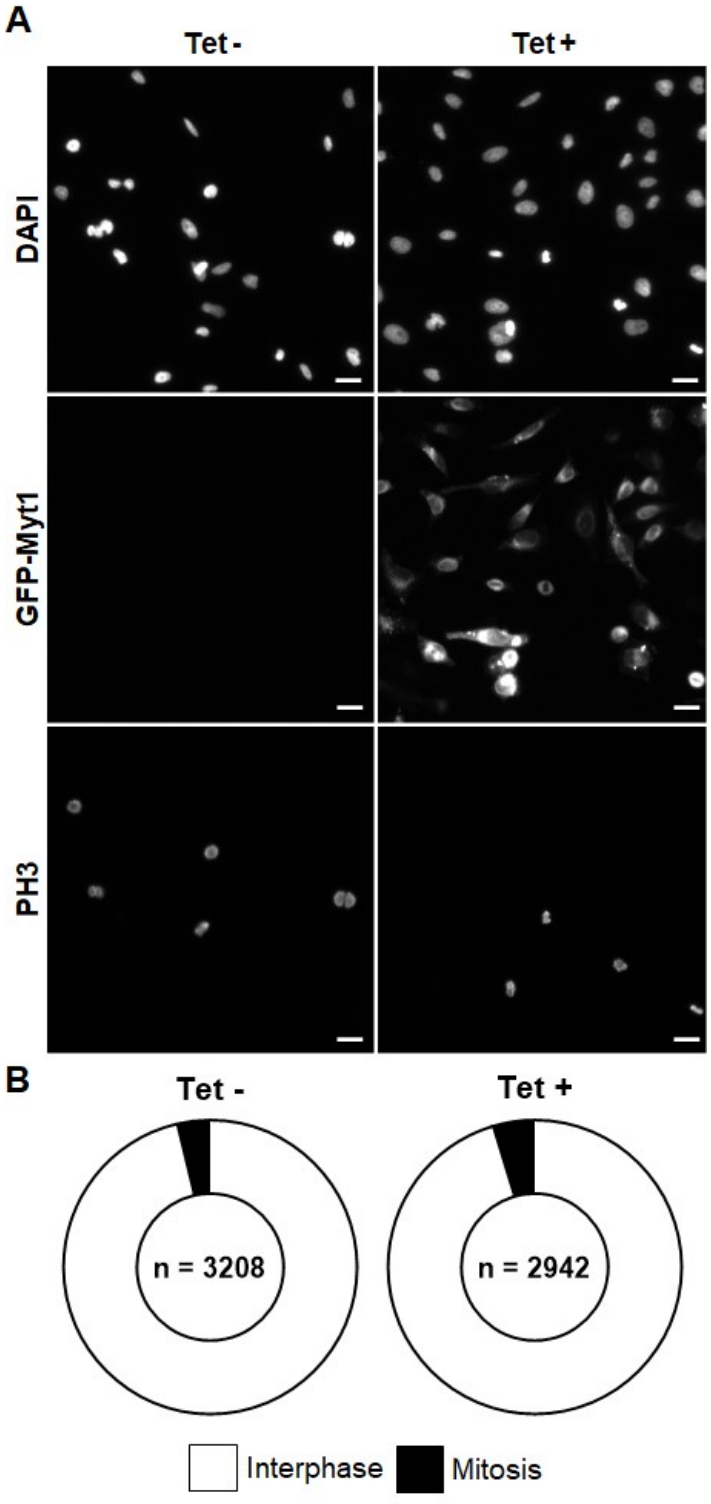
A
Tet -
Tet +
DAPI
GFP-Myt1
PH3
B
Tet -
Tet +
n = 3208
n = 2942
Interphase
Mitosis

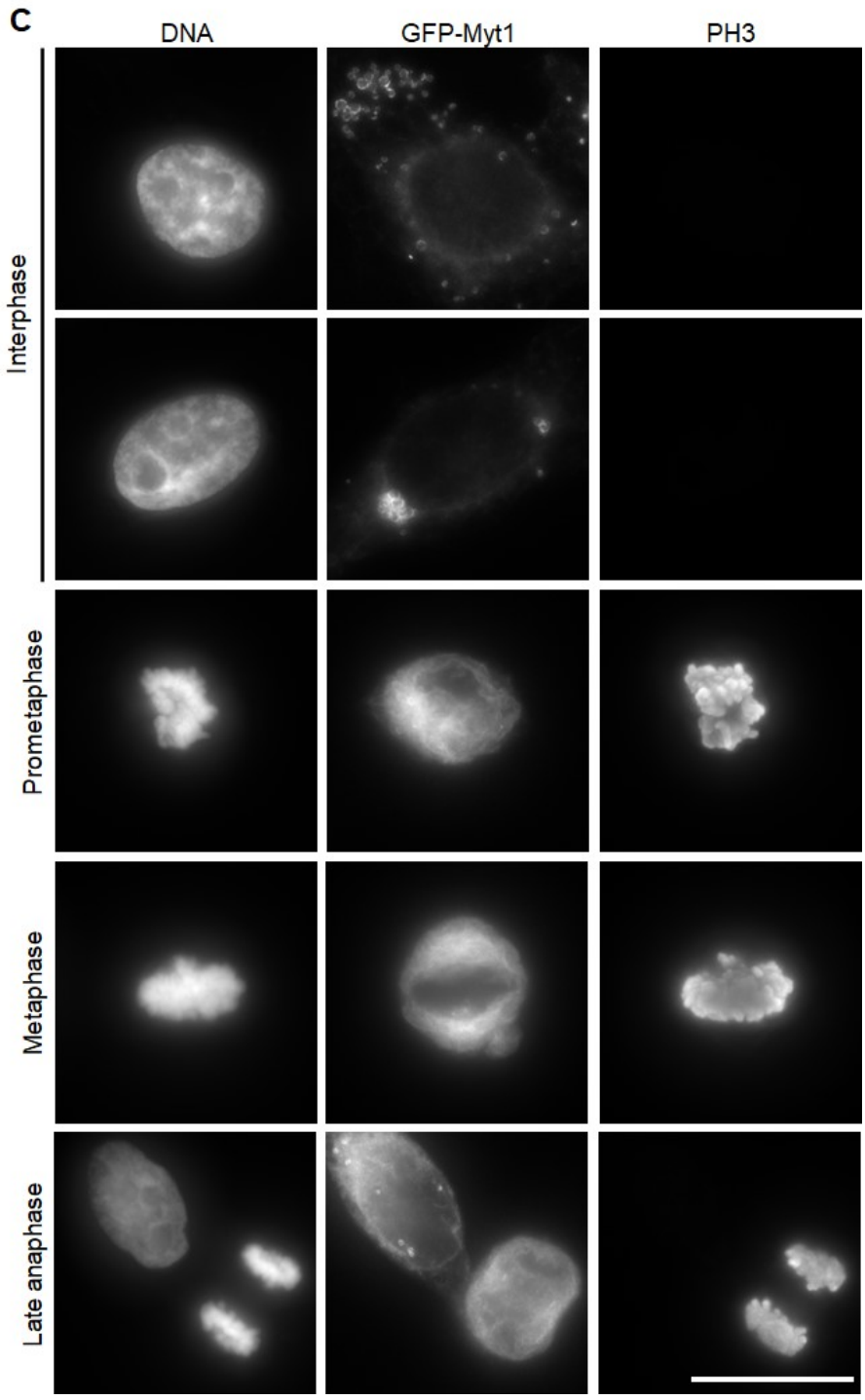

Figure 4.2. GFP-Myt1 does not induce a cell cycle arrest.
A) HeLa cells were either not treated or treated with 2 μM tetracycline for 48 h and then analyzed for total levels of PH3 by immunofluorescence microscopy. Scale bar = 20 μm. **B)** Donut plot show the portion of PH3 positive cells relative to DAPI. The number of cells counted for each treatment is presented in the centre of each plot. **C)** Representative interphase and mitotic cells (at indicated stages) expressing GFP-Myt1 are shown. Scale bar = 20 μm. Experiments were repeated three times.

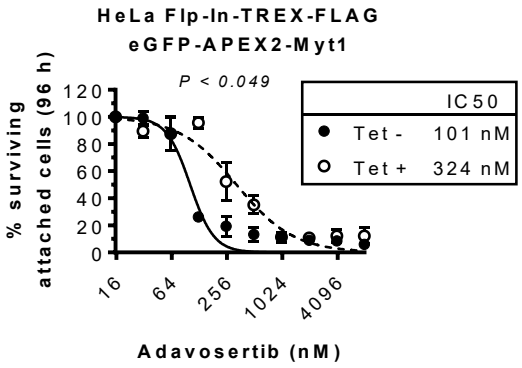

Figure 4.3. GFP-Myt1 induction promotes Adavosertib resistance.
HeLa cells were either not treated or treated with 2 μM tetracycline for 24 h and then treated with Adavosertib for an additional 96 h. Graph shows the average percent cell survival analyzed by crystal violet assay. Error bars represent SEM. Experiment was repeated three times.

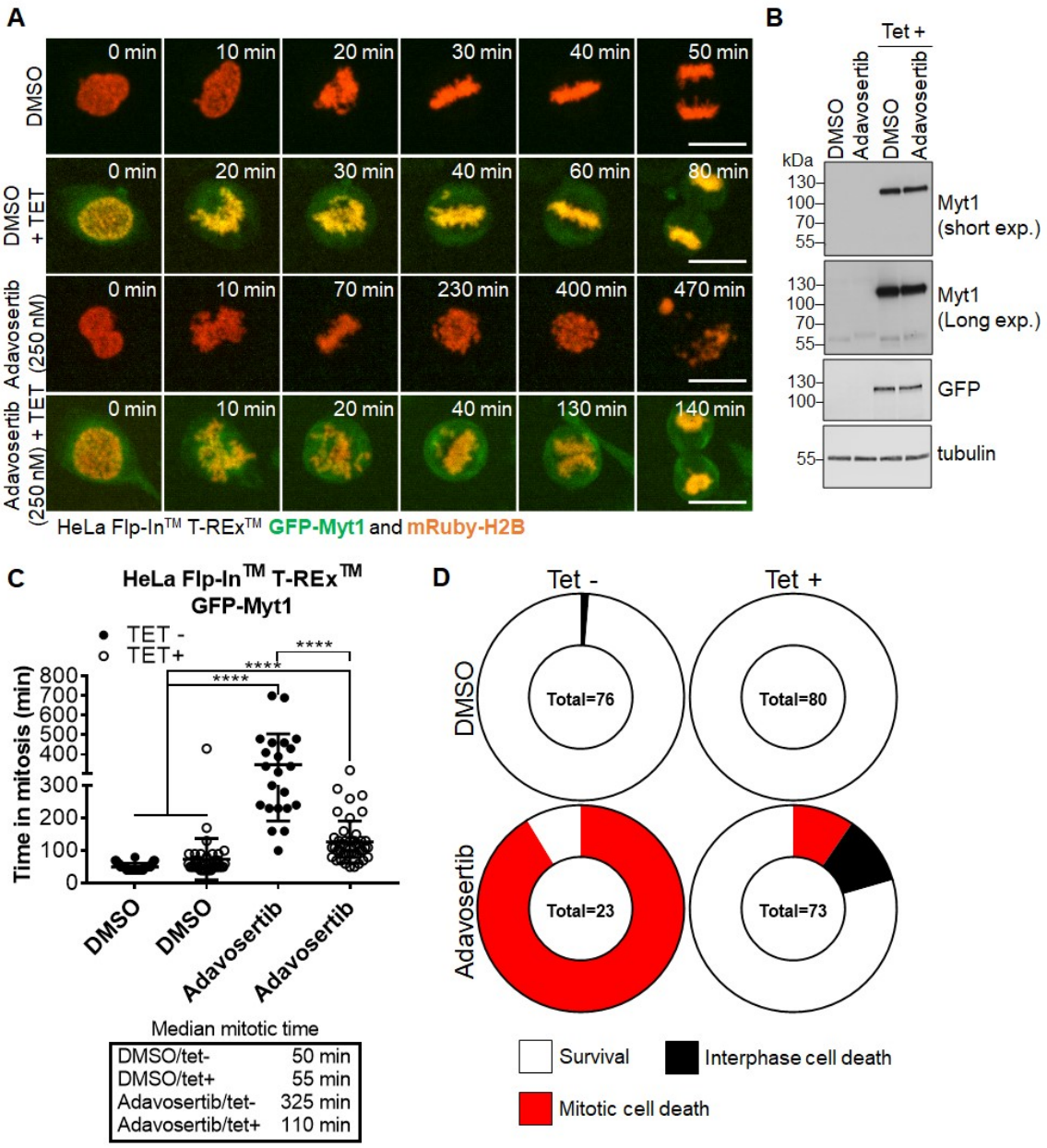

Figure 4.4. GFP-Myt1 induction rescues cells from Adavosertib induced mitotic arrest.
A) HeLa cells were treated with 250 nM Adavosertib in the presence or absence of 2 μM tetracycline and then analyzed by time-lapse microscopy. Scale bar = 10 μm. **B)** Immunoblot shows total levels of GFP, Myt1, and tubulin. **C)** Time in mitosis for indicated treatments is shown. **** denotes $P < 0.0001$ (ANOVA). Median mitotic times are included in table below. **D)** Donut plot show the proportion of cell death for each treatment. Number of cells counted is shown within each donut plot. Experiments were repeated at least three times.

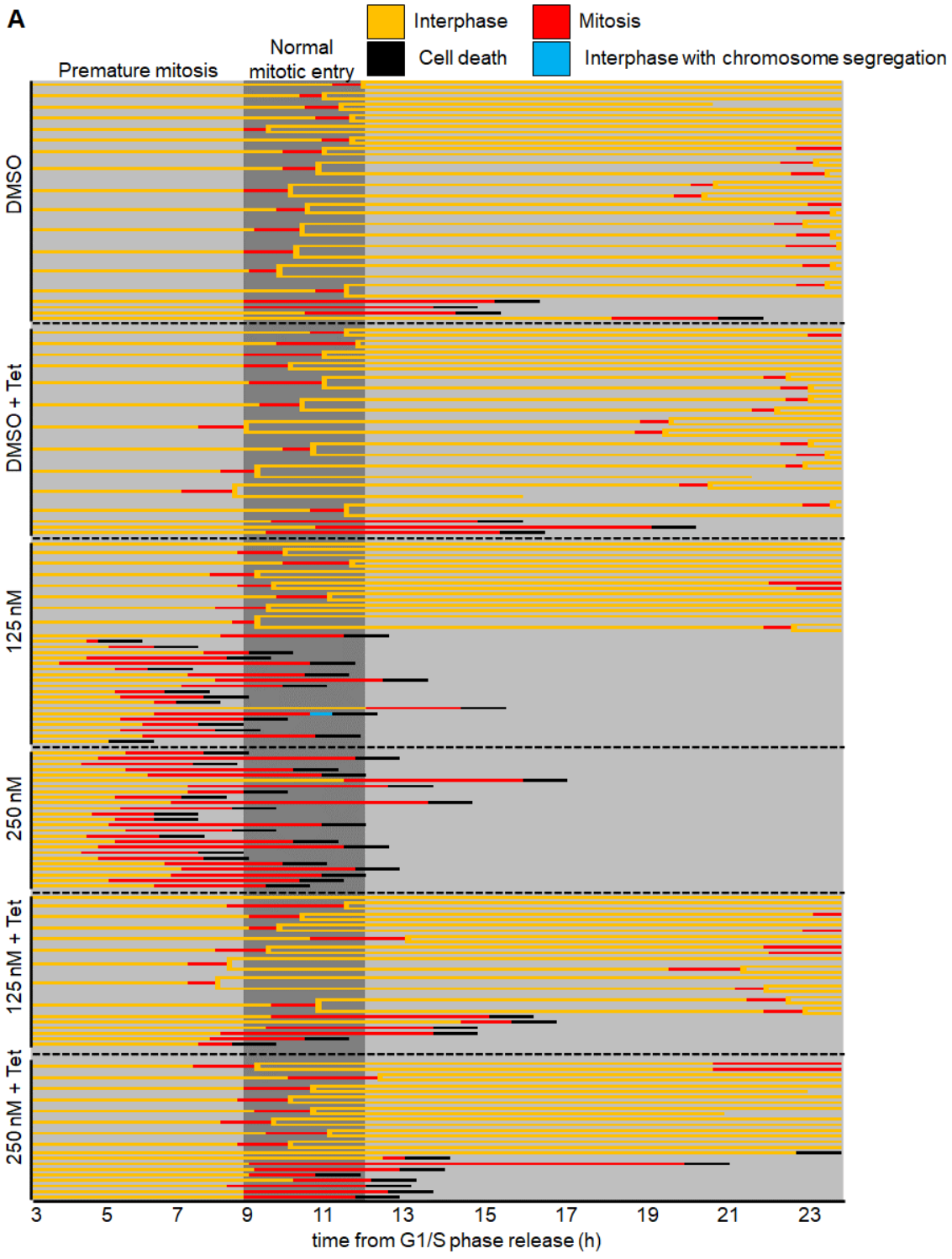
A
Interphase
Mitosis
Cell death
Interphase with chromosome segregation
Premature mitosis
Normal mitotic entry
DMSO
DMSO + Tet
125 nM
250 nM
125 nM + Tet
250 nM + Tet
3
5
7
9
11
13
15
17
19
21
23
time from G1/S phase release (h)

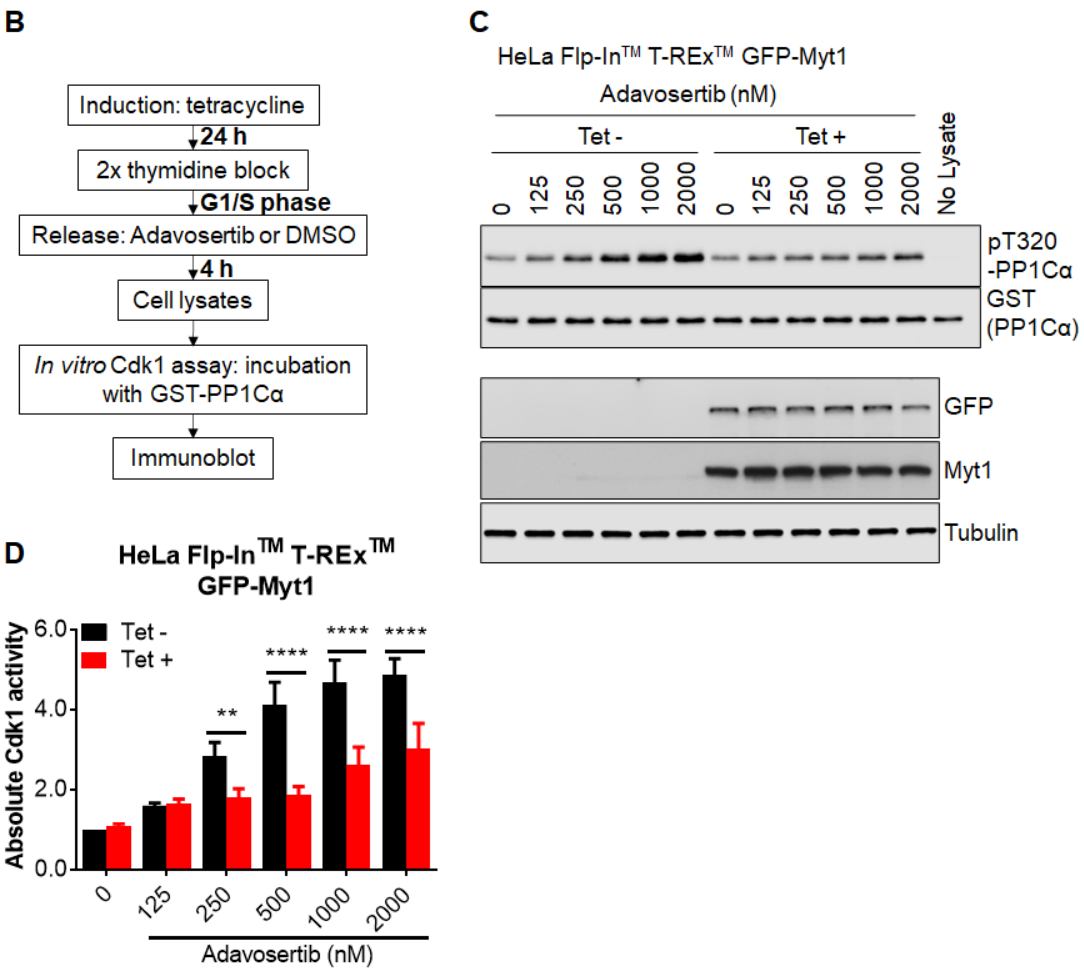

Figure 4.5. GFP-Myt1 prevents premature mitotic entry from S phase in the presence of Adavosertib.
A) Not treated or tetracycline treated HeLa cells were released from G1/S phase into media containing either DMSO or Adavosertib and then analyzed by time-lapse microscopy (3 post G1/S release). Each line represents a single cell and forked lines indicate cell division. Dark grey box indicates the time when nontreated cells are expected to enter mitosis (9-11 h). **B)** Flow chart depicts *in vitro* kinase assay. Cdk1 activity in lysates from cells 4 h after G1/S release was assessed *in vitro* by incubation with GST-PP1Cα (a Cdk1 substrate). Total pT320-PP1Cα peptide and GST levels were determined by immunoblot. **C)** *In vitro* Cdk1 activity (top two panels) was assessed in HeLa cells (treatments are indicated). GFP, Myt1, and tubulin levels were analyzed by immunoblot (bottom two panels). **D)** Graph shows the quantitation of average Cdk1 activity (relative to control Tet-/DMSO). Error bars represent SEM. ** and *** denote $P < 0.01$ and $P < 0.0001$ (Two-way ANOVA). Experiments were repeated at least three times.

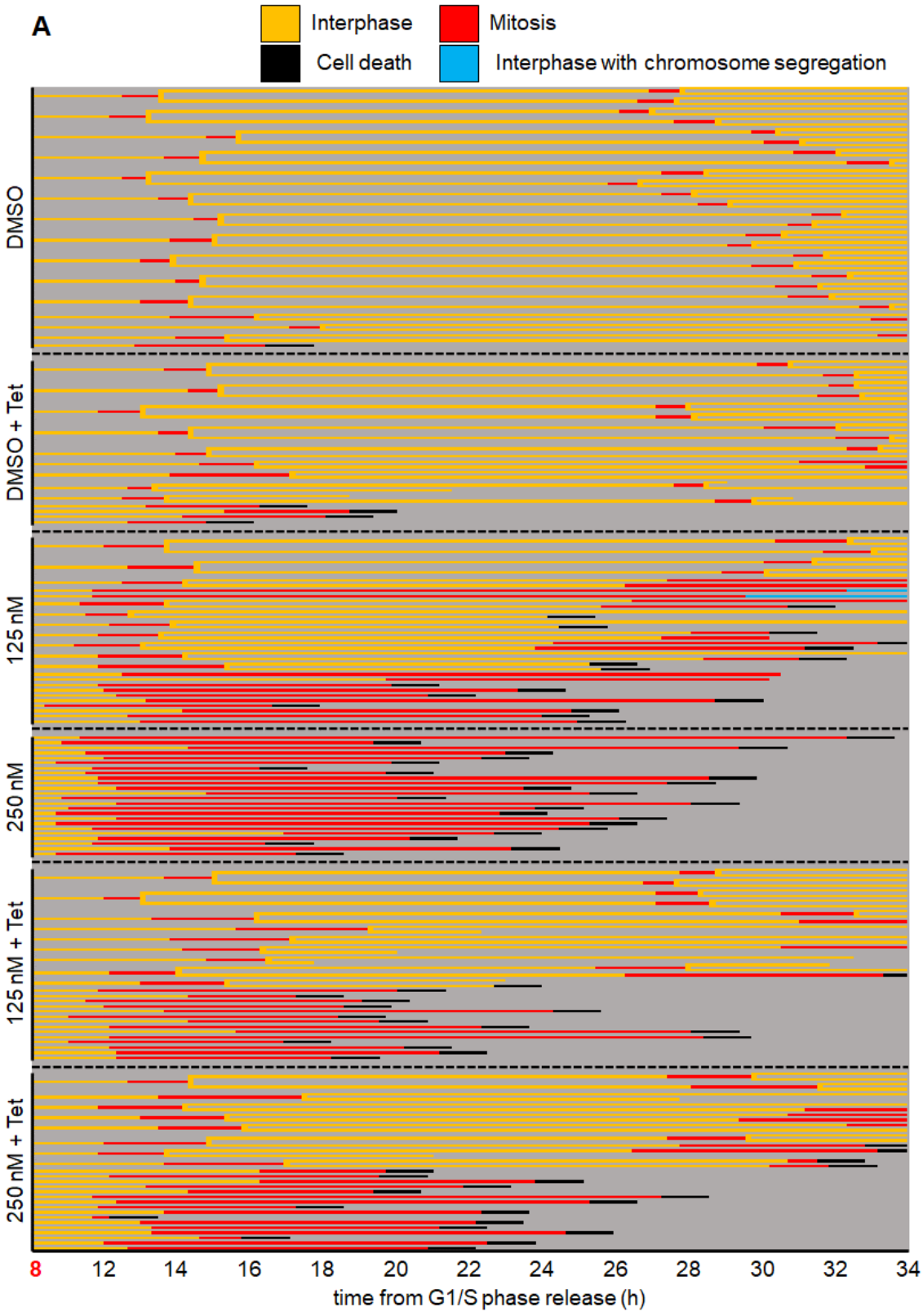
A
Interphase
Mitosis
Cell death
Interphase with chromosome segregation
DMSO
DMSO + Tet
125 nM
250 nM
125 nM + Tet
250 nM + Tet
8
12
14
16
18
20
22
24
26
28
30
32
34
time from G1/S phase release (h)

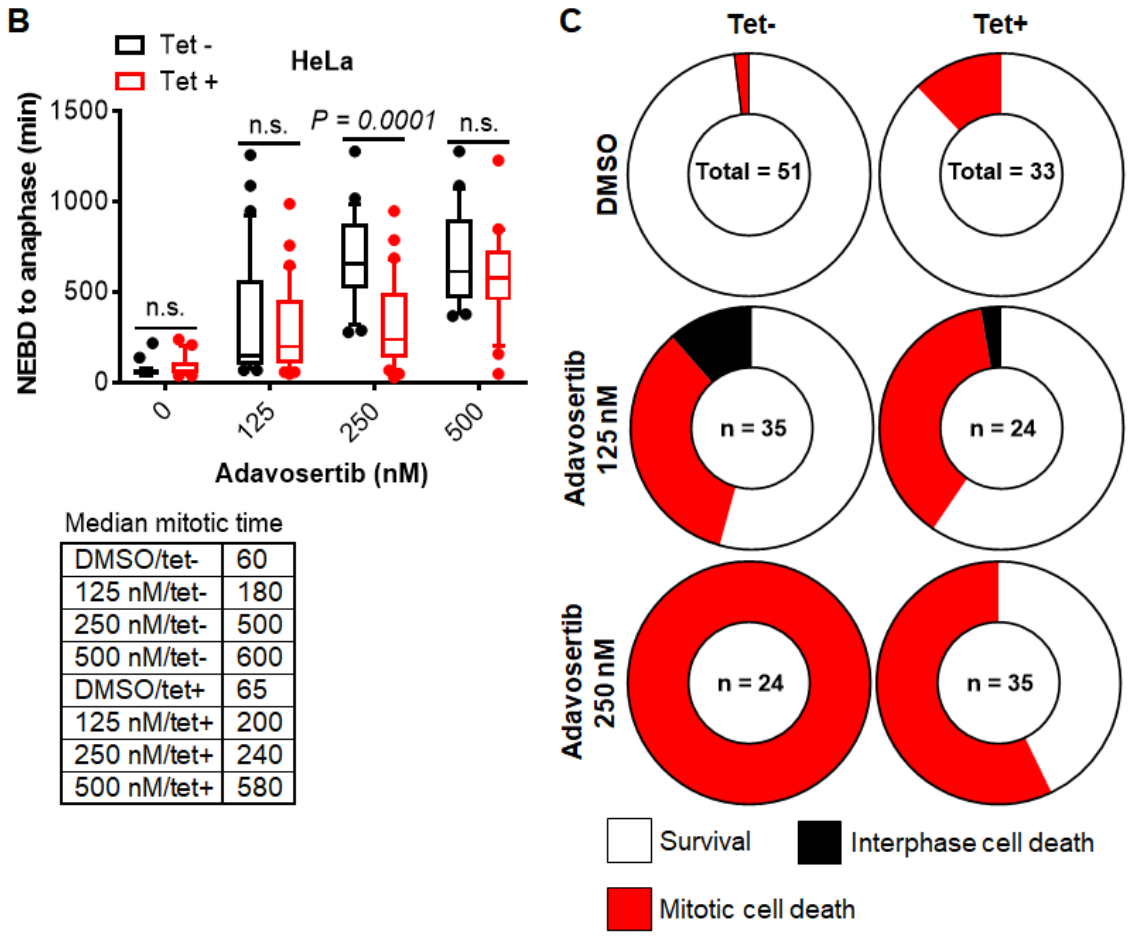

Median mitotic time

DMSO/tet-	60
125 nM/tet-	180
250 nM/tet-	500
500 nM/tet-	600
DMSO/tet+	65
125 nM/tet+	200
250 nM/tet+	240
500 nM/tet+	580

Figure 4.6. GFP-Myt1 induction promotes mitotic exit in the presence of Adavosertib.
A) Nontreated and tetracycline treated HeLa cells were released from G1/S for 8 h into media containing either DMSO or Adavosertib and then analyzed by time-lapse microscopy. Each line represents a single cell and forked lines indicate cell division. **B)** Graph indicates the duration of mitosis (NEBD to anaphase/mitotic slippage). Median mitotic times are included in table below. **C)** Donut plots indicate the proportion of cell death observed for each treatment. Number of cells counted is indicated within each donut plot. Experiments were repeated at least three times.

4.3 Discussion

Upregulation of Myt1 induces intrinsic and acquired Adavosertib resistance in cancer cells; high Myt1 expression is associated with reduced ectopic Cdk1 activity, resistance to premature mitotic entry, and increased cancer cell survival in the presence of Adavosertib (Lewis et al., 2019). We previously showed that siRNA knockdown of Myt1 increased the number of cells that prematurely entered mitosis as well as increased the duration of mitotic arrest in HeLa and MDA-MB-231 cells (Lewis et al., 2019). However, the effects of Myt1 overexpression on mitotic timing in Wee1 inhibited was not directly addressed. Here we demonstrate that Myt1 rescues cells from aberrant mitosis induced by Wee1 inhibition.

Wee1 inhibition by Adavosertib disrupts the cell cycle by two independent mechanisms. First, Wee1 inhibition by Adavosertib in S-phase leads to an upregulation in Cdk1 activity, which forces cells into mitosis with under-replicated chromosomes leading to chromosome fragmentation (Aarts et al., 2012; Duda et al., 2016; Lewis et al., 2017). Chromosome fragmentation prevents bipolar chromosomal alignment, which prolongs MCC activation and Cdk1 activity. Second, Cdk1 re-phosphorylation and cyclin B degradation are key steps required for mitotic exit (Chow et al., 2011; Jin et al., 1998; Lewis et al., 2017; Visconti et al., 2015; Visconti et al., 2012). Mitotic synchronized cells released from nocodazole into media containing Adavosertib also arrest in mitosis despite having fully replicated undamaged chromosomes (Lewis et al., 2017). We show that Myt1 induced expression prevents premature entry into mitosis in cells synchronized in G1/S and treated with Adavosertib (**Figure 4.5**). We also show that Myt1 induced expression also promotes mitotic exit in cells treated with Adavosertib (**Figure 4.6**).

A previous study reported that mitotic synchronized HeLa cells expressing an inactive Wee1 mutant cannot exit mitosis, a finding that was attributed to loss of Cdk1 re-phosphorylation (Visconti et al., 2015). Although siRNA knockdown of Myt1 alone in HeLa cells does not affect the timing of mitosis (Chow and Poon, 2013; Lewis et al., 2019; Lewis et al., 2017; Nakajima et al., 2008), Myt1 phosphorylates residual Cdk1/cyclin B complexes at the Golgi and endoplasmic reticulum during anaphase and telophase, a process that is essential for reassembly of these organelles after mitosis (Nakajima et al., 2008). We previously showed that Myt1 expression in HeLa cells is low relative to other cancer cell lines (Lewis et al., 2019). As such, it remains unclear if the loss of functional redundancy between Wee1 and Myt1 in HeLa cells is the reason why Myt1 cannot compensate for the loss of Wee1 activity in terms of regulating mitotic timing. Loss of the functional redundancy between Wee1 and Myt1 has been previously described in a subset of patient derived glioblastoma cells (Toledo et al., 2015). In these cells, Wee1 is downregulated relative to normal neural cells and as a result glioblastoma cells rely on Myt1 for Cdk1 regulation and mitotic timing. Myt1 knockdown or knockout by siRNA or CRISPR/Cas9 respectively, induces a mitotic arrest and cell death in mitosis. Therefore, we hypothesize that higher Myt1 levels in other cancer cells allow Myt1 to function more redundantly with Wee1 in regulating Cdk1 activity during interphase and during mitotic exit.

5 Chapter 5. Comparing the effects of PD0166285 and Adavosertib in cancer cells

5.1 Background/rationale

We previously showed that Myt1 upregulation induces Adavosertib resistance in HeLa and breast cancer cells (Lewis et al., 2019). In this study, we found that knockdown of Myt1 by siRNA could sensitize resistance cells to Wee1 inhibition, which suggested that co-inhibition of Wee1 and Myt1 could be an effective means of overcoming Adavosertib resistance. Currently, there are no selective small molecule Myt1 inhibitors; however, there are several broad-spectrum inhibitors, such as PD0166285 that inhibit both Wee1 and Myt1 (Najjar et al., 2019; Wang et al., 2001). Wang *et al.* reported that PD0166285 inhibits the *in vitro* kinase activity of Wee1 and Myt1 at IC50s of 24 nM and 72 nM respectively (Wang et al., 2001). Furthermore, in human colorectal cell lines, 500 nM PD0166285 was found to reduce Cdk1 phosphorylation on both T14 and Y15 (biomarkers for Wee1 and Myt1 activity respectively) (Wang et al., 2001).

In contrast, *in vitro* studies show that Adavosertib inhibits Wee1 and Myt1 at 5 nM and >500 nM (Hirai et al., 2009). In breast cancer cell lines (MDA-MB-231 and MDA-MB-468), Adavosertib treatment reduces pY15-Cdk1 at concentrations as low as 125 nM, but has little effect on pT14-Cdk1 even at concentrations as high as 1000 nM (Lewis et al., 2019). To take advantage of the dual specificity of PD0166285, we set out to evaluate the efficacy of PD0166285 in the presence or absence of Adavosertib.

5.2 Results

5.2.1 PD0166285 reduces both pT14- and pY15-Cdk1 in HeLa cells

To compare Adavosertib and PD0166285 potency against Wee1 and Myt1, HeLa and MDA-MB-231 cells were treated with 250 nM and 500 nM of each inhibitor for 4 h and then analyzed for total levels of pT14- and pY15-Cdk1 relative to total Cdk1 levels (**Figure 5.1**). Consistent with previous studies (Lewis et al., 2019), Adavosertib reduced pY15-Cdk1 in a dose dependent manner but did not affect pT14-Cdk1 in either HeLa or MDA-MB-231 cells, confirming that Adavosertib inhibits Wee1 but not Myt1 (n = 2). In contrast, PD0166285 reduced both pT14- and pY15-Cdk1 levels (Wang et al., 2001); however, at both concentrations tested (250 nM and 500 nM) pY15-Cdk1 levels decreased greater than pT14-Cdk1 suggesting that PD0166285 inhibits Wee1 slightly better than Myt1 (N = 2 for HeLa and N = 1 for MDA-MB-231).

5.2.2 PD0166285 is less cytotoxic towards cancer cells than Adavosertib

We compared HeLa and breast cancer cell sensitivity to PD0166285 and Adavosertib. HeLa, MDA-MB-231, SK-BR-3, and BT-474 cells were treated with increasing concentrations of either PD0166285 or Adavosertib for 96 h and then analyzed for cell survival by crystal violet assay (Bukhari et al., 2019; Feoktistova et al., 2016; Lewis et al., 2019) (**Figure 5.2A-D**). In three of the cell lines examined (HeLa, SK-BR-3, and BT-474), the IC50s for Adavosertib were lower compared to PD0166285, suggesting that monotreatment with Adavosertib induce more cell killing relative to that of PD0166285 (n = 3). Both Adavosertib and PD0166285 exhibited similar IC50s in MDA-MB-231 cells (n = 3).

5.2.3 Adavosertib has little to no effect on PD0166285 induced-cell death

We next tested if low dose Adavosertib could enhance the effects of PD0166285. HeLa and MDA-MB-231 cells were pre-treated with either DMSO or a sublethal concentration of Adavosertib (100 nM) for 16 h and then treated with increasing concentrations of PD0166285 for an additional 96 h (**Figure 5.3A & B**). Adavosertib slightly reduced the PD0166285 IC50 in HeLa cells from 241 nM to 122 nM but had no effect on MDA-MB-231 cells (n =2).

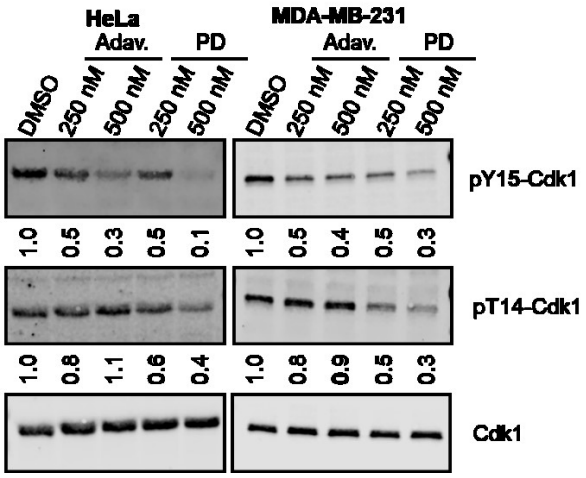

Figure 5.1. PD0166285 inhibits Cdk1 phosphorylation on T14 and Y15. HeLa and MDA-MB-231 cells were treated with indicated concentrations of Adavosertib (Adav) or PD0166285 (PD) for 4 h and then analyzed for total levels of pY15-Cdk1, pT14-Cdk1, and Cdk1 by immunoblot. The quantitation of pT14- and pY15-Cdk1 relative to total Cdk1 levels are presented below respective immunoblots. For HeLa, quantitation reflects an average of 2 experiments whereas for MDA-MB-231 the quantitation is from a single experiment.

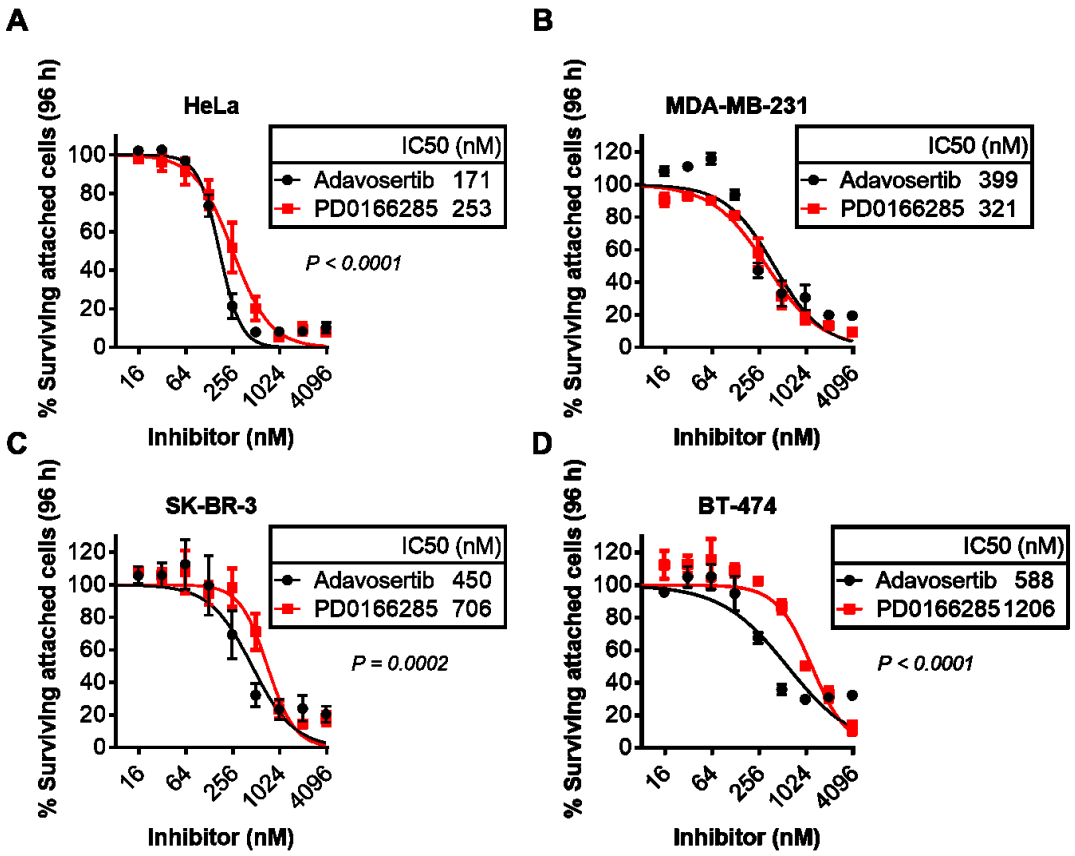

Figure 5.2. PD0166285 is less cytotoxic to cancer cells compared Adavosertib.

A) HeLa, **B)** MDA-MB-231, **C)**, SK-BR-3, and **D)** BT-474 cells treated with Adavosertib or PD0166285 for 96 h and then analyzed for cell survival by crystal violet assay. Calculated IC50 values are presented in tables for each cell line. Experiments were repeated twice.

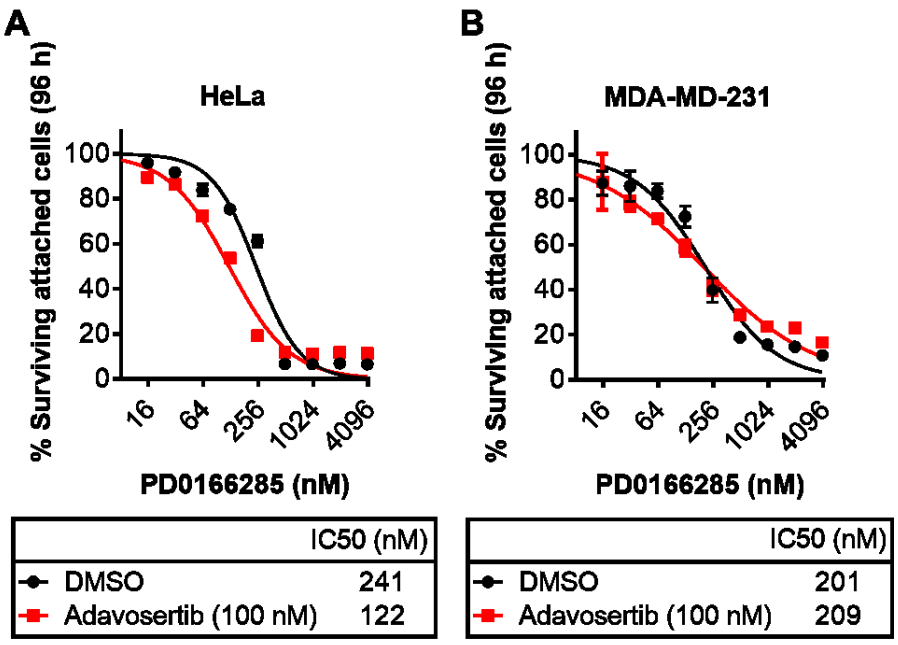

Figure 5.3. Adavosertib has little to no effect on PD0166285 induced-cell death.

A) HeLa and **B)** MDA-MB-231 cells were pre-treated with DMSO or 100 nM Adavosertib for 16 h and then treated with PD0166285 for an additional 96 h. Cell survival was analyzed by crystal violet assay. Calculated IC50 values are presented below graphs. Experiments were repeated twice.

5.3 Discussion

A one to one comparison of PD0166285 and Adavosertib showed that PD0166285 reduced both pT14- and Y15-Cdk1 levels in HeLa and MDA-MB-231 cells, whereas Adavosertib only reduced the levels of Y15-Cdk1. This data confirms previous studies that PD0166285 inhibits both Wee1 and Myt1 whereas Adavosertib inhibits Wee1 but not Myt1 in cancer cells (Lewis et al., 2019; Wang et al., 2001). We previously showed that Myt1 knockdown by siRNA enhanced the efficacy of Adavosertib treatment in HeLa and a subset of breast cancer cell lines (Lewis et al., 2019), suggesting that Myt1 inhibition may enhance the effects of Wee1 inhibition. Given the dual specificity of PD0166285 against both Wee1 and Myt1, we predicted that PD0166285 would exhibit higher cancer cell cytotoxicity compared to Adavosertib. However, PD0166285 was found to be less cytotoxic compared to Adavosertib in three of the four cell lines tested. Furthermore, Adavosertib only slightly enhanced the effects of PD0166285 in HeLa but not MDA-MB-231 cells.

A major limitation of small molecule inhibitors is that they often have unintended off-target effects. Adavosertib is reported to exhibit activity against several other kinases including Plk1, Yes, and Src at concentrations of 100-1000 nM (Hirai et al., 2009; Wright et al., 2017; Zhu et al., 2017). Similarly, PD0166285 has been shown to exhibit activity against Chk1, Src, epidermal growth factor receptor (EGFR), fibroblast growth factor receptor 1 (FGFR1), and platelet-derived growth factor receptor b (PDGFRb) in the low nanomolar range (De Witt Hamer et al., 2011; Dimitroff et al., 1999; Panek et al., 1997; Wang et al., 2001). The unintended inhibition of one or more of these kinases may enhance Wee1 inhibition by Adavosertib or diminished the effects of Wee1/Myt1 inhibition by PD0166285.

Another issue was that PD0166285 only partially inhibited Myt1 activity. At 250-500 nM, PD0166285 only reduces pT14-Cdk1 levels by 40-60% in HeLa and 50-70% in MDA-MB-231 cells. Therefore, the pool of uninhibited Myt1 may have been enough to protect cells from premature mitosis in Wee1 inhibited cells. In future experiments, it would be useful to compare how mitotic timing is affected by mono- and co-treatment with PD0166285 and Adavosertib.

It is worth mentioning that Myt1 kinase activity might not be required for Cdk1 inhibition in cells that overexpress Myt1. Wells *et al.* reported that overexpression of either wild-type or catalytically inactive Myt1 (Myt1 D251A) equally arrested HeLa cell populations in G2 phase (Wells et al., 1999). This G2 arrest was attributed to the ability of Myt1 to sequester Cdk1/cyclin B at the Golgi and endoplasmic reticulum independent of Cdk1 phosphorylation (Wells et al., 1999). Cytoplasmic sequestration of a non-phosphorylatable Cdk1 mutant (Cdk1 T14A/Y15F) was also reported to maintain G2 arrest in U-2 OS cells (Heald et al., 1993). If Myt1 kinase activity is not required to inhibit Cdk1 activity, then small molecule Myt1 inhibitors are unlikely to exhibit a strong effect on cell cycle progression. In future experiments, it will be important to elucidate whether Myt1 kinase activity is required to inhibit Cdk1 activity in the presence of Adavosertib or PD0166285. This could be tested by independently overexpressing wild-type or kinase dead Myt1 with these inhibitors and then analyzing Cdk1 activity both *in vitro* and in intact cells expressing a Cdk1 FRET biosensor (Gavet and Pines, 2010).

Several groups are currently in the process of developing novel selective Myt1 inhibitors (Najjar et al., 2019; Platzer et al., 2018). Once these inhibitors become available it will be important to re-evaluate these inhibitors with Adavosertib.

6 Chapter 6. Discussion and future directions

6.1 Wee1 inhibitors were developed to override DNA damage checkpoints

Wee1 is reported to be overexpressed in triple negative breast cancer (Iorns et al., 2009; Murrow et al., 2010), glioblastomas (Mir et al., 2010; Wuchty et al., 2011), malignant melanomas (Magnussen et al., 2012), malignant squamous cell carcinomas (Magnussen et al., 2013), and osteosarcomas (PosthumaDeBoer et al., 2011). Radiation and other DNA damaging therapies are the mainstays in anticancer therapy [Reviewed in (Baskar et al., 2012; Cheung-Ong et al., 2013)]. Most cancer cells have one or more defective DNA damage checkpoints, which causes cells to enter mitosis with damaged DNA, resulting in cell death by mitotic catastrophe [Reviewed in (Aleem et al., 2005; Visconti et al., 2016)]. However, Wee1 overexpression reinforces DNA damage checkpoints and prevents mitotic catastrophe (Mir et al., 2010). Additionally, Wee1 upregulation also decreases DNA packaging through histone H2B phosphorylation, which has been suggested to enhance DNA accessibility to repair machinery, further promoting resistance to DNA damaging therapies [(Mahajan et al., 2012) and reviewed in (Mahajan and Mahajan, 2013)]. As such, the Wee1 inhibitors such as Adavosertib and PD0166285 were developed as means of enhancing the efficacy of DNA damaging therapies (Hirai et al., 2009; Wang et al., 2001). Adavosertib is the only Wee1 inhibitor currently in clinical trials for the treatment of cancer. Currently, most Adavosertib trials are focused on combination therapies with one or more DNA damaging agents (**ClinicalTrial.gov)**. However, Adavosertib alone also exhibits strong anti-cancer effects in the clinic (Do et al., 2015; Sanai et al., 2018). Understanding why some cancer cells are sensitive to Wee1 inhibition alone is important

for understanding mechanisms of Adavosertib resistance, and for developing novel combination treatments.

6.2 Monotreatment with Adavosertib disrupts S-phase and mitosis

We show that Adavosertib disrupts both S-phase and mitosis in a subset of cancer cells (**Figure 6.1A-C**). Adavosertib forces cancer cells into mitosis directly from S-phase (**Figure 6.1B**). Normally, mitotic entry from G1/S release requires 8-10 h in HeLa cells. However, within 4 h of G1/S release mitosis was detected in Adavosertib-treated cells. Analysis of DNA content showed that Adavosertib treated cells had less than 4N DNA, confirming that these cells had entered mitosis with under-replicated chromosomes. Previous groups have shown that loss of Wee1 activity during S-phase promotes ectopic Cdk1 activity resulting in replication stress, aberrant nuclease activity, and premature mitotic entry and condensation of under-replicated chromosomes (**Figure 1.10**) (Aarts et al., 2012; Dominguez-Kelly et al., 2011; Duda et al., 2016; Hauge et al., 2017; Moiseeva et al., 2019a; Pfister et al., 2015; Szmyd et al., 2019). Consistent with premature Cdk1 activation in S-phase, we observed centromere fragmentation in nearly all cells that prematurely entered mitosis.

HeLa and breast cancer cells exhibiting centromere fragmentation displayed abnormal mitotic spindles and could not align chromosomes, which resulted in mitotic arrest and cell division failure. Moreover, we also observed that cells treated with Adavosertib *after* normal mitotic entry also arrested in mitosis (**Figure 6.1C**). These cells displayed normal mitotic spindles and were able to achieve chromosome alignment. However, progression from metaphase to anaphase was much slower in Adavosertib-

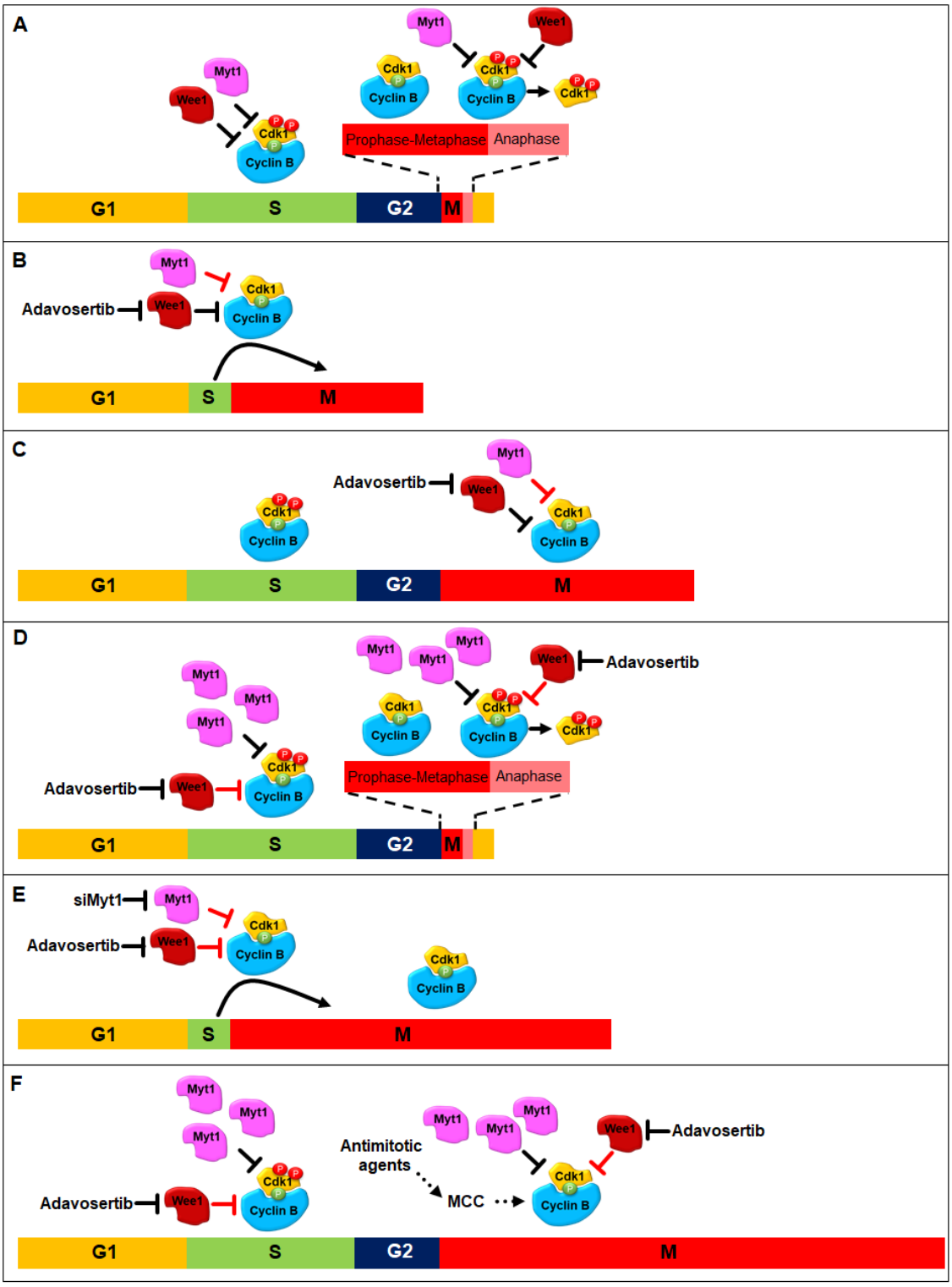

Figure 6.1. Adavosertib disrupts S-phase and mitosis.
A) Wee1 and Myt1 inhibit Cdk1 activity during interphase and during the metaphase to anaphase transition. **B)** Wee1 inhibition by Adavosertib permits premature Cdk1 activation in S-phase (See also **Figure 1.10**) and **C)** delays

mitotic exit. **D)** High Myt1 levels maintain Cdk1 inhibition in Wee1 inhibited cells resulting in normal cell cycle progression. **E)** siRNA knockdown of Myt1 in the presence of Adavosertib induces premature mitosis and mitotic arrest in Adavosertib resistant cells. **F)** Antimitotic agents that delay mitotic exit (e.g. paclitaxel or L-744-832) reinforce mitotic arrest induced by Adavosertib. Black lines are upregulated pathways whereas red lines are downregulated pathways. Solid lines represent direct regulatory processes whereas dotted lines represent indirect regulatory processes.

treated cells relative to DMSO controls. Our data is consistent with others who have reported that Wee1 is essential for normal mitotic exit in HeLa and other cancer cell lines (Visconti et al., 2015; Visconti et al., 2012).

Importantly, some breast cancer cell lines exhibited intrinsic Adavosertib resistance (**Figure 6.1D**). Other groups have also reported Adavosertib resistance in breast and other cancer cell lines (Aarts et al., 2012; Guertin et al., 2013; Sen et al., 2017). Knowing that both S-phase and mitotic cells were vulnerable to Adavosertib, we selectively examined how the downregulation of other regulatory proteins in these phases affected cell sensitivity to the Wee1 inhibitor.

6.3 High Myt1 levels facilitate resistance to Adavosertib

6.3.1 Myt1 protein levels determine cell sensitivity to Adavosertib

Both Wee1 and Myt1 negatively regulate Cdk1 activity; however, previous studies using cancer cell lines such as HeLa and U-2 OS showed that inhibition or knockdown of Wee1, but not Myt1, was sufficient to override DNA damage checkpoints and trigger premature mitotic entry (Chow and Poon, 2013; Nakajima et al., 2008). This suggested that Wee1 exhibited a more dominant role in Cdk1 regulation in cancer cells. However, Myt1 was recently shown to be essential for cell survival in a subset of patient-derived glioblastoma cell lines that had downregulated Wee1 (Toledo et al., 2015). In the study by Toledo *et al*., knockout or knockdown of Myt1 arrested cells in mitosis, a phenotype that is consistent

with HeLa cells depleted of Wee1 activity (Toledo et al., 2015). This study confirmed that Myt1 can compensate for the loss of Wee1 activity in at least some cancer cells. As such, we focussed on elucidating the role of Myt1 in breast cancer cells that are resistant to Wee1 inhibition.

In our experiments, breast cancer cell sensitivity to Adavosertib was strongly correlated with Myt1 protein expression. Cell lines with low Myt1 protein expression (e.g. HeLa and MDA-MB-231) were prone to both premature mitotic entry, centromere fragmentation, and prolonged mitotic arrest in the presence of Adavosertib suggesting that Wee1 exhibits a more dominant role in Cdk1 regulation in these cells. In contrast, high Myt1 expressing cell lines (e.g. BT-474, and SK-BR-3) were resistant to premature mitosis in the presence of Adavosertib (**Figure 6.1B & D**).

Depletion of Myt1 activity is reported to induce meiotic and mitotic defects in some cell systems. For instance, *Drosophila* expressing a homozygous loss-of-function Myt1 mutant are prone to premeiotic centriole disengagement, which induces a multipolar spindle during meiosis (Varadarajan et al., 2016). In our study, Myt1 knockdown alone did not induce multipolar spindle formation in any of the cell lines analyzed. Furthermore, Myt1 knockdown alone did not induce centromere fragmentation, disrupt chromosome alignment, or arrest cells in mitosis. This suggests that HeLa and the breast cancer cell lines examined here are not dependent on Myt1 for mitosis, which contrasts with observation in glioblastoma cells (Toledo et al., 2015).

siRNA knockdown of Myt1 strongly sensitized all cell lines to Adavosertib. Adavosertib treatment in the presence of siMyt1 increased ectopic Cdk1 activity in S-phase cells leading to increased premature mitosis and centromere fragmentation relative to Wee1

inhibition in siSc transfected cells (**Figure 6.1E**). Furthermore, Myt1 knockdown reinforced the Adavosertib induced mitotic arrest. In contrast, exogenous overexpression of Myt1 in HeLa cells reduced ectopic Cdk1 activity in S phase, prevented premature mitotic entry, and facilitated mitotic exit in cells treated with Adavosertib. This data confirms that Myt1 plays a role in Cdk1 regulation in both S-phase and mitosis, highlighting a major mechanism of intrinsic resistance to Adavosertib.

We also showed that cell lines that initially exhibited high sensitivity to Adavosertib (HeLa and MDA-MB-231) acquired resistance to Wee1 inhibition through the upregulation of Myt1 both *in vitro* and *in vivo*. The increased Myt1 levels correlated with reduced Cdk1 activity, suggesting that the functional redundancy between Wee1 and Myt1 had been restored. Myt1 knockdown by siRNA restored cell sensitivity to Adavosertib, resulting in enhanced Cdk1 activity and increased cell death. Together, our data argues that Myt1 upregulation is also a major mechanism of acquired Adavosertib resistance.

In the future, it would be useful to investigate if high Myt1 protein levels could be used as a predictive biomarker for tumour resistance to Adavosertib in the clinic. It would also be useful to know if Myt1 levels increase in tumours that acquire Adavosertib resistance. If Myt1 levels are found to play a role in Adavosertib resistance in the clinic, there would be a rationale for developing small molecule Myt1 inhibitors to counteract Wee1 inhibitor resistance.

6.3.2 Myt1 mRNA levels are weakly correlated with Adavosertib sensitivity

In contrast to Myt1 protein levels, Myt1 mRNA levels obtained from the **Cancer Cell Line Encyclopedia (CCLE)** exhibited only a weak correlation with Adavosertib sensitivity (**Figure 8.13**; $R^2 = 0.2610$). Furthermore, despite R500 HeLa cells having upregulated

Myt1 protein levels relative to parental cells, Myt1 mRNA levels were similar in R500 and parental cells (**Figure 8.14**). This data confirms that the increased Myt1 protein levels in R500 cells are not due to increased mRNA transcription. Besides transcription, other factors can affect protein levels including rate of protein translation or degradation [reviewed in (Vogel and Marcotte, 2012)]. In the future, it would be important to test if the rate of protein synthesis or degradation are altered in R500 cells relative to parental cells. Additionally, it will also be important to examine Myt1 mRNA levels in parental and R500 MDA-MB-231 cells.

6.3.3 High Myt1 mRNA levels correlate with poor cancer prognosis

Our data shows that Myt1 mRNA is overexpressed in patient breast cancer tissue relative to normal breast tissue. Moreover, high Myt1 mRNA levels are associated with a higher tumour grade, lower overall patient survival, higher disease relapse and triple negative receptor status. High Myt1 expression is also associated with reduced patient survival and higher tumour grade in non-small cell lung carcinoma, esophageal squamous cell carcinoma and colorectal cancer (Jeong et al., 2018; Sun et al., 2019; Zhang et al., 2019). Interestingly, Myt1 knockdown by siRNA was recently found to reduce cell invasion and migration in colorectal cancer cells (Jeong et al., 2018), which may suggest that Myt1 may function in oncogenic pathways independent of Cdk1. However, mRNA levels do not always predict protein levels and therefore it remains unclear if Myt1 protein levels are upregulated in breast cancer and other cancer tissue relative to normal tissue. If Myt1 protein levels are indeed upregulated in these cancers, there may be additional reasons for developing small molecule Myt1 inhibitors beyond enhancing Adavosertib sensitivity.

6.3.4 PD0166285 does not sensitize cells to Adavosertib

We showed that siMyt1 knockdown reduces pT14-Cdk1 but not Y15-Cdk1 in HeLa cells, whereas siWee1 reduced pY15-Cdk1 but not pT14-Cdk1 (**Figure 2.3**). In a one to one comparison of Adavosertib and PD0166285, Adavosertib was found to only reduce pY15-Cdk1 levels, while PD0166285 reduced both pY15- and pT14-Cdk1 levels (**Figure 5.1**). This suggests that Adavosertib inhibits Wee1 activity while PD0166285 inhibits both Wee1 and Myt1 activity. Based on this data, we predicted that PD0166285 would exhibit higher cytotoxicity compared to Adavosertib, possibly mimicking the effects of Adavosertib in the presence of siMyt1. Surprisingly, PD0166285 was found to be less cytotoxic than Adavosertib in HeLa and two other cell lines tested (SK-BR-3, and BT-474). There are several reasons that may explain the lack of cytotoxicity induced by PD0166285 relative to that of Adavosertib. Both Adavosertib and PD0166285 are reported to inhibit off target kinases, which may enhance or counteract the effects of Wee1 and/or Myt1 inhibition (De Witt Hamer et al., 2011; Dimitroff et al., 1999; Hirai et al., 2009; Panek et al., 1997; Wang et al., 2001; Wright et al., 2017; Zhu et al., 2017). Additionally, HeLa cells treated with 500 nM PD0166285 retained at least 40% of T14-Cdk1, which may have been enough to maintain Cdk1 inhibition. Alternatively, Myt1 may inhibit Cdk1 by a mechanism independent of Y15 and T14 phosphorylation in the presence of either PD0166285 or Adavosertib. Wells *et al*. reported that catalytically dead Myt1 can at least partially inhibit Cdk1 activity and maintain a G2 arrest through cytoplasmic sequestration (Wells et al., 1999). If Myt1 kinase activity is not required for Cdk1 inhibition, this might explain why PD0166285 does not exhibit higher cytotoxicity compared to Adavosertib. In the future, it would be interesting to test if transient overexpression of kinase dead Myt1

mimics the effects of wildtype Myt1 in inducing resistance to either Adavosertib or PD0166285. If kinase dead Myt1 mimics the wild type protein, then small molecule Myt1 kinase inhibitors are unlikely to affect mitotic entry (on their own or in the presence of Wee1 inhibitors). As such, it may be necessary to develop inhibitors that disrupt the physical interaction between Cdk1 and Myt1.

6.4 Inhibition of either Chk1 or ATR enhances cell sensitivity to Adavosertib

Given that there are no Myt1 specific inhibitors alternative approaches are required to enhance Adavosertib efficacy. The ATR-Chk1 pathway downregulates Cdk1 activity by inhibiting the Cdc25 family in response to replication stress [reviewed in (Qiu et al., 2018)]. Based on their effect on Cdc25 and Cdk1, ATR and Chk1 likely counteract the effects of Adavosertib by reducing ectopic Cdk1 activity. Lung cancer cells that acquire Adavosertib resistance are reported to have upregulated ATR and Chk1 activity, which suggests that these kinases play an important role in determining cancer cell sensitivity to Adavosertib (Sen et al., 2017).

We observed that inhibition of Chk1 by UCN-01 enhanced Adavosertib-induced premature mitosis in HeLa cells, which is consistent with publications reporting that Adavosertib synergizes with other Chk1 inhibitors (Aarts et al., 2012; Hauge et al., 2017; Sen et al., 2017). Although co-inhibition of Wee1 and Chk1 induces synergistic cancer cell killing, combined inhibition of Wee1 and Chk1 might not be safely tolerated in humans. Several Chk1/2 inhibitors including UCN-01 have been recently pulled from clinical trials owing to their toxicity in normal tissue [Reviewed in (Pilie et al., 2019)]. However, three selective Chk1 inhibitors are still being evaluated in ongoing clinical trials and could potentially be tested in combination with Adavosertib. Alternatively, inhibitors of ATR can

also be used to enhance Adavosertib efficacy. In collaboration with the Gamper lab, we recently showed that inhibition of ATR by AZD6738 also enhances Adavosertib-induced premature mitosis and centromere fragmentation in HeLa and breast cancer cells (Bukhari et al., 2019). Importantly, ATR and Wee1 inhibitors exhibit synergistic cell killing in Adavosertib resistant breast cancer cell lines with high Myt1 expression (T-47D, MDA-MB-468 and SK-BR-3) but not in non-tumorigenic cells (MCF 10A and HME-1). Relative to Chk1 inhibitors, ATR inhibitors exhibit less toxicity in normal cells and can be used in combination with Adavosertib to selectively kill breast cancer cells in xenograft mouse models (Bukhari et al., 2019). AZD6738 is currently being tested in the clinic and is generally found to be well tolerated by patients [Reviewed in (Pilie et al., 2019)]. As such, cotreatment with AZD6738 and Adavosertib may prove to be a safer alternative to Chk1 inhibitors.

6.5 Total Cdc25C protein levels do not correlate with Adavosertib sensitivity

Despite the role of Cdc25C in Cdk1 activation, we did not observe a correlation between total Cdc25C protein levels and Adavosertib sensitivity. However, there is evidence that reduced Cdc25 activity can counteract the effects of Wee1 inhibition. Potapova *et al.* showed co-inhibition of Cdc25C and Wee1/Myt1 in G1/S synchronised cells by NSC663284 and PD0166285, respectively, reduced Cdk1 activity and the percentage of mitotic cells relative to Wee1/Myt1 inhibition alone (Potapova et al., 2011). Moreover, ATR and Chk1 activity, which negatively regulates the Cdc25 family, is upregulated in lung cancer cells that acquire Adavosertib resistance (Sen et al., 2017). In our experiments we did not test the effects of Cdc25C knockdown or inhibition in the presence of Adavosertib. As such, we cannot exclude the possibility that low Cdc25C protein levels

may play a role in Adavosertib resistance. We also did not directly assay Cdc25C phosphatase activity in cell lines. In the study by Sen *et al.,* nuclear accumulation of phospho-active Chk1 (e.g. pS280-, pS196-, and pS345-Chk1), as opposed to total Chk1 levels, were associated with Adavosertib resistance (Sen et al., 2017). As such, pS216- and pS198-Cdc25C, which are biomarkers for inactive and active Cdc25C respectively, may correlate better with Adavosertib sensitivity (Cho et al., 2015; Toyoshima-Morimoto et al., 2002).

It will also be important to assay the levels and activity of Cdc25C homologues (Cdc25A and B) which also participate in Cdk1 dephosphorylation [Reviewed in (Boutros et al., 2007; Shaltiel et al., 2015)]. Both Cdc25A and B are reported to affect mitotic timing in cancer cells. For instance, Cdc25B overexpression overrides Chk1-mediated arrest and can induce premature mitosis in the presence of damaged DNA (Varmeh and Manfredi, 2008). Cdc25A deficiency was recently reported to induce resistance to ATR inhibition by preventing premature mitotic entry in embryonic stem cells (Ruiz et al., 2016). Therefore, the combined expression and/or activity of Cdc25A, B and C may be better indicators of cell sensitivity to Adavosertib.

6.6 p53 status is a poor predictor of cancer cell sensitivity to Adavosertib

p53 is a key transcriptional activator of the CDK inhibitor p21 as well as several apoptotic genes. Previous studies have reported that Adavosertib selectively kills cancer cells that lack p53 activity (Aarts et al., 2012; Hirai et al., 2009; Rajeshkumar et al., 2011). However, we did not observe a strong correlation between the functional status of p53 and Adavosertib sensitivity. HeLa and MDA-MB-231 cells, which are highly sensitive to Adavosertib, have downregulated and mutant p53, respectively (Lacroix et al., 2006; Leroy

et al., 2014); yet, three of the top four most resistant cell lines (BT-474, T-47D, and SK-BR-3) also have mutant p53 (Lacroix et al., 2006; Leroy et al., 2014). Furthermore, HME-1 cells have wild type p53 and exhibit Adavosertib sensitivity comparable to HeLa or MDA-MB-231 cells. Our data suggests that p53 status is a poor predictor of Adavosertib sensitivity. Nevertheless, we did not test if p53 knockdown in cells with mutant p53 could be used to enhance Adavosertib sensitivity. Depending on how p53 is mutated, p53 may gain *or* lose function. Therefore, downstream p53 targets such as p21, maybe a better indicator of Adavosertib sensitivity. p21 expression is reported to protect against Adavosertib induced DNA damage, suggesting that p21 levels may correlate with Wee1 inhibitor sensitivity (Aarts et al., 2012; Hauge et al., 2019).

6.7 Adavosertib treatment enhances the effects of other anti-mitotic agents

Most preclinical Adavosertib studies have focused on S-phase cell vulnerability to Wee1 inhibition and few studies have investigated mitotic cell vulnerability to Adavosertib. Our data shows that Wee1 inhibition in mitotic synchronized cells induces a mitotic arrest and promotes cell death either during mitosis or following mitotic exit/slippage (**Figure 6.1F**). Wee1 inhibition in HeLa cells has been previously reported to downregulate the anti-apoptotic protein Mcl-1 in a Cdk1 dependent manner (Visconti et al., 2015). Moreover, Adavosertib treatment has been shown to downregulate Mcl-1 and XIAP in head and neck squamous cell carcinomas (Tanaka et al., 2015). Likewise, Cdk1, in concert with other kinases, downregulate Mcl-1 and other anti-apoptotic proteins (Bcl-2, Bcl-XL, and XIAP) and upregulate of pro-apoptotic proteins (Bim and Bid) in cells arrested in mitosis by siRNA knockdown of Cdc20 or treatment with antimitotic agents such as paclitaxel, nocodazole or vinblastine (**Figure 1.11**) (Harley et al., 2010; Hou et al., 2017; Poruchynsky

et al., 1998; Sloss et al., 2016; Terrano et al., 2010; Topham et al., 2015; Wang et al., 2014b). As such, cells arrested in mitosis activate caspases and frequently undergo apoptosis. Additionally, cells arrested in mitosis acquire *de novo* DNA damage through partial caspase activity (also known as sublethal apoptosis) (Hain et al., 2016; Hayashi et al., 2012; Hayashi and Karlseder, 2013; Orth et al., 2012). While partial caspase activity may not induce mitotic cell death, it can trigger interphase cell death or senescence.

Given that Adavosertib induced a mitotic arrest, we predicted that the combined activity of Adavosertib with other anti-mitotic agents that delay mitotic progression could be used to enhance cancer cell killing. Here we show that paclitaxel, L-744-832, and ZM447439 delay mitotic exit and can be used to enhance cell sensitivity to Adavosertib. Furthermore, we also show that siRNA knockdown of SDS22 (a PP1 regulatory subunit) enhances cell sensitivity to Adavosertib.

6.7.1 Paclitaxel enhances Adavosertib efficacy

Paclitaxel disrupts microtubule dynamics leading to defects in chromosome congression, which prolongs mitotic checkpoint activation, delays mitotic exit, and induces cell death. Our data shows that low dose paclitaxel sensitizes HeLa and breast cancer cell lines to Adavosertib. Our data is consistent with that of Visconti *et al.* who reported that paclitaxel and Adavosertib co-treatment increases apoptotic activity and sensitizes leukemia cells to Adavosertib (Visconti et al., 2015).

T-47D, MCF7, and MDA-MB-468 were among the cell lines confirmed to exhibit high sensitivity to co-treatment with Adavosertib and paclitaxel. Notably, these cells exhibit high Myt1 levels and were found to be resistant to mono-treatment with Adavosertib. As such, our data suggests that paclitaxel maybe used to overcome

Adavosertib resistance in high Myt1 expressing cells, although this would need to be further tested. Likewise, Adavosertib may be used to overcome paclitaxel resistance. Triple negative breast cancer cell lines MDA-MB-231 and MDA-MB-468 are reported to be resistant to mono-treatment with paclitaxel (Craik et al., 2010). In our study, both cell lines exhibited high sensitivity to co-treatment with Adavosertib and paclitaxel. Given that 1) paclitaxel is used as a frontline chemotherapeutic agent for treating metastatic breast cancer, and 2) that cancer cells frequently acquire paclitaxel resistance (Nemcova-Furstova et al., 2016; Senkus et al., 2015), there is a strong rationale to investigate the combined efficacy of Adavosertib and paclitaxel in animal models.

6.7.2 L-744-832 enhances Adavosertib efficacy

L-744-832 has been previously shown to exhibit anti-mitotic activity in HeLa cells (Moudgil et al., 2015). L-744-832 and other FTIs inhibit Spindly farnesylation leading to loss of Spindly kinetochore localization. Spindly kinetochore localization is required for the recruitment of motor proteins dynein/dynactin (Chan et al., 2009). Importantly, dynein/dynactin is required for chromosome congression and for the removal of mitotic checkpoint proteins from kinetochores following bipolar kinetochore microtubule attachment [reviewed in (Lewis and Chan, 2017)]. Therefore, it is likely that the loss of Spindly farnesylation and kinetochore localization accounts for at least part of the mitotic exit delay. Although L-744-832 is not in clinical trials, two FTI inhibitors (Tipifarnib and Lonafarnib) are being tested in phase I/II clinical trials against different cancer types, including breast cancers [**ClinicalTrials.gov** and (Sparano et al., 2009; Yam et al., 2018)]. The efficacy of FTIs in cancer treatment is unclear. Several clinical trials have reported that FTIs exhibit little anti-cancer activity, either alone or in combination with other anti-

cancer drugs (Van Cutsem et al., 2004; Yam et al., 2018) and most clinical trials are evaluating FTIs in other diseases (progeria and Alzheimer's disease). Regardless, L-744-832 enhanced Adavosertib efficacy in HeLa cells (and vice versa), which provides a rationale for their continued examination in cancer models. Currently, our lab is testing combination treatments with Tipifarnib with Adavosertib in breast cancer cells.

6.7.3 ZM447439 enhances Adavosertib efficacy

ZM447439 treatment has been previously reported to disrupt the alignment and segregation of chromosomes as well as disrupt cytokinesis (Bekier et al., 2009; Ditchfield et al., 2003; Kaestner et al., 2009). In our experiments ZM447439 prevented chromosome alignment and segregation, consistent with these studies. However, we also observed that ZM447439 delayed mitotic exit in HeLa cells, which was inconsistent with the previously cited studies. These studies show that ZM447439 treatment alone and in combination with other antimitotic agents (e.g. MG132, paclitaxel, or nocodazole) promote premature mitotic exit through Aurora B inhibition and downregulation of mitotic checkpoint signals (Bekier et al., 2009; Ditchfield et al., 2003; Kaestner et al., 2009). However, a recent report by Isokane *et al.* showed that Aurora B inhibition by hesperadin can delay chromosome alignment and mitotic exit in HeLa cells (Isokane et al., 2016), which is consistent with our observations. One reason for the discrepancy in the phenotypes observed in these different studies may be related to the concentration of ZM447439 or hesperadin. In studies where premature mitotic exit was observed, three to eight fold higher concentrations of ZM447439 were used relative to the concentration used in our experiments (1000-2500 nM vs 300 nM) (Bekier et al., 2009; Ditchfield et al., 2003; Kaestner et al., 2009). Kaestner *et al.* reported that ZM-447439 concentrations below 500 nM did not cause cells to undergo

premature mitotic exit; however, mitotic arrest was also not observed (Kaestner et al., 2009). A low concentration of ZM447439 might partially inhibit, rather than completely inhibit Aurora B, leading to prolonged (rather than premature) mitotic exit. Alternatively, the discrepancy may be due to the inhibition of an off-target kinase or specific to the HeLa cell clone generated for our experiments. Further experiments will be needed to clarify this issue. In any case, we observed that cells co-treated with Adavosertib and ZM447439 exhibited longer mitotic durations and more cell death compared to cells treated with either inhibitor alone.

6.7.4 SDS22 knockdown enhances Adavosertib efficacy

PP1-SDS22 is required for kinetochore-microtubule attachment stabilization during metaphase, and the loss of SDS22 is reported to delay anaphase onset (Eiteneuer et al., 2014; Posch et al., 2010; Wurzenberger et al., 2012). PP1-SDS22 also promotes cytokinesis through polar relaxation, which is characterized by localized cellular blebbing adjacent to the mitotic spindle (Rodrigues et al., 2015). We observed that siRNA knockdown of SDS22 in HeLa, MCF7, T-47D and A549 cells significantly reduced colony formation relative to siRNA controls. Although we did not measure mitotic duration, we did confirm that SDS22 knockdown in the presence of Adavosertib increased the number of PH3-positive HeLa cells relative to either DMSO/siSDS22 or Adavosertib/siSc controls. This may indicate a longer mitotic duration in Adavosertib/siSDS22 treated cells, but this will need to be confirmed through additional experiments.

6.8 Conclusions

Wee1 inhibition by Adavosertib is a promising means of inducing mitotic catastrophe in some cancer cells, but intrinsic and acquired resistance to Wee1 inhibition are likely to be major obstacles as Adavosertib progresses through clinical trials. Validation of Myt1 as a predictive biomarker for Adavosertib cell sensitivity will likely aid in the understanding of clinical resistance. Additionally, development of selective Myt1 inhibitors are likely to improve tumour response to Adavosertib.

In the meantime, our data suggests that Adavosertib efficacy can be enhanced by treating cancer cells with Chk1 and ATR inhibitors, which are currently being tested in the clinic. Our data also show that Adavosertib efficacy can be enhanced by antimitotic agents that induce a mitotic arrest including paclitaxel and farnesyl transferase inhibitors. Given paclitaxel is already used as a frontline therapy for breast and other cancer types, our findings are likely to have a direct translational outcome.

7 References

Aarts, M., I. Bajrami, M.T. Herrera-Abreu, R. Elliott, R. Brough, A. Ashworth, C.J. Lord, and N.C. Turner. 2015. Functional Genetic Screen Identifies Increased Sensitivity to WEE1 Inhibition in Cells with Defects in Fanconi Anemia and HR Pathways. *Mol Cancer Ther*. 14:865-876.

Aarts, M., R. Sharpe, I. Garcia-Murillas, H. Gevensleben, M.S. Hurd, S.D. Shumway, C. Toniatti, A. Ashworth, and N.C. Turner. 2012. Forced mitotic entry of S-phase cells as a therapeutic strategy induced by inhibition of WEE1. *Cancer discovery*. 2:524-539.

Abe, S., K. Nagasaka, Y. Hirayama, H. Kozuka-Hata, M. Oyama, Y. Aoyagi, C. Obuse, and T. Hirota. 2011. The initial phase of chromosome condensation requires Cdk1-mediated phosphorylation of the CAP-D3 subunit of condensin II. *Genes Dev*. 25:863-874.

Adams, R.R., H. Maiato, W.C. Earnshaw, and M. Carmena. 2001. Essential roles of Drosophila inner centromere protein (INCENP) and aurora B in histone H3 phosphorylation, metaphase chromosome alignment, kinetochore disjunction, and chromosome segregation. *J Cell Biol*. 153:865-880.

Agami, R., and R. Bernards. 2000. Distinct initiation and maintenance mechanisms cooperate to induce G1 cell cycle arrest in response to DNA damage. *Cell*. 102:55-66.

Aleem, E., H. Kiyokawa, and P. Kaldis. 2005. Cdc2-cyclin E complexes regulate the G1/S phase transition. *Nat Cell Biol*. 7:831-836.

Alexander, J.L., and T.L. Orr-Weaver. 2016. Replication fork instability and the consequences of fork collisions from rereplication. *Genes Dev*. 30:2241-2252.

Ayeni, J.O., R. Varadarajan, O. Mukherjee, D.T. Stuart, F. Sprenger, M. Srayko, and S.D. Campbell. 2014. Dual phosphorylation of cdk1 coordinates cell proliferation with key developmental processes in Drosophila. *Genetics*. 196:197-210.

Bajar, B.T., E.S. Wang, A.J. Lam, B.B. Kim, C.L. Jacobs, E.S. Howe, M.W. Davidson, M.Z. Lin, and J. Chu. 2016. Improving brightness and photostability of green and red fluorescent proteins for live cell imaging and FRET reporting. *Scientific reports*. 6:20889.

Baldin, V., and B. Ducommun. 1995. Subcellular localisation of human wee1 kinase is regulated during the cell cycle. *J Cell Sci*. 108 (Pt 6):2425-2432.

Barra, V., and D. Fachinetti. 2018. The dark side of centromeres: types, causes and consequences of structural abnormalities implicating centromeric DNA. *Nat Commun*. 9:4340.

Baskar, R., K.A. Lee, R. Yeo, and K.W. Yeoh. 2012. Cancer and radiation therapy: current advances and future directions. *Int J Med Sci*. 9:193-199.

Bauer, T.M., S.F. Jones, C. Greenlees, C. Cook, P.J. Jewsbury, G. Mugundu, T. French, A.J. Pierce, M.J. O'Connor, N. Laing, J.C. Barrett, D.M. Stults, M.L. Johnson, J.T. Beck, K.N. Moore, J.R. Infante, H.A. Burris, and D.R. Spigel. 2016. A Phase Ib, Open-Label, Multi-Center Study to Assess the Safety, Tolerability, Pharmacokinetics, and Anti-tumor Activity of AZD1775 Monotherapy in Patients

with Advanced Solid Tumors: Expansion Cohorts. *J Clin Oncol*. 34:TPS2608-TPS2608.

Beck, H., V. Nahse-Kumpf, M.S. Larsen, K.A. O'Hanlon, S. Patzke, C. Holmberg, J. Mejlvang, A. Groth, O. Nielsen, R.G. Syljuasen, and C.S. Sorensen. 2012. Cyclin-dependent kinase suppression by WEE1 kinase protects the genome through control of replication initiation and nucleotide consumption. *Mol Cell Biol*. 32:4226-4236.

Beeharry, N., J.B. Rattner, J.P. Caviston, and T. Yen. 2013. Centromere fragmentation is a common mitotic defect of S and G2 checkpoint override. *Cell cycle (Georgetown, Tex.)*. 12:1588-1597.

Bekier, M.E., R. Fischbach, J. Lee, and W.R. Taylor. 2009. Length of mitotic arrest induced by microtubule-stabilizing drugs determines cell death after mitotic exit. *Mol Cancer Ther*. 8:1646-1654.

Bennett, A., O. Sloss, C. Topham, L. Nelson, A. Tighe, and S.S. Taylor. 2016. Inhibition of Bcl-xL sensitizes cells to mitotic blockers, but not mitotic drivers. *Open biology*. 6.

Booher, R.N., P.S. Holman, and A. Fattaey. 1997. Human Myt1 is a cell cycle-regulated kinase that inhibits Cdc2 but not Cdk2 activity. *J Biol Chem*. 272:22300-22306.

Boutros, R., V. Lobjois, and B. Ducommun. 2007. CDC25 phosphatases in cancer cells: key players? Good targets? *Nat Rev Cancer*. 7:495-507.

Bridges, K.A., H. Hirai, C.A. Buser, C. Brooks, H. Liu, T.A. Buchholz, J.M. Molkentine, K.A. Mason, and R.E. Meyn. 2011. MK-1775, a novel Wee1 kinase inhibitor, radiosensitizes p53-defective human tumor cells. *Clin Cancer Res*. 17:5638-5648.

Brinkley, B.R., R.P. Zinkowski, W.L. Mollon, F.M. Davis, M.A. Pisegna, M. Pershouse, and P.N. Rao. 1988. Movement and segregation of kinetochores experimentally detached from mammalian chromosomes. *Nature*. 336:251-254.

Bukhari, A.B., C.W. Lewis, J.J. Pearce, D. Luong, G.K. Chan, and A.M. Gamper. 2019. Inhibiting Wee1 and ATR kinases produces tumor-selective synthetic lethality and suppresses metastasis. *J Clin Invest*. 129:1329-1344.

Cahu, J., A. Olichon, C. Hentrich, H. Schek, J. Drinjakovic, C. Zhang, A. Doherty-Kirby, G. Lajoie, and T. Surrey. 2008. Phosphorylation by Cdk1 increases the binding of Eg5 to microtubules in vitro and in Xenopus egg extract spindles. *PloS one*. 3:e3936.

Cancer Genome Atlas Research, N. 2008. Comprehensive genomic characterization defines human glioblastoma genes and core pathways. *Nature*. 455:1061-1068.

Cancer Genome Atlas Research, N. 2012. Comprehensive molecular characterization of human colon and rectal cancer. *Nature*. 487:330-337.

Carmena, M., M. Wheelock, H. Funabiki, and W.C. Earnshaw. 2012. The chromosomal passenger complex (CPC): from easy rider to the godfather of mitosis. *Nat Rev Mol Cell Biol*. 13:789-803.

Cerami, E., J. Gao, U. Dogrusoz, B.E. Gross, S.O. Sumer, B.A. Aksoy, A. Jacobsen, C.J. Byrne, M.L. Heuer, E. Larsson, Y. Antipin, B. Reva, A.P. Goldberg, C. Sander, and N. Schultz. 2012. The cBio cancer genomics portal: an open platform for exploring multidimensional cancer genomics data. *Cancer discovery*. 2:401-404.

Chan, G.K., S.A. Jablonski, D.A. Starr, M.L. Goldberg, and T.J. Yen. 2000. Human Zw10 and ROD are mitotic checkpoint proteins that bind to kinetochores. *Nat Cell Biol*. 2:944-947.

Chan, Y.W., L.L. Fava, A. Uldschmid, M.H. Schmitz, D.W. Gerlich, E.A. Nigg, and A. Santamaria. 2009. Mitotic control of kinetochore-associated dynein and spindle orientation by human Spindly. *J Cell Biol*. 185:859-874.

Chan, Y.W., A.A. Jeyaprakash, E.A. Nigg, and A. Santamaria. 2012. Aurora B controls kinetochore-microtubule attachments by inhibiting Ska complex-KMN network interaction. *J Cell Biol*. 196:563-571.

Chang, B.H., L. Smith, J. Huang, and M. Thayer. 2007. Chromosomes with delayed replication timing lead to checkpoint activation, delayed recruitment of Aurora B and chromosome instability. *Oncogene*. 26:1852-1861.

Chang, Q., M. Chandrashekhar, T. Ketela, Y. Fedyshyn, J. Moffat, and D. Hedley. 2016. Cytokinetic effects of Wee1 disruption in pancreatic cancer. *Cell cycle (Georgetown, Tex.)*. 15:593-604.

Charrier-Savournin, F.B., M.T. Chateau, V. Gire, J. Sedivy, J. Piette, and V. Dulic. 2004. p21-Mediated nuclear retention of cyclin B1-Cdk1 in response to genotoxic stress. *Mol Biol Cell*. 15:3965-3976.

Cheang, M.C., S.K. Chia, D. Voduc, D. Gao, S. Leung, J. Snider, M. Watson, S. Davies, P.S. Bernard, J.S. Parker, C.M. Perou, M.J. Ellis, and T.O. Nielsen. 2009. Ki67 index, HER2 status, and prognosis of patients with luminal B breast cancer. *Journal of the National Cancer Institute*. 101:736-750.

Cheung-Ong, K., G. Giaever, and C. Nislow. 2013. DNA-damaging agents in cancer chemotherapy: serendipity and chemical biology. *Chemistry & biology*. 20:648-659.

Cho, Y.C., J.E. Park, B.C. Park, J.H. Kim, D.G. Jeong, S.G. Park, and S. Cho. 2015. Cell cycle-dependent Cdc25C phosphatase determines cell survival by regulating apoptosis signal-regulating kinase 1. *Cell Death Differ*. 22:1605-1617.

Choi, Y.H., and Y.H. Yoo. 2012. Taxol-induced growth arrest and apoptosis is associated with the upregulation of the Cdk inhibitor, p21WAF1/CIP1, in human breast cancer cells. *Oncology reports*. 28:2163-2169.

Chow, J.P., and R.Y. Poon. 2013. The CDK1 inhibitory kinase MYT1 in DNA damage checkpoint recovery. *Oncogene*. 32:4778-4788.

Chow, J.P., R.Y. Poon, and H.T. Ma. 2011. Inhibitory phosphorylation of cyclin-dependent kinase 1 as a compensatory mechanism for mitosis exit. *Mol Cell Biol*. 31:1478-1491.

Ciferri, C., S. Pasqualato, E. Screpanti, G. Varetti, S. Santaguida, G. Dos Reis, A. Maiolica, J. Polka, J.G. De Luca, P. De Wulf, M. Salek, J. Rappsilber, C.A. Moores, E.D. Salmon, and A. Musacchio. 2008. Implications for kinetochore-microtubule attachment from the structure of an engineered Ndc80 complex. *Cell*. 133:427-439.

Clijsters, L., W. van Zon, B.T. Riet, E. Voets, M. Boekhout, J. Ogink, C. Rumpf-Kienzl, and R.M. Wolthuis. 2014. Inefficient degradation of cyclin B1 re-activates the spindle checkpoint right after sister chromatid disjunction. *Cell cycle (Georgetown, Tex.)*. 13:2370-2378.

Colin, D.J., K.O. Hain, L.A. Allan, and P.R. Clarke. 2015. Cellular responses to a prolonged delay in mitosis are determined by a DNA damage response controlled by Bcl-2 family proteins. *Open biology*. 5:140156.

Cornwell, W.D., P.J. Kaminski, and J.R. Jackson. 2002. Identification of Drosophila Myt1 kinase and its role in Golgi during mitosis. *Cellular signalling*. 14:467-476.

Coulonval, K., L. Bockstaele, S. Paternot, and P.P. Roger. 2003. Phosphorylations of cyclin-dependent kinase 2 revisited using two-dimensional gel electrophoresis. *J Biol Chem*. 278:52052-52060.

Coulonval, K., H. Kooken, and P.P. Roger. 2011. Coupling of T161 and T14 phosphorylations protects cyclin B-CDK1 from premature activation. *Mol Biol Cell*. 22:3971-3985.

Craik, A.C., R.A. Veldhoen, M. Czernick, T.W. Buckland, K. Kyselytzia, S. Ghosh, R. Lai, S. Damaraju, D.A. Underhill, J.R. Mackey, and I.S. Goping. 2010. The BH3-only protein Bad confers breast cancer taxane sensitivity through a nonapoptotic mechanism. *Oncogene*. 29:5381-5391.

Crown, J., M. O'Leary, and W.S. Ooi. 2004. Docetaxel and paclitaxel in the treatment of breast cancer: a review of clinical experience. *The oncologist*. 9 Suppl 2:24-32.

Dai, X., T. Li, Z. Bai, Y. Yang, X. Liu, J. Zhan, and B. Shi. 2015. Breast cancer intrinsic subtype classification, clinical use and future trends. *American journal of cancer research*. 5:2929-2943.

Dai, Y., M. Rahmani, X.Y. Pei, P. Khanna, S.I. Han, C. Mitchell, P. Dent, and S. Grant. 2005. Farnesyltransferase inhibitors interact synergistically with the Chk1 inhibitor UCN-01 to induce apoptosis in human leukemia cells through interruption of both Akt and MEK/ERK pathways and activation of SEK1/JNK. *Blood*. 105:1706-1716.

De Witt Hamer, P.C., S.E. Mir, D. Noske, C.J. Van Noorden, and T. Wurdinger. 2011. WEE1 kinase targeting combined with DNA-damaging cancer therapy catalyzes mitotic catastrophe. *Clin Cancer Res*. 17:4200-4207.

DeLuca, J.G., W.E. Gall, C. Ciferri, D. Cimini, A. Musacchio, and E.D. Salmon. 2006. Kinetochore microtubule dynamics and attachment stability are regulated by Hec1. *Cell*. 127:969-982.

DeLuca, K.F., S.M. Lens, and J.G. DeLuca. 2011. Temporal changes in Hec1 phosphorylation control kinetochore-microtubule attachment stability during mitosis. *J Cell Sci*. 124:622-634.

Di Fiore, B., C. Wurzenberger, N.E. Davey, and J. Pines. 2016. The Mitotic Checkpoint Complex Requires an Evolutionary Conserved Cassette to Bind and Inhibit Active APC/C. *Mol Cell*. 64:1144-1153.

Dimitroff, C.J., W. Klohs, A. Sharma, P. Pera, D. Driscoll, J. Veith, R. Steinkampf, M. Schroeder, S. Klutchko, A. Sumlin, B. Henderson, T.J. Dougherty, and R.J. Bernacki. 1999. Anti-angiogenic activity of selected receptor tyrosine kinase inhibitors, PD166285 and PD173074: implications for combination treatment with photodynamic therapy. *Investigational New Drugs*. 17:121-135.

Diril, M.K., X. Bisteau, M. Kitagawa, M.J. Caldez, S. Wee, J. Gunaratne, S.H. Lee, and P. Kaldis. 2016. Loss of the Greatwall Kinase Weakens the Spindle Assembly Checkpoint. *PLoS genetics*. 12:e1006310.

Ditchfield, C., V.L. Johnson, A. Tighe, R. Ellston, C. Haworth, T. Johnson, A. Mortlock, N. Keen, and S.S. Taylor. 2003. Aurora B couples chromosome alignment with anaphase by targeting BubR1, Mad2, and Cenp-E to kinetochores. *J Cell Biol*. 161:267-280.

Do, K., D. Wilsker, J. Ji, J. Zlott, T. Freshwater, R.J. Kinders, J. Collins, A.P. Chen, J.H. Doroshow, and S. Kummar. 2015. Phase I Study of Single-Agent AZD1775 (MK-

1775), a Wee1 Kinase Inhibitor, in Patients With Refractory Solid Tumors. *J Clin Oncol*. 33:3409-3415.

Dominguez-Kelly, R., Y. Martin, S. Koundrioukoff, M.E. Tanenbaum, V.A. Smits, R.H. Medema, M. Debatisse, and R. Freire. 2011. Wee1 controls genomic stability during replication by regulating the Mus81-Eme1 endonuclease. *J Cell Biol*. 194:567-579.

Dong, L., L. Yu, C. Bai, L. Liu, H. Long, L. Shi, and Z. Lin. 2018. USP27-mediated Cyclin E stabilization drives cell cycle progression and hepatocellular tumorigenesis. *Oncogene*. 37:2702-2713.

Duda, H., M. Arter, J. Gloggnitzer, F. Teloni, P. Wild, M.G. Blanco, M. Altmeyer, and J. Matos. 2016. A Mechanism for Controlled Breakage of Under-replicated Chromosomes during Mitosis. *Dev Cell*. 39:740-755.

Dumitru, A.M.G., S.F. Rusin, A.E.M. Clark, A.N. Kettenbach, and D.A. Compton. 2017. Cyclin A/Cdk1 modulates Plk1 activity in prometaphase to regulate kinetochore-microtubule attachment stability. *eLife*. 6.

Eaton, S.L., M.L. Hurtado, K.J. Oldknow, L.C. Graham, T.W. Marchant, T.H. Gillingwater, C. Farquharson, and T.M. Wishart. 2014. A guide to modern quantitative fluorescent western blotting with troubleshooting strategies. *Journal of visualized experiments : JoVE*:e52099.

Eckelman, B.P., G.S. Salvesen, and F.L. Scott. 2006. Human inhibitor of apoptosis proteins: why XIAP is the black sheep of the family. *EMBO reports*. 7:988-994.

Eichhorn, J.M., N. Sakurikar, S.E. Alford, R. Chu, and T.C. Chambers. 2013. Critical role of anti-apoptotic Bcl-2 protein phosphorylation in mitotic death. *Cell Death Dis*. 4:e834.

Eiteneuer, A., J. Seiler, M. Weith, M. Beullens, B. Lesage, V. Krenn, A. Musacchio, M. Bollen, and H. Meyer. 2014. Inhibitor-3 ensures bipolar mitotic spindle attachment by limiting association of SDS22 with kinetochore-bound protein phosphatase-1. *EMBO J*. 33:2704-2720.

El Achkar, E., M. Gerbault-Seureau, M. Muleris, B. Dutrillaux, and M. Debatisse. 2005. Premature condensation induces breaks at the interface of early and late replicating chromosome bands bearing common fragile sites. *Proc Natl Acad Sci U S A*. 102:18069-18074.

Elowe, S., S. Hummer, A. Uldschmid, X. Li, and E.A. Nigg. 2007. Tension-sensitive Plk1 phosphorylation on BubR1 regulates the stability of kinetochore microtubule interactions. *Genes Dev*. 21:2205-2219.

Enders, G.H. 2010. Gauchos and ochos: a Wee1-Cdk tango regulating mitotic entry. *Cell division*. 5:12.

Espert, A., P. Uluocak, R.N. Bastos, D. Mangat, P. Graab, and U. Gruneberg. 2014. PP2A-B56 opposes Mps1 phosphorylation of Knl1 and thereby promotes spindle assembly checkpoint silencing. *J Cell Biol*. 206:833-842.

Famulski, J.K., and G.K. Chan. 2007. Aurora B kinase-dependent recruitment of hZW10 and hROD to tensionless kinetochores. *Curr Biol*. 17:2143-2149.

Famulski, J.K., L.J. Vos, J.B. Rattner, and G.K. Chan. 2011. Dynein/Dynactin-mediated transport of kinetochore components off kinetochores and onto spindle poles induced by nordihydroguaiaretic acid. *PloS one*. 6:e16494.

Fang, Y., X. Liang, W. Jiang, J. Li, J. Xu, and X. Cai. 2015. Cyclin B1 Suppresses Colorectal Cancer Invasion and Metastasis by Regulating E-Cadherin. *PloS one*. 10:e0126875.

Fenech, M., M. Kirsch-Volders, A.T. Natarajan, J. Surralles, J.W. Crott, J. Parry, H. Norppa, D.A. Eastmond, J.D. Tucker, and P. Thomas. 2011. Molecular mechanisms of micronucleus, nucleoplasmic bridge and nuclear bud formation in mammalian and human cells. *Mutagenesis*. 26:125-132.

Feoktistova, M., P. Geserick, and M. Leverkus. 2016. Crystal Violet Assay for Determining Viability of Cultured Cells. *Cold Spring Harb Protoc*. 2016:pdb prot087379.

Feoktistova, M., P. Geserick, D. Panayotova-Dimitrova, and M. Leverkus. 2012. Pick your poison: the Ripoptosome, a cell death platform regulating apoptosis and necroptosis. *Cell cycle (Georgetown, Tex.)*. 11:460-467.

Ferlay, J., I. Soerjomataram, R. Dikshit, S. Eser, C. Mathers, M. Rebelo, D.M. Parkin, D. Forman, and F. Bray. 2015. Cancer incidence and mortality worldwide: sources, methods and major patterns in GLOBOCAN 2012. *International journal of cancer*. 136:E359-386.

Fernandez-Medarde, A., and E. Santos. 2011. Ras in cancer and developmental diseases. *Genes & cancer*. 2:344-358.

Foley, E.A., and T.M. Kapoor. 2013. Microtubule attachment and spindle assembly checkpoint signalling at the kinetochore. *Nat Rev Mol Cell Biol*. 14:25-37.

Fujimitsu, K., M. Grimaldi, and H. Yamano. 2016. Cyclin-dependent kinase 1-dependent activation of APC/C ubiquitin ligase. *Science (New York, N.Y.)*. 352:1121-1124.

Fung, T.K., H.T. Ma, and R.Y. Poon. 2007. Specialized roles of the two mitotic cyclins in somatic cells: cyclin A as an activator of M phase-promoting factor. *Mol Biol Cell*. 18:1861-1873.

Galluzzi, L., I. Vitale, J.M. Abrams, E.S. Alnemri, E.H. Baehrecke, M.V. Blagosklonny, T.M. Dawson, V.L. Dawson, W.S. El-Deiry, S. Fulda, E. Gottlieb, D.R. Green, M.O. Hengartner, O. Kepp, R.A. Knight, S. Kumar, S.A. Lipton, X. Lu, F. Madeo, W. Malorni, P. Mehlen, G. Nunez, M.E. Peter, M. Piacentini, D.C. Rubinsztein, Y. Shi, H.U. Simon, P. Vandenabeele, E. White, J. Yuan, B. Zhivotovsky, G. Melino, and G. Kroemer. 2012. Molecular definitions of cell death subroutines: recommendations of the Nomenclature Committee on Cell Death 2012. *Cell Death Differ*. 19:107-120.

Gao, J., B.A. Aksoy, U. Dogrusoz, G. Dresdner, B. Gross, S.O. Sumer, Y. Sun, A. Jacobsen, R. Sinha, E. Larsson, E. Cerami, C. Sander, and N. Schultz. 2013. Integrative analysis of complex cancer genomics and clinical profiles using the cBioPortal. *Science signaling*. 6:pl1.

Gao, L., L. Shao, C.D. Higgins, J.S. Poulton, M. Peifer, M.W. Davidson, X. Wu, B. Goldstein, and E. Betzig. 2012. Noninvasive imaging beyond the diffraction limit of 3D dynamics in thickly fluorescent specimens. *Cell*. 151:1370-1385.

Gao, Y.F., T. Li, Y. Chang, Y.B. Wang, W.N. Zhang, W.H. Li, K. He, R. Mu, C. Zhen, J.H. Man, X. Pan, T. Li, L. Chen, M. Yu, B. Liang, Y. Chen, Q. Xia, T. Zhou, W.L. Gong, A.L. Li, H.Y. Li, and X.M. Zhang. 2011. Cdk1-phosphorylated CUEDC2 promotes spindle checkpoint inactivation and chromosomal instability. *Nat Cell Biol*. 13:924-933.

Gascoigne, K.E., and S.S. Taylor. 2008. Cancer cells display profound intra- and interline variation following prolonged exposure to antimitotic drugs. *Cancer cell*. 14:111-122.

Gascoigne, K.E., and S.S. Taylor. 2009. How do anti-mitotic drugs kill cancer cells? *J Cell Sci*. 122:2579-2585.

Gavet, O., and J. Pines. 2010. Progressive Activation of CyclinB1-Cdk1 Coordinates Entry to Mitosis. *Dev Cell*. 18:533-543.

Germain, D.R., K. Graham, D.D. Glubrecht, J.C. Hugh, J.R. Mackey, and R. Godbout. 2011. DEAD box 1: a novel and independent prognostic marker for early recurrence in breast cancer. *Breast cancer research and treatment*. 127:53-63.

Gharbi-Ayachi, A., J.C. Labbe, A. Burgess, S. Vigneron, J.M. Strub, E. Brioudes, A. Van-Dorsselaer, A. Castro, and T. Lorca. 2010. The substrate of Greatwall kinase, Arpp19, controls mitosis by inhibiting protein phosphatase 2A. *Science (New York, N.Y.)*. 330:1673-1677.

Gheghiani, L., D. Loew, B. Lombard, J. Mansfeld, and O. Gavet. 2017. PLK1 Activation in Late G2 Sets Up Commitment to Mitosis. *Cell reports*. 19:2060-2073.

Giunta, S., and S.P. Jackson. 2011. Give me a break, but not in mitosis: the mitotic DNA damage response marks DNA double-strand breaks with early signaling events. *Cell cycle (Georgetown, Tex.)*. 10:1215-1221.

Gligorov, J., and S. Richard. 2015. Breast cancer: weekly paclitaxel--still preferred first-line taxane for mBC. *Nature reviews. Clinical oncology*. 12:508-509.

Gordon, D.J., B. Resio, and D. Pellman. 2012. Causes and consequences of aneuploidy in cancer. *Nature reviews. Genetics*. 13:189-203.

Green, D.R., and F. Llambi. 2015. Cell Death Signaling. *Cold Spring Harbor perspectives in biology*. 7.

Guertin, A.D., J. Li, Y. Liu, M.S. Hurd, A.G. Schuller, B. Long, H.A. Hirsch, I. Feldman, Y. Benita, C. Toniatti, L. Zawel, S.E. Fawell, D.G. Gilliland, and S.D. Shumway. 2013. Preclinical evaluation of the WEE1 inhibitor MK-1775 as single-agent anticancer therapy. *Mol Cancer Ther*. 12:1442-1452.

Guzman, J.R., S. Fukuda, and L.M. Pelus. 2009. Inhibition of caspase-3 by Survivin prevents Wee1 Kinase degradation and promotes cell survival by maintaining phosphorylation of p34Cdc2. *Gene therapy & molecular biology*. 13b:264-273.

Hached, K., P. Goguet, S. Charrasse, S. Vigneron, M.P. Sacristan, T. Lorca, and A. Castro. 2019. ENSA and ARPP19 differentially control cell cycle progression and development. *J Cell Biol*. 218:541-558.

Hain, K.O., D.J. Colin, S. Rastogi, L.A. Allan, and P.R. Clarke. 2016. Prolonged mitotic arrest induces a caspase-dependent DNA damage response at telomeres that determines cell survival. *Scientific reports*. 6:26766.

Han, S.J., R. Chen, M.P. Paronetto, and M. Conti. 2005. Wee1B is an oocyte-specific kinase involved in the control of meiotic arrest in the mouse. *Current biology : CB*. 15:1670-1676.

Harbour, J.W., R.X. Luo, A. Dei Santi, A.A. Postigo, and D.C. Dean. 1999. Cdk phosphorylation triggers sequential intramolecular interactions that progressively block Rb functions as cells move through G1. *Cell*. 98:859-869.

Harley, M.E., L.A. Allan, H.S. Sanderson, and P.R. Clarke. 2010. Phosphorylation of Mcl-1 by CDK1-cyclin B1 initiates its Cdc20-dependent destruction during mitotic arrest. *EMBO J*. 29:2407-2420.

Harvey, S.L., G. Enciso, N. Dephoure, S.P. Gygi, J. Gunawardena, and D.R. Kellogg. 2011. A phosphatase threshold sets the level of Cdk1 activity in early mitosis in budding yeast. *Mol Biol Cell*. 22:3595-3608.

Hauge, S., L. Macurek, and R.G. Syljuasen. 2019. p21 limits S phase DNA damage caused by the Wee1 inhibitor MK1775. *Cell cycle (Georgetown, Tex.)*. 18:834-847.

Hauge, S., C. Naucke, G. Hasvold, M. Joel, G.E. Rodland, P. Juzenas, T. Stokke, and R.G. Syljuasen. 2017. Combined inhibition of Wee1 and Chk1 gives synergistic DNA damage in S-phase due to distinct regulation of CDK activity and CDC45 loading. *Oncotarget*. 8:10966-10979.

Hayashi, M.T., A.J. Cesare, J.A. Fitzpatrick, E. Lazzerini-Denchi, and J. Karlseder. 2012. A telomere-dependent DNA damage checkpoint induced by prolonged mitotic arrest. *Nat Struct Mol Biol*. 19:387-394.

Hayashi, M.T., and J. Karlseder. 2013. DNA damage associated with mitosis and cytokinesis failure. *Oncogene*. 32:4593-4601.

Hayward, D., T. Alfonso-Perez, M.J. Cundell, M. Hopkins, J. Holder, J. Bancroft, L.H. Hutter, B. Novak, F.A. Barr, and U. Gruneberg. 2019a. CDK1-CCNB1 creates a spindle checkpoint-permissive state by enabling MPS1 kinetochore localization. *J Cell Biol*. 218:1182-1199.

Hayward, D., T. Alfonso-Perez, and U. Gruneberg. 2019b. Orchestration of the spindle assembly checkpoint by CDK1-cyclin B1. *FEBS Lett*. 593:2889-2907.

Heald, R., and F. McKeon. 1990. Mutations of phosphorylation sites in lamin A that prevent nuclear lamina disassembly in mitosis. *Cell*. 61:579-589.

Heald, R., M. McLoughlin, and F. McKeon. 1993. Human wee1 maintains mitotic timing by protecting the nucleus from cytoplasmically activated Cdc2 kinase. *Cell*. 74:463-474.

Hegarat, N., C. Vesely, P.K. Vinod, C. Ocasio, N. Peter, J. Gannon, A.W. Oliver, B. Novak, and H. Hochegger. 2014. PP2A/B55 and Fcp1 regulate Greatwall and Ensa dephosphorylation during mitotic exit. *PLoS genetics*. 10:e1004004.

Hendzel, M.J., Y. Wei, M.A. Mancini, A. Van Hooser, T. Ranalli, B.R. Brinkley, D.P. Bazett-Jones, and C.D. Allis. 1997. Mitosis-specific phosphorylation of histone H3 initiates primarily within pericentromeric heterochromatin during G2 and spreads in an ordered fashion coincident with mitotic chromosome condensation. *Chromosoma*. 106:348-360.

Hirai, H., T. Arai, M. Okada, T. Nishibata, M. Kobayashi, N. Sakai, K. Imagaki, J. Ohtani, T. Sakai, T. Yoshizumi, S. Mizuarai, Y. Iwasawa, and H. Kotani. 2010. MK-1775, a small molecule Wee1 inhibitor, enhances anti-tumor efficacy of various DNA-damaging agents, including 5-fluorouracil. *Cancer Biol Ther*. 9:514-522.

Hirai, H., Y. Iwasawa, M. Okada, T. Arai, T. Nishibata, M. Kobayashi, T. Kimura, N. Kaneko, J. Ohtani, K. Yamanaka, H. Itadani, I. Takahashi-Suzuki, K. Fukasawa, H. Oki, T. Nambu, J. Jiang, T. Sakai, H. Arakawa, T. Sakamoto, T. Sagara, T. Yoshizumi, S. Mizuarai, and H. Kotani. 2009. Small-molecule inhibition of Wee1 kinase by MK-1775 selectively sensitizes p53-deficient tumor cells to DNA-damaging agents. *Mol Cancer Ther*. 8:2992-3000.

Hiruma, Y., C. Sacristan, S.T. Pachis, A. Adamopoulos, T. Kuijt, M. Ubbink, E. von Castelmur, A. Perrakis, and G.J.P.L. Kops. 2015. Competition between MPS1 and microtubules at kinetochores regulates spindle checkpoint signaling. *Science (New York, N.Y.)*. 348:1264-1267.

Holland, A.J., and D.W. Cleveland. 2012. Chromoanagenesis and cancer: mechanisms and consequences of localized, complex chromosomal rearrangements. *Nat Med*. 18:1630-1638.

Holland, A.J., R.M. Reis, S. Niessen, C. Pereira, D.A. Andres, H.P. Spielmann, D.W. Cleveland, A. Desai, and R. Gassmann. 2015. Preventing farnesylation of the dynein adaptor Spindly contributes to the mitotic defects caused by farnesyltransferase inhibitors. *Mol Biol Cell*. 26:1845-1856.

Hou, Y., L.A. Allan, and P.R. Clarke. 2017. Phosphorylation of XIAP by CDK1–cyclin-B1 controls mitotic cell death. *J Cell Sci*. 130:502-511.

Howell, B.J., D.B. Hoffman, G. Fang, A.W. Murray, and E.D. Salmon. 2000. Visualization of Mad2 dynamics at kinetochores, along spindle fibers, and at spindle poles in living cells. *J Cell Biol*. 150:1233-1250.

Huang, H., J. Hittle, F. Zappacosta, R.S. Annan, A. Hershko, and T.J. Yen. 2008. Phosphorylation sites in BubR1 that regulate kinetochore attachment, tension, and mitotic exit. *J Cell Biol*. 183:667-680.

Hughes, B.T., J. Sidorova, J. Swanger, R.J. Monnat, Jr., and B.E. Clurman. 2013. Essential role for Cdk2 inhibitory phosphorylation during replication stress revealed by a human Cdk2 knockin mutation. *Proc Natl Acad Sci U S A*. 110:8954-8959.

Hummer, S., and T.U. Mayer. 2009. Cdk1 negatively regulates midzone localization of the mitotic kinesin Mklp2 and the chromosomal passenger complex. *Current biology : CB*. 19:607-612.

Inoue, D., and N. Sagata. 2005. The Polo-like kinase Plx1 interacts with and inhibits Myt1 after fertilization of Xenopus eggs. *EMBO J*. 24:1057-1067.

Iorns, E., C.J. Lord, A. Grigoriadis, S. McDonald, K. Fenwick, A. Mackay, C.A. Mein, R. Natrajan, K. Savage, N. Tamber, J.S. Reis-Filho, N.C. Turner, and A. Ashworth. 2009. Integrated functional, gene expression and genomic analysis for the identification of cancer targets. *PloS one*. 4:e5120.

Isokane, M., T. Walter, R. Mahen, B. Nijmeijer, J.K. Heriche, K. Miura, S. Maffini, M.P. Ivanov, T.S. Kitajima, J.M. Peters, and J. Ellenberg. 2016. ARHGEF17 is an essential spindle assembly checkpoint factor that targets Mps1 to kinetochores. *J Cell Biol*. 212:647-659.

Jeong, D., H. Kim, D. Kim, S. Ban, S. Oh, S. Ji, D. Kang, H. Lee, T.S. Ahn, H.J. Kim, S.B. Bae, M.S. Lee, C.J. Kim, H.Y. Kwon, and M.J. Baek. 2018. Protein kinase, membrane-associated tyrosine/threonine 1 is associated with the progression of colorectal cancer. *Oncology reports*. 39:2829-2836.

Ji, Z., H. Gao, L. Jia, B. Li, and H. Yu. 2017. A sequential multi-target Mps1 phosphorylation cascade promotes spindle checkpoint signaling. *eLife*. 6.

Ji, Z., H. Gao, and H. Yu. 2015. Cell division cycle. Kinetochore attachment sensed by competitive Mps1 and microtubule binding to Ndc80C. *Science (New York, N.Y.)*. 348:1260-1264.

Jin, H.S., and T.H. Lee. 2006. Cell cycle-dependent expression of cIAP2 at G2/M phase contributes to survival during mitotic cell cycle arrest. *Biochem J*. 399:335-342.

Jin, P., S. Hardy, and D.O. Morgan. 1998. Nuclear localization of cyclin B1 controls mitotic entry after DNA damage. *J Cell Biol*. 141:875-885.

Jin, Z., E. Homola, S. Tiong, and S.D. Campbell. 2008. Drosophila myt1 is the major cdk1 inhibitory kinase for wing imaginal disc development. *Genetics*. 180:2123-2133.

Jin, Z., E.M. Homola, P. Goldbach, Y. Choi, J.A. Brill, and S.D. Campbell. 2005. Drosophila Myt1 is a Cdk1 inhibitory kinase that regulates multiple aspects of cell cycle behavior during gametogenesis. *Development (Cambridge, England)*. 132:4075-4085.

Jones, M.C., J.A. Askari, J.D. Humphries, and M.J. Humphries. 2018. Cell adhesion is regulated by CDK1 during the cell cycle. *J Cell Biol*. 217:3203-3218.

Jordan, M.A., R.J. Toso, D. Thrower, and L. Wilson. 1993. Mechanism of mitotic block and inhibition of cell proliferation by taxol at low concentrations. *Proc Natl Acad Sci U S A*. 90:9552-9556.

Jordan, M.A., and L. Wilson. 2004. Microtubules as a target for anticancer drugs. *Nat Rev Cancer*. 4:253-265.

Kaestner, P., A. Stolz, and H. Bastians. 2009. Determinants for the efficiency of anticancer drugs targeting either Aurora-A or Aurora-B kinases in human colon carcinoma cells. *Mol Cancer Ther*. 8:2046-2056.

Kaisari, S., D. Sitry-Shevah, S. Miniowitz-Shemtov, A. Teichner, and A. Hershko. 2017. Role of CCT chaperonin in the disassembly of mitotic checkpoint complexes. *Proc Natl Acad Sci U S A*. 114:956-961.

Kallio, M.J., M.L. McCleland, P.T. Stukenberg, and G.J. Gorbsky. 2002. Inhibition of aurora B kinase blocks chromosome segregation, overrides the spindle checkpoint, and perturbs microtubule dynamics in mitosis. *Current biology : CB*. 12:900-905.

Karess, R. 2005. Rod-Zw10-Zwilch: a key player in the spindle checkpoint. *Trends in cell biology*. 15:386-392.

Karlsson, C., S. Katich, A. Hagting, I. Hoffmann, and J. Pines. 1999. Cdc25B and Cdc25C differ markedly in their properties as initiators of mitosis. *J Cell Biol*. 146:573-584.

Kasahara, K., H. Goto, M. Enomoto, Y. Tomono, T. Kiyono, and M. Inagaki. 2010. 14-3-3gamma mediates Cdc25A proteolysis to block premature mitotic entry after DNA damage. *EMBO J*. 29:2802-2812.

Katayama, K., N. Fujita, and T. Tsuruo. 2005. Akt/protein kinase B-dependent phosphorylation and inactivation of WEE1Hu promote cell cycle progression at G2/M transition. *Mol Cell Biol*. 25:5725-5737.

Kausar, T., J.S. Schreiber, D. Karnak, L.A. Parsels, J.D. Parsels, M.A. Davis, L. Zhao, J. Maybaum, T.S. Lawrence, and M.A. Morgan. 2015. Sensitization of Pancreatic Cancers to Gemcitabine Chemoradiation by WEE1 Kinase Inhibition Depends on Homologous Recombination Repair. *Neoplasia (New York, N.Y.)*. 17:757-766.

Kikuchi, I., Y. Nakayama, T. Morinaga, Y. Fukumoto, and N. Yamaguchi. 2010. A decrease in cyclin B1 levels leads to polyploidization in DNA damage-induced senescence. *Cell biology international*. 34:645-653.

Kim, S.Y., E.J. Song, K.J. Lee, and J.E. Ferrell, Jr. 2005. Multisite M-phase phosphorylation of Xenopus Wee1A. *Mol Cell Biol*. 25:10580-10590.

Kishimoto, T. 2015. Entry into mitosis: a solution to the decades-long enigma of MPF. *Chromosoma*. 124:417-428.

Ku, B.M., Y.H. Bae, J. Koh, J.M. Sun, S.H. Lee, J.S. Ahn, K. Park, and M.J. Ahn. 2017. Mutational status of TP53 defines the efficacy of Wee1 inhibitor AZD1775 in KRAS-mutant non-small cell lung cancer. *Oncotarget*. 8:67526-67537.

Kubara, P.M., S. Kerneis-Golsteyn, A. Studeny, B.B. Lanser, L. Meijer, and R.M. Golsteyn. 2012. Human cells enter mitosis with damaged DNA after treatment with pharmacological concentrations of genotoxic agents. *Biochem J*. 446:373-381.

Kumagai, A., A. Shevchenko, A. Shevchenko, and W.G. Dunphy. 2011. Direct regulation of Treslin by cyclin-dependent kinase is essential for the onset of DNA replication. *J Cell Biol*. 193:995-1007.

Kumar, G., P. Tajpara, A.B. Bukhari, A.G. Ramchandani, A. De, and G.B. Maru. 2014. Dietary curcumin post-treatment enhances the disappearance of B(a)P-derived DNA adducts in mouse liver and lungs. *Toxicology reports*. 1:1181-1194.

Kwon, Y.G., S.Y. Lee, Y. Choi, P. Greengard, and A.C. Nairn. 1997. Cell cycle-dependent phosphorylation of mammalian protein phosphatase 1 by cdc2 kinase. *Proc Natl Acad Sci U S A*. 94:2168-2173.

Lacroix, M., R.A. Toillon, and G. Leclercq. 2006. p53 and breast cancer, an update. *Endocrine-related cancer*. 13:293-325.

Lambrus, B.G., V. Daggubati, Y. Uetake, P.M. Scott, K.M. Clutario, G. Sluder, and A.J. Holland. 2016. A USP28-53BP1-p53-p21 signaling axis arrests growth after centrosome loss or prolonged mitosis. *J Cell Biol*. 214:143-153.

Lan, W., X. Zhang, S.L. Kline-Smith, S.E. Rosasco, G.A. Barrett-Wilt, J. Shabanowitz, D.F. Hunt, C.E. Walczak, and P.T. Stukenberg. 2004. Aurora B phosphorylates centromeric MCAK and regulates its localization and microtubule depolymerization activity. *Current biology : CB*. 14:273-286.

Langan, T.A., J. Gautier, M. Lohka, R. Hollingsworth, S. Moreno, P. Nurse, J. Maller, and R.A. Sclafani. 1989. Mammalian growth-associated H1 histone kinase: a homolog of cdc2+/CDC28 protein kinases controlling mitotic entry in yeast and frog cells. *Mol Cell Biol*. 9:3860-3868.

Leijen, S., R.M. van Geel, A.C. Pavlick, R. Tibes, L. Rosen, A.R. Razak, R. Lam, T. Demuth, S. Rose, M.A. Lee, T. Freshwater, S. Shumway, L.W. Liang, A.M. Oza, J.H. Schellens, and G.I. Shapiro. 2016. Phase I Study Evaluating WEE1 Inhibitor AZD1775 As Monotherapy and in Combination With Gemcitabine, Cisplatin, or Carboplatin in Patients With Advanced Solid Tumors. *J Clin Oncol*. 34:4371-4380.

Leise, W., 3rd, and P.R. Mueller. 2002. Multiple Cdk1 inhibitory kinases regulate the cell cycle during development. *Dev Biol*. 249:156-173.

Leroy, B., L. Girard, A. Hollestelle, J.D. Minna, A.F. Gazdar, and T. Soussi. 2014. Analysis of TP53 mutation status in human cancer cell lines: a reassessment. *Human mutation*. 35:756-765.

Lewis, C.W., A.B. Bukhari, E.J. Xiao, W.S. Choi, J.D. Smith, E. Homola, J.R. Mackey, S.D. Campbell, A.M. Gamper, and G.K. Chan. 2019. Upregulation of Myt1 promotes acquired resistance of cancer cells to Wee1 inhibition. *Cancer Res*.

Lewis, C.W., and G.K. Chan. 2017. Role of cytoplasmic dynein and dynactin in mitotic silencing. Elsevier Science. 684 pp.

Lewis, C.W., and R.M. Golsteyn. 2016. Cancer cells that survive checkpoint adaptation contain micronuclei that harbor damaged DNA. *Cell cycle (Georgetown, Tex.)*. 15:3131-3145.

Lewis, C.W., Z. Jin, D. Macdonald, W. Wei, X.J. Qian, W.S. Choi, R. He, X. Sun, and G. Chan. 2017. Prolonged mitotic arrest induced by Wee1 inhibition sensitizes breast cancer cells to paclitaxel. *Oncotarget*. 8:73705-73722.

Lewis, C.W., R.G. Taylor, and R.M. Golsteyn. 2016. Measurement of Cdk1/Cyclin B Kinase Activity by Specific Antibodies and Western Blotting. *Methods in molecular biology (Clifton, N.J.)*. 1342:337-348.

Lewis, C.W., R.G. Taylor, P.M. Kubara, K. Marshall, L. Meijer, and R.M. Golsteyn. 2013. A western blot assay to measure cyclin dependent kinase activity in cells or in vitro without the use of radioisotopes. *FEBS Lett*. 587:3089-3095.

Li, C., M. Andrake, R. Dunbrack, and G.H. Enders. 2010. A bifunctional regulatory element in human somatic Wee1 mediates cyclin A/Cdk2 binding and Crm1-dependent nuclear export. *Mol Cell Biol*. 30:116-130.

Li, P., H. Goto, K. Kasahara, M. Matsuyama, Z. Wang, Y. Yatabe, T. Kiyono, and M. Inagaki. 2012. P90 RSK arranges Chk1 in the nucleus for monitoring of genomic integrity during cell proliferation. *Mol Biol Cell*. 23:1582-1592.

Lianga, N., E.C. Williams, E.K. Kennedy, C. Dore, S. Pilon, S.L. Girard, J.S. Deneault, and A.D. Rudner. 2013. A Wee1 checkpoint inhibits anaphase onset. *J Cell Biol*. 201:843-862.

Littler, S., O. Sloss, B. Geary, A. Pierce, A.D. Whetton, and S.S. Taylor. 2019. Oncogenic MYC amplifies mitotic perturbations. *Open biology*. 9:190136.

Liu, D., M. Vleugel, C.B. Backer, T. Hori, T. Fukagawa, I.M. Cheeseman, and M.A. Lampson. 2010. Regulated targeting of protein phosphatase 1 to the outer kinetochore by KNL1 opposes Aurora B kinase. *J Cell Biol*. 188:809-820.

Liu, F., C. Rothblum-Oviatt, C.E. Ryan, and H. Piwnica-Worms. 1999. Overproduction of human Myt1 kinase induces a G2 cell cycle delay by interfering with the intracellular trafficking of Cdc2-cyclin B1 complexes. *Mol Cell Biol*. 19:5113-5123.

Liu, F., J.J. Stanton, Z. Wu, and H. Piwnica-Worms. 1997. The human Myt1 kinase preferentially phosphorylates Cdc2 on threonine 14 and localizes to the endoplasmic reticulum and Golgi complex. *Mol Cell Biol*. 17:571-583.

Liu, Q., S. Guntuku, X.S. Cui, S. Matsuoka, D. Cortez, K. Tamai, G. Luo, S. Carattini-Rivera, F. DeMayo, A. Bradley, L.A. Donehower, and S.J. Elledge. 2000. Chk1 is an essential kinase that is regulated by Atr and required for the G(2)/M DNA damage checkpoint. *Genes Dev*. 14:1448-1459.

Liu, R.Z., K. Graham, D.D. Glubrecht, D.R. Germain, J.R. Mackey, and R. Godbout. 2011. Association of FABP5 expression with poor survival in triple-negative breast cancer: implication for retinoic acid therapy. *The American journal of pathology*. 178:997-1008.

Liu, R.Z., K. Graham, D.D. Glubrecht, R. Lai, J.R. Mackey, and R. Godbout. 2012. A fatty acid-binding protein 7/RXRbeta pathway enhances survival and proliferation in triple-negative breast cancer. *The Journal of pathology*. 228:310-321.

Liu, S.T., and H. Zhang. 2016. The mitotic checkpoint complex (MCC): looking back and forth after 15 years. *AIMS molecular science*. 3:597-634.

London, N., S. Ceto, J.A. Ranish, and S. Biggins. 2012. Phosphoregulation of Spc105 by Mps1 and PP1 regulates Bub1 localization to kinetochores. *Current biology : CB*. 22:900-906.

Lundberg, A.S., and R.A. Weinberg. 1998. Functional inactivation of the retinoblastoma protein requires sequential modification by at least two distinct cyclin-cdk complexes. *Mol Cell Biol*. 18:753-761.

Lundgren, K., N. Walworth, R. Booher, M. Dembski, M. Kirschner, and D. Beach. 1991. mik1 and wee1 cooperate in the inhibitory tyrosine phosphorylation of cdc2. *Cell*. 64:1111-1122.

Luo, X., and H. Yu. 2008. Protein metamorphosis: the two-state behavior of Mad2. *Structure (London, England : 1993)*. 16:1616-1625.

Madan, K., J.W. Allen, P.S. Gerald, and S.A. Latt. 1976. Fluorescence analysis of late DNA replication in mouse metaphase chromosomes using BUdR and 33258 Hoechst. *Exp Cell Res*. 99:438-444.

Magnussen, G.I., E. Hellesylt, J.M. Nesland, C.G. Trope, V.A. Florenes, and R. Holm. 2013. High expression of wee1 is associated with malignancy in vulvar squamous cell carcinoma patients. *BMC cancer*. 13:288.

Magnussen, G.I., R. Holm, E. Emilsen, A.K. Rosnes, A. Slipicevic, and V.A. Florenes. 2012. High expression of Wee1 is associated with poor disease-free survival in malignant melanoma: potential for targeted therapy. *PloS one*. 7:e38254.

Mahajan, K., B. Fang, J.M. Koomen, and N.P. Mahajan. 2012. H2B Tyr37 phosphorylation suppresses expression of replication-dependent core histone genes. *Nat Struct Mol Biol*. 19:930-937.

Mahajan, K., and N.P. Mahajan. 2013. WEE1 tyrosine kinase, a novel epigenetic modifier. *Trends in genetics : TIG*. 29:394-402.

Malumbres, M., and M. Barbacid. 2005. Mammalian cyclin-dependent kinases. *Trends Biochem Sci*. 30:630-641.

Malumbres, M., and M. Barbacid. 2009. Cell cycle, CDKs and cancer: a changing paradigm. *Nat Rev Cancer*. 9:153-166.

Marcelain, K., R. Armisen, A. Aguirre, N. Ueki, J. Toro, C. Colmenares, and M.J. Hayman. 2012. Chromosomal instability in mouse embryonic fibroblasts null for the transcriptional co-repressor Ski. *J Cell Physiol*. 227:278-287.

Marzluff, W.F., P. Gongidi, K.R. Woods, J. Jin, and L.J. Maltais. 2002. The human and mouse replication-dependent histone genes. *Genomics*. 80:487-498.

Marzluff, W.F., E.J. Wagner, and R.J. Duronio. 2008. Metabolism and regulation of canonical histone mRNAs: life without a poly(A) tail. *Nature reviews. Genetics*. 9:843-854.

Matheson, C.J., D.S. Backos, and P. Reigan. 2016a. Targeting WEE1 Kinase in Cancer. *Trends in pharmacological sciences*. 37:872-881.

Matheson, C.J., S. Venkataraman, V. Amani, P.S. Harris, D.S. Backos, A.M. Donson, M.F. Wempe, N.K. Foreman, R. Vibhakar, and P. Reigan. 2016b. A WEE1 Inhibitor Analog of AZD1775 Maintains Synergy with Cisplatin and Demonstrates Reduced Single-Agent Cytotoxicity in Medulloblastoma Cells. *ACS chemical biology*. 11:921-930.

Matsushime, H., D.E. Quelle, S.A. Shurtleff, M. Shibuya, C.J. Sherr, and J.Y. Kato. 1994. D-type cyclin-dependent kinase activity in mammalian cells. *Mol Cell Biol*. 14:2066-2076.

McGowan, C.H., and P. Russell. 1995. Cell cycle regulation of human WEE1. *EMBO J*. 14:2166-2175.

Mendez, E., C.P. Rodriguez, M.C. Kao, S. Raju, A. Diab, R.A. Harbison, E.Q. Konnick, G.M. Mugundu, R. Santana-Davila, R. Martins, N.D. Futran, and L.Q.M. Chow. 2018. A Phase I Clinical Trial of AZD1775 in Combination with Neoadjuvant Weekly Docetaxel and Cisplatin before Definitive Therapy in Head and Neck Squamous Cell Carcinoma. *Clin Cancer Res*. 24:2740-2748.

Meyerson, M., and E. Harlow. 1994. Identification of G1 kinase activity for cdk6, a novel cyclin D partner. *Mol Cell Biol*. 14:2077-2086.

Mikhailov, A., R.W. Cole, and C.L. Rieder. 2002. DNA damage during mitosis in human cells delays the metaphase/anaphase transition via the spindle-assembly checkpoint. *Current biology : CB*. 12:1797-1806.

Mir, S.E., P.C. De Witt Hamer, P.M. Krawczyk, L. Balaj, A. Claes, J.M. Niers, A.A. Van Tilborg, A.H. Zwinderman, D. Geerts, G.J. Kaspers, W. Peter Vandertop, J. Cloos, B.A. Tannous, P. Wesseling, J.A. Aten, D.P. Noske, C.J. Van Noorden, and T. Wurdinger. 2010. In silico analysis of kinase expression identifies WEE1 as a gatekeeper against mitotic catastrophe in glioblastoma. *Cancer cell*. 18:244-257.

Moasser, M.M., L. Sepp-Lorenzino, N.E. Kohl, A. Oliff, A. Balog, D.S. Su, S.J. Danishefsky, and N. Rosen. 1998. Farnesyl transferase inhibitors cause enhanced mitotic sensitivity to taxol and epothilones. *Proc Natl Acad Sci U S A*. 95:1369-1374.

Mochida, S., S.L. Maslen, M. Skehel, and T. Hunt. 2010. Greatwall phosphorylates an inhibitor of protein phosphatase 2A that is essential for mitosis. *Science (New York, N.Y.)*. 330:1670-1673.

Moiseeva, T.N., C. Qian, N. Sugitani, H.U. Osmanbeyoglu, and C.J. Bakkenist. 2019a. WEE1 kinase inhibitor AZD1775 induces CDK1 kinase-dependent origin firing in unperturbed G1- and S-phase cells. *Proc Natl Acad Sci U S A*.

Moiseeva, T.N., Y. Yin, M.J. Calderon, C. Qian, S. Schamus-Haynes, N. Sugitani, H.U. Osmanbeyoglu, E. Rothenberg, S.C. Watkins, and C.J. Bakkenist. 2019b. An ATR and CHK1 kinase signaling mechanism that limits origin firing during unperturbed DNA replication. *Proc Natl Acad Sci U S A*. 116:13374-13383.

Moudgil, D.K., N. Westcott, J.K. Famulski, K. Patel, D. Macdonald, H. Hang, and G.K. Chan. 2015. A novel role of farnesylation in targeting a mitotic checkpoint protein, human Spindly, to kinetochores. *J Cell Biol*. 208:881-896.

Mueller, P.R., T.R. Coleman, A. Kumagai, and W.G. Dunphy. 1995. Myt1: a membrane-associated inhibitory kinase that phosphorylates Cdc2 on both threonine-14 and tyrosine-15. *Science (New York, N.Y.)*. 270:86-90.

Mukhtar, E., V.M. Adhami, and H. Mukhtar. 2014. Targeting microtubules by natural agents for cancer therapy. *Mol Cancer Ther*. 13:275-284.

Muller, P.A., and K.H. Vousden. 2014. Mutant p53 in cancer: new functions and therapeutic opportunities. *Cancer cell*. 25:304-317.

Murrow, L.M., S.V. Garimella, T.L. Jones, N.J. Caplen, and S. Lipkowitz. 2010. Identification of WEE1 as a potential molecular target in cancer cells by RNAi screening of the human tyrosine kinome. *Breast cancer research and treatment*. 122:347-357.

Musacchio, A. 2015. The Molecular Biology of Spindle Assembly Checkpoint Signaling Dynamics. *Current biology : CB*. 25:R1002-1018.

Musacchio, A., and A. Desai. 2017. A Molecular View of Kinetochore Assembly and Function. *Biology*. 6.

Najjar, A., C. Platzer, A. Luft, C.A. Assmann, N.H. Elghazawy, F. Erdmann, W. Sippl, and M. Schmidt. 2019. Computer-aided design, synthesis and biological characterization of novel inhibitors for PKMYT1. *Eur J Med Chem*. 161:479-492.

Nakajima, H., S. Yonemura, M. Murata, N. Nakamura, H. Piwnica-Worms, and E. Nishida. 2008. Myt1 protein kinase is essential for Golgi and ER assembly during mitotic exit. *J Cell Biol*. 181:89-103.

Nakanishi, M., H. Ando, N. Watanabe, K. Kitamura, K. Ito, H. Okayama, T. Miyamoto, T. Agui, and M. Sasaki. 2000. Identification and characterization of human Wee1B, a new member of the Wee1 family of Cdk-inhibitory kinases. *Genes to cells : devoted to molecular & cellular mechanisms*. 5:839-847.

Nakayama, K.I., and K. Nakayama. 2006. Ubiquitin ligases: cell-cycle control and cancer. *Nat Rev Cancer*. 6:369-381.

Nakayama, Y., A. Igarashi, I. Kikuchi, Y. Obata, Y. Fukumoto, and N. Yamaguchi. 2009. Bleomycin-induced over-replication involves sustained inhibition of mitotic entry through the ATM/ATR pathway. *Exp Cell Res*. 315:2515-2528.

Nalepa, G., and D.W. Clapp. 2018. Fanconi anaemia and cancer: an intricate relationship. *Nat Rev Cancer*. 18:168-185.

Nemcova-Furstova, V., D. Kopperova, K. Balusikova, M. Ehrlichova, V. Brynychova, R. Vaclavikova, P. Daniel, P. Soucek, and J. Kovar. 2016. Characterization of acquired paclitaxel resistance of breast cancer cells and involvement of ABC transporters. *Toxicology and applied pharmacology*. 310:215-228.

Nilsson, J. 2015. Mps1-Ndc80: one interaction to rule them all. *Oncotarget*. 6:16822-16823.

Okamoto, K., and N. Sagata. 2007. Mechanism for inactivation of the mitotic inhibitory kinase Wee1 at M phase. *Proc Natl Acad Sci U S A*. 104:3753-3758.

Okumura, E., T. Fukuhara, H. Yoshida, S. Hanada Si, R. Kozutsumi, M. Mori, K. Tachibana, and T. Kishimoto. 2002. Akt inhibits Myt1 in the signalling pathway that leads to meiotic G2/M-phase transition. *Nat Cell Biol*. 4:111-116.

Okumura, E., A. Morita, M. Wakai, S. Mochida, M. Hara, and T. Kishimoto. 2014. Cyclin B-Cdk1 inhibits protein phosphatase PP2A-B55 via a Greatwall kinase-independent mechanism. *J Cell Biol*. 204:881-889.

Olivier, M., M. Hollstein, and P. Hainaut. 2010. TP53 mutations in human cancers: origins, consequences, and clinical use. *Cold Spring Harbor perspectives in biology*. 2:a001008.

Orth, J.D., A. Loewer, G. Lahav, and T.J. Mitchison. 2012. Prolonged mitotic arrest triggers partial activation of apoptosis, resulting in DNA damage and p53 induction. *Mol Biol Cell*. 23:567-576.

Osman, A.A., M.M. Monroe, M.V. Ortega Alves, A.A. Patel, P. Katsonis, A.L. Fitzgerald, D.M. Neskey, M.J. Frederick, S.H. Woo, C. Caulin, T.K. Hsu, T.O. McDonald, M. Kimmel, R.E. Meyn, O. Lichtarge, and J.N. Myers. 2015. Wee-1 kinase inhibition overcomes cisplatin resistance associated with high-risk TP53 mutations in head and neck cancer through mitotic arrest followed by senescence. *Mol Cancer Ther*. 14:608-619.

Padron, A., S. Iwasaki, and N.T. Ingolia. 2019. Proximity RNA Labeling by APEX-Seq Reveals the Organization of Translation Initiation Complexes and Repressive RNA Granules. *Mol Cell*. 75:875-887 e875.

Palmer, A., A.C. Gavin, and A.R. Nebreda. 1998. A link between MAP kinase and p34(cdc2)/cyclin B during oocyte maturation: p90(rsk) phosphorylates and inactivates the p34(cdc2) inhibitory kinase Myt1. *EMBO J*. 17:5037-5047.

Panek, R.L., G.H. Lu, S.R. Klutchko, B.L. Batley, T.K. Dahring, J.M. Hamby, H. Hallak, A.M. Doherty, and J.A. Keiser. 1997. In vitro pharmacological characterization of PD 166285, a new nanomolar potent and broadly active protein tyrosine kinase inhibitor. *J Pharmacol Exp Ther*. 283:1433-1444.

Passer, B.J., V. Nancy-Portebois, N. Amzallag, S. Prieur, C. Cans, A. Roborel de Climens, G. Fiucci, V. Bouvard, M. Tuynder, L. Susini, S. Morchoisne, V. Crible, A. Lespagnol, J. Dausset, M. Oren, R. Amson, and A. Telerman. 2003. The p53-inducible TSAP6 gene product regulates apoptosis and the cell cycle and interacts with Nix and the Myt1 kinase. *Proc Natl Acad Sci U S A*. 100:2284-2289.

Peng, C.Y., P.R. Graves, R.S. Thoma, Z. Wu, A.S. Shaw, and H. Piwnica-Worms. 1997. Mitotic and G2 checkpoint control: regulation of 14-3-3 protein binding by phosphorylation of Cdc25C on serine-216. *Science (New York, N.Y.)*. 277:1501-1505.

Peter, M., J. Nakagawa, M. Doree, J.C. Labbe, and E.A. Nigg. 1990. In vitro disassembly of the nuclear lamina and M phase-specific phosphorylation of lamins by cdc2 kinase. *Cell*. 61:591-602.

Pfister, S.X., E. Markkanen, Y. Jiang, S. Sarkar, M. Woodcock, G. Orlando, I. Mavrommati, C.C. Pai, L.P. Zalmas, N. Drobnitzky, G.L. Dianov, C. Verrill, V.M. Macaulay, S. Ying, N.B. La Thangue, V. D'Angiolella, A.J. Ryan, and T.C. Humphrey. 2015. Inhibiting WEE1 Selectively Kills Histone H3K36me3-Deficient Cancers by dNTP Starvation. *Cancer cell*. 28:557-568.

Pilie, P.G., C. Tang, G.B. Mills, and T.A. Yap. 2019. State-of-the-art strategies for targeting the DNA damage response in cancer. *Nature reviews. Clinical oncology*. 16:81-104.

Platzer, C., A. Najjar, A. Rohe, F. Erdmann, W. Sippl, and M. Schmidt. 2018. Identification of PKMYT1 inhibitors by screening the GSK published protein kinase inhibitor set I and II. *Bioorganic & medicinal chemistry*.

Pontano, L.L., P. Aggarwal, O. Barbash, E.J. Brown, C.H. Bassing, and J.A. Diehl. 2008. Genotoxic stress-induced cyclin D1 phosphorylation and proteolysis are required for genomic stability. *Mol Cell Biol*. 28:7245-7258.

Poruchynsky, M.S., E.E. Wang, C.M. Rudin, M.V. Blagosklonny, and T. Fojo. 1998. Bcl-xL is phosphorylated in malignant cells following microtubule disruption. *Cancer Res*. 58:3331-3338.

Posch, M., G.A. Khoudoli, S. Swift, E.M. King, J.G. Deluca, and J.R. Swedlow. 2010. Sds22 regulates aurora B activity and microtubule-kinetochore interactions at mitosis. *J Cell Biol*. 191:61-74.

PosthumaDeBoer, J., T. Wurdinger, H.C. Graat, V.W. van Beusechem, M.N. Helder, B.J. van Royen, and G.J. Kaspers. 2011. WEE1 inhibition sensitizes osteosarcoma to radiotherapy. *BMC cancer*. 11:156.

Potapova, T.A., S. Sivakumar, J.N. Flynn, R. Li, and G.J. Gorbsky. 2011. Mitotic progression becomes irreversible in prometaphase and collapses when Wee1 and Cdc25 are inhibited. *Mol Biol Cell*. 22:1191-1206.

Powers, A.F., A.D. Franck, D.R. Gestaut, J. Cooper, B. Gracyzk, R.R. Wei, L. Wordeman, T.N. Davis, and C.L. Asbury. 2009. The Ndc80 kinetochore complex forms load-bearing attachments to dynamic microtubule tips via biased diffusion. *Cell*. 136:865-875.

Price, D., S. Rabinovitch, P.H. O'Farrell, and S.D. Campbell. 2000. Drosophila wee1 has an essential role in the nuclear divisions of early embryogenesis. *Genetics*. 155:159-166.

Qiu, Z., N.L. Oleinick, and J. Zhang. 2018. ATR/CHK1 inhibitors and cancer therapy. *Radiother Oncol*. 126:450-464.

Rago, F., K.E. Gascoigne, and I.M. Cheeseman. 2015. Distinct organization and regulation of the outer kinetochore KMN network downstream of CENP-C and CENP-T. *Current biology : CB*. 25:671-677.

Rajeshkumar, N.V., E. De Oliveira, N. Ottenhof, J. Watters, D. Brooks, T. Demuth, S.D. Shumway, S. Mizuarai, H. Hirai, A. Maitra, and M. Hidalgo. 2011. MK-1775, a potent Wee1 inhibitor, synergizes with gemcitabine to achieve tumor regressions, selectively in p53-deficient pancreatic cancer xenografts. *Clin Cancer Res*. 17:2799-2806.

Rata, S., M.F. Suarez Peredo Rodriguez, S. Joseph, N. Peter, F. Echegaray Iturra, F. Yang, A. Madzvamuse, J.G. Ruppert, K. Samejima, M. Platani, M. Alvarez-Fernandez, M. Malumbres, W.C. Earnshaw, B. Novak, and H. Hochegger. 2018. Two Interlinked Bistable Switches Govern Mitotic Control in Mammalian Cells. *Current biology : CB*. 28:3824-3832.e3826.

Rausch, T., D.T. Jones, M. Zapatka, A.M. Stutz, T. Zichner, J. Weischenfeldt, N. Jager, M. Remke, D. Shih, P.A. Northcott, E. Pfaff, J. Tica, Q. Wang, L. Massimi, H. Witt, S. Bender, S. Pleier, H. Cin, C. Hawkins, C. Beck, A. von Deimling, V. Hans, B. Brors, R. Eils, W. Scheurlen, J. Blake, V. Benes, A.E. Kulozik, O. Witt, D. Martin, C. Zhang, R. Porat, D.M. Merino, J. Wasserman, N. Jabado, A. Fontebasso, L. Bullinger, F.G. Rucker, K. Dohner, H. Dohner, J. Koster, J.J. Molenaar, R. Versteeg, M. Kool, U. Tabori, D. Malkin, A. Korshunov, M.D. Taylor, P. Lichter, S.M. Pfister, and J.O. Korbel. 2012. Genome sequencing of pediatric medulloblastoma links catastrophic DNA rearrangements with TP53 mutations. *Cell*. 148:59-71.

Rezacova, M., G. Rudolfova, A. Tichy, A. Bacikova, D. Mutna, R. Havelek, J. Vavrova, K. Odrazka, E. Lukasova, and S. Kozubek. 2011. Accumulation of DNA damage and cell death after fractionated irradiation. *Radiat Res*. 175:708-718.

Rodrigues, N.T., S. Lekomtsev, S. Jananji, J. Kriston-Vizi, G.R. Hickson, and B. Baum. 2015. Kinetochore-localized PP1-Sds22 couples chromosome segregation to polar relaxation. *Nature*. 524:489-492.

Rodriguez-Rodriguez, J.A., C. Lewis, K.L. McKinley, V. Sikirzhytski, J. Corona, J. Maciejowski, A. Khodjakov, I.M. Cheeseman, and P.V. Jallepalli. 2018. Distinct Roles of RZZ and Bub1-KNL1 in Mitotic Checkpoint Signaling and Kinetochore Expansion. *Current biology : CB*. 28:3422-3429 e3425.

Rogers, S., D. Fey, R.A. McCloy, B.L. Parker, N.J. Mitchell, R.J. Payne, R.J. Daly, D.E. James, C.E. Caldon, D.N. Watkins, D.R. Croucher, and A. Burgess. 2016. PP1 initiates the dephosphorylation of MASTL, triggering mitotic exit and bistability in human cells. *J Cell Sci*. 129:1340-1354.

Rogers, S., R. Wells, and M. Rechsteiner. 1986. Amino acid sequences common to rapidly degraded proteins: the PEST hypothesis. *Science (New York, N.Y.)*. 234:364-368.

Ruiz, S., C. Mayor-Ruiz, V. Lafarga, M. Murga, M. Vega-Sendino, S. Ortega, and O. Fernandez-Capetillo. 2016. A Genome-wide CRISPR Screen Identifies CDC25A as a Determinant of Sensitivity to ATR Inhibitors. *Mol Cell*. 62:307-313.

Russell, P., and P. Nurse. 1986a. cdc25+ functions as an inducer in the mitotic control of fission yeast. *Cell*. 45:145-153.

Russell, P., and P. Nurse. 1986b. Schizosaccharomyces pombe and Saccharomyces cerevisiae: a look at yeasts divided. *Cell*. 45:781-782.

Russell, P., and P. Nurse. 1987. Negative regulation of mitosis by wee1+, a gene encoding a protein kinase homolog. *Cell*. 49:559-567.

Sanai, N., J. Li, J. Boerner, K. Stark, J. Wu, S. Kim, A. Derogatis, S. Mehta, H.D. Dhruv, L.K. Heilbrun, M.E. Berens, and P.M. LoRusso. 2018. Phase 0 Trial of AZD1775 in First-Recurrence Glioblastoma Patients. *Clin Cancer Res*. 24:3820-3828.

Sanchez, Y., C. Wong, R.S. Thoma, R. Richman, Z. Wu, H. Piwnica-Worms, and S.J. Elledge. 1997. Conservation of the Chk1 checkpoint pathway in mammals: linkage of DNA damage to Cdk regulation through Cdc25. *Science (New York, N.Y.)*. 277:1497-1501.

Santamaria, D., C. Barriere, A. Cerqueira, S. Hunt, C. Tardy, K. Newton, J.F. Caceres, P. Dubus, M. Malumbres, and M. Barbacid. 2007. Cdk1 is sufficient to drive the mammalian cell cycle. *Nature*. 448:811-815.

Sartorius, C.A., S.D. Groshong, L.A. Miller, R.L. Powell, L. Tung, G.S. Takimoto, and K.B. Horwitz. 1994. New T47D breast cancer cell lines for the independent study of progesterone B- and A-receptors: only antiprogestin-occupied B-receptors are switched to transcriptional agonists by cAMP. *Cancer Res*. 54:3868-3877.

Satyanarayana, A., M.B. Hilton, and P. Kaldis. 2008. p21 Inhibits Cdk1 in the absence of Cdk2 to maintain the G1/S phase DNA damage checkpoint. *Mol Biol Cell*. 19:65-77.

Sauer, B. 1994. Site-specific recombination: developments and applications. *Current Opinion in Biotechnology*. 5:521-527.

Saurin, A.T., M.S. van der Waal, R.H. Medema, S.M. Lens, and G.J. Kops. 2011. Aurora B potentiates Mps1 activation to ensure rapid checkpoint establishment at the onset of mitosis. *Nat Commun*. 2:316.

Seibert, M., M. Kruger, N.A. Watson, O. Sen, J.R. Daum, J.A. Slotman, T. Braun, A.B. Houtsmuller, G.J. Gorbsky, R. Jacob, M. Kracht, J.M.G. Higgins, and M.L. Schmitz. 2019. CDK1-mediated phosphorylation at H2B serine 6 is required for mitotic chromosome segregation. *J Cell Biol*. 218:1164-1181.

Sen, T., P. Tong, L. Diao, L. Li, Y. Fan, J. Hoff, J.V. Heymach, J. Wang, and L.A. Byers. 2017. Targeting AXL and mTOR Pathway Overcomes Primary and Acquired Resistance to WEE1 Inhibition in Small-Cell Lung Cancer. *Clin Cancer Res*. 23:6239-6253.

Senkus, E., S. Kyriakides, S. Ohno, F. Penault-Llorca, P. Poortmans, E. Rutgers, S. Zackrisson, and F. Cardoso. 2015. Primary breast cancer: ESMO Clinical Practice Guidelines for diagnosis, treatment and follow-up. *Annals of oncology : official journal of the European Society for Medical Oncology*. 26 Suppl 5:v8-30.

Serpico, A.F., G. D'Alterio, C. Vetrei, R. Della Monica, L. Nardella, R. Visconti, and D. Grieco. 2019. Wee1 Rather Than Plk1 Is Inhibited by AZD1775 at Therapeutically Relevant Concentrations. *Cancers*. 11.

Shaltiel, I.A., L. Krenning, W. Bruinsma, and R.H. Medema. 2015. The same, only different - DNA damage checkpoints and their reversal throughout the cell cycle. *J Cell Sci*. 128:607-620.

Shen, M., P.T. Stukenberg, M.W. Kirschner, and K.P. Lu. 1998. The essential mitotic peptidyl-prolyl isomerase Pin1 binds and regulates mitosis-specific phosphoproteins. *Genes Dev*. 12:706-720.

Shi, J., J.D. Orth, and T. Mitchison. 2008. Cell type variation in responses to antimitotic drugs that target microtubules and kinesin-5. *Cancer Res*. 68:3269-3276.

Shorter, J., and G. Warren. 2002. Golgi architecture and inheritance. *Annu Rev Cell Dev Biol*. 18:379-420.

Silva, P.M., N. Ribeiro, R.T. Lima, C. Andrade, V. Diogo, J. Teixeira, C. Florindo, A. Tavares, M.H. Vasconcelos, and H. Bousbaa. 2017. Suppression of spindly delays mitotic exit and exacerbates cell death response of cancer cells treated with low doses of paclitaxel. *Cancer Lett*. 394:33-42.

Sivakumar, S., P.L. Janczyk, Q. Qu, C.A. Brautigam, P.T. Stukenberg, H. Yu, and G.J. Gorbsky. 2016. The human SKA complex drives the metaphase-anaphase cell cycle transition by recruiting protein phosphatase 1 to kinetochores. *eLife*. 5.

Sloss, O., C. Topham, M. Diez, and S. Taylor. 2016. Mcl-1 dynamics influence mitotic slippage and death in mitosis. *Oncotarget*. 7:5176-5192.

Smith, E., N. Hegarat, C. Vesely, I. Roseboom, C. Larch, H. Streicher, K. Straatman, H. Flynn, M. Skehel, T. Hirota, R. Kuriyama, and H. Hochegger. 2011. Differential control of Eg5-dependent centrosome separation by Plk1 and Cdk1. *EMBO J*. 30:2233-2245.

Solomon, M.J., T. Lee, and M.W. Kirschner. 1992. Role of phosphorylation in p34cdc2 activation: identification of an activating kinase. *Mol Biol Cell*. 3:13-27.

Sorlie, T., R. Tibshirani, J. Parker, T. Hastie, J.S. Marron, A. Nobel, S. Deng, H. Johnsen, R. Pesich, S. Geisler, J. Demeter, C.M. Perou, P.E. Lonning, P.O. Brown, A.L. Borresen-Dale, and D. Botstein. 2003. Repeated observation of breast tumor subtypes in independent gene expression data sets. *Proc Natl Acad Sci U S A*. 100:8418-8423.

Sparano, J.A., S. Moulder, A. Kazi, D. Coppola, A. Negassa, L. Vahdat, T. Li, C. Pellegrino, S. Fineberg, P. Munster, M. Malafa, D. Lee, S. Hoschander, U. Hopkins, D. Hershman, J.J. Wright, C. Kleer, S. Merajver, and S.M. Sebti. 2009. Phase II trial of tipifarnib plus neoadjuvant doxorubicin-cyclophosphamide in patients with clinical stage IIB-IIIC breast cancer. *Clin Cancer Res*. 15:2942-2948.

Sperka, T., J. Wang, and K.L. Rudolph. 2012. DNA damage checkpoints in stem cells, ageing and cancer. *Nat Rev Mol Cell Biol*. 13:579-590.

Squire, C.J., J.M. Dickson, I. Ivanovic, and E.N. Baker. 2005. Structure and inhibition of the human cell cycle checkpoint kinase, Wee1A kinase: an atypical tyrosine kinase

with a key role in CDK1 regulation. *Structure (London, England : 1993)*. 13:541-550.

Subik, K., J.F. Lee, L. Baxter, T. Strzepek, D. Costello, P. Crowley, L. Xing, M.C. Hung, T. Bonfiglio, D.G. Hicks, and P. Tang. 2010. The Expression Patterns of ER, PR, HER2, CK5/6, EGFR, Ki-67 and AR by Immunohistochemical Analysis in Breast Cancer Cell Lines. *Breast cancer : basic and clinical research*. 4:35-41.

Sudakin, V., G.K. Chan, and T.J. Yen. 2001. Checkpoint inhibition of the APC/C in HeLa cells is mediated by a complex of BUBR1, BUB3, CDC20, and MAD2. *J Cell Biol*. 154:925-936.

Sun, Q.S., M. Luo, H.M. Zhao, and H. Sun. 2019. Overexpression of PKMYT1 indicates the poor prognosis and enhances proliferation and tumorigenesis in non-small cell lung cancer via activation of Notch signal pathway. *European review for medical and pharmacological sciences*. 23:4210-4219.

Swift, L.H., and R.M. Golsteyn. 2016. Cytotoxic amounts of cisplatin induce either checkpoint adaptation or apoptosis in a concentration-dependent manner in cancer cells. *Biology of the cell*. 108:127-148.

Szmyd, R., J. Niska-Blakie, M.K. Diril, P. Renck Nunes, K. Tzelepis, A. Lacroix, N. van Hul, L.W. Deng, J. Matos, O. Dreesen, X. Bisteau, and P. Kaldis. 2019. Premature activation of Cdk1 leads to mitotic events in S phase and embryonic lethality. *Oncogene*. 38:998-1018.

Tanaka, N., A.A. Patel, J. Wang, M.J. Frederick, N.N. Kalu, M. Zhao, A.L. Fitzgerald, T.X. Xie, N.L. Silver, C. Caulin, G. Zhou, H.D. Skinner, F.M. Johnson, J.N. Myers, and A.A. Osman. 2015. Wee-1 Kinase Inhibition Sensitizes High-Risk HPV+ HNSCC to Apoptosis Accompanied by Downregulation of MCl-1 and XIAP Antiapoptotic Proteins. *Clin Cancer Res*. 21:4831-4844.

Teft, W.A., S.E. Mansell, and R.B. Kim. 2011. Endoxifen, the active metabolite of tamoxifen, is a substrate of the efflux transporter P-glycoprotein (multidrug resistance 1). *Drug metabolism and disposition: the biological fate of chemicals*. 39:558-562.

Teichner, A., E. Eytan, D. Sitry-Shevah, S. Miniowitz-Shemtov, E. Dumin, J. Gromis, and A. Hershko. 2011. p31comet Promotes disassembly of the mitotic checkpoint complex in an ATP-dependent process. *Proc Natl Acad Sci U S A*. 108:3187-3192.

Terrano, D.T., M. Upreti, and T.C. Chambers. 2010. Cyclin-Dependent Kinase 1-Mediated Bcl-xL/Bcl-2 Phosphorylation Acts as a Functional Link Coupling Mitotic Arrest and Apoptosis. *Mol Cell Biol*. 30:640-656.

Tighe, A., O. Staples, and S. Taylor. 2008. Mps1 kinase activity restrains anaphase during an unperturbed mitosis and targets Mad2 to kinetochores. *J Cell Biol*. 181:893-901.

Timofeev, O., O. Cizmecioglu, F. Settele, T. Kempf, and I. Hoffmann. 2010. Cdc25 phosphatases are required for timely assembly of CDK1-cyclin B at the G2/M transition. *J Biol Chem*. 285:16978-16990.

Tipton, A.R., W. Ji, B. Sturt-Gillespie, M.E. Bekier, 2nd, K. Wang, W.R. Taylor, and S.T. Liu. 2013. Monopolar spindle 1 (MPS1) kinase promotes production of closed MAD2 (C-MAD2) conformer and assembly of the mitotic checkpoint complex. *J Biol Chem*. 288:35149-35158.

Tipton, A.R., K. Wang, L. Link, J.J. Bellizzi, H. Huang, T. Yen, and S.T. Liu. 2011. BUBR1 and closed MAD2 (C-MAD2) interact directly to assemble a functional mitotic checkpoint complex. *J Biol Chem*. 286:21173-21179.

Toledo, C.M., Y. Ding, P. Hoellerbauer, R.J. Davis, R. Basom, E.J. Girard, E. Lee, P. Corrin, T. Hart, H. Bolouri, J. Davison, Q. Zhang, J. Hardcastle, B.J. Aronow, C.L. Plaisier, N.S. Baliga, J. Moffat, Q. Lin, X.N. Li, D.H. Nam, J. Lee, S.M. Pollard, J. Zhu, J.J. Delrow, B.E. Clurman, J.M. Olson, and P.J. Paddison. 2015. Genome-wide CRISPR-Cas9 Screens Reveal Loss of Redundancy between PKMYT1 and WEE1 in Glioblastoma Stem-like Cells. *Cell reports*. 13:2425-2439.

Tominaga, Y., C. Li, R.H. Wang, and C.X. Deng. 2006. Murine Wee1 plays a critical role in cell cycle regulation and pre-implantation stages of embryonic development. *International journal of biological sciences*. 2:161-170.

Topham, C., A. Tighe, P. Ly, A. Bennett, O. Sloss, L. Nelson, R.A. Ridgway, D. Huels, S. Littler, C. Schandl, Y. Sun, B. Bechi, D.J. Procter, O.J. Sansom, D.W. Cleveland, and S.S. Taylor. 2015. MYC is a major determinant of mitotic cell fate. *Cancer cell*. 28:129-140.

Toyoshima-Morimoto, F., E. Taniguchi, and E. Nishida. 2002. Plk1 promotes nuclear translocation of human Cdc25C during prophase. *EMBO reports*. 3:341-348.

Trimarchi, J.M., and J.A. Lees. 2002. Sibling rivalry in the E2F family. *Nat Rev Mol Cell Biol*. 3:11-20.

Trinkle-Mulcahy, L. 2019. Recent advances in proximity-based labeling methods for interactome mapping. *F1000Research*. 8.

Tseng, L.M., N.C. Hsu, S.C. Chen, Y.S. Lu, C.H. Lin, D.Y. Chang, H. Li, Y.C. Lin, H.K. Chang, T.C. Chao, F. Ouyang, and M.F. Hou. 2013. Distant metastasis in triple-negative breast cancer. *Neoplasma*. 60:290-294.

Tsukahara, T., Y. Tanno, and Y. Watanabe. 2010. Phosphorylation of the CPC by Cdk1 promotes chromosome bi-orientation. *Nature*. 467:719-723.

Ubersax, J.A., E.L. Woodbury, P.N. Quang, M. Paraz, J.D. Blethrow, K. Shah, K.M. Shokat, and D.O. Morgan. 2003. Targets of the cyclin-dependent kinase Cdk1. *Nature*. 425:859-864.

Uetake, Y., and G. Sluder. 2010. Prolonged prometaphase blocks daughter cell proliferation despite normal completion of mitosis. *Current biology : CB*. 20:1666-1671.

Vakifahmetoglu, H., M. Olsson, and B. Zhivotovsky. 2008. Death through a tragedy: mitotic catastrophe. *Cell Death Differ*. 15:1153-1162.

Valente, C., and A. Colanzi. 2015. Mechanisms and Regulation of the Mitotic Inheritance of the Golgi Complex. *Frontiers in cell and developmental biology*. 3:79.

Van Cutsem, E., H. van de Velde, P. Karasek, H. Oettle, W.L. Vervenne, A. Szawlowski, P. Schoffski, S. Post, C. Verslype, H. Neumann, H. Safran, Y. Humblet, J. Perez Ruixo, Y. Ma, and D. Von Hoff. 2004. Phase III trial of gemcitabine plus tipifarnib compared with gemcitabine plus placebo in advanced pancreatic cancer. *J Clin Oncol*. 22:1430-1438.

Van Linden, A.A., D. Baturin, J.B. Ford, S.P. Fosmire, L. Gardner, C. Korch, P. Reigan, and C.C. Porter. 2013. Inhibition of Wee1 sensitizes cancer cells to antimetabolite chemotherapeutics in vitro and in vivo, independent of p53 functionality. *Mol Cancer Ther*. 12:2675-2684.

Varadarajan, R., J. Ayeni, Z. Jin, E. Homola, and S.D. Campbell. 2016. Myt1 inhibition of Cyclin A/Cdk1 is essential for fusome integrity and premeiotic centriole engagement in Drosophila spermatocytes. *Mol Biol Cell*. 27:2051-2063.

Varghese, F., A.B. Bukhari, R. Malhotra, and A. De. 2014. IHC Profiler: an open source plugin for the quantitative evaluation and automated scoring of immunohistochemistry images of human tissue samples. *PloS one*. 9:e96801.

Varmeh, S., and J.J. Manfredi. 2008. Overexpression of the dual specificity phosphatase, Cdc25C, confers sensitivity on tumor cells to doxorubicin-induced cell death. *Mol Cancer Ther*. 7:3789-3799.

Vassilopoulos, A., Y. Tominaga, H.S. Kim, T. Lahusen, B. Li, H. Yu, D. Gius, and C.X. Deng. 2014. WEE1 murine deficiency induces hyper-activation of APC/C and results in genomic instability and carcinogenesis. *Oncogene*. 0.

Villeneuve, J., M. Scarpa, M. Ortega-Bellido, and V. Malhotra. 2013. MEK1 inactivates Myt1 to regulate Golgi membrane fragmentation and mitotic entry in mammalian cells. *EMBO J*. 32:72-85.

Visconti, R., R. Della Monica, and D. Grieco. 2016. Cell cycle checkpoint in cancer: a therapeutically targetable double-edged sword. *Journal of experimental & clinical cancer research : CR*. 35:153.

Visconti, R., R. Della Monica, L. Palazzo, F. D'Alessio, M. Raia, S. Improta, M.R. Villa, L. Del Vecchio, and D. Grieco. 2015. The Fcp1-Wee1-Cdk1 axis affects spindle assembly checkpoint robustness and sensitivity to antimicrotubule cancer drugs. *Cell Death Differ*. 22:1551-1560.

Visconti, R., L. Palazzo, R. Della Monica, and D. Grieco. 2012. Fcp1-dependent dephosphorylation is required for M-phase-promoting factor inactivation at mitosis exit. *Nat Commun*. 3:894.

Vitale, I., L. Galluzzi, M. Castedo, and G. Kroemer. 2011. Mitotic catastrophe: a mechanism for avoiding genomic instability. *Nat Rev Mol Cell Biol*. 12:385-392.

Vleugel, M., E. Tromer, M. Omerzu, V. Groenewold, W. Nijenhuis, B. Snel, and G.J. Kops. 2013. Arrayed BUB recruitment modules in the kinetochore scaffold KNL1 promote accurate chromosome segregation. *J Cell Biol*. 203:943-955.

Vogel, C., and E.M. Marcotte. 2012. Insights into the regulation of protein abundance from proteomic and transcriptomic analyses. *Nature reviews. Genetics*. 13:227-232.

von Schubert, C., F. Cubizolles, J.M. Bracher, T. Sliedrecht, G. Kops, and E.A. Nigg. 2015. Plk1 and Mps1 Cooperatively Regulate the Spindle Assembly Checkpoint in Human Cells. *Cell reports*. 12:66-78.

Vos, L.J., J.K. Famulski, and G.K. Chan. 2011. hZwint-1 bridges the inner and outer kinetochore: identification of the kinetochore localization domain and the hZw10-interaction domain. *Biochem J*. 436:157-168.

Wan, L., M. Tan, J. Yang, H. Inuzuka, X. Dai, T. Wu, J. Liu, S. Shaik, G. Chen, J. Deng, M. Malumbres, A. Letai, M.W. Kirschner, Y. Sun, and W. Wei. 2014. APC(Cdc20) suppresses apoptosis through targeting Bim for ubiquitination and destruction. *Dev Cell*. 29:377-391.

Wang, H., S. Li, J. Oaks, J. Ren, L. Li, and X. Wu. 2018. The concerted roles of FANCM and Rad52 in the protection of common fragile sites. *Nat Commun*. 9:2791.

Wang, J., X. Yao, and J. Huang. 2017. New tricks for human farnesyltransferase inhibitor: cancer and beyond. *MedChemComm*. 8:841-854.

Wang, K., B. Sturt-Gillespie, J.C. Hittle, D. Macdonald, G.K. Chan, T.J. Yen, and S.T. Liu. 2014a. Thyroid hormone receptor interacting protein 13 (TRIP13) AAA-ATPase is a novel mitotic checkpoint-silencing protein. *J Biol Chem*. 289:23928-23937.

Wang, P., J. Lindsay, T.W. Owens, E.J. Mularczyk, S. Warwood, F. Foster, C.H. Streuli, K. Brennan, and A.P. Gilmore. 2014b. Phosphorylation of the proapoptotic BH3-only protein bid primes mitochondria for apoptosis during mitotic arrest. *Cell reports*. 7:661-671.

Wang, Y., J. Li, R.N. Booher, A. Kraker, T. Lawrence, W.R. Leopold, and Y. Sun. 2001. Radiosensitization of p53 mutant cells by PD0166285, a novel G(2) checkpoint abrogator. *Cancer Res*. 61:8211-8217.

Ward, R.J., E. Alvarez-Curto, and G. Milligan. 2011. Using the Flp-In T-Rex system to regulate GPCR expression. *Methods in molecular biology (Clifton, N.J.)*. 746:21-37.

Watanabe, N., H. Arai, Y. Nishihara, M. Taniguchi, N. Watanabe, T. Hunter, and H. Osada. 2004. M-phase kinases induce phospho-dependent ubiquitination of somatic Wee1 by SCFbeta-TrCP. *Proc Natl Acad Sci U S A*. 101:4419-4424.

Watanabe, N., M. Broome, and T. Hunter. 1995. Regulation of the human WEE1Hu CDK tyrosine 15-kinase during the cell cycle. *EMBO J*. 14:1878-1891.

Watanabe, R., M. Hara, E.I. Okumura, S. Herve, D. Fachinetti, M. Ariyoshi, and T. Fukagawa. 2019. CDK1-mediated CENP-C phosphorylation modulates CENP-A binding and mitotic kinetochore localization. *J Cell Biol*. 218:4042-4062.

Wei, R.R., J. Al-Bassam, and S.C. Harrison. 2007. The Ndc80/HEC1 complex is a contact point for kinetochore-microtubule attachment. *Nat Struct Mol Biol*. 14:54-59.

Welburn, J.P., E.L. Grishchuk, C.B. Backer, E.M. Wilson-Kubalek, J.R. Yates, 3rd, and I.M. Cheeseman. 2009. The human kinetochore Ska1 complex facilitates microtubule depolymerization-coupled motility. *Dev Cell*. 16:374-385.

Welburn, J.P., M. Vleugel, D. Liu, J.R. Yates, 3rd, M.A. Lampson, T. Fukagawa, and I.M. Cheeseman. 2010. Aurora B phosphorylates spatially distinct targets to differentially regulate the kinetochore-microtubule interface. *Mol Cell*. 38:383-392.

Welch, P.J., and J.Y. Wang. 1992. Coordinated synthesis and degradation of cdc2 in the mammalian cell cycle. *Proc Natl Acad Sci U S A*. 89:3093-3097.

Wells, N.J., N. Watanabe, T. Tokusumi, W. Jiang, M.A. Verdecia, and T. Hunter. 1999. The C-terminal domain of the Cdc2 inhibitory kinase Myt1 interacts with Cdc2 complexes and is required for inhibition of G(2)/M progression. *J Cell Sci*. 112 (Pt 19):3361-3371.

Whitfield, M.L., G. Sherlock, A.J. Saldanha, J.I. Murray, C.A. Ball, K.E. Alexander, J.C. Matese, C.M. Perou, M.M. Hurt, P.O. Brown, and D. Botstein. 2002. Identification of genes periodically expressed in the human cell cycle and their expression in tumors. *Mol Biol Cell*. 13:1977-2000.

Whyte, D.B., P. Kirschmeier, T.N. Hockenberry, I. Nunez-Oliva, L. James, J.J. Catino, W.R. Bishop, and J.K. Pai. 1997. K- and N-Ras are geranylgeranylated in cells treated with farnesyl protein transferase inhibitors. *J Biol Chem*. 272:14459-14464.

Williams, B.C., J.J. Filter, K.A. Blake-Hodek, B.E. Wadzinski, N.J. Fuda, D. Shalloway, and M.L. Goldberg. 2014. Greatwall-phosphorylated Endosulfine is both an inhibitor and a substrate of PP2A-B55 heterotrimers. *eLife*. 3:e01695.

Woo, R.A., and R.Y. Poon. 2003. Cyclin-dependent kinases and S phase control in mammalian cells. *Cell cycle (Georgetown, Tex.)*. 2:316-324.

Wordeman, L., M. Wagenbach, and G. von Dassow. 2007. MCAK facilitates chromosome movement by promoting kinetochore microtubule turnover. *J Cell Biol*. 179:869-879.

Wright, G., V. Golubeva, L.L. Remsing Rix, N. Berndt, Y. Luo, G.A. Ward, J.E. Gray, E. Schonbrunn, H.R. Lawrence, A.N.A. Monteiro, and U. Rix. 2017. Dual Targeting of WEE1 and PLK1 by AZD1775 Elicits Single Agent Cellular Anticancer Activity. *ACS chemical biology*. 12:1883-1892.

Wuchty, S., D. Arjona, A. Li, Y. Kotliarov, J. Walling, S. Ahn, A. Zhang, D. Maric, R. Anolik, J.C. Zenklusen, and H.A. Fine. 2011. Prediction of Associations between microRNAs and Gene Expression in Glioma Biology. *PloS one*. 6:e14681.

Wurzenberger, C., M. Held, M.A. Lampson, I. Poser, A.A. Hyman, and D.W. Gerlich. 2012. Sds22 and Repo-Man stabilize chromosome segregation by counteracting Aurora B on anaphase kinetochores. *J Cell Biol*. 198:173-183.

Wyatt, H.D., S. Sarbajna, J. Matos, and S.C. West. 2013. Coordinated actions of SLX1-SLX4 and MUS81-EME1 for Holliday junction resolution in human cells. *Mol Cell*. 52:234-247.

Xia, G., X. Luo, T. Habu, J. Rizo, T. Matsumoto, and H. Yu. 2004. Conformation-specific binding of p31(comet) antagonizes the function of Mad2 in the spindle checkpoint. *EMBO J*. 23:3133-3143.

Xiao, Z., Z. Chen, A.H. Gunasekera, T.J. Sowin, S.H. Rosenberg, S. Fesik, and H. Zhang. 2003. Chk1 mediates S and G2 arrests through Cdc25A degradation in response to DNA-damaging agents. *J Biol Chem*. 278:21767-21773.

Yam, C., R.K. Murthy, V. Valero, J. Szklaruk, G.S. Shroff, C.J. Stalzer, A.U. Buzdar, J.L. Murray, W. Yang, G.N. Hortobagyi, S.L. Moulder, and B. Arun. 2018. A phase II study of tipifarnib and gemcitabine in metastatic breast cancer. *Investigational New Drugs*. 36:299-306.

Yamazaki, S., A. Ishii, Y. Kanoh, M. Oda, Y. Nishito, and H. Masai. 2012. Rif1 regulates the replication timing domains on the human genome. *EMBO J*. 31:3667-3677.

Yao, F., T. Svensjo, T. Winkler, M. Lu, C. Eriksson, and E. Eriksson. 1998. Tetracycline repressor, tetR, rather than the tetR-mammalian cell transcription factor fusion derivatives, regulates inducible gene expression in mammalian cells. *Human Gene Therapy*. 9:1939-1950.

Yudkovsky, Y., M. Shteinberg, T. Listovsky, M. Brandeis, and A. Hershko. 2000. Phosphorylation of Cdc20/fizzy negatively regulates the mammalian cyclosome/APC in the mitotic checkpoint. *Biochemical and biophysical research communications*. 271:299-304.

Zasadil, L.M., K.A. Andersen, D. Yeum, G.B. Rocque, L.G. Wilke, A.J. Tevaarwerk, R.T. Raines, M.E. Burkard, and B.A. Weaver. 2014. Cytotoxicity of paclitaxel in breast cancer is due to chromosome missegregation on multipolar spindles. *Science translational medicine*. 6:229ra243.

Zerjatke, T., I.A. Gak, D. Kirova, M. Fuhrmann, K. Daniel, M. Gonciarz, D. Muller, I. Glauche, and J. Mansfeld. 2017. Quantitative Cell Cycle Analysis Based on an Endogenous All-in-One Reporter for Cell Tracking and Classification. *Cell reports*. 19:1953-1966.

Zhang, C.Z., A. Spektor, H. Cornils, J.M. Francis, E.K. Jackson, S. Liu, M. Meyerson, and D. Pellman. 2015a. Chromothripsis from DNA damage in micronuclei. *Nature*. 522:179-184.

Zhang, G., T. Lischetti, D.G. Hayward, and J. Nilsson. 2015b. Distinct domains in Bub1 localize RZZ and BubR1 to kinetochores to regulate the checkpoint. *Nat Commun*. 6:7162.

Zhang, Q., X. Zhao, C. Zhang, W. Wang, F. Li, D. Liu, K. Wu, D. Zhu, S. Liu, C. Shen, X. Yuan, K. Zhang, Y. Yang, Y. Zhang, and S. Zhao. 2019. Overexpressed PKMYT1 promotes tumor progression and associates with poor survival in esophageal squamous cell carcinoma. *Cancer Management and Research*. 11:7813—7824.

Zhao, H., and H. Piwnica-Worms. 2001. ATR-mediated checkpoint pathways regulate phosphorylation and activation of human Chk1. *Mol Cell Biol*. 21:4129-4139.

Zheng, H., F. Shao, S. Martin, X. Xu, and C.X. Deng. 2017. WEE1 inhibition targets cell cycle checkpoints for triple negative breast cancers to overcome cisplatin resistance. *Scientific reports*. 7:43517.

Zhu, J.Y., R.A.D. Cuellar, N. Berndt, H.E. Lee, S.H. Olesen, M.P. Martin, J.T. Jensen, G.I. Georg, and E. Schonbrunn. 2017. Structural basis of Wee kinases functionality and inactivation by diverse small molecule inhibitors. *J Med Chem*.

8 Appendix

8.1 Appendix A: Co-inhibition of Wee1 and ATR

This appendix includes published and unpublished data characterizing the effects of combined inhibition of Wee1 and ATR on mitosis in HeLa and other cancer cell lines. The Chan lab contributed to this project by providing stably fluorescent cell lines and performing some of the mitotic assays included in this appendix. Additionally, our lab performed survival assays showing that siWee1 mimics the effects of Adavosertib in the presence of AZD6783. Portions of **Figure 8.1**, **Figure 8.2**, and **Figure 8.3** are published in Bukhari AB, Lewis CW, Pearce JJ, Luong D, Chan GK, and AM Gamper, "Inhibiting Wee1 and ATR kinases produces tumor-selective synthetic lethality and suppresses metastasis," The Journal of Clinical Investigations, volume 129, issue 3, 1329-1344 (2019).

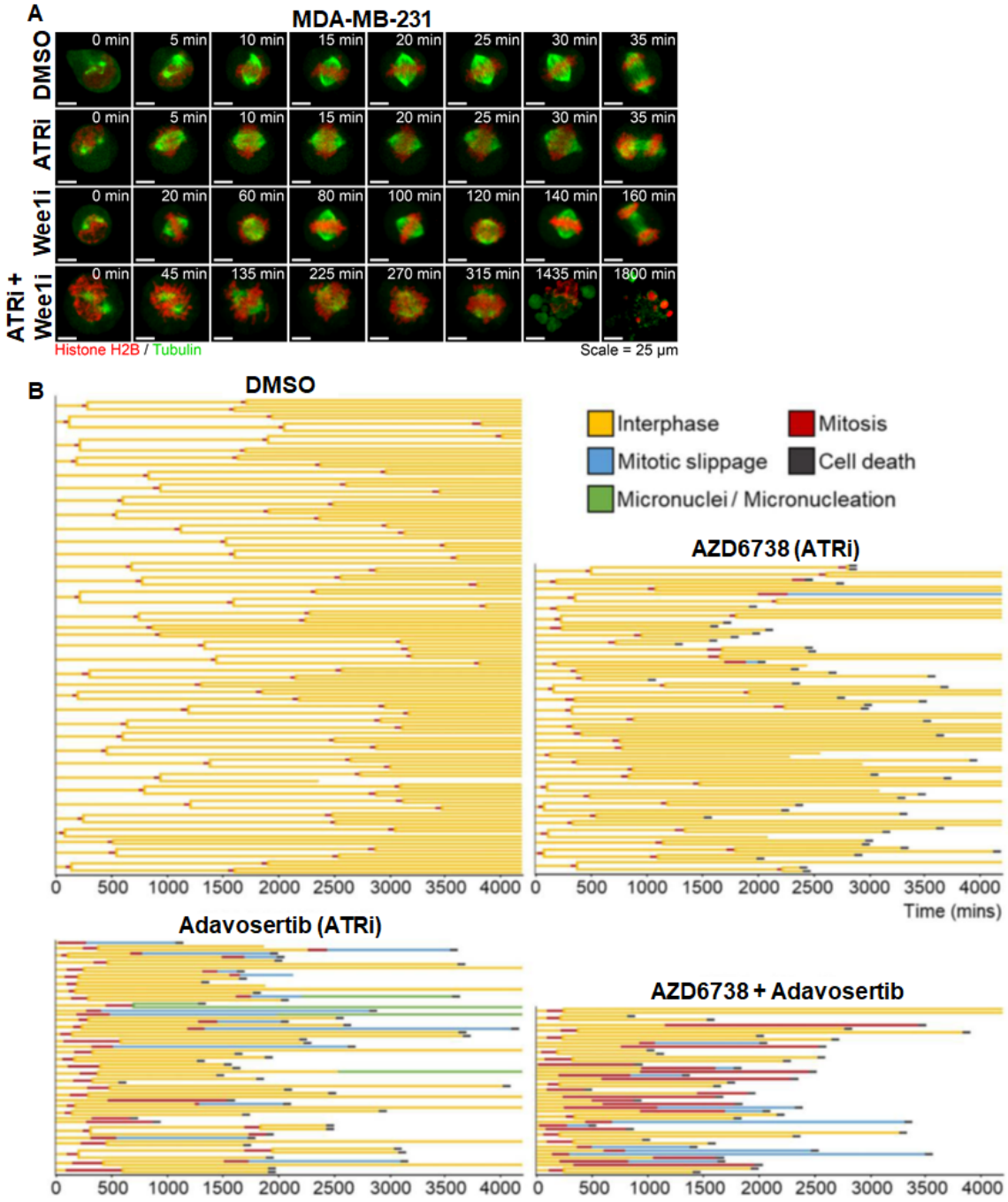

Figure 8.1. Co-inhibition of ATR and Wee1 leads to mitotic defects and cancer cell death.
Live cell imaging of. **A)** MDA-MB-231 cells expressing mCherry–histone H2B and GFP-tubulin were analyzed by time lapse-microscopy. Representative images of cells following nuclear envelope breakdown (NEBD) are shown. **B)** Line graph for individual mitotic cells tracked by time-lapse microscopy is shown, which includes times for indicated cellular events. A fork in the line indicates cell division and cell fate of daughter cells is also shown. Adapted from (Bukhari et al., 2019).

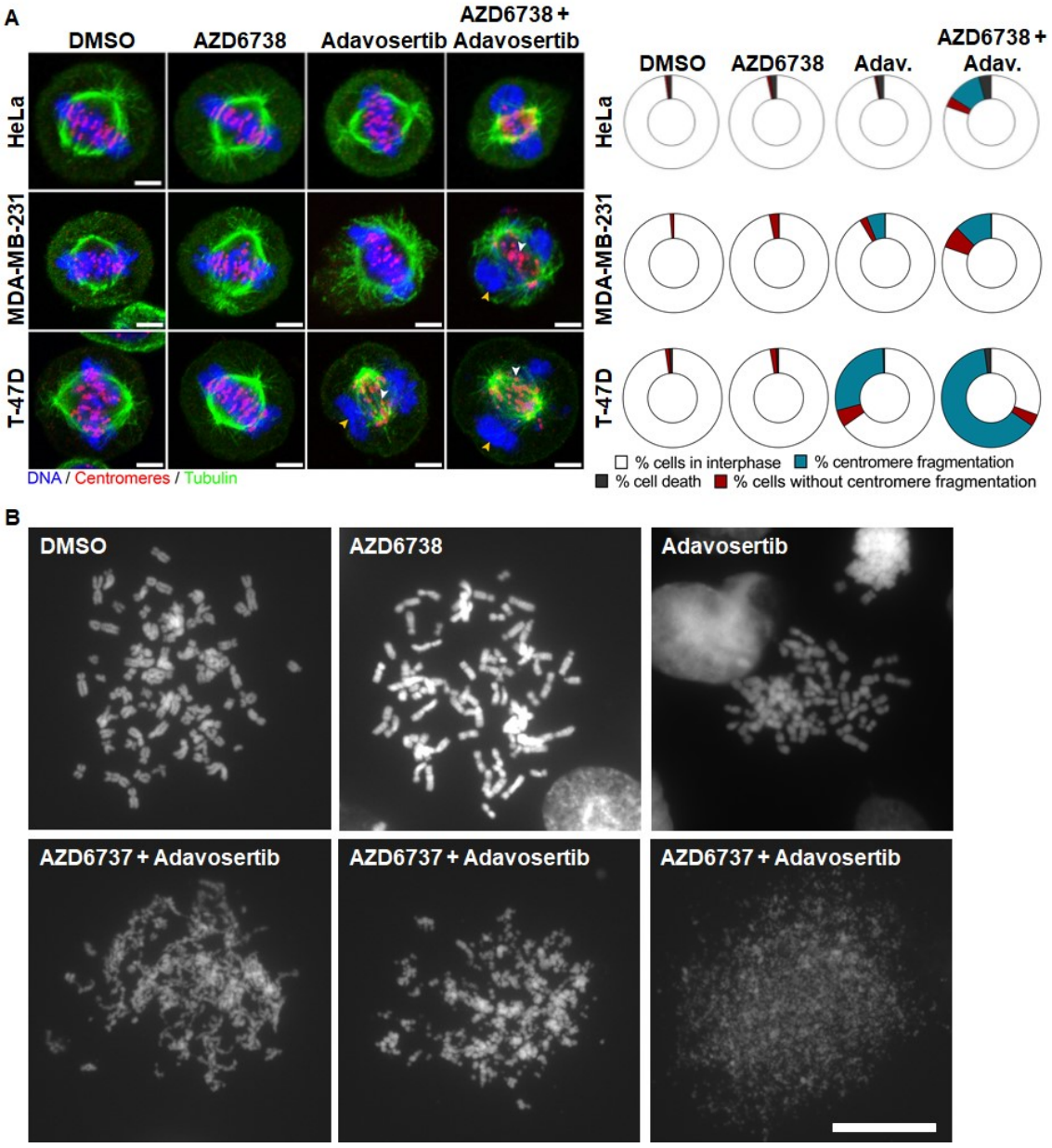

Figure 8.2. Wee1 and ATR inhibition induces centromere fragmentation. **A)** Representative images of mitotic HeLa, MDA-MB-231, and T-47D cells treated with ATR and/or Wee1 inhibitor (1 μM AZD6738; 300 nM Adavosertib). Fixed cells were stained for centromeres (red) and tubulin (green) by immunofluorescence and for DNA with DAPI (blue). Drug-induced clustering of centromeres spatially separated from the main mass of chromosome, a feature of centromere fragmentation, is clearly visible. Quantification of cells (n > 1000), fixed 4 h after release from a double thymidine block in the presence of the indicated inhibitors, that are in mitosis (red and blue) and display centromere fragmentation (blue). Adapted from (Bukhari et al., 2019). **B)** Metaphase spreads of representative HeLa cells is shown for indicated treatment. Scale bar = 12 μm. This data was *not* published in 2019 Bukhari *et al.* manuscript.

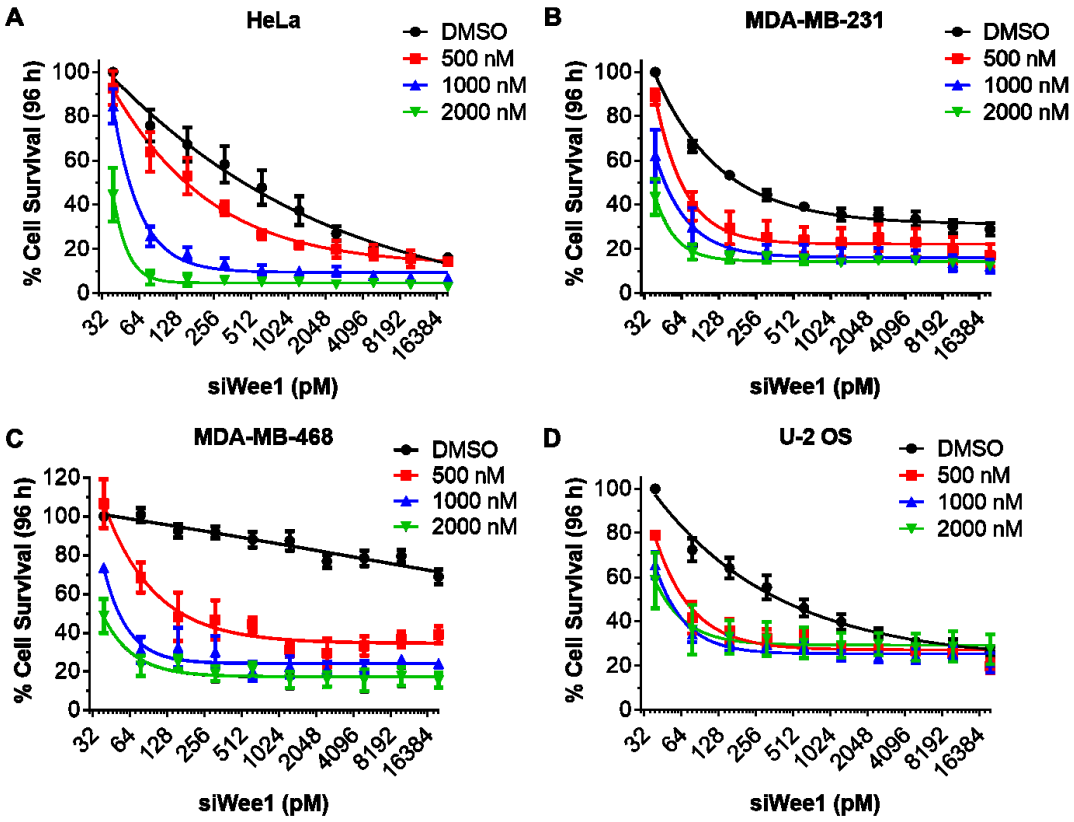

Figure 8.3. siRNA knockdown of Wee1 enhances AZD6783 induced cell death.
A) HeLa, **B)** MDA-MB-231, **C)** MDA-MB-468, and **D)** U-2 OS cells were treated with DMSO or with indicated amounts of AZD6738 in the presence of increasing concentrations of siWee1 and 0.2% lipofectamine for 96 h. The average percent surviving attached cells was analyzed by violet assay. Error bars represent SEM. Experiments were repeated at least three times. Adapted from (Bukhari et al., 2019).

8.2 Appendix B: Co-inhibition of Wee1 and farnesyl transferases

8.2.1 Inhibition of Farnesyl transferases prolongs mitosis.

Farnesyl transferases are enzymes that add a 15-carbon isoprenoid (farnesyl group) to proteins, which can be used to targeting a protein to the membrane. Several proteins are known to be farnesylated including the oncogenic protein Ras GTPase [reviewed in (Wang et al., 2017)]. The Ras signalling pathway is frequently dysregulated in cancer cells [reviewed in (Fernandez-Medarde and Santos, 2011)]. As such, small molecule inhibitors [known to as farnysel transferase inhibitors (FTIs)] were developed to block farnesyl transferase activity as a means of downregulating Ras signaling. However, blocking Ras farnesylation by FTI treatment promoted Ras geranylgeranylation (addition of a geranylgeranyl isoprene group), which allowed Ras to maintain its membrane association and signalling (Whyte et al., 1997). As such, many FTIs failure to show strong efficacy against cancers in the clinic [reviewed in (Wang et al., 2017)]. FTIs can disrupt chromosomal alignment and induce a mitotic arrest and are known to sensitize cancer cells to other antimitotic drugs such as paclitaxel (Moasser et al., 1998). Our lab has shown that HeLa cells treated with the FTI L-744-832, progress though mitosis 2 times slower compared to controls (Moudgil et al., 2015). FTI inhibits the farnesylation of at least three kinetochore proteins (CENP-E, CENP-F, and Spindly) [reviewed in (Wang et al., 2017)]. Although FTI treatment does not affect the kinetochore localization of CENP-E or CENP-F, FTIs do disrupt the kinetochore localization of Spindly (Moudgil et al., 2015). Non-farnesylatable Spindly mutants fail to localize to the kinetochore and loss of Spindly localization delays chromosome segregation (Moudgil et al., 2015). This suggest that loss of Spindly farnesylation drives the mitotic arrest phenotype observed by FTIs.

FTIs synergistically induce apoptosis in breast cancer cells when combined with the Chk1 inhibitors (Dai et al., 2005). Chk1 inhibition induces ectopic Cdk1 activity, which induces premature mitosis and mitotic arrest, a mechanism comparable Adavosertib. As such, we tested if

L744832 could also enhance death induced by Adavosertib.

8.2.2 Cells cotreated with L-744-832 and Adavosertib arrest in mitosis longer and exhibit more cell death compared to either inhibitor alone

We first established the cellular response to mono-treatment with either L-744-832 or Adavosertib in HeLa cells by colony formation assay (**Figure 8.4**). We determined that both inhibitors reduced colony formation in a dose-dependent manner but concentrations less than 300 nM L-744-832 and < 125 nM Adavosertib did not appear to effect colony formation in HeLa cells.

Using this information, we examined the effect of co-treating HeLa cells with both inhibitors. HeLa cells were treated with increasing concentrations of Adavosertib in the presence or absence of 100 nM or 300 nM L-744-832 for 48 h (**Figure 8.5A**). Relative to the DMSO control, L-744-832 decreased the number of colonies formed in HeLa cells treated with Adavosertib. We then performed a reciprocal experiment in which increasing concentrations of L-744-832 were added to cells in the presence or absence of 62.5 nM or 125 nM Adavosertib (**Figure 8.5B**). Relative to the DMSO control, Adavosertib treatment reduced colony formation in HeLa cells treated with L-744-832.

We next examined the duration of mitosis (NEBD to anaphase/mitotic slippage) in HeLa cells stably expressing GFP-H2B by live-cell imaging. DMSO treated cells exhibited a median mitotic duration of 65 min, which is consistent with a normal mitosis (**Figure**

8.6A). Cells treated with either 300 nM L-744-832 or 125 nM Adavosertib had median mitotic durations of 85 min. Consistent with the colony forming assay, neither inhibitor alone increased cell death relative to DMSO control (**Figure 8.6B**). However, cells co-treated with both Adavosertib and L-744-832 had a median mitotic time of 145 min, which resulted in 32% cell death over 48 h (**Figure 8.6A & B**). This data suggests that prolonged mitotic arrest increased cell death.

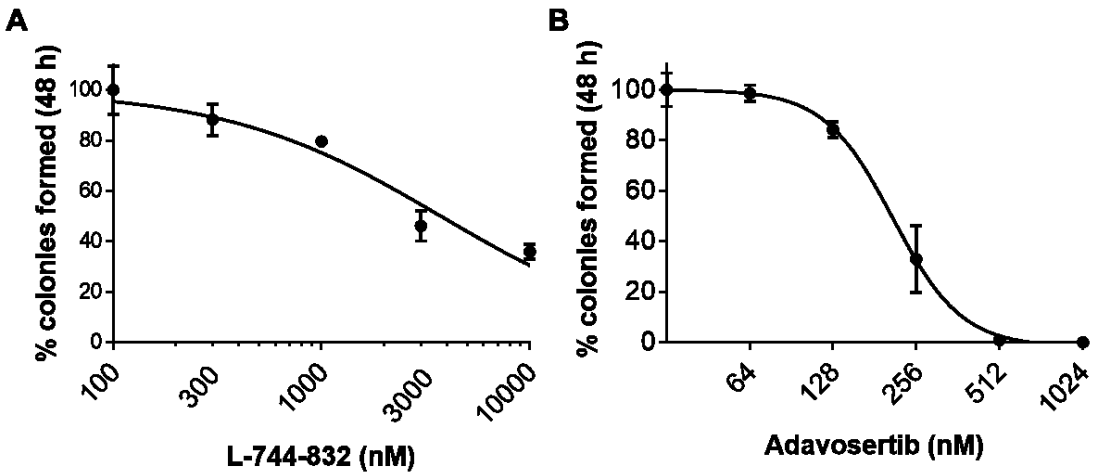

Figure 8.4. Mono-treatment with L-744-832 and Adavosertib reduces the colony forming ability of HeLa cells.
HeLa cells were treated with with either L-744832 **(A)** or Adavosertib **(B)** and then analyzed for colony forming ability. Average percent colonies formed (relative to DMSO control) is shown. Error bar represent standard deviation.

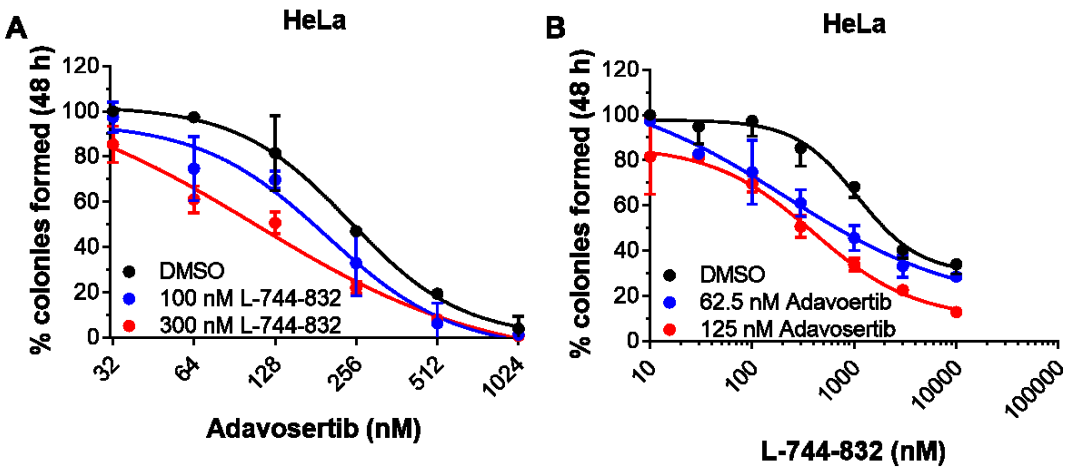

Figure 8.5. Co-treatment with Adavosertib and L-744-832 inhibits colony formation in HeLa cells more than mono-treatment.
Colony formation was assayed in HeLa cells. **A)** Cells were treated with DMSO or L-744832 (100 nM or 300 nM) in the presence of increasing concentration of Adavosertib for 48 h. **B)** Cells were treated with DMSO or Adavosertib (62.5 nM or 125 nM) in the presence of increasing concentration of L-744832 for 48 h.

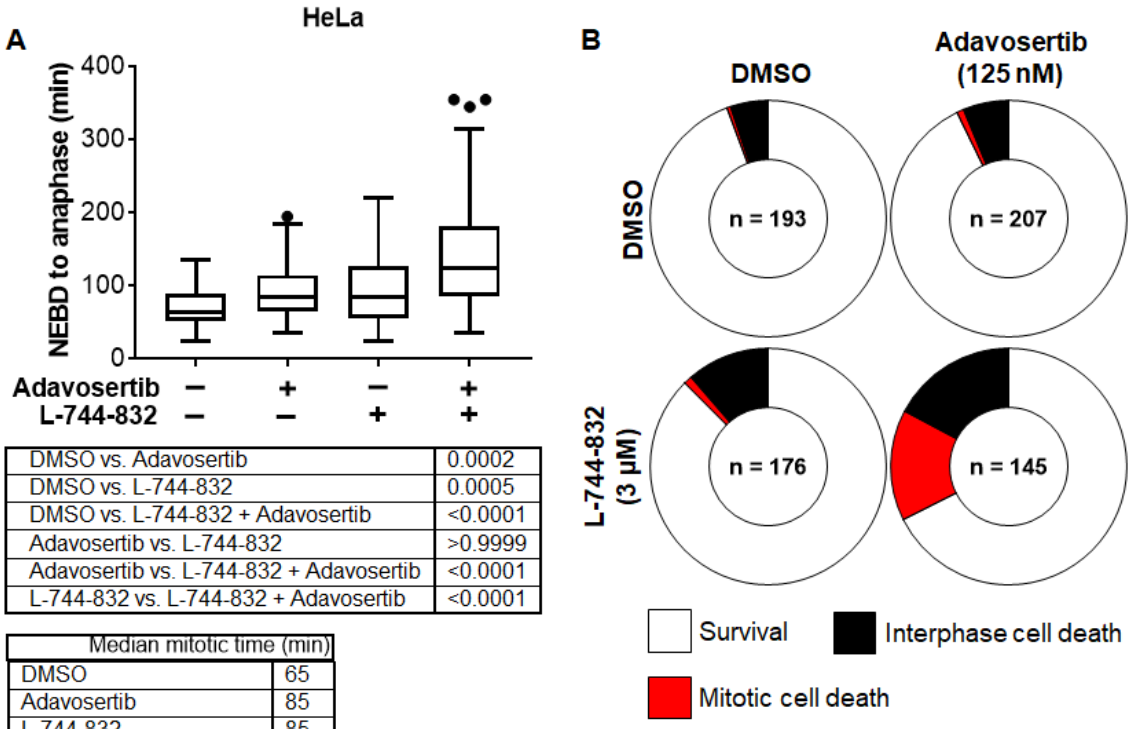

DMSO vs. Adavosertib	0.0002
DMSO vs. L-744-832	0.0005
DMSO vs. L-744-832 + Adavosertib	<0.0001
Adavosertib vs. L-744-832	>0.9999
Adavosertib vs. L-744-832 + Adavosertib	<0.0001
L-744-832 vs. L-744-832 + Adavosertib	<0.0001

Median mitotic time (min)	
DMSO	65
Adavosertib	85
L-744-832	85
L-744-832 + Adavosertib	125

Figure 8.6. Adavosertib and L-744-832 cotreatment exhibit a stronger mitotic arrest compared to either inhibitor alone.
HeLa cells stably expressing GFP-H2B were released from G1/S for 9 h and then treated with either DMSO (lane 1 denoted as -/-), Adavosertib, L-744-832, or Adavosertib and L-744-832. Cells were analyzed by time-lapse imaging. **A)** Whisker-box plots show the duration of mitosis for each treatment. Tables show median mitotic time and statistical differences between median mitotic times. *P*-values are shown in table below (One-way ANOVA and Tukey's multiple comparisons test). **B)** Proportion of cell death in mitosis and interphase are shown in donut plots. Number of cells counted for each treatment is shown within donut plots.

8.3 Appendix C: Co-inhibition of Wee1 and Aurora B

8.3.1 Aurora B inhibition by ZM447439 impairs chromosomal congression and induces chromosome segregation errors

Incorrect kinetochore-microtubule attachments can be destabilized by Aurora B in concert with other kinases (Cdk1 and Plk1). Aurora B phosphorylates Ncd80 subunit Hec1 on several sites, which induce a charge repulsion between Ndc80 and the negatively charged C-terminal tail of tubulin weakening microtubule binding (Ciferri et al., 2008; DeLuca et al., 2006; DeLuca et al., 2011). Aurora B is also phosphorylates the Mis12 subunit Dsn1, the N-terminal microtubule-binding domain of KNL1 (Welburn et al., 2010), and Ska subunit Ska1 and Ska3 (Chan et al., 2012), which also disrupt kinetochore-microtubule binding. Moreover, Aurora B also downregulates the activity of the kinesin 13 mitotic centromere–associated kinesin (MCAK), a potent microtubule depolymerizing enzyme that facilitates chromosome movement (Lan et al., 2004; Wordeman et al., 2007). Micro-injection of antibodies against Aurora B (Kallio et al., 2002), small molecule Aurora B inhibitors (ZM447439 and Hesperadin) (Ditchfield et al., 2003; Isokane et al., 2016), and siRNA knockdown of Aurora B (Adams et al., 2001; Ditchfield et al., 2003) leads to defect in chromosome congression. As a result, cells mitotic exit without proper chromosome alignment.

Following error correction of kinetochore-microtubule attachments, PP1 along with targeting subunits Sds22 and repo man) and PP2A-B55 dephosphorylate Aurora B substrates (Wurzenberger et al., 2012), allowing new bipolar attachments to be made. siRNA (or shRNA) knockdown of Sds22, prevents dephosphorylation of Aurora B

substrates leading to prolonged activation of the mitotic checkpoint, and mitotic arrest (Eiteneuer et al., 2014; Posch et al., 2010; Wurzenberger et al., 2012).

ZM447439 is a potent Aurora B inhibitor that has been previously reported to disrupt the alignment and segregation of chromosomes as well as disrupt cytokinesis (Bekier et al., 2009; Ditchfield et al., 2003; Kaestner et al., 2009).

8.3.2 Cells cotreated with ZM447439 and Adavosertib arrest in mitosis longer and exhibit more cell death compared to either inhibitor alone

We treated A549 lung cancer cells with increasing concentration of ZM447439 in the presence or absence of 300 nM Adavosertib and then analyzed cells by CellTiter-Blue® Cell Viability Assay (a metabolic assay used to screen for potential cell killing) (**Figure 8.7**). We observed a reduction in metabolic activity in a dose dependent manner with ZM447439, which was further enhanced with Adavosertib treatment. A549 cells were used here because they were shown to be Adavosertib resistant by a project student; however, subsequent experiments were performed in HeLa Flp-In T-Rex GFP-Myt1 cells. Although we planned to study the effects of Myt1 overexpression in these cells, Myt1 induction was not tested at the time this document was written.

To study the effects of Aurora B and Wee1 inhibition in mitotic cells, we released cells from G1/S for 9 hours and then treated cells with either DMSO, Adavosertib, ZM447439, or both Adavosertib and ZM447439 (**Figure 8.8A**). Normal mitotic progression and cell division was observed in DMSO-treated cells (median mitotic duration = 50 min). Consistent with the Aurora B inhibition phenotype, we observed chromosome congression failure and mitotic slippage in ZM447439 treated cells. Adavosertib and ZM447439 increased the median mitotic time from 50 min in DMSO treated cells to 140

min and 145 min respectively (**Figure 8.8B**). However, combined treatment with both Adavosertib and ZM447439 resulted in the longest mitotic arrest (320 min). Individually, Adavosertib and ZM447439 induced greater than 50% cell killing, but combined the two inhibitors resulted in nearly 75% cell killing (**Figure 8.8C**).

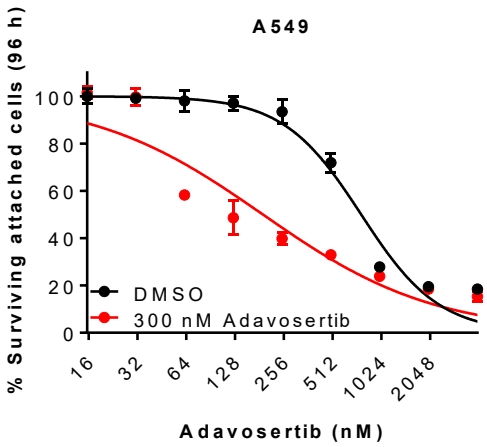

Figure 8.7. ZM447439 enhances Adavosertib mediated cell killing.
A549 cells were treated with increasing concentrations of Adavosertib alone or in combination with 300 nM ZM447439. Cell survival was analyzed by crystal violet assay. Experiments were repeated two times.

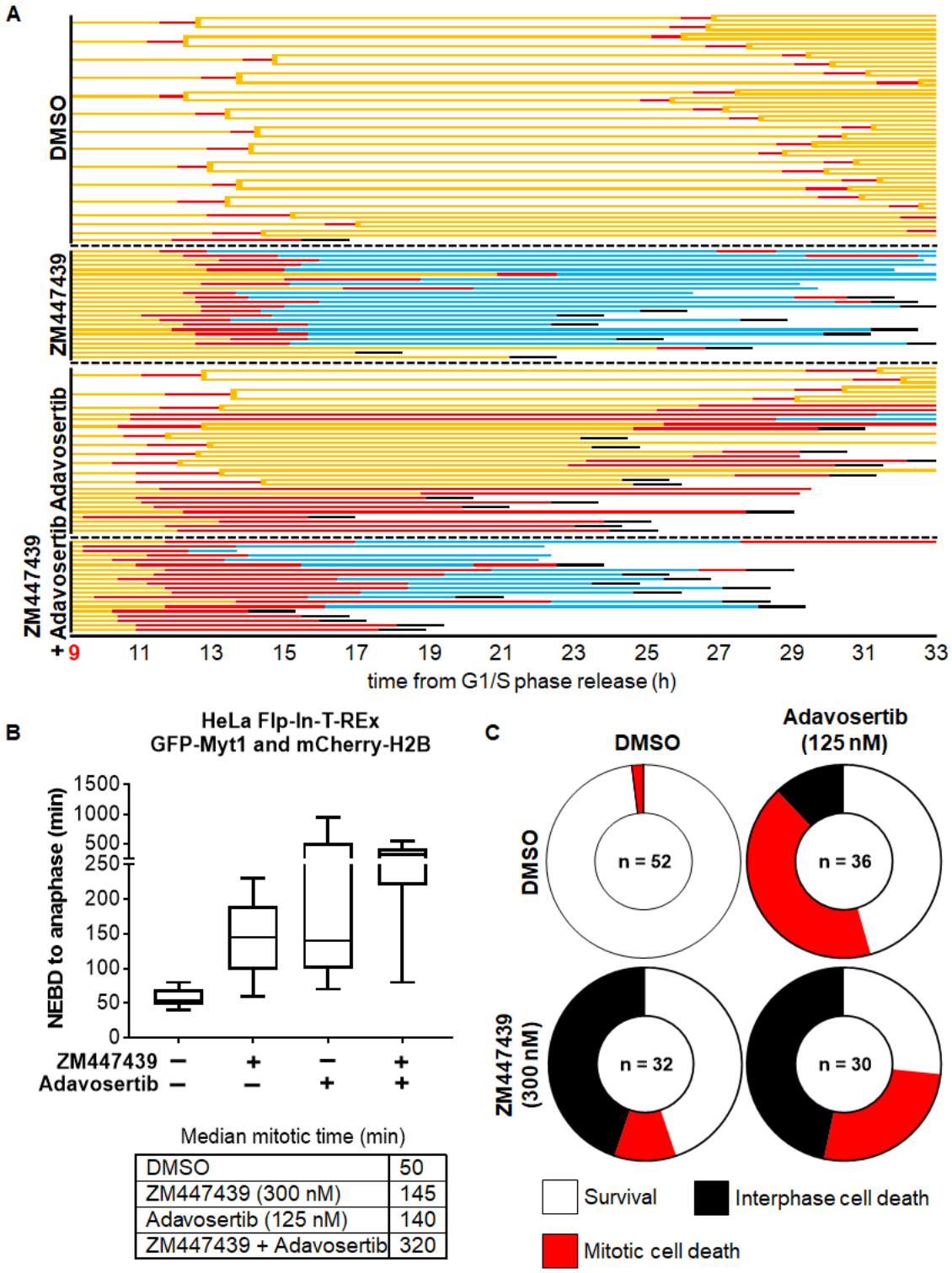

Figure 8.8. ZM447439 enhances Adavosertib induced cell killing by delaying mitotic exit.

HeLa Flp-In GFP-Myt1 cells stably expressing mCherry-H2B were released from G1/S for 9 hours and then treated with DMSO, Adavosertib, ZM447439, or both Adavosertib and ZM447439. Duration for mitosis was analyzed by time-lapse imaging. **A**) Line graph for individual mitotic cells tracked by time-lapse

microscopy is shown, which includes times for indicated cellular events. A fork in the line indicates cell division and cell fate of daughter cells is also shown. **B)** Whisker-box plots show the duration of mitosis for each treatment. **C)** Proportion of cell death in mitosis and interphase are shown in donut plots. Number of cells counted for each treatment is shown within donut plots. *P*-values are shown in table below (One-way ANOVA and Tukey's multiple comparisons test).

8.4 Appendix D: SDS22 enhances Adavosertib induced cancer cell killing

8.4.1 siRNA phosphatase screen with Adavosertib

We completed a preliminary RNAi screen of a human phosphatase library (267 gene; Ambion) in the presence of Adavosertib as means of identify genes that when knocked down enhanced cancer killing compared to Adavosertib alone. We transfected HeLa cells with a pool of 3 siRNAs targeting different phosphatases alone or in the presence of a sublethal concentration of Adavosertib (250 nM). We used the CellTiter-Blue® Cell Viability Assay as a high throughput surrogate measure for cancer cell killing. We identified 16 "positive gene hits" that when knockdown, enhanced Adavosertib efficacy in this assay (**Figure 8.9**). Despite the name, CellTiter-Blue® Cell Viability Assay is metabolic assay and not a survival assay. Therefore, further assays were used to validate select gene hits.

Our preliminary screens identified Protein phosphatase 1 regulatory subunit (PPP1R7) also known as SDS22 as a possible "positive gene hit". SDS22 is a kinetochore protein and a PP1 regulator (Posch et al., 2010; Rodrigues et al., 2015; Wurzenberger et al., 2012). To validate SDS22 as a positive gene hit, we transfect HeLa, A549, MCF7, and T-47D cells with a single siRNA targeting SDS22 alone or in the presence of Adavosertib for 48 h and then analyzed colony formation (**Figure 8.10A-D**). We observed that siSDS22 knockdown enhanced the effects of Adavosertib and reduced colony formation in all four cell lines. SDS22 and tubulin protein levels were analyzed in HeLa and A549 cells by immunoblot (**Figure 8.10A & B**). As expected, cells transfected siSDS22 had lower SDS22 levels relative to cells transfected with siSc.

To test if SDS22 knockdown affected the number of cells in mitosis, we transfected Hela cells with siSDS22 or siSc for 24 h and then treated cells with Adavosertib for an additional 4 h. Cells were then analyzed for PH3 (relative to DAPI) by immunofluorescence (**Figure 8.11A & B**). In the absence of Adavosertib, SDS22 knockdown has little effect on the percentage of PH3 positive cells (3% in siSc verses 5% in siSDS22). However, siSDS22 in the presence of Adavosertib increased the percentage of PH3 positive cells from 25% to 35%.

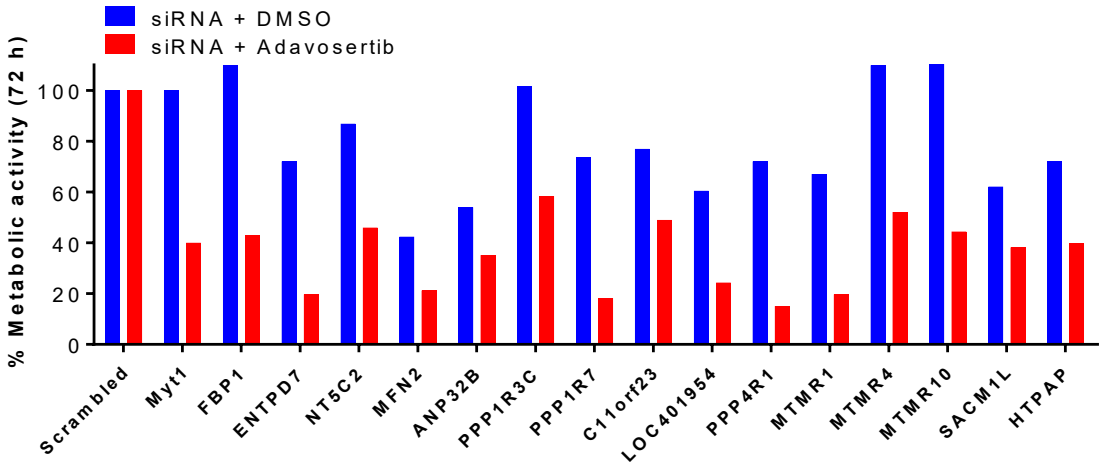

Figure 8.9. siRNA screen of human phosphatases with Adavosertib.
HeLa cells were transfected with a pool of three siRNAs targeting different human phosphatases for 24 h and then treated with 250 nM Adavosertib for an additional 72 h. siRNAs that reduced metabolic activity in the presence of Adavosertib compared to DMSO (as assayed by CellTiter Blue®) were considered positive hits.

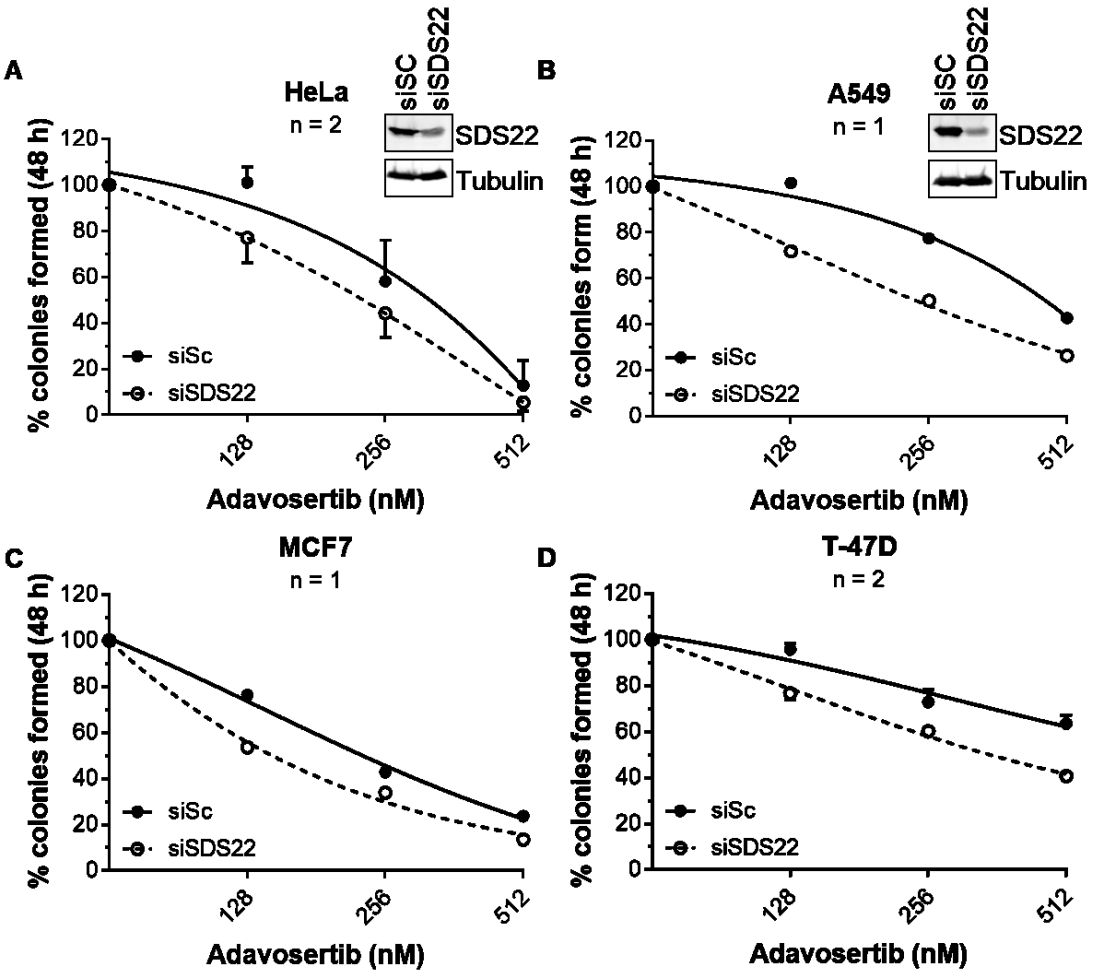

Figure 8.10. Knockdown of SDS22 sensitizes cancer cells to Adavosertib. **A)** HeLa, **B)** A549, **C)** MCF7 and **D)** T-47D cells were transfected with either siSc or siSDS22 for 24 h and then treated with increasing concentration of Adavosertib for 48 h. Cells were then analyzed for colony forming ability. Number of repeats are included below each cell line. Knockdown efficiency of SDS22 (relative to tubulin) was determined in HeLa and A549 by immunoblot.

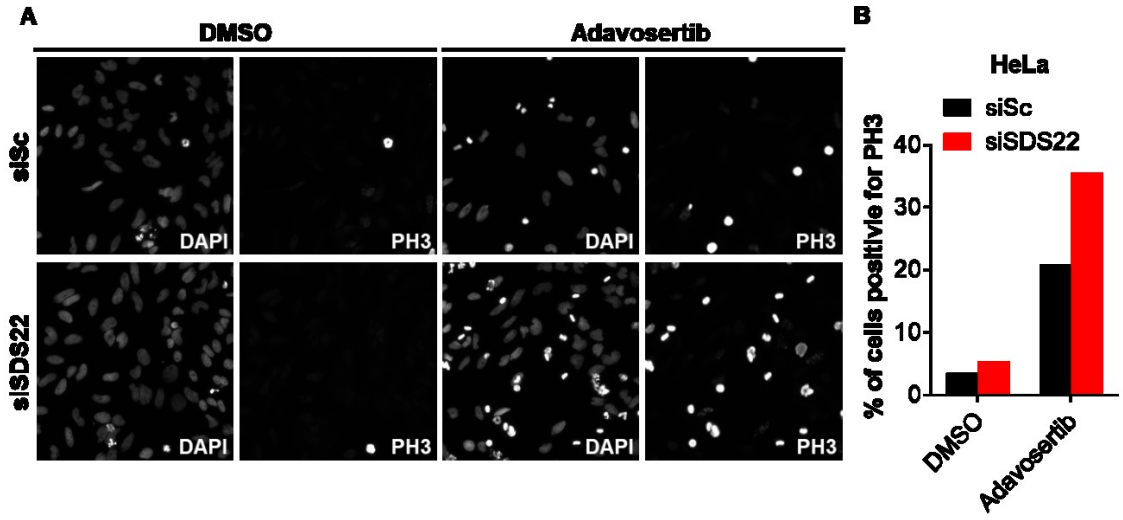

Figure 8.11. SDS22 knockdown promotes mitotic arrest in the presence of Adavosertib.
HeLa cells were transfected with either siSc or siSDS22 for 24 h and then treated with Adavosertib for 4 h. Cells were than analyzed by immunofluorescence microscopy for the percentage of PH3-positive cells relative to DAPI. **A)** Representative images for treatments are shown. **B)** Graph shows the percentage of cells that were PH3 positive. At least 500 cells were scored for each treatment. Experiment has *not* been repeated.

8.5 Appendix E:

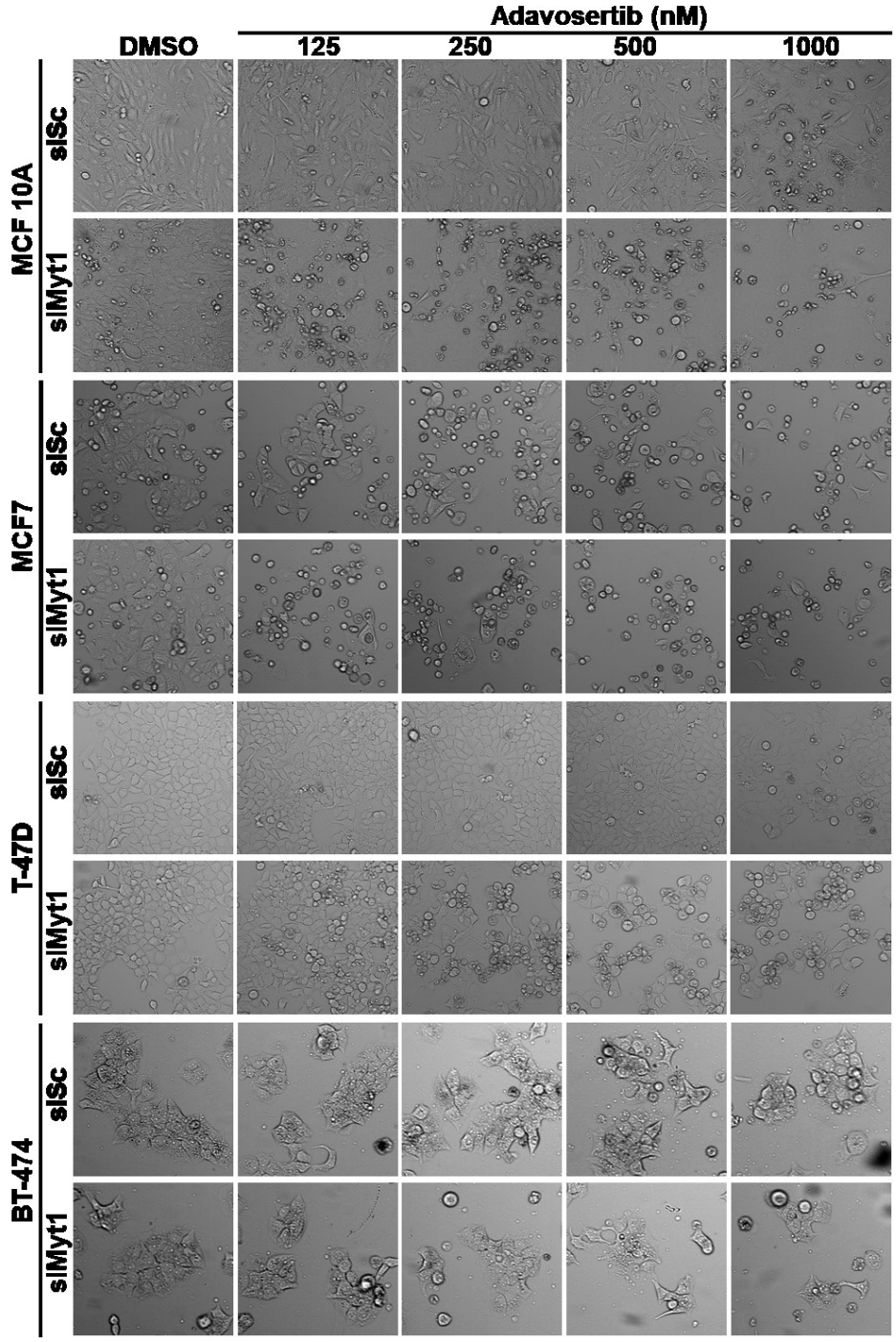

Figure 8.12. Myt1 knockdown induces cell rounding, shrinkage, and detachment in the presence of Adavosertib.
Indicated cells were transfected with siSc or siMyt1 and then treated with Adavosertib for 72 h. Representative images are shown for treatments.

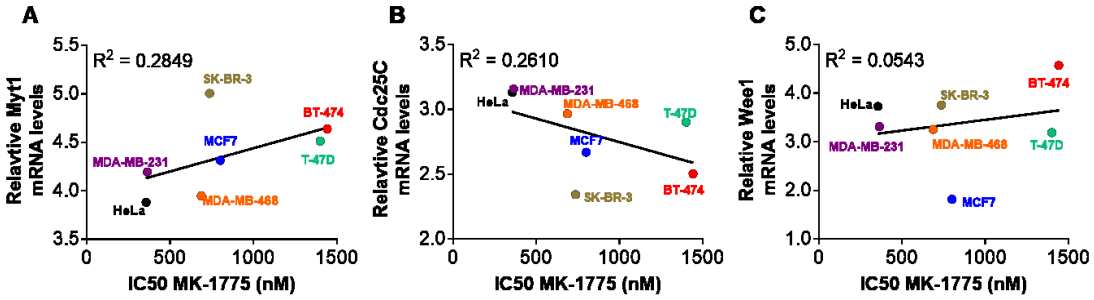

Figure 8.13. Myt1 and Cdc25C mRNA levels are weakly correlated with Adavosertib sensitivity in cell lines.
mRNA expression z-scores obtained from the Cancer cell Line Encyclopedia (CCLE) were plotted against IC50 values calculated from crystal violet assay (**Table 3.2**; siSc + Adavosertib).

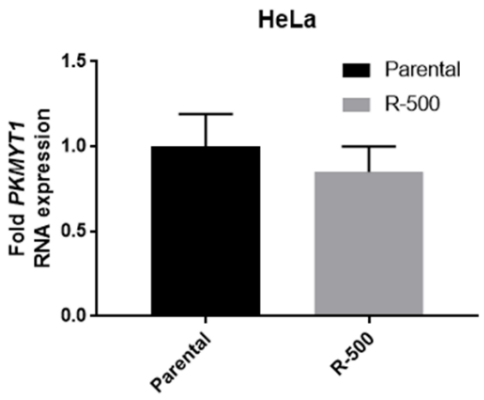

Figure 8.14. Cell that acquire resistance to Adavosertib have similarly Myt1 mRNA levels.
Myt1 mRNA levels were analyzed by real time quantitative polymerase chain reaction (RT-qPCR) in parental and R500 HeLa cells. mRNA levels were normalized to parental cells. Error bar equal standard deviation (three replicates).